JOURNAL OF FLUID MECHANICS

VOLUME 6 PART 3

OCTOBER 1959

THE UNIVERSITY OF MICHIGAN
NOV 4 1959
ENGINEERING LIBRARY

PUBLISHED BY

CAMBRIDGE UNIVERSITY PRESS

BENTLEY HOUSE, 200 EUSTON ROAD, LONDON, N.W.1

AMERICAN BRANCH: 32 EAST 57TH STREET, NEW YORK 22, N.Y.

Price 30*s.* (*U.S.A.* $5.00)

The JOURNAL OF FLUID MECHANICS exists for the publication of theoretical and experimental investigations of all aspects of the mechanics of fluids, and is issued in four parts per volume.

EDITOR

DR G. K. BATCHELOR

Cavendish Laboratory, University of Cambridge, Cambridge, England

ASSISTANT EDITORS

DR T. B. BENJAMIN, DR I. PROUDMAN, DR P. G. SAFFMAN

Cavendish Laboratory, University of Cambridge, Cambridge, England

ASSOCIATE EDITORS

PROF. G. F. CARRIER

Pierce Hall, Harvard University, Cambridge 38, *Massachusetts, U.S.A.*

DR W. C. GRIFFITH

Research and Development Laboratory, Missile Systems Division, Lockheed Aircraft Corporation, Palo Alto, California, U.S.A.

PROF. M. J. LIGHTHILL

Department of Mathematics, The University, Manchester, England

PROF. R. R. LONG

School of Engineering, The Johns Hopkins University, Baltimore 18, *Maryland, U.S.A.*

Authors wishing to have papers published in the JOURNAL should communicate them to any one of the persons named above, choosing one in their own country where possible.

Authors are urged to ensure that their papers are written clearly and attractively, in order that their work will be readily accessible to readers.

Manuscripts should be typed in double spacing on one side of the paper only, with references listed at the end in alphabetical order of authors. Drawings should be done on a large scale in Indian ink on tracing cloth or drawing paper, the lettering being shown clearly in pencil for reproduction by the printer; the list of captions should be typed at the end of the manuscript. Proofs of papers from overseas will usually be despatched to authors by airmail. There is no charge for publication. Authors are entitled to receive 50 offprints of a paper in the JOURNAL free of charge, and additional offprints can be purchased if ordered in advance.

SUBSCRIPTIONS

The subscription price for a volume of four parts is £5. 10*s*. net, post free, payable in advance; separate parts 30*s*. net, plus postage. Subscriptions may be sent to any bookseller, or to the Cambridge University Press, Bentley House, 200 Euston Road, London, N.W.1.

Subscribers in the United States should send their orders to the Cambridge University Press, American Branch, 32 East 57th Street, New York 22. The subscription price per volume is $18.50, post free, payable in advance; separate parts $5.00, plus postage.

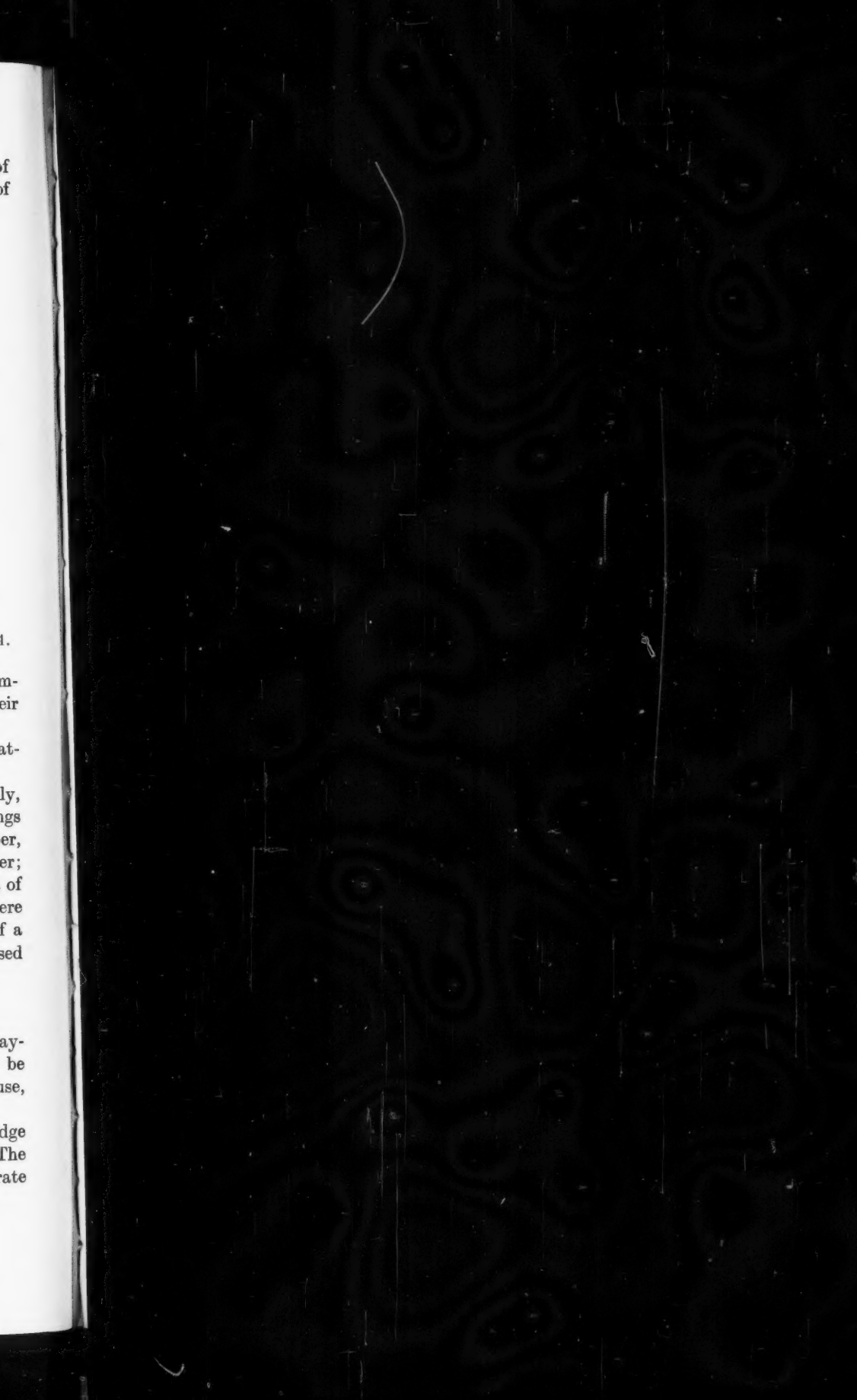

A theory of dispersion in a porous medium

By P. G. SAFFMAN

Cavendish Laboratory, University of Cambridge

(Received 16 January 1959)

This paper is concerned with the dispersion of a dynamically neutral material quantity in a fluid flowing through a porous medium. The medium is regarded as an assemblage of randomly orientated straight pores, and it is assumed that the path of a marked element of the material quantity consists of a sequence of statistically independent steps whose direction and duration vary in some random manner. The probability density function for the displacement of a single marked element is calculated and values for the dispersion of a cloud of marked elements then follow.

The case is examined in which the flow satisfies Darcy's law (i.e. the mean velocity is linearly proportional to the mean pressure gradient), and the molecular diffusivity is sufficiently small for the dispersion to be primarily due to the randomness of the streamlines, but it is not assumed that effects of molecular diffusion can be altogether neglected. It is shown that the longitudinal dispersion in the direction of the mean flow may be described asymptotically by an effective diffusivity which is a function of U, l, a, κ and T. (U denotes the average velocity, l the pore length, a the pore radius which is shown to be related to the permeability, κ the molecular diffusivity, and T the time from the initial instant.) Expressions for the longitudinal diffusivity κ_l are obtained according to the relative values of l/U, T, $t_0 = l^2/2\kappa$ and $t_1 = a^2/8\kappa$. These are given in §4, equations (4.3), (4.4) and (4.5). Speaking roughly, when $t_0 \gg T \gg l/U$, κ_l/Ul is a logarithmic function of UT/l and increases with T; when $T \gg t_0 \gg l/U$, which must eventually be the case however small κ, κ_l/Ul is a logarithmic function of Ul/κ and independent of T. The theoretical results are compared with experimental data reported in the literature and approximate agreement is obtained when l is put equal to the average diameter of the particles composing the porous medium.

The lateral dispersion in the direction perpendicular to that of the mean velocity is found to be governed asymptotically by an effective diffusivity $\kappa_l = \frac{3}{16}Ul$. However, it is pointed out that some of the assumptions, namely that successive steps are statistically independent and that the dispersion of a cloud follows immediately from the statistical properties of the displacement of a single marked element, may not be valid for the lateral dispersion and this result is therefore suspect.

Remarks are made in §5 on the dispersion for high values of the Reynolds number Ul/ν (ν = kinematic viscosity) when Darcy's law is not obeyed, and it is argued that κ_l/Ul should decrease as Ul/ν increases.

1. Introduction

When a viscous fluid flows through the pores and voids of a porous medium, such as a bed of sand, a tower of small glass beads, a porous rock like limestone, etc., a material quantity carried by the fluid (e.g. a substance in solution or heat) is dispersed by molecular diffusion and by what may be called 'convective' or 'mechanical diffusion'. The latter effect arises from the irregular pattern of the streamlines through the pores and voids, and the consequent tendency for fluid elements which are originally close together to become separated. The situation is in fact somewhat analogous to that of turbulent diffusion, the difference being that in a porous medium the irregularity of the streamlines arises from the complicated geometrical structure of the medium instead of from random solutions of the Navier–Stokes equations.

The purpose of this paper is to examine the 'convective diffusion' of a dynamically neutral material quantity or, as is equivalent, the phenomenon of 'miscible displacement' when a viscous fluid is expelled from a porous medium by another fluid of identical viscosity and density with which it is completely miscible, since in this case the relative concentrations of the fluids may be regarded as a dynamically neutral material quantity. In an actual flow further complications are often present; for example, adsorption of the material quantity on the solid material of the medium may occur, the physical properties of the fluid may vary significantly with the concentration of the material quantity, etc. Such effects are often of great practical importance, but we shall not consider them here at all.

The detailed structure of the medium is usually highly irregular and only a few statistical properties are in practice available. A detailed solution for the flow pattern is therefore not a practical possibility, and even if it were it is doubtful whether it would be useful because of its complexity. However, the quantities of interest are often spatial averages; for instance, the filter velocity which is the flux of fluid per unit area of the medium, the 'average' or interstitial velocity which is the spatial average of the velocity over the region occupied by fluid,* and the mean pressure gradient and mean concentration of a material quantity which may be likewise defined. (It need hardly be pointed out that the spatial average is a useful concept only if the medium and the flow are effectively statistically homogeneous over a region large compared with the dimensions of the grains or

* The average velocity is in fact the filter velocity divided by the porosity (the fraction of porous media actually occupied by fluid), since the filter velocity is

$$\int \mathbf{u}\,dS \Big/ \int dS = \int \mathbf{u}\,dV \Big/ \int dV$$

where dS and dV denote elements of area and volume of the porous media and $\mathbf{u}$ is the velocity of the fluid. The average velocity is

$$\int \mathbf{u}\,dV' \Big/ \int dV' = \int \mathbf{u}\,dV \Big/ \sigma \int dV,$$

where dV' is an element of volume entirely occupied by fluid, since $\mathbf{u} = 0$ if $dV \neq dV'$ and by definition

$$\int dV' = \sigma \int dV,$$

where σ denotes the porosity.

pores.) It seems reasonable to suppose that the various ways in which such averages may depend upon one another will not be greatly affected by changes in the detailed structure of the medium which leave its statistical properties unaltered, and that it will be profitable to consider not the flow through an actual porous medium but a simple model of such a flow, the model being constructed so that it appears to correspond in essentials with the actual flow, and is capable of mathematical analysis. Scheidegger (1957) gives an account of various models which have been put forward to calculate the permeability (i.e. resistance to flow) of porous media.

A 'random-residence-time' model for longitudinal dispersion has been put forward and developed by several writers (see, for example, McHenry & Wilhelm 1957, where other references are given). (When the average velocity is unidirectional, the dispersion in the same direction is termed longitudinal or axial dispersion, and that in the perpendicular directions lateral or transverse dispersion; there is no reason why these should be equal even though the medium is statistically isotropic.) Briefly, this theory considers the flow through a sequence of cells in each of which there is complete mixing, i.e. in which the probability of a fluid element leaving a cell in any interval of time is independent of the length of time it has been in the cell. The time of passage of a fluid element through a length of the porous medium is then the sum of the times spent in each cell, and is a random function which tends to a Gaussian form with a variance proportional to the number of cells as this number becomes large. It can then be shown that the longitudinal dispersion is described by the diffusion equation with an effective diffusivity proportional to the product of the average velocity and the length of each cell. Identifying this length with the diameter of the solid particles of which the medium is composed, one obtains values in reasonable agreement with experimental observations at values of the Reynolds number, based on the average velocity and average particle size, in the range 50–200. For these Reynolds numbers, the flow in the voids may be turbulent, producing fairly intensive mixing, so that the model appears to be a not unreasonable simplification of the actual flow. However, it does not lend itself to a study of lateral dispersion, and also the validity of the model to describe what happens at low Reynolds numbers is open to question.

An alternative approach to the problem of dispersion is to follow the motion of a marked fluid particle, supposing that its path varies in some postulated random manner. The probability distribution of the displacement of a single fluid particle after a given time may then be calculated. If the distance traversed or the time taken is sufficiently large for the assumption to be valid that the paths of initially neighbouring particles become statistically independent, the dispersion of a marked volume of fluid can be obtained.

Several writers (e.g. Baron 1952; Scheidegger 1954) have investigated dispersion on the assumption that a fluid particle carries out a random walk consisting of a succession of statistically independent straight steps in equal small intervals of time. It follows from the Central Limit Theorem of statistics that the probability distribution function of the displacement is Gaussian with a variance proportional to the time, and hence that the dispersion is described by the

diffusion equation with the effective diffusivity related to the parameters of the random walk.

This treatment is physically not entirely satisfactory, partly because the time is broken up into *equal* small intervals and it would be expected intuitively that a particle stays longer in a region where the velocity is small than where it is large, and also because it seems to predict that the dispersion is isotropic since there is no obvious mechanism whereby the velocity fluctuations about the mean, and thence the displacement about the mean position, are correlated with the direction of the average velocity.

The present work originated in a suggestion by Sir Geoffrey Taylor that the dispersion might be investigated by taking as a model of the flow through a porous medium that through an assembly of randomly orientated and distributed straight pores, in each of which the flow is uniform. The pores are supposed to be connected with one another at the ends and several pores may start or finish at these end-points. The dimensions of the pores are to be taken as comparable with the size of the particles composing the bed. In other words, the medium is visualized as a lattice in which a randomly distributed set of points are connected to their neighbours by straight uniform pores. The path of a fluid particle may then be regarded as a random walk in which the length, direction, and duration of each step are random variables. The probability distribution function of the displacement of a fluid particle after a given time may then be calculated and a value for the dispersion obtained.

One condition which must be satisfied in order that this model should apply to the actual dispersion of a material quantity is that the amount of dispersion that takes place is large compared with the dispersion there would be due to molecular diffusion acting alone as under static conditions, i.e. the effective diffusivity must be large compared with the molecular diffusivity. It will be assumed throughout this paper that this is the case. This is not to say, however, that molecular diffusion is entirely negligible; on the contrary, it will be found that the theory to be developed below predicts that in some cases the effective diffusivity is a logarithmic function of the molecular diffusivity (cf. Taylor (1953, 1954) where it is shown that the effective diffusivity describing the dispersion of a material quantity in a fluid flowing through a long capillary tube is inversely proportional to the molecular diffusivity). But it is expected that this theory is valid only if the molecular diffusivity is sufficiently small compared with the product of the average pore length and average velocity which, as will be seen, determines the order of magnitude of the effective diffusivity. It is worth mentioning in passing that there are physical circumstances of great interest (e.g. geothermal flows) in which 'convective diffusion' is small compared with molecular diffusion and may be entirely neglected.

After this paper had been completed, it was discovered that Josselin de Jong (1958) had considered a similar model and obtained one of the results of this paper, namely that of equation (4.4*b*) below. However, the model discussed in this paper is rather more general, and various results are obtained, that given by Josselin de Jong being a particular case apparently valid only for a certain limited range of the physical parameters.

2. Description of the model and formulation of the random walk

In this section we describe the model for calculating dispersion in a porous medium which supposes that the medium is an assembly of randomly orientated straight uniform pores and that a marked particle moves along a random succession of straight steps, each step corresponding to passage through one pore, of variable direction and duration. It is supposed that the medium is statistically homogeneous and isotropic, and that the average velocity or mean pressure gradient is constant and unidirectional. We take a co-ordinate system with the x-axis in the direction of the average velocity, and denote by l the length of a step, by θ the angle between the direction of motion along the step and that of the average velocity, by ϕ the azimuthal angle between the y-axis and the projection of the step on the yz-plane ($0 \leqslant \phi < 2\pi$), by t the duration of the step, and by $q = l/t$ the velocity of the marked particle along the step. Then the displacement of a marked particle after n steps is a random variable with components parallel to the axes

$$X_n = \sum_1^n l_r \cos\theta_r, \quad Y_n = \sum_1^n l_r \sin\theta_r \cos\phi_r, \quad Z_n = \sum_1^n l_r \sin\theta_r \sin\phi_r, \tag{2.1}$$

and the time for n steps is the random variable

$$T_n = \sum_1^n t_r = \sum_1^n l_r/q_r, \tag{2.2}$$

where the suffix r refers to the rth step. In order to obtain the probability distributions of the various random variables, we must now examine the flow through the model.

The velocity of the fluid through the pores

Let us consider the average speed, $\hat{q}$ say, of the fluid flowing through a particular pore, i.e. $\hat{q}$ is the flux of fluid through the pore divided by its cross-section area; it is in general a random quantity which varies from pore to pore. (It is called here the 'average speed' to distinguish it from the 'average velocity' which in this paper is a spatial mean over many pores.)

We shall now suppose that the inertia of the fluid is negligible and that the motion through the pores is dominated by viscosity. In this case the Navier–Stokes equations which describe the motion of the fluid through the pores become linear and the average velocity will be linearly proportional to the mean pressure gradient and inversely proportional to the viscosity of the fluid. That is, Darcy's law is satisfied according to which

$$Q = kP'/\mu, \tag{2.3}$$

where Q is the filter velocity, P' is the mean pressure gradient, μ is the viscosity, and k is a constant with dimensions (length)^2 which is a property of the porous medium and is called the permeability. The range of validity of Darcy's law depends upon the Reynolds number of the motion through the voids and the structure of the medium (see Scheidegger 1957).

Further, the average speed $\hat{q}$ is proportional to the pressure drop between the ends of the pore divided by the length of the pore, i.e. to the pressure gradient

along the pore. Now the pressure in the fluid is $P'x+p$, where p is a random quantity whose spatial average over many pores is zero, and if the fluid inertia is negligible it is not unreasonable to suppose that p does not vary too rapidly with position and that the pressure gradient in a pore making an angle θ with the x-axis and with azimuthal angle ϕ is

$$\left(P'+\frac{\partial p}{\partial x}\right)\cos\theta+\frac{\partial p}{\partial y}\sin\theta\cos\phi+\frac{\partial p}{\partial z}\sin\theta\sin\phi$$
$$=P'\{(1+p_1)\cos\theta+p_2\sin\theta\cos\phi+p_3\sin\theta\sin\phi\}, \quad (2.4)$$

where $(p_1, p_2, p_3) = (1/P')\operatorname{grad} p$ are dimensionless random quantities with zero mean whose statistical properties depend entirely upon the medium and are independent of the magnitude of P (since the equations of motion are linear) and also of θ and ϕ. Then,

$$\hat{q}=\frac{AP'}{\mu}\{(1+p_1)\cos\theta+p_2\sin\theta\cos\phi+p_3\sin\theta\sin\phi\}, \quad (2.5)$$

where A is the cross-section area of the pore multiplied by some function of its shape. By definition, $\hat{q}$ is a positive quantity and the values of θ and ϕ for a pore (or step) are defined as those ($0\leqslant\theta\leqslant\pi$; $0\leqslant\phi<2\pi$) for which (2.5) is positive.

In general, A will be a random quantity varying from pore to pore. However, we shall assume, primarily for the sake of simplicity, that all the pores are of circular cross-section and of equal radius a, say, so that $A=\frac{1}{8}a^2$. This assumption is physically not very good, but it actually involves no real loss of generality and does not affect the results significantly. It is perfectly possible to go through the analysis with A as a random variable (and even with the cross-section of a pore varying), but since we do not know the statistical properties of A and in any case the model is only an approximation to an actual porous medium, it seems hardly worth while introducing extra complications of this kind. For similar reasons, all the pores will be supposed to be of the same length l, say, where a should be small compared with l for the model to be strictly meaningful.

The average velocity and permeability of the model

The probability density function (p.d.f.) of $(p_1, p_2, p_3,)$ will be supposed Gaussian and isotropic* so that the probability that it lies in the range (p_1, p_2, p_3) to $(p_1+dp_1, p_2+dp_2, p_3+dp_3)$ is

$$\left(\frac{\lambda}{\pi}\right)^{\frac{3}{2}}\exp\left[-\lambda(p_1^2+p_2^2+p_3^2)\right]dp_1\,dp_2\,dp_3, \quad (2.6)$$

where λ is some dimensionless constant parameter which will depend only on the structure of the porous medium. The value of λ is a measure of the relative magnitude of the mean pressure gradient and the fluctuations; $(p_1, p_2, p_3)=0$ corresponds with $\lambda=\infty$.

* The assumption that this p.d.f. is isotropic is unlikely to be strictly correct since there is in fact a preferred direction, namely that of the average velocity, but it considerably simplifies the analysis and is unlikely to lead to a significant error.

The proportion of pores such that the values of θ, ϕ, p_1, p_2 and p_3 lie in the element of generalized volume $d\theta\, d\phi\, dp_1\, dp_2\, dp_3 = d\Sigma$, say, is therefore proportional to the product of $\sin\theta\, d\theta\, d\phi$ and (2.6), and is

$$\frac{1}{2\pi}\sin\theta\left(\frac{\lambda}{\pi}\right)^{\frac{3}{2}}\exp\left[-\lambda(p_1^2+p_2^2+p_3^2)\right]d\theta\, d\phi\, dp_1\, dp_2\, dp_3, \tag{2.7}$$

where the domain of Σ is $0 \leqslant \theta \leqslant \pi$, $0 \leqslant \phi < 2\pi$, $\hat{q} > 0$, and the constant of proportionality was chosen to make the integral of (2.7) over the domain Σ equal to one, so that (2.7) is a true proportion.

The components parallel to the x-, y- and z-axes of the average speed through a pore are

$$\hat{q}\cos\theta, \quad \hat{q}\sin\theta\cos\phi, \quad \hat{q}\sin\theta\sin\phi, \tag{2.8}$$

and, by definition, the components of the average velocity are the values of (2.8) averaged over many pores. The components of average speed in the y- and z-directions clearly average to zero. The average velocity in the x-direction is denoted by U, where

$$\begin{aligned} U &= \int_\Sigma \hat{q}\cos\theta\,\frac{1}{2\pi}\sin\theta\left(\frac{\lambda}{\pi}\right)^{\frac{3}{2}}\exp\left[-\lambda(p_1^2+p_2^2+p_3^2)\right]d\Sigma \\ &= \frac{a^2P'}{24\mu}, \end{aligned} \tag{2.9}$$

on substituting from (2.5) for $\hat{q}$ and integrating (see the Appendix).

The filter velocity Q is σU, where σ is the porosity and thus $Q = (\sigma a^2 P')/24\mu$, whence the permeability $k = (\sigma a^2)/24$. Note that k is independent of λ. This expression may be used to obtain an estimate of a which is otherwise very much an unknown quantity. For instance, Mr R. Wooding in the Cavendish Laboratory has measured the permeability of a bed of glass spheres of average diameter 2×10^{-2} cm and obtained the value $k = 3\times10^{-7}\,\mathrm{cm}^2$, the value of the porosity being 0·37. Substituting into the formula for the permeability, we obtain $a \doteqdot 4\times10^{-3}$ cm. Taking as a value for l the average diameter of the spheres, we have $a/l = \frac{1}{5}$, which seems reasonable. The question of what value to give λ will be deferred for a little while.

The duration of the steps in the random walk

We can now return to discuss the properties of the random walk. The velocity of an idealized fluid particle in a pore is

$$q = 2\hat{q}\left(1-\frac{r^2}{a^2}\right), \tag{2.10}$$

where r is the distance of the fluid particle from the axis of the pore and the velocity profile has been assumed parabolic. The duration t of a step by an idealized fluid particle would then be

$$t = \frac{l}{q} = \frac{l}{2\hat{q}(1-r^2/a^2)}. \tag{2.11}$$

At first sight it might be thought that infinitesimal elements of the material quantity may be assumed to move through the pores like idealized fluid particles so that the duration of a step is given by (2.11). Speaking roughly, this is permissible if the duration of a step is small compared with the time required for

effects of molecular diffusion to be appreciable. However, t is large without bound for steps in which r is nearly equal to a or $\hat{q}$ is very small; so that even though the molecular diffusivity is as small as we please, there will be some elements of material quantity which are so long in a pore that molecular diffusion may be appreciable and it is not obvious that it is meaningful to regard them as moving like idealized fluid particles. We may intuitively expect this effect to be negligible if the proportion of idealized fluid particles undergoing steps of very long duration is sufficiently small, but exactly how small remains to be determined. To anticipate, it may be shown (see §3) that the condition of being sufficiently small is that $\int_0^\infty tf(t)\,dt$ is finite, where $f(t)\,dt$ is the proportion of idealized fluid particles which at any instant are undergoing steps of duration in the range t to $t+dt$. The proportion of pores in which the average speed is $\hat{q}$ is given by (2.7), the duration is given by (2.11), the proportion of fluid particles in a pore whose distance from the axis is between r and $r+dr$ is $2r\,dr/a^2$; hence for fluid particles

$$\int_0^\infty tf(t)\,dt = \int_0^a \frac{2r\,dr}{a^2} \int_\Sigma \frac{l}{2\hat{q}(1-r^2/a^2)} \frac{\sin\theta}{2\pi} \left(\frac{\lambda}{\pi}\right)^{\frac{3}{2}} \exp\left[-\lambda(p_1^2+p_2^2+p_3^2)\right] d\Sigma$$

$$= \int_0^1 \frac{d\rho}{1-\rho} \times \iint\limits_{\substack{0<\theta<\pi \\ p+\cos\theta>0}} \frac{l}{6U} \frac{\sin\theta}{p+\cos\theta} \left(\frac{\lambda}{\pi}\right)^{\frac{1}{2}} e^{-\lambda p^2}\,dp\,d\theta, \tag{2.12}$$

on substituting for $\hat{q}$ from (2.5) and (2.9), writing $\rho = r^2/a^2$, and using the method of integration described in the Appendix. Each of the integrals in (2.12) is divergent, and this as it turns out is the mathematical reason why it is necessary to make some attempt at estimating the effect of molecular diffusion on the motion through a pore.

Molecular diffusion affects the material quantity moving through a pore in two ways. First, the material quantity diffuses sideways across the pore so that an element of material quantity does not stay on a streamline r = constant but spreads out over neighbouring streamlines. It may be expected that this effect is negligible if $t \ll t_1$, where t is the time spent by the material element in the pore and t_1 is the time for appreciable molecular diffusion over a distance comparable with that in which the velocity differs by a factor of order unity. An estimate of the value of t_1 is $t_1 = a^2/8\kappa$, where κ is the molecular diffusivity (this expression is obtained by analogy from the formula for diffusion $x^2 = 2\kappa t$ with $x = \frac{1}{2}a$).

If the average speed through the pore is so small that $l/\hat{q} \gg t_1$, then any material quantity has ample time to diffuse across the pore. This is the case discussed by Taylor (1953, 1954) and Aris (1956) who have shown that if a material quantity is introduced into a fluid flowing through a long thin straight tube, then after a time large compared with t_1 the concentration of the material quantity is approximately uniform over the pore cross-section and the material quantity is convected with the average speed in the tube, at the same time diffusing along the tube, relative to axes moving with the mean speed, with an effective diffusivity

$$\kappa' = \frac{a^2\hat{q}^2}{48\kappa} + \kappa. \tag{2.13}$$

If we neglect for the moment the diffusion along the pore, it does not therefore seem unreasonable to suppose that the transport of material quantity along a pore for which $l/\hat{q} \gg t_1$ is approximately the same as the transport calculated on the assumption that elements of the material quantity remain elements and all move with the average speed. In other words, it is assumed that the duration of all steps through such a pore is $t = l/\hat{q}$.

If an element of material quantity enters a pore with $l/\hat{q} \ll t_1$ on a streamline close to the wall for which the duration of passage of an idealized fluid particle is large compared with t_1, then this element will have ample time to diffuse sideways on to streamlines where the velocity is not small and be convected along to the end of the pore. It again does not seem unreasonable to suppose that the transport of this material element is taken account of approximately by supposing that it remains an element and reaches the end of the pore in a time $t = t_1 + l/\hat{q}$.

Let us now consider the second effect of molecular diffusion which is transport of material quantity by diffusion along the pore. This effect will be negligible if $t \ll t_0$, where $t_0 = l^2/2\kappa$ is an estimate of the time for appreciable diffusion along the pore. If, on the other hand, $l/\hat{q} \gg t_0$, then the transport of a material element along the pore by convection will be negligible compared with the transport by diffusion, and it does not seem an unreasonable approximation to suppose that the transport along these pores is adequately represented by the passage of material elements in a time $t = t_0$. Note that the assumption $a \ll l$ implies $t_1 \ll t_0$.

The preceding remarks may be combined in an approximate manner to give the following rule for specifying the duration of a step made by a material element:

$$t = \frac{l}{2\hat{q}(1-r^2/a^2)} \quad \text{if} \quad t \leqslant t_1 \quad (t_1 = a^2/8\kappa), \tag{2.14a}$$

$$t = t_1 + l/\hat{q} \quad \text{if} \quad t_1 < t \leqslant t_0 \quad (t_0 = l^2/2\kappa), \tag{2.14b}$$

$$t = t_0 \quad \text{otherwise.} \tag{2.14c}$$

Now the above discussion of the effects of molecular diffusion is somewhat crude and limited, but it is not easy to see how it can be improved. The essential difficulty, which also occurs in the theory of turbulent diffusion, lies in the problem of combining the Lagrangian and Eulerian descriptions of a fluid motion, the former being the natural way of calculating how a marked particle moves and the latter of treating molecular diffusion. The rules (2.14) are probably alright if the molecular diffusivity is small enough for t_0 and t_1 to be large compared with the average duration $\bar{t}$, say, of a step (a precise value for $\bar{t}$ is obtained later but it is clearly $O(l/U)$), so that relatively few material elements are affected by molecular diffusion. Further, the values that will be obtained for the dispersion are logarithmic functions of $t_0/\bar{t}$ and $t_1/\bar{t}$, and are thus fairly insensitive to the numerical values in the definitions of t_0 and t_1. This reinforces belief in the adequacy of (2.14) to represent the effects of molecular diffusion. A smooth function of $\hat{q}$, t_0, t_1 and r with essentially the same behaviour as (2.14), apart from the discontinuities at $t = t_1$ and $t = t_0$, may easily be constructed; but there is no real gain and the analysis becomes much more complicated.

It is possible that the structure of the medium is such that the pores should be regarded as exceptionally thin compared with their length and the average

velocity is such that $t_1 \ll \bar{t} \ll t_0$. In this case we shall suppose that the concentration of the material quantity is uniform over the pore cross-section and that the material quantity is convected with the average speed. The rule analogous to (2.14) for this case is

$$t = l/\hat{q} \quad \text{if} \quad t \leqslant t_0 \quad (t_0 = l^2/2\kappa), \tag{2.15a}$$

$$t = t_0 \text{ otherwise.} \tag{2.15b}$$

The objection may be raised that the effective diffusivity κ' as given by (2.13) should be used in the definition of t_0 rather than κ. However, when t as given by (2.14*b*) or (2.15*a*) is close to t_0, $(a^2\hat{q}^2/48\kappa)/\kappa \doteq \frac{1}{12}a^2/l^2$, so that κ' may be replaced by κ to a good approximation in the definition of t_0.

The probability that a given step occurs in the random walk

To complete the formulation of the random walk, it remains to evaluate the probability that a marked material element chooses a step with angles in the range θ to $\theta + d\theta$ and ϕ to $\phi + d\phi$, and of duration in the range t to $t + dt$, where t is defined as a function of $\hat{q}$ and r by either (2.14) or (2.15), and $\hat{q}$ is a function of θ, ϕ, p_1, p_2 and p_3. The values of $\hat{q}$ and r for a step by an infinitesimal material element are assumed to be the values of these quantities for the fluid particle with which it coincides at the beginning of the step (and remains coincident if $t_1 \gg l/\{2\hat{q}(1-r^2/a^2)\}$, otherwise they separate and the element completes the step in the time given by (2.14) or (2.15)). The required probability is hence the probability that an idealized fluid particle chooses a streamline with values of $\theta, \phi, p_1, p_2, p_3$ and r in the element of generalized volume $d\theta\, d\phi\, dp_1\, dp_2\, dp_3\, dr$. The proportion of pores with appropriate values of the variables is given by (2.7), and the proportion of a pore with r in the range r to $r + dr$ is $2r dr/a^2$, and thus the proportion of such streamlines existing in the model is (2.7) multiplied by $2r\, dr/a^2$, namely

$$\frac{1}{2\pi}\sin\theta\left(\frac{\lambda}{\pi}\right)^{\frac{3}{2}} \exp\left[-\lambda(p_1^2+p_2^2+p_3^2)\right]\frac{2r}{a^2}\, d\theta\, d\phi\, dp_1\, dp_2\, dp_3\, dr. \tag{2.16}$$

Now this is *not* the probability that a fluid particle will choose such a streamline because the rate at which fluid particles go along a streamline is proportional to the velocity on the streamline. Suppose, for the sake of example, that a large number of particles arrive at a junction from which start two streamlines, then the relative number of fluid particles which go along the streamlines is proportional to the ratio of the velocities of the streamlines. Thus, the required probability is, apart from a normalizing factor, (2.16) multiplied by the velocity of the streamline, $2\hat{q}(1-r^2/a^2)$, and is

$$\frac{2}{N}\hat{q}\left(1-\frac{r^2}{a^2}\right)\frac{1}{2\pi}\sin\theta\left(\frac{\lambda}{\pi}\right)^{\frac{3}{2}} \exp\left[-\lambda(p_1^2+p_2^2+p_3^2)\right]\frac{2r}{a^2}\, d\theta\, d\phi\, dp_1\, dp_2\, dp_3\, dr, \tag{2.17}$$

where $\hat{q}$ is given by (2.5), the range of the variables is the domain $0 \leqslant \theta \leqslant \pi$, $0 \leqslant \phi < 2\pi$, $0 \leqslant r \leqslant a$, $\hat{q} \geqslant 0$, denoted here by P, and N is a normalizing factor so that the integral of (2.17) over P is equal to unity. In fact, see the Appendix,

$$N = \frac{3U}{2}\left[\left(1+\frac{1}{2\lambda}\right)\operatorname{erf}\sqrt{\lambda} + \left(\frac{1}{\lambda\pi}\right)^{\frac{1}{2}} e^{-\lambda}\right]. \tag{2.18}$$

For brevity of writing, we shall denote (2.17) symbolically by $d\mathbf{P}$.

Statistical independence of successive steps

The remaining assumption to be made is that successive steps in the random walk are statistically independent. This is necessary in order to keep the analysis of the random walk tractable and seems alright as a beginning, but it is in fact not as good as might be thought. It appears reasonable as far as the values of θ and r for successive steps are concerned since there is no apparent mechanism for correlating successive values, but this is not the case for $\hat{q}$ and ϕ. Since fluid cannot accumulate, it follows that pores with large (or small) values of $\hat{q}$ are more likely to be followed by pores with large (or small) values of $\hat{q}$ than with small (or large) values. If many pores start and finish together, this effect is likely to be small; if only a few, then this effect will not be entirely negligible, but the indications are that the error due to this cause in the results to be obtained consists in the numerical coefficients being inaccurate by a factor not too different from unity.

The statistical independence of successive values of ϕ is rather more of a problem. However, it does not affect the longitudinal dispersion, owing to the statistical isotropy of the model, so we shall defer consideration until we examine the results for the lateral dispersion, which, of course, will depend upon whether there is correlation between successive values of ϕ.

Ensemble averages

We can now evaluate the random variables X_n, Y_n, Z_n and T_n, defined in (2.1) and (2.2), which give the displacement and time after n steps of the random walk, and evaluate the probability that the displacement of an element of material quantity has a given value after a given time. This probability distribution is strictly speaking an ensemble average over many realizations of the model. That is, if we take a large number of samples of the medium, each with a different arrangement of pores but with the same statistical properties, and observe the displacement of a single material element through each of them, the calculated probability is equal to the proportion of samples in which the displacement has a given value after a given time as the number of samples tends to infinity. However, by the properties of ergodic theory, and assuming statistical homogeneity of the medium, the probability distribution gives the proportion of elements which have a given displacement after a given time if a large number of elements are started from different points scattered randomly through the same sample. All average properties of the random walk and of individual steps of the random walk are likewise ensemble averages, as distinct from spatial averages as in the definition of average velocity.

It is perhaps worth while demonstrating, for the sake of example, the equality of the spatial average and ensemble average (after many steps) of the velocity of an idealized fluid particle, i.e. a particle whose velocity is always given by (2.10). The (ensemble) average of the displacement after one step has components parallel to the axes:

$$\bar{x} = \int_P l\cos\theta\, d\mathbf{P} = lU/N \quad \text{on performing the integration,}$$

$$\bar{y} = \int_P l\sin\theta\cos\phi\, d\mathbf{P} = 0, \quad \bar{z} = \int_P l\sin\theta\sin\theta\, d\mathbf{P} = 0,$$

where $d\mathbf{P}$ is given by (2.17) and the bar denotes an ensemble average. The average duration of a step is

$$\bar{t} = \int_P \frac{l}{2\hat{q}(1-r^2/a^2)}\, d\mathbf{P} = l/N.$$

Then $$\bar{X}_n = \sum_1^n \bar{x}_r = n\bar{x}, \quad \bar{Y}_n = \bar{Z}_n = 0, \quad \bar{T}_n = \sum_1^n \bar{t}_r = n\bar{t}.$$

Hence, $\bar{X}_n/\bar{T}_n = U$ from which it follows that $X_n/T_n \to U$ in probability as $n \to \infty$, since (as follows rigorously from the results of the next section) $X_n/\bar{X}_n$ and $T_n/\bar{T}_n$ tend in probability to one as $n \to \infty$; and *a fortiori* $(\overline{X_n/T_n}) \to U$. Note that these results are independent of λ.

The dispersion of a cloud of marked particles can be calculated from the statistical properties of the displacement of a single marked particle if the time or displacement are large enough for the paths to become statistically independent.* Exactly how large the time or displacement should be for this condition to be approximately satisfied is far from clear, but it seems plausible that not too many, of the order of 100 say, will suffice for the longitudinal dispersion, although (for reasons which shall be given later) more may be required for the lateral dispersion.

The assumption $\lambda = \infty$

In the analysis of the random walk, we shall for the sake of mathematical simplicity put $\lambda = \infty$. This is equivalent to $(p_1, p_2, p_3) = 0$. The average speed in a pore is then

$$\hat{q} = 3U\cos\theta \quad (0 \leqslant \theta \leqslant \tfrac{1}{2}\pi), \tag{2.19}$$

and the expression (2.17) for the probability of a step being such that θ, ϕ and r lie in a range of extent $d\theta\, d\phi\, dr$ becomes

$$d\mathbf{P} = \frac{4}{\pi}\sin\theta\cos\theta\frac{r}{a^2}\left(1-\frac{r^2}{a^2}\right)d\theta\, d\phi\, dr, \tag{2.20}$$

where the domain, P, of the variables is $0 \leqslant \theta \leqslant \frac{1}{2}\pi$, $0 \leqslant \phi < 2\pi$, $0 \leqslant r \leqslant a$. The rules (2.14) or (2.15) for the duration of a step by an element of material quantity remain unaltered.

There is no loss of physical generality in this assumption. The analysis may be carried out for a general value of λ, but it is found that the results for λ finite differ from those for $\lambda = \infty$ only by a numerical factor of order $\operatorname{erf}\sqrt{\lambda}$ $(= 1$ when $\lambda = \infty)$. Now from (2.7), the proportion of steps, for a general value of λ, whose direction lies in the element of solid angle $\frac{1}{4}\pi\sin\theta\, d\theta\, d\phi$ is

$$\frac{1}{2}\iiint_{\hat{q}>0}\left(\frac{\lambda}{\pi}\right)^{\frac{3}{2}}\exp\left[-\lambda(p_1^2+p_2^2+p_3^2)\right]dp_1\,dp_2\,dp_3 = \tfrac{1}{2}\{1+\operatorname{erf}(\sqrt{\lambda}\cos\theta)\}.$$

We may intuitively expect this number to be small when $\theta = \pi$, i.e. in the direction exactly opposite to that of the average velocity, so that there are reasonable

* I am indebted to Dr G. K. Batchelor for pointing out the proper interpretation of the mean values of the random walk as ensemble averages and the necessity for the paths of different marked particles to become statistically independent before the results for the displacement of a single particle may be used to calculate the dispersion of a cloud.

grounds for believing that $\operatorname{erf}\sqrt{\lambda}$ is close to one. In view of the fact that the model is a considerable simplification of an actual porous medium, there is therefore no real loss in putting $\lambda = \infty$, especially as there is no point in making the analysis more complicated than is necessary and the analysis with λ finite is lengthy and cumbersome.

3. Analysis of the random walk

This section is devoted to the calculation of the statistical properties of the displacement of a single marked element after many steps. It is mathematical in character and no further physical assumptions will be introduced. The results of the section will be summarized at the beginning of §4 for the benefit of the reader who does not wish to follow the mathematics in detail.

3.1. *Statistical properties of the displacement after many steps*

Consider the displacement of an element of the material quantity after n steps, where n is for the moment a fixed number. The components along the axes are given by (2.1). X_n is the sum of n independent random variables, and therefore

$$\overline{X}_n = nl\,\overline{\cos\theta};$$

similarly, $\overline{Y}_n = nl\,\overline{\sin\theta\cos\phi}$ and $\overline{Z}_n = nl\,\overline{\sin\theta\sin\phi}$, where the bar denotes an ensemble average and the probability distribution of θ and ϕ is given by (2.20). Thus, $\overline{\cos\theta} = \int_P \cos\theta\, d\mathbf{P} = \frac{2}{3}$ and $\overline{\sin\theta\cos\phi} = \overline{\sin\theta\sin\phi} = 0$, the integrations being elementary. Hence,

$$\overline{X}_n = \tfrac{2}{3}nl, \quad \overline{Y}_n = 0, \quad \overline{Z}_n = 0. \tag{3.1}$$

The variance of X_n is the sum of the variances of the longitudinal displacement of the individual steps. Hence,

$$\left.\begin{aligned} \overline{(X_n - \overline{X}_n)^2} &= nl^2 \int_P (\cos\theta - \tfrac{2}{3})^2\, d\mathbf{P} = \tfrac{1}{18}(nl^2) = nl^2\sigma_X^2, \text{ say,} \\ \text{and similarly} \qquad \overline{Y}_n^2 &= \overline{Z}_n^2 = \tfrac{1}{4}(nl^2) = nl^2\sigma_Y^2, \text{ say.} \end{aligned}\right\} \tag{3.2}$$

Define dimensionless random variables

$$\mathbf{x}_n = \frac{X_n - \overline{X}_n}{ln^{\frac{1}{2}}} = \frac{X_n}{ln^{\frac{1}{2}}} - \tfrac{2}{3}n^{\frac{1}{2}}, \quad \mathbf{y}_n = \frac{Y_n}{ln^{\frac{1}{2}}}, \quad \mathbf{z}_n = \frac{Z_n}{ln^{\frac{1}{2}}}. \tag{3.3}$$

Then $\mathbf{x}_n$, $\mathbf{y}_n$ and $\mathbf{z}_n$ have zero mean and variances σ_X^2, σ_Y^2, σ_Y^2, respectively. Also, it is immediate that $\overline{\mathbf{x}_n\mathbf{y}_n} = \overline{\mathbf{x}_n\mathbf{z}_n} = \overline{\mathbf{y}_n\mathbf{z}_n} = 0$. It follows from the Central Limit Theorem of statistics (see, for example, Cramér 1946) that the probability distributions of $\mathbf{x}_n$, $\mathbf{y}_n$ and $\mathbf{z}_n$ are asymptotically normal and statistically independent as $n \to \infty$, the departure from normality for a fixed value of n being $O(n^{-\frac{1}{2}})$.

3.2. *Statistical properties of the time for n steps according to the rules* (2.14)

Consider now the time for n steps, supposing that the rules (2.14) for the duration of a single step apply. (The rules (2.15) will be considered later.) These rules are an approximation and are expected to be valid only if t_1 and t_0 are large

compared with the average duration of a step. We shall therefore neglect in the analysis all terms which vanish as t_0 and t_1 tend to infinity. The case of an idealized fluid particle is obtained by putting $t_0 = t_1 = \infty$. On substituting from (2.19) for $\hat{q}$ and using (2.14), we have for the average duration of a single step

$$\bar{t} = \int_P t\,d\mathbf{P} = \int_{P_1} \frac{l}{6U(1-r^2/a^2)\cos\theta}\,d\mathbf{P} + \int_{P_2} \left(\frac{l}{3U\cos\theta} + t_1\right) d\mathbf{P} + \int_{P_3} t_0\,d\mathbf{P},$$

where the domain P_1 is that part of P in which $l/\{6U(1-r^2/a^2)\cos\theta\} \leqslant t_1$; P_2 is that part of $P - P_1$ in which $t_1 < t_1 + l/(3U\cos\theta) < t_0$; and $P_3 = P - P_1 - P_2$. Substituting for $d\mathbf{P}$ from (2.20), integrating with respect to ϕ, and writing $\rho = 1 - r^2/a^2$, we obtain

$$\bar{t} = \iint_{\mathrm{I}} \frac{2l}{3U}\sin\theta\,d\theta\,d\rho + \iint_{\mathrm{II}} 4\left(\frac{l}{3U} + t_1\cos\theta\right)\rho\sin\theta\,d\theta\,d\rho + \iint_{\mathrm{III}} 4t_0\rho\sin\theta\cos\theta\,d\theta\,d\rho,$$

where the domain of integration I is $0 < \theta < \frac{1}{2}\pi$, $0 < \rho < 1$, $\rho\cos\theta > l/6Ut_1$; II is $0 < \rho < 1$, $\rho\cos\theta < l/6Ut_1$, $\cos\theta > l/\{3U(t_0 - t_1)\} \doteqdot l/3Ut_0$; and III is $0 < \rho < 1$, $0 < \cos\theta < l/3Ut_0$. The integration is straightforward and gives, neglecting terms which vanish as t_0 and t_1 tend to infinity,

$$\bar{t} = 2l/3U, \tag{3.4}$$

the largest term neglected being $-(l^2/18U^2t_1)\log(6Ut_1/l)$. It follows immediately that

$$\overline{T}_n = 2nl/3U. \tag{3.5}$$

The value of $\overline{(t-\bar{t})^2} = \int_P (t-\bar{t})^2\,d\mathbf{P}$ may be calculated in exactly the same manner. The calculation is straightforward, though a little lengthy, and gives

$$\overline{(t-\bar{t})^2} = \frac{l^2}{U^2}\left\{\tfrac{2}{9}\log\frac{3Ut_0}{l} + \frac{1}{18}\left(\log\frac{6Ut_1}{l}\right)^2 - \tfrac{1}{6}\log\frac{6Ut_1}{l} + \tfrac{1}{4}\right\}$$

$$= \frac{l^2}{U^2}\sigma_T^2, \text{ say.} \tag{3.6}$$

Note that this variance does not exist if t_1 and t_0 are infinite, and we may therefore expect the statistical properties of the path of an idealized fluid particle to be very different from those of an element of material quantity, even though the molecular diffusivity is very small. This is why the rules (2.14) and (2.15) were formulated, a rough attempt at estimating the effects of molecular diffusion being thought better than none at all.

It follows from (3.6) that $\overline{(T_n - \overline{T}_n)^2} = nl^2\sigma_T^2/U^2$, and that the dimensionless random variable

$$\mathbf{t}_n = \frac{T_n - \overline{T}_n}{(l/U)\,n^{\frac{1}{2}}} = \frac{T_n}{(l/U)\,n^{\frac{1}{2}}} - \tfrac{2}{3}n^{\frac{1}{2}} \tag{3.7}$$

has zero mean and variance σ_T^2.

Since σ_T is large when t_1 and t_0 are large compared with l/U, we must be cautious in applying the Central Limit Theorem to $\mathbf{t}_n$. As a rough estimate (a more precise

argument based on the results of § 3.7 below gives a slightly different one), $\mathbf{t}_n$ will be normally distributed when $\mathbf{t}_n^3$ is small compared with one. Now,

$$\overline{(T_n - \overline{T}_n)^3} = \overline{n(t-\bar{t})^3}$$

and it may be shown that $\overline{(t-\bar{t})^3} \sim \frac{1}{3}l^2 t_0/U^2$; thus

$$\overline{\mathbf{t}_n^3} \sim \frac{1}{3}\frac{Ut_0}{ln^{\frac{1}{2}}}. \tag{3.8}$$

Hence, $\mathbf{t}_n$ is normally distributed to a good approximation only if the number of steps is so large that $n^{\frac{1}{2}} \gg \frac{1}{3}Ut_0/l$; i.e. the smaller κ and the larger t_0, then the larger is the number of steps before (3.7) is normally distributed.

The covariance of $\mathbf{x}_n$ and $\mathbf{t}_n$ is

$$\overline{\mathbf{x}_n \mathbf{t}_n} = \frac{\overline{(X_n - \overline{X}_n)(T_n - \overline{T}_n)}}{nl^2/U} = \frac{\overline{(\cos\theta - \overline{\cos\theta})(t-\bar{t})}}{l/U} = -\tfrac{1}{9} = \sigma_{XT}, \text{ say}, \tag{3.9}$$

terms which vanish when t_1 and t_0 equal infinity being neglected. It is immediate that $\overline{\mathbf{y}_n \mathbf{t}_n} = \overline{\mathbf{z}_n \mathbf{t}_n} = 0$, because the terms in ϕ integrate to zero.

3.3. *Probability distribution of the number of steps in a given time*

So far we have examined the displacement and time after n steps, where n is a fixed number. In order to calculate the dispersion, it is necessary to know the probability distribution (p.d.) of the displacement after a given time T, say, where T is in general large compared with l/U.

The first step is to calculate the p.d. of the number of steps made in the time T. The probability that more than n steps are required before the time exceeds T is equal to the probability that $T_n < T$, since each event implies the other, which in turn is equal to the probability that $\mathbf{t}_n < \mathbf{t}$, where

$$\mathbf{t} = \frac{T}{(l/U)n^{\frac{1}{2}}} - \tfrac{2}{3}n^{\frac{1}{2}}. \tag{3.10}$$

Hence, the probability that $\mathbf{t}$ (with T fixed and n variable) lies in the range $\mathbf{t}$ to $\mathbf{t}+d\mathbf{t}$ is equal to the probability that $\mathbf{t}_n$ lies between $\mathbf{t}$ and $\mathbf{t}+d\mathbf{t}$ when the value of n satisfies (3.10), i.e.

$$n = \frac{3}{2}\frac{UT}{l} + \tfrac{9}{8}\mathbf{t}^2 - \frac{9\mathbf{t}}{8}\left(\mathbf{t}^2 + \frac{8UT}{3l}\right)^{\frac{1}{2}}. \tag{3.11}$$

(The positive square root is taken in (3.11) so that n goes from 0 to ∞ as $\mathbf{t}$ goes from $+\infty$ to $-\infty$. Also, it is supposed that n is sufficiently large for it to be regarded as a continuous variable.)

The p.d. of $\mathbf{t}$ is in general a complicated function, being dependent upon the p.d. of $\mathbf{t}_n$ for all n, but if the mean value of n for given T, denoted by $\bar{n}$, is large, the p.d. of $\mathbf{t}$ will depend mainly upon the p.d.'s of $\mathbf{t}_n$ for values of n not too different from $\bar{n}$ and the p.d. of $\mathbf{t}$ will approximate to that of $\mathbf{t}_{\bar{n}}$. Indeed, as $\bar{n} \to \infty$ the p.d.'s of $\mathbf{t}$ and $\mathbf{t}_{\bar{n}}$ become identical since the p.d. of $\mathbf{t}_n$ is independent of n for sufficiently large n.

Equation (3.11) may be written approximately as

$$n = \frac{3}{2}\frac{UT}{l} - \frac{9\mathbf{t}}{8}\left(\frac{8UT}{3l}\right)^{\frac{1}{2}}, \tag{3.12}$$

the terms neglected being $O(\sigma_T^2)$. It follows that

$$\overline{n} = \frac{3}{2}\frac{UT}{l} \tag{3.13}$$

with error $O(\sigma_T^2/\overline{n})$.

3.4. *The p.d. of the lateral displacement after a given time*

Denote the component of the displacement in the y-direction after time T by Y. From (3.3), $Y = ln^{\frac{1}{2}}\mathbf{y}_n$, and if $\overline{n}^{\frac{1}{2}} \gg 1$ we may write $\mathbf{y}_n = \mathbf{y}_{\overline{n}}$ except for a negligible set of values of n. Further, if $\sigma_T/\overline{n}^{\frac{1}{2}} \ll 1$, n is given by (3.12) and, to the same approximation,

$$n^{\frac{1}{2}} = \left(\frac{3}{2}\frac{UT}{l}\right)^{\frac{1}{2}} - \tfrac{3}{4}\mathbf{t}. \tag{3.14}$$

Hence $$Y = (\tfrac{3}{2}UTl)^{\frac{1}{2}}\mathbf{y}_{\overline{n}} - \tfrac{3}{4}\mathbf{t}\mathbf{y}_{\overline{n}} \doteq (\tfrac{3}{2}UTl)^{\frac{1}{2}}\mathbf{y}_{\overline{n}}.$$

Thus, when $\sigma_T/\overline{n}^{\frac{1}{2}} \ll 1$, Y is normally distributed with zero mean and

$$\overline{Y}^2 = \tfrac{3}{2}UlT\sigma_Y^2 = \tfrac{3}{8}UlT, \tag{3.15}$$

on substituting from (3.2).*

Identical results hold for the displacement in the z-direction. Note that the p.d. of the lateral displacement is independent of molecular diffusion and the same result should hold for idealized fluid particles; it will be verified later that this is indeed so.

3.5. *The p.d. of the longitudinal displacement after a given time*

Denote the longitudinal displacement after time T by X. From (3.3)

$$X = ln^{\frac{1}{2}}\mathbf{x}_n + \tfrac{2}{3}ln,$$

and if $\overline{n}^{\frac{1}{2}} \gg 1$, we may again write $\mathbf{x}_n = \mathbf{x}_{\overline{n}}$. Substituting for n from (3.12) and (3.14), we have

$$X = UT - (\tfrac{3}{2}UTl)^{\frac{1}{2}}(\mathbf{t} - \mathbf{x}_{\overline{n}}), \tag{3.16}$$

neglecting terms of order $l\mathbf{t}\mathbf{x}_{\overline{n}}$. Then

$$\overline{X} = UT = \tfrac{2}{3}l\overline{n}. \tag{3.17}$$

Suppose now that T is sufficiently large for

$$\overline{n}^{\frac{1}{2}} \gg \frac{1}{3}\frac{Ut_0}{l}. \tag{3.18}$$

Then the p.d. of $\mathbf{t}_{\overline{n}}$ is normally distributed with variance σ_T^2, and so also will be the p.d. of $\mathbf{t}$. Hence,

$$\frac{X - UT}{T^{\frac{1}{2}}} = -(\tfrac{3}{2}Ul)^{\frac{1}{2}}(\mathbf{t} - \mathbf{x}_{\overline{n}})$$

* In the interests of conciseness, the argument is presented here and in § 3.5 in an heuristic manner. Rigorous arguments can be formulated, but they are more complicated and less direct, and appear to be out of place in the present context.

is the sum of two normally distributed variables with finite variances and is therefore itself normally distributed with zero mean and variance given by

$$\frac{1}{T}\overline{(X-UT)^2} = \tfrac{3}{2}Ul(\overline{\mathbf{t}^2} - 2\overline{\mathbf{t}\mathbf{x}_{\bar{n}}} + \overline{\mathbf{x}_{\bar{n}}^2}) = \tfrac{3}{2}Ul(\sigma_T^2 + \sigma_X^2 - 2\sigma_{XT})$$

$$= Ul\left\{\tfrac{1}{3}\log\frac{3Ut_0}{l} + \frac{1}{12}\left(\log\frac{6Ut_1}{l}\right)^2 - \tfrac{1}{4}\log\frac{6Ut_1}{l} + \tfrac{19}{24}\right\}, \quad (3.19)$$

on substituting from (3.2), (3.6) and (3.9).

It should perhaps be mentioned that this analysis proves only that the p.d. of $X/T^{\frac{1}{2}}$ is asymptotically normal, it does not prove that the p.d. of $X-UT$ is asymptotically normal. Indeed, from (3.16) and (3.8),

$$(X-UT)^3 \sim -(\tfrac{3}{2}UTl)^{\frac{3}{2}}\bar{\mathbf{t}}^3 \sim -\tfrac{3}{4}U^2Tlt_0, \quad (3.20)$$

which becomes large as $T\to\infty$, so that the analysis predicts that the p.d. of X, as opposed to that of $X/T^{\frac{1}{2}}$, becomes increasingly skew as T increases.

3.6. *The random walk according to the rules* (2.15)

The results obtained so far have been based on the rules (2.14) which are for the case $l/U \ll t_1 \ll t_0$. It is expected, however, that the rules (2.15) for the case $t_1 \ll l/U \ll t_0$ may sometimes apply.

The previous analysis depends upon the duration of a single step only in so far as the statistical properties of T_n are affected. That is to say, the previous analysis is unaffected apart from §3.2 which must be repeated using the new rules. It is then sufficient to replace the value of σ_T used above by a new value, σ_{T_1} say, obtained using (2.15).

We have
$$\bar{t} = \int_P t\,d\mathbf{P} = \int_{P_1}\frac{l}{3U\cos\theta}d\mathbf{P} + \int_{P_2} t_0\,d\mathbf{P},$$

where P_1 is that part of P in which $l/\{3U\cos\theta\} < t_0$, and $P_2 = P - P_1$. Substituting for $d\mathbf{P}$ from (2.20), integrating with respect to ϕ and r, and neglecting terms which vanish as $t_0\to\infty$ (these are at most $l^2/9U^2t_0$), one obtains

$$\bar{t} = \int_{\cos\theta=l/3Ut_0}^{1}\frac{2l}{3U}\sin\theta\,d\theta + \int_{\cos\theta=0}^{l/3Ut_0} 2t_0\sin\theta\cos\theta\,d\theta = \frac{2l}{3U}$$

as before. Similarly, the variance of the duration may be calculated, giving

$$\overline{(t-\bar{t})^2} = \frac{l^2}{U^2}\left\{\tfrac{2}{9}\log\frac{3Ut_0}{l} - \tfrac{1}{3}\right\} = \frac{l^2}{U^2}\sigma_{T_1}^2, \quad \text{say.} \quad (3.21)$$

The values of $\overline{\mathbf{x}_n\mathbf{t}_n}$ and $\overline{\mathbf{t}_n^3}$ are again given by (3.9) and (3.8).

The results of §§3.4 and 3.5 now apply with σ_T replaced by σ_{T_1}. Thus, the statistical properties of the lateral displacement remain unaltered. So do those of X except that now

$$\frac{1}{T}\overline{(X-UT)^2} = Ul\left\{\tfrac{1}{3}\log\frac{3Ut_0}{l} - \tfrac{1}{12}\right\} \quad (3.22)$$

when (3.18) is satisfied.

It seems plausible to suppose that the lateral displacement is independent of t_1, since the same result is obtained for $t_1 \gg l/U$ and $t_1 \ll l/U$. For the longitudinal

displacement, the leading terms of (3.19) and (3.22) are the same and it seems plausible that the variance of the displacement for intermediate values of t_1 will be intermediate between the values of (3.19) and (3.22).

3.7. *Further analysis of the random walk*

The reason why the statistical properties of the longitudinal displacement involve the molecular diffusivity (through t_1 and t_0) is that the mean square duration of a step by an idealized fluid particle is not finite,* and therefore the Central Limit Theorem cannot be applied to the variable $\mathbf{t}_n$ evaluated for such particles. It is then not possible to prove that $(1/T)\,(\overline{X-UT})^2$ tends asymptotically to a value independent of T as is usually the case for random processes occurring in nature. As we have seen, this difficulty does not arise if molecular diffusion is taken into account. However, the expressions (3.19) and (3.22) tend to infinity as $\kappa \to 0$, and also the value of T which must obtain for these expressions to apply becomes infinite as $\kappa \to 0$, because of (3.18).

It is natural to inquire what happens if κ, or more precisely l/Ut_0, is so small that (3.18) is not satisfied even though T is sufficiently large for $\overline{n}^{\frac{1}{2}} \gg 1$, or alternatively what are the statistical properties of the displacement of an idealized fluid particle whose velocity is given by (2.10) for all values of t. To answer these questions, it is necessary to investigate the statistical properties of the random walk in rather more detail.

Consider the joint probability distribution function (j.p.d.f.) of $\mathbf{x}_n$, $\mathbf{y}_n$, $\mathbf{z}_n$ and $\mathbf{t}_n$, where these random variables are defined by (3.3) and (3.7) but for the moment we do not specify the value of the duration of a step. The joint characteristic function (j.c.f.) of these quantities is the fourier transform of the j.p.d.f.; that is, the j.c.f., $C_n(\xi, \eta, \zeta, \tau)$ say, is the expectation of $\exp i(\xi\mathbf{x}_n + \eta\mathbf{y}_n + \zeta\mathbf{z}_n + \tau\mathbf{t}_n)$. By well-known results (see Cramér 1946), if $\Phi(\xi, \eta)$ is the j.c.f. of random variables x and y with a j.p.d.f. $\phi(x, y)$, the j.c.f. of $ax+b$ and $cy+d$ (a, b, c and d being constants) is $e^{b\xi+d\eta}\Phi(a\xi, c\eta)$. Also, the j.c.f. of $\sum_1^n x_r$ and $\sum_1^n y_r$ is $\{\Phi(\xi, \eta)\}^n$.

It follows from these results that

$$C_n(\xi, \eta, \zeta, \tau) = \left\{\int_P d\mathbf{P} \exp \frac{i}{n^{\frac{1}{2}}}\left[\xi\,(\cos\theta - \overline{\cos\theta}) + \eta \sin\theta\cos\phi + \zeta\sin\theta\sin\phi + \frac{U\tau}{l}\,(t-\bar{t})\right]\right\}^n. \tag{3.23}$$

We require the value of (3.23) when n is large compared with unity. The analysis is not particularly difficult, but the details are very tedious and we shall confine ourselves to a brief description of the principal steps. The essential difficulty is that the exponential in the integrand in (3.23) may be expanded as a power series in ξ, η and ζ, but not in τ, since τ is multiplied by t which ranges up to t_0 (or infinity), unless $Ut_0/ln^{\frac{1}{2}} \ll 1$ which is now not necessarily the case.

* The mean square duration of a step by an idealized fluid particle is $\int t^2 d\mathbf{P}$ which is proportional to $\int_0^\infty tf(t)\,dt$, where $f(t)\,dt$ is the (spatial) proportion of particles at any instant undergoing steps of duration between t and $t+dt$, since, as explained in § 2, $d\mathbf{P}$ is proportional to this proportion multiplied by the velocity of the step. According to (2.12), this integral diverges for all λ so that the above result does not arise from the assumption $\lambda = \infty$.

Suppose now that $d\mathbf{P}$ is given by (2.20), and t is given by one of (2.11), (2.14) or (2.15). We then take the logarithm of (3.23) and expand the exponential as a power series in ξ, η and ζ, giving after some reduction

$$\log C_n = n\left\{\int_P \exp\left[iU\tau(t-\bar{t})/ln^{\frac{1}{2}}\right]d\mathbf{P} - 1\right\} - \tfrac{1}{2}(\xi^2\sigma_X^2 + \eta^2\sigma_Y^2 + \zeta^2\sigma_Y^2 + 2\xi\tau\sigma_{XT}) + O(n^{-\frac{1}{2}}), \quad (3.24)$$

where use has been made of the result

$$\int_P f(\theta,\phi)\exp\left[iU\tau t/ln^{\frac{1}{2}}\right]d\mathbf{P} = \int_P f(\theta,\phi)\left\{1 + i\frac{U\tau t}{ln^{\frac{1}{2}}}\right\}d\mathbf{P} + o(n^{-\frac{1}{2}}), \quad (3.25)$$

for $f(\theta,\phi)$ a regular function, and the values of σ_X^2, σ_Y^2 and σ_{XT} are those given in (3.2) and (3.9). The result (3.25) follows from the fact that differentiation with respect to τ under the integral sign is permissible if the resulting integral is absolutely convergent.

It remains to evaluate

$$n\left\{\int_P \exp\left[iU\tau\frac{(t-\bar{t})}{ln^{\frac{1}{2}}}\right]d\mathbf{P} - 1\right\} = -\tfrac{1}{2}\Sigma^2\tau^2, \quad \text{say.}$$

Suppose the rules (2.14) apply. Then the integral may be broken up as in the derivation of (3.4) into integrals with respect to θ and ρ. In the domain I (see §3.3) introduce new variables $\psi = \tau/(6n^{\frac{1}{2}}\rho\cos\theta)$, $\rho = \rho$; and in the domain II put $\psi = \tau/(3n^{\frac{1}{2}}\cos\theta)$. Integration with respect to ρ gives after some reduction

$$\begin{aligned}\Sigma^2 = {} & -\tfrac{2}{9}\exp\left[-iU\tau\bar{t}/ln^{\frac{1}{2}}\right]\int_{\tau/6n^{\frac{1}{2}}}^{Ut_1\tau/ln^{\frac{1}{2}}}\frac{e^{i\psi}}{\psi^3}\log\frac{6n^{\frac{1}{2}}\psi}{\tau}\,d\psi \\ & -\frac{2nl^2}{9U^2t_0^2\tau^2}\exp\left[iU\tau(t_0-\bar{t})/ln^{\frac{1}{2}}\right] + \frac{2n}{\tau^2} - \exp\left[iU\tau(t_1-\bar{t})/ln^{\frac{1}{2}}\right] \\ & \times\left\{\frac{4}{9}\int_{2Ut_0\tau/ln^{\frac{1}{2}}}^{Ut_0\tau/ln^{\frac{1}{2}}} e^{i\psi}\,d\psi/\psi^3 + \frac{nl^2}{9U^2t_1^2\tau^2}\int_{\tau/3n^{\frac{1}{2}}}^{2Ut_1\tau/ln^{\frac{1}{2}}}\frac{e^{i\psi}}{\psi}\,d\psi\right\}. \quad (3.26)\end{aligned}$$

By integration by parts and use of the results

$$\int_{1/\epsilon}^{\infty}\frac{e^{i\psi}}{\psi}\,d\psi = O(\epsilon), \quad \int_{1/\epsilon}^{\infty}\frac{e^{i\psi}}{\psi}\log\psi\,d\psi = O(\epsilon\log(1/\epsilon)),$$

$$\int_{\epsilon}^{\infty}\frac{e^{i\psi}}{\psi}\,d\psi = -\log\epsilon + (\gamma + i(\tfrac{1}{2}\pi)) + O(\epsilon),$$

$$\int_{\epsilon}^{\infty}\frac{e^{i\psi}}{\psi}\log(\psi/\epsilon)\,d\psi = \tfrac{1}{2}(\log\epsilon)^2 + (\gamma + i(\tfrac{1}{2}\pi))\log\epsilon + O(1),$$

where γ is Euler's constant (see Jeffreys & Jeffreys 1950, p. 471), it may be shown that Σ^2 is given approximately by

$$\Sigma^2 = \tfrac{2}{9}\log\frac{3Ut_0}{l} + \frac{1}{18}\left(\log\frac{6Ut_1}{l}\right)^2 - \tfrac{1}{6}\log\frac{6Ut_1}{l} + \tfrac{1}{4} \quad \text{if} \quad \frac{\tau Ut_0}{3ln^{\frac{1}{2}}} \ll 1; \quad (3.27a)$$

$$\Sigma^2 = \tfrac{2}{9}\log\frac{3n^{\frac{1}{2}}}{\tau} + \frac{1}{18}\left(\log\frac{6Ut_1}{l}\right)^2 - \tfrac{1}{6}\log\frac{6Ut_1}{l} + \tfrac{1}{4}$$

$$\text{if} \quad \log\frac{3n^{\frac{1}{2}}}{\tau} \gg 1, \quad \frac{\tau Ut_1}{ln^{\frac{1}{2}}} \ll 1, \quad \frac{\tau Ut_0}{ln^{\frac{1}{2}}} \gg 1; \quad (3.27b)$$

$$\Sigma^2 = \frac{1}{18}\left(\log\frac{6n^{\frac{1}{2}}}{\tau}\right)^2 \quad \text{if} \quad \log\frac{6n^{\frac{1}{2}}}{\tau} \gg 1, \quad \frac{\tau Ut_1}{ln^{\frac{1}{2}}} \gg 1, \quad \frac{\tau Ut_0}{ln^{\frac{1}{2}}} \gg 1. \quad (3.27c)$$

Actually, the conditions given here for these formulae to hold are more restrictive than is strictly necessary, but more precise conditions are rather complicated.

Similarly, if the rules (2.15) hold,

$$\Sigma^2 = \tfrac{2}{9}\log\frac{3Ut_0}{l} - \tfrac{1}{3} \quad \text{if} \quad \frac{\tau U t_0}{3ln^{\frac{1}{2}}} \ll 1; \tag{3.28a}$$

$$\Sigma^2 = \tfrac{2}{9}\log\frac{3n^{\frac{1}{2}}}{\tau} \quad \text{if} \quad \log\frac{3n^{\frac{1}{2}}}{\tau} \gg 1, \quad \frac{\tau U t_0}{ln^{\frac{1}{2}}} \gg 1. \tag{3.28b}$$

The j.p.d.f. of $\mathbf{x}_n$, $\mathbf{y}_n$, $\mathbf{z}_n$ and $\mathbf{t}_n$ is the fourier transform of C_n and is, for $n^{\frac{1}{2}} \gg 1$,

$$\left(\frac{1}{2\pi}\right)^2 \iiiint \exp\left[i(\xi\mathbf{x}_n + \eta\mathbf{y}_n + \zeta\mathbf{z}_n + \tau\mathbf{t}_n)\right]$$
$$\times \exp\left[-\tfrac{1}{2}(\xi^2\sigma_X^2 + \eta^2\sigma_Y^2 + \zeta^2\sigma_Y^2 + \tau^2\Sigma^2 + 2\xi\tau\sigma_{XT})\right] d\xi\, d\eta\, d\zeta\, d\tau. \tag{3.29}$$

If Σ were constant, it would follow immediately that the j.p.d.f. is normal with $\overline{\mathbf{x}_n^2} = \sigma_X^2$, $\overline{\mathbf{y}_n^2} = \overline{\mathbf{z}_n^2} = \sigma_Y^2$, $\overline{\mathbf{t}_n^2} = \Sigma^2$ and $\overline{\mathbf{x}_n\,\mathbf{t}_n} = \sigma_{XT}$, the other covariances being zero. Now Σ is actually a function of τ, but it is a slowly varying function and the main contribution to the integration with respect to τ comes from values of τ for which $\Sigma\tau = O(1)$, and it may be proved that to a sufficient approximation (3.29) may be evaluated with Σ independent of τ and having the value determined by $\Sigma\tau = 1$.

It follows that for the rules (2.14), the value of $\Sigma^2\,(=\overline{\mathbf{t}_n^2})$ is approximately

$$\Sigma^2 = \tfrac{2}{9}\log\frac{3Ut_0}{l} + \frac{1}{18}\left(\log\frac{6Ut_1}{l}\right)^2 - \tfrac{1}{6}\log\frac{6Ut_1}{l} + \tfrac{1}{4} \quad \text{if} \quad \frac{Ut_0}{n^{\frac{1}{2}}l\,(\log 3Ut_0/l)^{\frac{1}{2}}} \ll 1; \tag{3.30a}$$

$$\Sigma^2 = \tfrac{2}{9}\log 3n^{\frac{1}{2}} + \frac{1}{18}\left(\log\frac{6Ut_1}{l}\right)^2 - \tfrac{1}{6}\log\frac{6Ut_1}{l} + \tfrac{1}{4} \quad \text{if} \quad \log n^{\frac{1}{2}} \gg 1,$$
$$\frac{3Ut_1}{n^{\frac{1}{2}}l(\log n^{\frac{1}{2}})^{\frac{1}{2}}} \ll 1, \quad \frac{3Ut_0}{n^{\frac{1}{2}}l(\log n^{\frac{1}{2}})^{\frac{1}{2}}} \gg 1; \tag{3.30b}$$

$$\Sigma^2 = \tfrac{1}{18}(\log 6n^{\frac{1}{2}})^2 \quad \text{if} \quad \log n^{\frac{1}{2}} \gg 1, \quad \frac{4Ut_1}{n^{\frac{1}{2}}l\log n^{\frac{1}{2}}} \gg 1, \quad \frac{4Ut_0}{n^{\frac{1}{2}}l\log n^{\frac{1}{2}}} \gg 1; \tag{3.30c}$$

and for the rules (2.15)

$$\Sigma^2 = \tfrac{2}{9}\log\frac{3Ut_0}{l} - \tfrac{1}{4} \quad \text{if} \quad \frac{Ut_0}{n^{\frac{1}{2}}l(\log 3Ut_0/l)^{\frac{1}{2}}} \ll 1; \tag{3.31a}$$

$$\Sigma^2 = \tfrac{2}{9}\log 3n^{\frac{1}{2}} \quad \text{if} \quad \log n^{\frac{1}{2}} \gg 1, \quad \frac{3Ut_0}{n^{\frac{1}{2}}l(\log n^{\frac{1}{2}})^{\frac{1}{2}}} \gg 1. \tag{3.31b}$$

The cases (3.30*a*) and (3.31*a*) are those which we have in fact already considered when (3.18) is satisfied. The case (3.30*c*) describes the motion of an idealized fluid particle since these conditions apply when t_1 and t_0 become infinite.

3.8. *The statistical properties of the displacement after a fixed time*

The analysis of §3.3 for the probability distribution of the number of steps in a given time may now be repeated with the variance of $\mathbf{t}_n$ given by the above results. The statistical properties of $\mathbf{t}$ will again not be very different from those of $\mathbf{t}_{\bar{n}}$, the difference between them becoming smaller as $\bar{n}$ becomes larger since Σ is a slowly varying function of n.

The analysis of §§3.4 and 3.5 for the lateral and longitudinal displacement may then be repeated with σ_T replaced by $(\Sigma)_{n=\bar{n}}$. Thus Y is normally distributed in all cases with zero mean and variance given by (3.15), and $(X-UT)/T^{\frac{1}{2}}$ is normally distributed with zero mean and variance

$$\frac{1}{T}\overline{(X-UT)^2} = \tfrac{3}{2}Ul\{(\Sigma^2)_{n=\bar{n}} + \sigma_X^2 - 2\sigma_{XT}\} = UlS^2, \quad \text{say.} \tag{3.32}$$

It seems worth adding here a word of comment about the apparent contradiction between the results of (3.30*b*), (3.30*c*) and (3.31*b*) and the fact that $\mathbf{t}_n$ has exactly the variance σ_T^2 or $\sigma_{T_1}^2$, as the case may be, for all n. The explanation is that the p.d. of $\mathbf{t}_n$ is approximately that of a normal distribution with variance Σ^2 provided the value of $\mathbf{t}_n$ is not too large. For very large values of $\mathbf{t}_n$, the p.d. is significantly different from that of the normal distribution with variance Σ^2, and it is this tail which makes the exact p.d. of $\mathbf{t}_n$ have variance σ_T^2 or $\sigma_{T_1}^2$. Examination of the analysis of §3.3 shows that only the values of $\mathbf{t}$ in the neighbourhood of $\mathbf{t}=0$ are relevant to the calculation of $X-UT$, and that the long tail to the p.d. of $\mathbf{t}_n$ may be neglected.

4. The lateral and longitudinal dispersion

We obtain from the analysis of the previous section the following results for the statistical properties of the displacement of a single particle after a given (large) time T.

The mean number of steps and mean longitudinal displacement are, respectively,

$$\bar{n} = \frac{3}{2}\frac{UT}{l} \quad \text{and} \quad \bar{X} = UT \quad \text{if} \quad \bar{n} \gg 1. \tag{4.1}$$

The mean lateral displacement is $\bar{Y} = \bar{Z} = 0$.

The lateral displacement is normally distributed and

$$\bar{Y}^2 = \bar{Z}^2 = \tfrac{3}{8}UlT \quad \text{if} \quad \bar{n}^{\frac{1}{2}} \gg 1. \tag{4.2}*$$

For the longitudinal displacement when the rules (2.14) apply, necessary conditions being $Ut_1/l \gg 1, Ut_0/l \gg 1$ where $t_1 = a^2/8\kappa, t_0 = l^2/2\kappa$, then $(X-UT)/T^{\frac{1}{2}}$ is approximately normally distributed with variance UlS^2 given by (3.32): from (3.30) the approximate values are given by

$$S^2 = \tfrac{1}{3}\log\frac{3Ut_0}{l} + \frac{1}{12}\left(\log\frac{6Ut_1}{l}\right)^2 - \tfrac{1}{4}\log\frac{6Ut_1}{l} + \tfrac{19}{24} \quad \text{if} \quad \frac{Ut_0/l}{\bar{n}^{\frac{1}{2}}(\log 3Ut_0/l)^{\frac{1}{2}}} \ll 1; \tag{4.3a}$$

$$S^2 = \tfrac{1}{6}\log\frac{27UT}{2l} + \frac{1}{12}\left(\log\frac{6Ut_1}{l}\right)^2 - \tfrac{1}{4}\log\frac{6Ut_1}{l} + \tfrac{19}{24}$$

$$\text{if} \quad \log\bar{n}^{\frac{1}{2}} \gg 1, \quad \frac{3Ut_1/l}{\bar{n}^{\frac{1}{2}}(\log\bar{n}^{\frac{1}{2}})^{\frac{1}{2}}} \ll 1, \quad \frac{3Ut_0/l}{\bar{n}^{\frac{1}{2}}(\log\bar{n}^{\frac{1}{2}})^{\frac{1}{2}}} \gg 1; \tag{4.3b}$$

$$S^2 = \frac{1}{48}\left(\log\frac{54UT}{l}\right)^2 \quad \text{if} \quad \log\bar{n}^{\frac{1}{2}} \gg 1, \quad \frac{4Ut_1/l}{\bar{n}^{\frac{1}{2}}\log\bar{n}^{\frac{1}{2}}} \gg 1, \quad \frac{4Ut_0/l}{\bar{n}^{\frac{1}{2}}\log\bar{n}^{\frac{1}{2}}} \gg 1. \tag{4.3c}$$

* This result is also obtained by Josselin de Jong (1958).

Thus idealized fluid particles ($t_0 = t_1 = \infty$) obey (4.3*c*), and the variance of their longitudinal displacement is an increasing function of T. This is also the case for elements of a material quantity subject to molecular diffusion provided the time for appreciable molecular diffusion across streamlines is sufficiently large compared with T; but as T (and $\overline{n}$) increase, the variance is given by (4.3*b*) and eventually by (4.3*a*). The value of S^2 is then independent of T.

If the rules (2.15) apply, necessary conditions being $Ut_1/l \ll 1$ and $Ut_0/l \gg 1$, then from (3.31) approximate values of S^2 are

$$S^2 = \tfrac{1}{3}\log\frac{3Ut_0}{l} - \tfrac{1}{12} \quad \text{if} \quad \frac{Ut_0/l}{\overline{n}^{\frac{1}{2}}(\log 3Ut_0/l)^{\frac{1}{2}}} \ll 1; \tag{4.4a}$$

$$S^2 = \tfrac{1}{6}\log\frac{27UT}{2l} \quad \text{if} \quad \log\overline{n}^{\frac{1}{2}} \gg 1, \quad \frac{3Ut_0/l}{\overline{n}^{\frac{1}{2}}(\log\overline{n}^{\frac{1}{2}})^{\frac{1}{2}}} \gg 1. \tag{4.4b}*$$

For this case, S^2 is again an increasing function of T provided T is sufficiently small compared with t_0, but when T is sufficiently large S^2 has a constant value independent of T.

It therefore appears that molecular diffusion is of great importance in determining the statistical properties of the longitudinal displacement however small it may be, provided it is not exactly zero and the value of T is sufficiently large. It is to be emphasized, however, that the present theory is tentative because of the simplifying assumptions that have been made about the way in which molecular diffusion works, and it should really be regarded as no more than a first approximation. It should also be mentioned that the numerical coefficients in the above results are not expected to be exactly correct because the geometry of the model is obviously a rough approximation to that of a porous medium.

Longitudinal dispersion

The dispersion of a cloud of marked particles relative to its centre follows from the statistics of the displacement of a single particle only if the time or number of steps is large enough for the paths of the different particles to become statistically independent. As far as the longitudinal dispersion is concerned, there is no apparent reason why this should not be so after the particles have made 100 or so steps, provided the original dimensions of the cloud are large compared with a step length, although it is difficult to formulate satisfactory arguments to make this statement rigorous. It is therefore reasonable to assume that the above results for the longitudinal displacement may be applied to the dispersion of a cloud. A longitudinal diffusivity, κ_l say, may be defined by the equation

$$\kappa_l = \frac{1}{2T}\overline{(X - UT)^2} = \tfrac{1}{2}UlS^2, \tag{4.5}$$

where S^2 is given by (4.3) or (4.4) as the case may be. The dimensionless ratio Ul/κ_l is not a constant but depends upon t_0, t_1, T and l/U. The longitudinal dispersion does not satisfy the ordinary diffusion equation unless T is sufficiently large for (4.3*a*) or (4.4*a*) to apply, since otherwise the diffusivity is a function of T.

* The result (4.4*b*) is essentially that given by Josselin de Jong (1958).

It seems worth while mentioning here one case of physical interest for which the result (4.4*b*) may possibly apply for all T, i.e. for which the dispersion may be calculated on the assumptions that all marked particles move with the average speed in the pore and that the duration of a step may be unbounded. Consider the displacement of a fluid in a porous medium by another fluid of identical viscosity (and density if hydrostatic pressures are important), and suppose that the two fluids do not mix. If the fluids are homogeneous, molecular diffusion does not enter the problem. When the interfacial tension is sufficiently large for the ratio of μU to the interfacial tension to be small compared with one, then to a good approximation the meniscus between the two fluids in a pore will extend across the pore and move with a velocity equal to that of the average speed through the pore.* Assuming that the presence of the menisci does not significantly affect the flow field through the porous medium, the relative motion of the two fluids may be calculated on the assumption that the meniscus does not exist and every fluid particle moves with the average speed in the pore, and the distribution of relative concentration in the mixing region should therefore be asymptotically normal with a variance given by (4.4*b*), with $t_0 = \infty$, for all sufficiently large T.

Lateral dispersion

It follows from the assumption of the statistical independence of the paths of different particles that the transverse or lateral dispersion may be described by an effective diffusivity, κ_l say, defined by

$$\kappa_l = \frac{1}{2T}\,\overline{Y}^2 = \tfrac{3}{16}Ul, \tag{4.6}$$

from (4.2). The lateral dispersion is therefore independent of molecular diffusion and the dimensionless number Ul/κ_l is constant.

There is, however, considerable doubt about the correctness of (4.6). Sir Geoffrey Taylor has pointed out that in an exactly two-dimensional flow through an exactly two-dimensional porous medium, the requirement that streamlines cannot cross implies that the width of a stream of marked fluid remains constant, variations of the order of the grain size being neglected. In other words, although the centre line of the stream may wander about from side to side with a mean square displacement given by a result similar to (4.2) (provided, of course, there are no rigid side walls) the paths of individual particles in the stream are so correlated that the width of the stream remains constant. Thus in two dimensions, either one or both are false of the assumptions that the paths of different fluid particles become statistically independent and that the lateral displacement in successive steps by a single particle are statistically uncorrelated. It is not obvious which of these assumptions is worse since the presence of rigid side walls parallel to the average velocity seems to make a difference. If side walls are there, the path of a single element is approximately a straight line, so there must be a high correlation between the lateral displacement in successive steps; if side walls are not there, there is no apparent reason why such a correlation should exist.

* This result was pointed out by Sir Geoffrey Taylor.

The situation in three dimensions is even more obscure. Streamlines may now pass round one another, but it is unlikely that both of the assumptions just mentioned are valid unless some other effect is present to reduce the correlation, e.g. a complicated streamline pattern at the pore junctions which would have the effect of twisting streamlines around each other, or even some turbulence, although this is very unlikely to be present when the average motion satisfies Darcy's law. There seems to be hardly any experimental evidence on the lateral dispersion.

Comparison between theory and experiment for the longitudinal dispersion

The experiments of Von Rosenberg (1956). Von Rosenberg observed the width of the mixing region or concentration front between two miscible liquids of equal viscosities and densities (benzene and ethyl *n*-butyrate) after passage with either of three velocities through three packed towers, filled with Ottawa sand, of various lengths, the front being initially sharp. Table 1 gives the value of lS^2, defined as $(1/UT)\,\overline{(X-UT)^2}$, calculated from the data on the assumption that the concentration curve is derived from a normal distribution.

Average velocity (cm/sec)	Length of tower (cm)		
	27·6	57·9	118·0
6×10^{-4}	0·085	0·075	0·058
48×10^{-4}	0·085	0·110	0·110
36×10^{-3}	0·078	0·128	0·158

TABLE 1. Values of lS^2 in cm calculated from the data of Von Rosenberg (1956). Each figure is the result of a separate experiment.

Exact quantitative comparison is not possible because Von Rosenberg does not give the average grain size of the sand. However, let us for the sake of example suppose that $l = 0{\cdot}1$ cm (which seems reasonable though possibly a little large) and $\kappa = 1{\cdot}5\times10^{-5}\,\mathrm{cm^2/sec}$ (this is of the same order of magnitude as the diffusivities of simple organic liquids in benzene); then $t_0 = 330$ sec. The values of l/U are 170, 21 and 3 sec, respectively, and the theory given here will therefore not apply to the experiments with the smallest velocity since for these Ut_0/l is not large compared with unity. If we suppose further that $a/l = \frac{1}{5}$ (the value which seems appropriate to glass beads and which will suffice here as an estimate) then $t_1 = 3$ sec, so that, for the purposes of rough comparison at least, the appropriate theoretical results are those of (4.4). On examining the relative values of Ut_0/l and $\bar{n}$, we find that all the experiments with $U = 48\times10^{-4}\,\mathrm{cm/sec}$ satisfy the conditions of (4.4*a*), according to which S^2 is independent of T and therefore of the length of the tower; whereas those with $U = 36\times10^{-3}\,\mathrm{cm/sec}$ are intermediate between the conditions of (4.4*a*) and (4.4*b*) with a tendency to satisfy the latter, rather than the former, according to which S^2 is a logarithmic function of the length of the tower. It is clear from table 1 that there is qualitative agreement between the theory and experiment. As regards quantitative agreement, it

follows from (4.4*a*) that the value of lS^2 for $U = 48 \times 10^{-4}$ cm/sec is 0·12 cm; and from (4.4*b*) the values of lS^2 are 0·13, 0·14, 0·16 cm, respectively, for the three tower lengths. The quantitative agreement would be improved by taking a slightly smaller value of l.

The experiments of Ebach & White (1958). In these, the dispersion was measured of Pontomine sky blue 6BX dye in water flowing through a 5·12 ft. long tower packed with glass beads of diameter 0·0083 in. For those experiments in which the Reynolds number based on the average velocity and bead diameter was less than one (so that Darcy's law may be satisfied), the observed values of Ul/κ_l, with l equal to the bead diameter, were scattered between 0·4 and 0·6 with no systematic variation for 9 values of U between 0·00077 and 0·0315 ft./sec.

With a value of $\kappa = 10^{-6}$ cm^2/sec (which seems appropriate for an organic dye), the value of t_0 is 220 sec and that of t_1 is 2·2 sec, taking $a/l = \frac{1}{5}$. The value of l/U lies between 0·9 sec and 0·02 sec and the appropriate theoretical results are those of (4.3). The value of $\overline{n}$ is the same for all the experiments and is $1{\cdot}1 \times 10^4$.

Comparison of the values of Ut_0/l, Ut_1/l and $\overline{n}$ shows that for the smallest velocities the conditions (4.3*b*) are satisfied, whereas for the largest velocities the conditions (4.3*c*) are satisfied. According to (4.3*b*) the value of S^2 increases from 2·8 to 3·7 as the velocity goes from 0·00077 ft./sec to 0·0315 ft./sec, and according to (4.3*c*) the value of S^2 is 3·4 for all velocities. Thus, according to the theory S^2 should go from 2·8 to 3·4 as the velocity goes from the smallest value to the largest, and the value of $Ul/\kappa_l = 2/S^2$ goes from 0·72 to 0·59. These results are in good agreement with the experimental observations bearing in mind the large experimental scatter.

The experiments of Josselin de Jong (1958). In these the width of a concentration front, which was initially sharp, between water and salt solution was measured after passage through a tower of glass beads of diameter 0·02 cm after distances of 2·5, 7·5, 12·5 and 17·5 cm. The value of U was $0{\cdot}92 \times 10^{-2}$ cm/sec. Josselin de Jong compared the observed values with the predictions of (4.4*b*) and found approximate agreement if the value of l was taken as 0·008 cm, i.e. about one-third the bead diameter.

Comparing his results with the theory of the present paper, we have $t_0 = 13$ sec with $\kappa = 1{\cdot}5 \times 10^{-5}$ cm^2/sec and $l = 0{\cdot}02$ cm, and $t_1 = 0{\cdot}13$ sec taking $a/l = \frac{1}{5}$. The value of l/U is 2·2 sec, so the appropriate theoretical results are (4.4). Further, the values of $\overline{n}$ are 190, 560, 940 and 1320, and comparison with (4.4) shows that it is the conditions of (4.4*a*) which appear to be satisfied, and (4.4*b*) does not appear to be valid.

Now from (4.4*a*), the value of $(2\kappa_l T/X)^{\frac{1}{2}} = l^{\frac{1}{2}}S$ is 0·13 cm$^{\frac{1}{2}}$, l being taken as the diameter of the beads 0·02 cm, and the value of this quantity according to the experimental data is approximately 0·14, so that the agreement with (4.4*a*) is better than that with (4.4*b*), in accordance with the present theory.

To sum up, the agreement between the present theory and the three sets of experimental data is encouraging, but a more thorough experimental investigation is clearly required.

5. Remarks on the dispersion when Darcy's law not satisfied

An essential feature of the model put forward in §2 is that the velocity of the fluid through a pore should be proportional to the pressure drop between the ends of the pore. This is so if the inertia of the fluid is negligible and the flow in the pores is dominated by viscosity, and it was pointed out in §2 that this is equivalent to assuming that the flow obeys Darcy's law, equation (2.3), and that the streamline pattern is independent of the average velocity. For sufficiently large values of the velocity, or more precisely of the Reynolds number based on the pore length, the average velocity and the kinematic velocity, the fluid inertia is not negligible, Darcy's law is not satisfied, and there is no reason to expect that the dispersion is described by the results of the previous section. Since this case obtains in many practical applications, it seems worth while examining our model to see if by means of suitable modifications predictions can be made about the dispersion at high values of the average velocity.

The difficulty is that the flow is then much more complicated and the calculation of the velocity field in the pores becomes troublesome. Also, the assumption that the pores are straight and uniform becomes suspect because the curvature of the streamlines is important when the fluid inertia is not negligible. However, the dispersion is primarily a kinematic, as opposed to a dynamic, property of the flow field, and there is no obvious reason why the path of a marked particle should not be approximated to by a random walk of randomly orientated straight steps of random duration. But in order to calculate the duration of the steps it is necessary to consider the dynamics of the flow, and it has not proved possible so far to do this in a satisfactory manner.

It seems worth while to examine qualitatively the model consisting of an assembly of straight uniform pores as the Reynolds number increases. It follows from dimensional analysis that

$$\frac{\kappa_l}{Ul} = F\left(\frac{UT}{l}, \frac{Ul}{\kappa}, \frac{Ul}{\nu}\right) \tag{5.1}$$

(ν denotes the kinematic viscosity), where F is independent of the Reynolds number Ul/ν when it is not too large (the value of Ul/ν for which departures from Darcy's law become significant varies greatly from one type of porous medium to another and will be anywhere between 10 and 100). Now as the Reynolds number increases, the velocity profile will cease to be parabolic all along the pore and will be flat at the ends, i.e. the extent of the inlet regions will increase with the Reynolds number. Thus one effect of increasing Ul/ν is to make the velocity of the fluid in a pore more uniform and hence to decrease the dispersion, until the limit is reached in which the velocity is uniform throughout the pore except for thin layers near the pore walls. It does not follow immediately that F decreases as Ul/ν increases because other Reynolds number effects are present; in particular, the ratio of the velocity in a pore to the average velocity of the fluid through the medium will be Reynolds number dependent. However, the longitudinal dispersion was calculated using a random walk model which takes this effect into account and it appears that the longitudinal dispersion again decreases with

increase of Reynolds number, so that the indications are that F is a decreasing function of Ul/ν.

This random walk model is rather crude, but the results are not without interest and it seems worth while placing them on record. With the same notation as used in §2, it is supposed that the average speed in a pore is proportional, owing to the effects of inertia, to some power of the pressure difference between the ends of the pore, and further that the pressure in the medium is $P'x$. Accordingly, $\hat{q} = KP'^s \cos^s\theta\,(0 \leqslant \theta \leqslant \frac{1}{2}\pi)$, where s is a function of the Reynolds number and K has the same value for every pore.

By means of the arguments of §2, the (spatial) average of velocity is

$$U = \int_0^{2\pi}\int_0^{\frac{1}{2}\pi} \frac{1}{2\pi}\hat{q}\cos\theta\sin\theta\,d\theta\,d\phi = \frac{KP'^s}{s+2}, \tag{5.2}$$

and hence

$$\hat{q} = (s+2)\,U\cos^s\theta. \tag{5.3}$$

It follows from (5.2) that the filter velocity is proportional to a power of the mean pressure gradient, and it is indeed found that this is sometimes so in practice (see Scheidegger 1957). A means of giving a value to s is thereby afforded, and s is usually between $\frac{1}{2}$ and 1. We should intuitively expect s to approach one when Ul/ν is small, and to approach $\frac{1}{2}$ when the Reynolds number is large enough for the flow in the pores to be turbulent and the pressure drop to be proportional to the square of the velocity, and that in general s decreases as Ul/ν increases.

The duration of a step is

$$t = \frac{l}{\hat{q}} = \frac{l}{(s+2)U\cos^s\theta}, \tag{5.4}$$

if it is supposed that the velocity profile in a pore is flat and that all fluid particles, except for a negligible fraction, move with the average speed $\hat{q}$. The probability of a given step occurring may then be calculated as in §2 and we have

$$d\mathbf{P} = \frac{s+1}{2\pi}\sin\theta\cos^s\theta\,d\theta\,d\phi \quad (0 \leqslant \theta \leqslant \tfrac{1}{2}\pi,\ 0 \leqslant \phi < 2\pi). \tag{5.5}$$

The (ensemble average) variance of t now exists and it is not necessary to bring in molecular diffusion.

The statistical properties of the displacement of a single particle may now be calculated exactly as in §3.1 to §3.5, apart from changes in numerical values. The results are, with the same notation as employed previously:

$$\overline{Y} = \overline{Z} = 0; \tag{5.6}$$

$$\overline{n} = \frac{s+2}{s+1}\frac{UT}{l}, \quad \overline{X} = UT, \quad \text{if} \quad \overline{n} \gg 1; \tag{5.7}$$

the lateral displacement is normally distributed with

$$\overline{Y}^2 = \overline{Z}^2 = \frac{s+2}{(s+1)(s+3)}\,UlT \quad \text{if} \quad \overline{n}^{\frac{1}{2}} \gg 1; \tag{5.8}$$

and $(X - UT)/T^{\frac{1}{2}}$ is normally distributed with

$$\frac{1}{T}\overline{(X-UT)^2} = \frac{(s+1)^2}{(1-s)(s+2)(s+3)}\,Ul \quad \text{if} \quad \overline{n}^{\frac{1}{2}(1-s)/s} \gg 1. \tag{5.9}$$

(This last condition on $\overline{n}$ requires that s is not too close to 1 and follows from an analysis similar to that carried out in §3.7. If it is not satisfied and $(1-s)\log\overline{n} \ll 1$, then it may be shown that the result (4.4*b*) applies, as is to be expected since when $s \to 1$ the duration of a step as given by (5.4) tends to the value used in calculating (4.4*b*).)

It follows from the assumption that the paths of different particles become statistically independent that

$$\frac{\kappa_t}{Ul} = \frac{s+2}{2(s+1)(s+3)}, \tag{5.10}$$

and

$$\frac{\kappa_l}{Ul} = \frac{(s+1)^2}{2(1-s)(s+2)(s+3)}, \tag{5.11}$$

where κ_t and κ_l denote the effective lateral and longitudinal diffusivities, respectively. It will be noted that (5.11) decreases as s decreases from 1 to $\frac{1}{2}$.

The values of κ_l/Ul reported in the literature for high Reynolds numbers show considerable scatter but seem to lie between 0·5 and 1. The value of (5.11) is 0·76 when $s = 0{\cdot}8$.

The values of κ_l/Ul given by (5.10) seem to be a little high, but this discrepancy may well be explained by the falseness of the assumption that the lateral displacement in successive steps are uncorrelated. As regards the variation of κ_l/Ul with Reynolds number, it seems that the main effect of increasing Reynolds number may be to decrease the correlation between the lateral displacement in successive steps, because of an increase in complexity of the streamline pattern at the pore junctions or because of some turbulent mixing taking place, and thus to increase the lateral dispersion.

I wish to thank Sir Geoffrey Taylor for suggesting this investigation and for the benefit of several discussions; also Dr G. K. Batchelor for constructive criticism of an earlier draft.

Appendix

Integrals of the form

$$I = \int f(\cos\theta)\, g\{(1+p_1)\cos\theta + p_2\sin\theta\cos\phi + p_3\sin\theta\sin\phi\}\sin\theta \times \exp\left[-\lambda(p_1^2+p_2^2+p_3^2)\right] d\theta\, d\phi\, dp_1\, dp_2\, dp_3$$

over the domain

$$0 < \theta < \pi, \quad 0 < \phi < 2\pi, \quad (1+p_1)\cos\theta + p_2\sin\theta\cos\phi + p_3\sin\theta\sin\phi > 0,$$

occur in §2. The method of evaluation consists in making the transformation

$$p_1' = p_1\cos\theta + p_2\sin\theta\cos\phi + p_3\sin\theta\sin\phi,$$
$$p_2' = -p_1\sin\theta + p_2\cos\theta\cos\phi + p_3\cos\theta\sin\phi,$$
$$p_3' = -p_2\sin\phi + p_3\cos\phi,$$

which gives

$$I = \int_{\substack{0<\theta<\pi \\ 0<\phi<2\pi \\ \cos\theta+p_1'>0}} f(\cos\theta)\, g(\cos\theta+p_1') \sin\theta \exp\left[-\lambda(p_1'^2+p_2'^2+p_3'^2)\right] d\theta\, d\phi\, dp_1'\, dp_2'\, dp_3'$$

$$= -\frac{2\pi^2}{\lambda} \iint_{\substack{0<\theta<\pi \\ p+\cos\theta>0}} f(\cos\theta)\, g(p+\cos\theta)\, dp\, d(\cos\theta)$$

on integration with respect to p_2', p_3' and ϕ, and writing $p_1' = p$. The evaluation of the last integral is straightforward for the cases which occur in §2.

REFERENCES

Aris, R. 1956 *Proc. Roy. Soc.* A, **235**, 67.

Baron, T. 1952 *Chem. Eng. Progr.* **48**, 118.

Cramér, H. 1946 *Mathematical Methods of Statistics.* Princeton University Press.

Ebach, E. A. & White, R. R. 1958 *J. Amer. Inst. Chem. Engrs*, **4**, 61.

Jeffreys, H. & Jeffreys, B. S. 1950 *Methods of Mathematical Physics.* 2nd ed. Cambridge University Press.

Josselin de Jong, G. de 1958 *Trans. Amer. Geophys. Un.* **39**, 67.

McHenry, K. W. & Wilhelm, R. H. 1957 *J. Amer. Inst. Chem. Engrs*, **3**, 83.

Scheidegger, A. E. 1954 *J. Appl. Phys.* **25**, 994.

Scheidegger, A. E. 1957 *The Physics of Flow through Porous Media.* Toronto University Press.

Taylor, G. I. 1953 *Proc. Roy. Soc.* A, **219**, 186.

Taylor, G. I. 1954 *Proc. Roy. Soc.* A, **225**, 473.

Von Rosenberg, D. V. 1956 *J. Amer. Inst. Chem. Engrs*, **2**, 55.

The motion of bubbles in a vertical temperature gradient

By N. O. YOUNG,* J. S. GOLDSTEIN,† AND M. J. BLOCK‡
Baird-Atomic, Inc., Cambridge, Massachusetts

(Received 9 October 1958 and in revised form 30 January 1959)

It has been observed experimentally that small bubbles in pure liquids can be held stationary or driven downwards by means of a sufficiently strong negative temperature gradient in the vertical direction. This effect is demonstrated to be due to the stresses resulting from the thermal variation of surface tension at the bubble surface. The flow field within and around the bubble is derived, and an expression for the magnitude of the temperature gradient required to hold the bubble stationary is obtained. This expression is verified experimentally.

1. Introduction

It has long been known that when variations in temperature are maintained on the free surface of a pure liquid a dynamic steady state is achieved, characterized by a bulk flow in the liquid and at the surface, together with small surface deformations (Hershey 1939). The nature of this flow is as follows. A local increase in temperature results in a local decrease in surface free energy, γ; a surface temperature distribution therefore is accompanied by a non-uniform tangential stress in the surface, the positive direction of which is opposite to the surface temperature gradient. In response to this stress occurs a flow, the details of which are determined by a balance between the viscous shearing stress at the surface and the thermally induced surface stress. It is of interest to contrast the behaviour of a liquid subjected to a surface temperature variation with that of an elastic membrane subjected to the same thermal variation. Because the membrane is elastic, it may deform in its own plane until the tension is uniform throughout; the steady state in this case is therefore static, while in the case of the liquid a dynamic steady state is reached.

The situation in the liquid is entirely different if the surface is contaminated by an insoluble monolayer. Such monolayers can indeed support tangential stress without steady state flow by means of local density variations (Harkins 1952). This fact has been used as a very sensitive test for distinguishing between surface-tension induced flows, and flows due to other causes, e.g. free convection (Block 1956).

The direction of the flow in the surface is in the direction of the tangential stress vector. The direction of the surface flow is therefore away from the warmer

* Now at Ericsson Telephone Co., Nottingham, England.
† Also at Brandeis University, Waltham 54, Massachusetts.
‡ Now at Naval Supersonic Laboratory, Massachusetts Institute of Technology.

regions, with liquid flowing to the surface from the bulk at the warm regions. Since the velocity does not vanish at the surface, a pressure variation is present at the surface. This variation in normal stress is balanced by a surface deformation; the excess normal stress necessary to balance the flow pressure is provided by the pressure due to surface curvature. Qualitatively, a depression in the surface is formed at a local hot spot, as has been shown by Hershey (1939).

In the course of a series of experiments on this phenomenon (other results of which will be published later), we have investigated the effect of temperature variations on a spherical free surface, e.g. that of a free bubble or droplet. According to the above argument, if the temperature increases monotonically from one pole to the other of a bubble surface, a flow must be produced if the liquid is uncontaminated. In the linear approximation to be described below, this flow is to be added to the normal Stokesian flow surrounding a freely rising bubble, so that the net effect must be to alter the motion of the bubble; this conclusion is, however, independent of whether the linear approximation is made.

It is easy to see in what direction the motion of the bubble will be altered. The capillary-type flow at the bubble surface, with respect to the bubble centre, is from the warmer to the cooler pole; with respect to the liquid bulk, therefore, the bubble will move in the direction of its warmer pole. Bubbles ought therefore to be 'attracted' by hot objects. This is easily demonstrated to be the case for small bubbles by touching a hot soldering iron to a test-tube containing any very clean liquid which has been shaken up to contain air bubbles.

2. Experiments and results

In order to avoid the effects of changing bubble solubility with temperature, the experiments were restricted to the determination of the relationship between the bubble radius and the (negative) vertical temperature gradient necessary to keep the bubble motionless with respect to the liquid at large distances. From dimensional analysis, this relationship may be expected to have the form

$$dT/dz = (K/\gamma')(\rho - \rho')gRF(\ldots), \tag{1}$$

where dT/dz is the temperature gradient, K is a numerical constant, R is the bubble radius, γ' is the temperature coefficient of surface tension, ρ and ρ' are the densities outside and inside the bubble, and g is the acceleration of gravity. The function $F(\ldots)$ is any function of dimensionless quantities, e.g. $(\mu/\rho)(gR^3)^{\frac{1}{2}}$, etc. The purpose of the experiment was to verify equation (1) and to determine the values of K and the function F.

The experiment was carried out by observing bubbles in a cylindrical sample of liquid carried in the gap between the anvils of a machinist's micrometer. The temperatures of the anvils were measured by means of mercury thermometers thrust into copper blocks borne by the anvils. The temperature of the lower block could be raised by increasing the current through a nichrome wire wrapped around the lower copper block. Measurements were confined to the region near the vertical axis of the liquid sample in order to minimize any effects associated with the free cylindrical surface. Bubble diameters were measured with a travelling microscope. The experimental arrangement is illustrated in figure 1.

In the experiment, small bubbles were found to collect at the lower (warmer) anvil. As the temperature gradient was slowly reduced, the larger of these were observed to detach and to rise slowly. A second adjustment of temperature gradient then made it possible to poise the bubble essentially motionless midway between the anvils. Measurements were made on all bubbles, the residual velocity being held by this means within the limits of $\pm 10\,\mu$/s. These bubbles were very nearly spherical in shape.

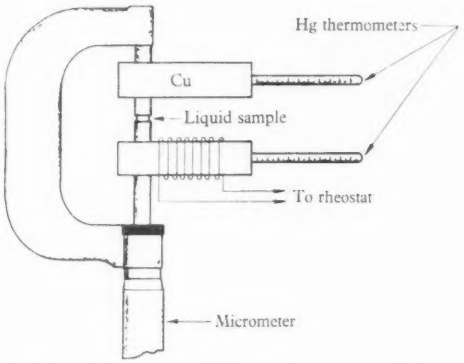

FIGURE 1. Schematic representation of experimental arrangement.

Fluid	ρ	$\mu \times 10^2$	γ	γ'* dyne cm^{-1} °C^{-1}	$\alpha \times 10^3$ deg^{-1}	$h \times 10^4$ cal/cm deg sec	c_p (cal/g)
n-hexadecane	0·773	3·52	27·66	−0·106	0·805	3·5	0·495
DC 200, 20 cs	0·955	19	20·50	−0·062	1·0	3·4	0·34
200 cs	0·971	193	21·04	−0·065	0·94	3·7	0·35
1000 cs	0·973	973	21·13	−0·061	0·94	3·8	0·37
Air, 20 °C, 1 atm.	0·0012	0·0018	—	—	—	0·57	0·25

ρ = density, μ = viscosity, γ = surface tension, γ' = therma. coefficient of surface tension, α = coefficient of volume expansion, h = thermal conductivity, c_p = heat capacity, c.g.s. units used throughout, temperature in °C.

* N. O. Young, 1955, *Rev. Sci. Inst.* **26**, 561. Probable error on γ' measurements is about 10 %.

TABLE 1. Fluid properties

In order to avoid free convective flow in the liquid sample, care was taken to keep the Rayleigh number, N, well below the critical value of about 2000.*

Measurements were carried out on air bubbles in the organic liquid *n*-hexadecane and in three Dow-Corning silicone oils of the DC 200 series. The viscosities of the three silicone oils differ widely while virtually all of their other specific properties are approximately the same. Specific parameters for each liquid are listed in table 1.

* The Rayleigh number is defined as $N = (\rho g \alpha b^4/\mu\sigma)\,(dT/dz)$, where α, b, μ and σ represent the thermal coefficient of expansion, depth of the liquid, viscosity and thermal diffusivity, respectively (see Lin 1955).

The liquid n-hexadecane is easily contaminated by the introduction of very slight amounts of silicone oil, and was included for this reason. It was found that the introduction of very small amounts of silicone contaminant was sufficient to prevent completely the abnormal bubble behaviour under consideration, and this is taken as convincing evidence that the effect in question is a surface tension effect. On the other hand, it is known that it is very difficult to form monolayers on silicone, since virtually all contaminants remain in the bulk phase. In the present experiment it was found that the addition of relatively large amounts of contaminant to the silicone oils was ineffective in preventing abnormal motion.

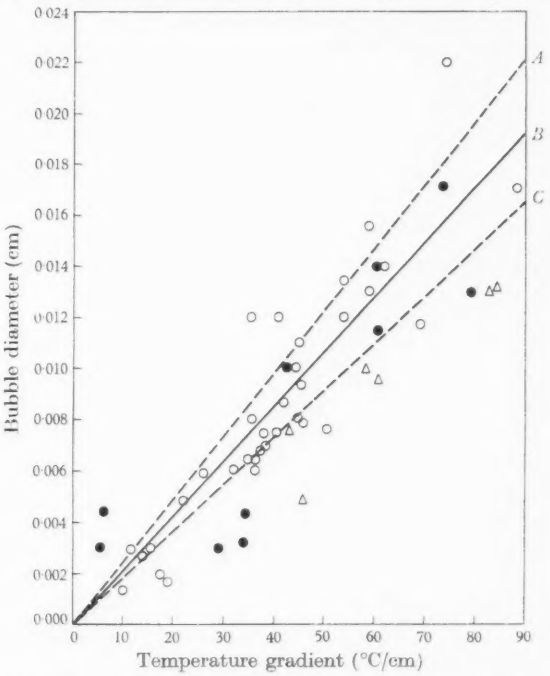

FIGURE 2. Bubble diameter, $2R$, *vs* temperature gradient necessary to hold bubble stationary. ○, DC 200, 20 cs; △, DC 200, 200 cs; ●, DC 200, 1000 cs.
$A = \gamma' = -0{\cdot}06$ dyne/cm; $B = \gamma' = -0{\cdot}07$ dyne/cm; $C = \gamma' = -0{\cdot}08$ dyne/cm.

The data for the three silicone oils is presented graphically in figure 2. The theory in the following section predicts that the value of K is $\frac{2}{3}$ and that the function F of equation (1) is equal to unity. Thus, the straight lines represent equation (1) (with $K = \frac{2}{3}$ and $F = 1$) for three different values of γ'. There are three principle sources of error involved in this determination; first, an uncertainty of about 10 % in the value of γ'; an estimated probable error of about 10 % in measuring bubble diameter (this error may perhaps be as large as 20–25 % for the smallest bubbles); and finally, an error resulting from the $\pm 10\,\mu$/s uncertainty in residual velocity. This error is greatest for those bubbles whose normal (Stokesian) velocity is smallest; thus, the residual velocity errors are greatest for the smallest bubbles, and for the highest viscosity.

It will be seen that the data confirm the theory within the limits of experimental accuracy. The critical temperature gradient is proportional to the bubble radius and is independent of viscosity (which varies by a factor of fifty among the three oils).

3. Derivation of the motion of a bubble in a vertical temperature gradient

In this section the flow field around a stationary undeformed bubble in a temperature field is derived. The analysis which follows is essentially a perturbation calculation, the unperturbed solution being one of no flow at all. It is then consistent with perturbation theory to neglect bubble deformations to the first order.

The centre of the bubble is taken as the origin of co-ordinates, and the z direction (direction of gravity) as the polar axis. Let ρ and μ be the density and viscosity, respectively, of the fluid outside the bubble (assumed to be infinite in extent) and let T be the temperature field outside the bubble. Corresponding quantities inside the bubble are denoted by the same symbols primed, e.g. ρ', μ', T'. The linearized Navier–Stokes equations describing the flow are (Birkhoff 1950)

$$\mu\nabla^2\mathbf{u} = \operatorname{grad}(p+\rho gz), \quad \operatorname{div}\mathbf{u} = 0, \tag{2}$$

where $\mathbf{u}$ is the flow field outside the bubble and p is the pressure. Identical equations describe the flow field $\mathbf{u}'$ inside the bubble. Quadratic (inertial) terms have been neglected in equation (2); this is the approximation of 'creeping flow' and may be expected to be valid for small bubbles under the same conditions which make valid Stokes's law for a freely rising bubble (Lamb 1945).

The energy equation governs the temperature distribution. If σ is the thermal diffusivity of the liquid outside the bubble, this equation has the form, for the steady state (Jakob 1942)

$$(\mathbf{u}.\operatorname{grad})T = \sigma\nabla^2 T. \tag{3}$$

A similar equation holds inside the bubbles for T'. If σ is sufficiently large, it is consistent with the approximation of creeping flow to neglect forced convection in determining the temperature distribution. With this approximation, T becomes a solution of Laplace's equation

$$\nabla^2 T = 0. \tag{4}$$

The axially symmetric solutions for flow around and within a spherical bubble have been derived by Rybczynski (1911) and by Hadamard (1911). If u_r and u_θ represent the radial and transverse components of the flow field outside the bubble, with u_r' and u_θ' their counterparts within the bubble, the solution is

$$u_r = [(a/\mu)(r^{-1} - R^2r^{-3}) + v_0(1 - R^3r^{-3})]\cos\theta, \tag{5a}$$

$$u_\theta = -[(a/\mu)(r^{-1} + R^2r^{-3}) + v_0(1 + \tfrac{1}{2}R^3r^{-3})]\sin\theta, \tag{5b}$$

$$u_r' = (a'/10\mu')(r^2 - R^2)\cos\theta, \tag{5c}$$

$$u_\theta' = -(a'/10\mu')(2r^2 - R^2)\sin\theta, \tag{5d}$$

$$p = (a/r^2)\cos\theta - \rho gr\cos\theta, \tag{5e}$$

$$p' = a'r\cos\theta - \rho' gr\cos\theta + a_0', \tag{5f}$$

where a, a' and a'_0 are constants to be determined by the boundary conditions, R is the bubble radius and v_0 is the velocity of rise of the bubble (later to be set equal to zero).*

We must include with these results the appropriate solutions of equation (4)

$$T = T_0 + T_1(r + k/r^2)\cos\theta, \tag{6a}$$

$$T' = T_0 + T_1 k' r\cos\theta, \tag{6b}$$

where k, k', T_0 and T_1 are constants also to be determined from the boundary conditions.

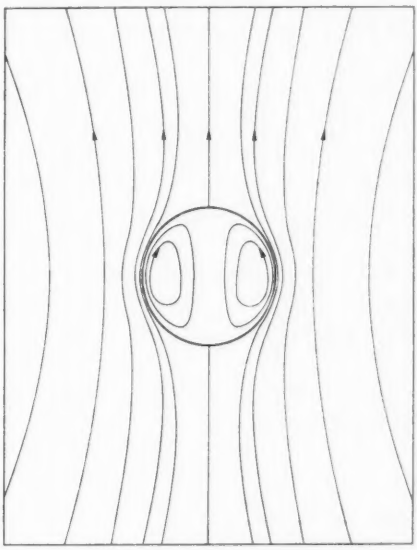

FIGURE 3. Flow field within and around the bubble.

The solutions expressed by equations (5) and (6) automatically satisfy conditions of regularity at the origin, and also satisfy the asymptotic conditions

$$\mathbf{u} \to (0, 0, v_0), \quad p \to -\rho g z, \quad T \to T_0 + T_1 z, \quad \text{as} \quad |\mathbf{r}| \to \infty. \tag{7}$$

Furthermore, the constants in these solutions have been chosen so that at the bubble surface $u_r = u'_r = 0$, since there can be no flow across the bubble surface.

Additional boundary conditions must be applied at $r = R$ to express (a) continuity of u_θ across the bubble surface, (b) continuity of shear stress across the surface, including that due to the thermal variation in surface tension, (c) continuity of normal stress across the surface, (d) continuity of temperature across the surface, and (e) continuity of heat flux across the surface. These conditions are expressed by

$$u_\theta(R, \theta) = u'_\theta(R, \theta), \tag{8a}$$

$$[\mu'(\partial u'_\theta/\partial r - u'_\theta/r) - \mu(\partial u_\theta/\partial r - u_\theta/r) - r^{-1}\partial\gamma/\partial\theta]_{r=R} = 0, \tag{8b}$$

$$[p' - p + 2\mu\,\partial u_r/\partial r - 2\mu'\,\partial u'_r/\partial r - 2\gamma/R]_{r=R} = 0, \tag{8c}$$

$$T(R, \theta) = T'(R, \theta), \tag{8d}$$

$$[h\,\partial T/\partial r - h'\,\partial T'/\partial r]_{r=R} = 0, \tag{8e}$$

* The solutions correctly describe the physical situation only when $v_0 = 0$.

where h and h' are the thermal conductivities outside and inside the bubble, respectively. When these five conditions are imposed on the solutions given by equations (7) and (8), the constants a, a', a_0, k and k' may be eliminated, and the single relation which obtains among the remaining parameters is

$$v_0 = (\tfrac{2}{3}\mu)\,[\mu\gamma' RT_c - (\rho - \rho')\,gR^2(\mu + \mu')]\,(3\mu + 2\mu')^{-1}, \tag{9}$$

where $T_c = 3T_1/(2 + h'/h)$. Setting $v_0 = 0$ in this equation gives the required relationship between the fluid parameters and dT/dz for the stationary bubble. Putting $\rho' = \mu' = h' = 0$, which is correct to within a few percent, yields equation (1) with $K = \frac{2}{3}$ and $F = 1$. The streamlines for the flow within and around the bubble are illustrated in figure 3.

Equation (9), it may be noted, agrees with the law derived by Hadamard and Rybczynski when $\gamma' = 0$. The term involving γ' enters in exactly the same way as the slip coefficient applied by Epstein (1924) to Stokes's law.

If in equation (9) we neglect unprimed quantities compared to primed ones, the case of the droplet falling in a gas results. It is seen that, by neglecting h and μ in equation (9), the term involving γ' disappears and Stokes's law is obtained. Thus the effect is extremely small for the case of droplets falling in a gas unless the droplet radius is of the order of $3\mu\gamma' hT_1/\mu' h' \rho' g$. It is possible that this situation is realized in the case of burning fuel droplets.

This work was supported in part by The Engineering Research and Development Laboratory, Fort Belvoir, Virginia.

REFERENCES

Birkhoff, G. 1950 *Hydrodynamics.* Princeton University Press.
Block, M. J. 1956 *Nature, Lond.*, **178**, 650.
Epstein, J. 1924 *Phys. Rev.* **23**, 710.
Hadamard, J. 1911 *C.R. Acad. Sci., Paris*, **152**, 1735.
Harkins, W. 1952 *The Physical Chemistry of Surface Films.* New York: Reinhold.
Hershey, A. V. 1939 *Phys. Rev.* **56**, 204.
Jakob, M. 1942 *Heat Transfer.* New York: Wiley.
Lamb, H. 1945 *Hydrodynamics.* New York: Dover.
Lin, C. C. 1955 *Hydrodynamic Stability.* Cambridge University Press.
Rybczynski, D. 1911 *Bull. Acad. Sci. Cracovie*, **1**, 40.

Two-dimensional convection from heated wires at low Reynolds numbers

By D. C. COLLIS AND M. J. WILLIAMS
Aeronautical Research Laboratories, Australian Defence Scientific Service

(Received 16 July 1958 and in revised form 21 March 1959)

Measurements of heat transfer from circular wires placed normal to a horizontal airstream have been made in the Reynolds number range 0·01 to 140. The Nusselt number can be related to the Reynolds number and temperature loading by an expression of the form

$$N\left(\frac{T_m}{T_\infty}\right)^{-0\cdot17} = A + BR^n,$$

where the values of n, A and B (see table 3) depend on whether the Reynolds number is above or below the value for which a vortex street exists in the wake of the wire. This value of the Reynolds number ($R \doteqdot 44$) is independent of the intensity and scale of the stream turbulence. The theoretical heat transfer relation based on the Oseen approximation is approached asymptotically as $R \to 0$, provided free convection is negligible.

Free convection effects diminish rapidly with increasing Reynolds number so that the orientation of the wire with respect to the vertical has a negligible influence on heat transfer except at very low velocities. For horizontal wires at very low Reynolds numbers, free convection is significant, when, roughly speaking, the Reynolds number is less than the cube root of the Grashof number.

1. Introduction

Heat transfer from circular cylinders by forced convection has been widely studied because of its engineering importance. This paper is concerned only with the range of variables encompassed in instruments employing heated cylindrical wires as sensing elements (Corrsin 1949). The most important application of hot-wire instruments is probably in fluid velocity and turbulence measurements. Unfortunately, the many advantages of the hot-wire anemometer in such work are somewhat offset by large uncertainties in the absolute magnitude of measured quantities. This deficiency is in part attributable to the use of inaccurate heat-transfer relations. The experimental investigation described below has yielded a new general relation governing heat-transfer by two-dimensional forced convection in air which should assist in improving the accuracy of hot-wire measurements.

Dimensional analysis of the equations for convection of heat by an incompressible fluid (Goldstein 1938) shows that the dimensionless heat-transfer

coefficient, or Nusselt number N, is a function of the flow parameters and fluid properties as follows:

$$N = f(R, G, \sigma), \tag{1}$$

where R is the Reynolds number, G the Grashof number, and σ is the Prandtl number. This analysis assumes that the fluid properties are independent of temperature and that it is a continuous medium. The former assumption is rarely valid, and it is customary to take account of this by introducing a parameter representing the temperature loading of the heated body, e.g. T_W/T_∞ or T_m/T_∞, where T denotes temperature and the suffixes W, ∞, m respectively signify conditions at the body surface, in the free stream, and the arithmetic mean of these. In the experiments reported here, some of the heated wires were sufficiently small in diameter for the effects of the molecular nature of air to be experienced. Molecular effects take the form of changed boundary conditions as compared with continuum flow—there is a jump in temperature between the surface of the wire and the gas adjacent to it, and the fluid slips or moves over the surface with a finite velocity. In rarefied gas dynamics the ratio of mean free path to cylinder-diameter, i.e. the Knudsen number K, is recognized as the parameter characterizing molecular effects. Thus, for the complete specification of convective heat transfer from fine hot wires, a relation of the following type is required:

$$N = f(R, G, \sigma, K, T_m/T_\infty). \tag{2}$$

There is still insufficient knowledge of the subject to permit the formulation of such a relation, and in any case it would be too unwieldy for practical purposes. In practice, free and forced convection are treated separately. As a result of recent investigations (e.g. Collis & Williams 1954), free convection from wires in air can be specified in the form

$$N = f(G, T_m/T_\infty) \tag{3}$$

for Grashof numbers as small as 10^{-10}. It has been further reported (Beckers *et al.* 1956) that free convection at Grashof numbers less than about unity is independent of Prandtl number, so that equation (3) is valid for other fluids in this case. Forced convection from hot wires in air has long been specified by simple relations of the following type, or by its equivalent in dimensional variables:

$$N = f(R, T_m/T_\infty). \tag{4}$$

The results of the present measurements are also given in this form. The variation of Prandtl number of air with temperature is small and can be combined with other temperature loading effects. Explicit introduction of the parameter K has been dispensed with, because molecular effects are small enough to be treated as a correction to the continuum heat transfer coefficient. This correction, described in Appendix A, is made on the assumption that temperature jump is solely responsible for the observed reduction in the Nusselt number. Rough estimates suggest that the effect of velocity slip would lie between $\frac{1}{3}$ and $\frac{1}{5}$ of the jump effect in the present experiments.

At sufficiently low Reynolds numbers, forced and free convection interact in a manner which has not yet been fully investigated. Ower & Johansen (1931) and Cooper & Linton (see Ower 1949) have described this interaction, essentially

in a qualitative manner. In the particular case of horizontal wires in a horizontal air stream, sufficient data was obtained in the present series of experiments to permit the formulation of a criterion for the onset of significant free convection as the Reynolds number is decreased from values where forced convection predominates. Further, it has been clearly shown that at higher Reynolds numbers beyond this small region of interaction, the effect of free convection is quite negligible. This observation shows that the method of hot-wire anemometer calibration which involves the measurement of heat transfer at zero Reynolds number is erroneously based.

Since the primary aim of this work was to establish precise heat transfer laws for forced convection at low Reynolds numbers the existing information on this subject will now be examined in more detail.

2. Review of data on forced convection at low Reynolds numbers

The results of the more important forced convection investigations have been collected and correlated by McAdams (1954). The scatter of results is rather large, but a correlation between N and R, satisfactory for many engineering purposes, has been achieved for temperature loadings up to 1000 °C by evaluating the thermal conductivity k and the dynamic viscosity μ of the gas at a temperature halfway between the cylinder temperature and the ambient or free-stream temperature, i.e. $\frac{1}{2}(T_W + T_\infty)$, and the density ρ at free stream temperature. In the Reynolds number range 0·1 to 250,000, McAdams gives co-ordinates of a recommended mean curve, whilst for the smaller range 0·1 to 1000, he gives the equation

$$N = 0{\cdot}32 + 0{\cdot}43R^{0{\cdot}52}. \tag{5}$$

Mean equations such as this smooth out the finer details, and therefore are too crude to form the basis for accurate measuring devices, particularly those which, like the turbulence hot wire, depend on the values of $\partial N/\partial R$ at the operating point. It is probable that a single careful investigation, covering perhaps a more restricted range of the variables, would yield more satisfactory heat-transfer relations.

Of the various sources quoted by McAdams, only two contribute extensive data at Reynolds numbers in the range of operation of hot-wire instruments (viz. $R < 100$), namely King (1914) and Hilpert (1933). Hot-wire anemometry is almost invariably based on an empirical relation obtained by King. If a wire of diameter d, placed normal to an airstream of velocity V, and temperature T_∞, is heated to a temperature T_W, then the heat transfer coefficient H W cm^{-1} deg^{-1} as given by King's law is

$$H = A[1 + \gamma(T_W - T_\infty)] + B[1 + \delta(T_W - T_\infty)]\sqrt{(Vd)}, \tag{6}$$

where $A = 2{\cdot}50 \times 10^{-4}(1 + 35d)$ with d in cm, $B = 1{\cdot}012 \times 10^{-2}\sqrt{d}$, and the temperature coefficients when $T_\infty = 17$ °C are $\gamma = 0{\cdot}00114$, $\delta = 0{\cdot}00008$.

King's experiments were performed with a whirling arm and consequently were subject to interference from draughts, both natural and induced. However, more recent investigations in wind tunnels or air jets of low turbulence level have been found to confirm King's law, but these investigations have generally

covered a very limited range of the variables, and it is doubtful whether the results have been examined sufficiently critically. It will be shown later, in fact, that King's results involved some fairly large systematic errors, and that because of this the results can be interpreted as being consistent with the proposed new heat transfer relation which differs somewhat from equation (6).

The work of Hilpert is exceptional in that it extends over a very wide Reynolds number range and exhibits a high degree of consistency throughout. Hilpert expressed his results in the form of a power law

$$N = C\left[R\left(\frac{T_W}{T_\infty}\right)^{\frac{1}{4}}\right]^n, \tag{7}$$

where C and n are constant in specified ranges of R. The method of correlation in this equation differs from that of McAdams in that the gas density as well as the conductivity and viscosity are evaluated at the mean temperature,† $\frac{1}{2}(T_W + T_\infty)$. Table 1 contains values of C and n for the ranges of interest here.

R	C	n
1–4	0·891	0·330
4–40	0·821	0·385
40–4000	0·615	0·466

TABLE 1

There are two reasons which possibly account for the fact that the results have not been applied extensively in instrument work. First, the temperature factor was based on a series of measurements in which the Reynolds number varied only through a small range. It was therefore not shown that this factor retains the same form in other ranges of Reynolds number, although some support was derived by correlating some of King's data at lower Reynolds numbers. Secondly, the series of simple power laws is probably only an approximate representation of the data, which could lead to appreciable errors in deriving the local slope of the heat-transfer curve. Although the experimental results were published in tabular form, no alternative analysis seems to have been attempted, and the discontinuities in the slope of the heat-transfer curve which Hilpert noted at $R = 4$ and $R = 40$, have been generally ignored in instrument work. The second of these irregularities obviously could arise from the sudden change in nature of the flow, which occurs when vortices begin to detach from the rear of the cylinder. The former, which was less well defined, might be due to the formation of standing vortices—a more gradual process.

A theoretical solution to the forced convection problem for Reynolds numbers in the range of 0·1 to 100 is extremely difficult, since neither the slow viscous flow approach on the one hand, nor the use of boundary layer approximations on the other, is allowable for most of the range. The one well-known solution for forced

† Allowance for this difference has not been made by McAdams (1954) in incorporating Hilpert's results in McAdams' figure 10–7. The required adjustment amounts to an increase of 13½% in Reynolds number. A rather smaller adjustment to McAdams' recommended curve seems indicated.

convection from wires, that due to King, avoids the difficulty by assuming potential flow. King's solution is somewhat tedious to evaluate, but can be approximated closely by two equations of simpler form. Written in non-dimensional terms these are†

$$N = \frac{2}{\log\left(2e^{1-\gamma_E}/R\sigma\right)} \qquad (R\sigma < 0{\cdot}08), \tag{8}$$

where $\gamma_E = 0{\cdot}577\ldots$ is Euler's constant, and

$$N = \frac{1}{\pi} + \sqrt{\left(\frac{2}{\pi} R\sigma\right)} \qquad (R\sigma > 0{\cdot}08). \tag{9}$$

The second equation is identical in form with King's experimental law, except that it does not include the effect of temperature on the physical properties of the gas. Comparison with experimental data shows that it overestimates the heat transfer by up to 40 %. Apart from this, the basic assumptions of the theory have been held to be unsatisfactory (Goldstein 1938). The theory thus is of no help in assessing the relative merits of experimental results.

A useful piece of theory (although of limited scope) is that based on the Oseen approximation. This is of course strictly valid only in the limit as $R \to 0$. Cole & Roshko (1954) find that this approximation yields the solution

$$\frac{2}{N} = \log\frac{8}{R\sigma} - \gamma_E. \tag{10}$$

Experimental work by the same authors failed to substantiate equation (10) due, it was thought, to disturbance of the two-dimensional convection by three-dimensional effects.

The investigation which is now described was provoked by observations that hot-wire anemometer calibrations made under near-ideal conditions tended to deviate systematically, and always in the same manner, from King's law (equation (6)). The nature of these deviations was such as to indicate a somewhat different dependence of heat-transfer on velocity from that of equation (6). A modification of King's law is proposed in this paper following careful measurements involving a wide range of air velocities, wire diameters and temperature loading. The existence of at least one discontinuity in the heat transfer relation as previously observed by Hilpert has been verified. The dependence on temperature loading was found to agree in magnitude with Hilpert's finding rather than with that of King.

3. Description of measurements

3.1. *Equipment*

Heat transfer measurements in the speed range 6–140 ft./sec were made with electrically heated wires in a small closed-return wind-tunnel (test-section area $10\frac{1}{2} \times 13\frac{1}{2}$ in.) of conventional design. An excellent distribution of velocity and a low turbulence level were obtained by using a single wire gauze screen in the

† The specific heat at constant volume has been replaced by that at constant pressure, which seems to be more appropriate in this problem.

settling chamber followed by a 4 : 1 contraction of area. The longitudinal component of turbulence was found to be 0·08 % at 50 ft./sec. Air speed was determined from the pressure drop across the contraction, which was calibrated by means of a Pitot-static tube placed at the position later occupied by the heated wires. The temperature of the air in the tunnel was slightly sensitive to changes in atmospheric conditions, and also changed several degrees during runs at the higher speeds due to viscous dissipation. As heat-transfer measurements were made for temperature loadings as small as 30 °C, a check on changes in ambient temperature was thus essential. This was made by means of a rapid response, platinum thermometer placed near to, but clear of, the wake of the heated wire. From time to time an ambient temperature reading was obtained from the test wire itself. Comparison of such readings with those of the monitoring thermometer served as a check on changes in the test wire arising from strain or other causes. Ambient temperature varied between 10 and 25 °C during the experiments.

For measurements at lower air speeds, namely, from 0·08 to 1·42 ft./sec, a cylindrical duct fitted at the intake end with a bell mouth, honeycomb and gauze was used. Air speed was measured by means of a Simmons' shielded anemometer (Simmons 1949), which was originally calibrated on a whirling arm at the National Physical Laboratory.† Flow conditions in this duct were much less steady than in the wind-tunnel, and velocity measurements were less accurate. Thus, in the experimental results presented later, there is a greater scatter amongst data taken at speeds less than 6 ft./sec.

3.2. *Wire assemblies*

In some earlier work in this field the effect of finite wire length has been largely eliminated by attaching potential taps to the heated wire, so that end losses are not included in the measured heat transfer. This device is not practicable for the finer wire used in the present work. The procedure adopted was to use very long wires and correct the results for the small residual transmission of heat to the supports by the method given by Simmons & Beavan (1934). The maximum correction necessary was 3·6 %.

The heavier gauges of wire were mounted by soldering them between slender steel prongs as in figure 1 (*a*). Tension was applied subsequently by a screw adjustment. The finest gauge wires which were prepared from Wollaston wire could not be mounted under tension without risk of breakage by vibration. An arrangement in which tension is maintained by air-drag was therefore used. An assembly of this type is shown in figure 1 (*b*). The Wollaston wire is soldered in a slack loop trailing downstream of the prongs. The silver layer is then etched from the centre of the loop and the platinum is straightened by manipulation of the remaining silver supports. At the maximum speed at which the finest wire was used, namely, 100 ft./sec, the platinum was deformed into a catenary with the tangent at either end inclined at about 5° to the normal to the air stream. This deformation would have a negligible effect on the rate of heat transfer.

† In using the Simmons' anemometer as a transfer device, no assumption about the heat transfer law applicable to this instrument is involved.

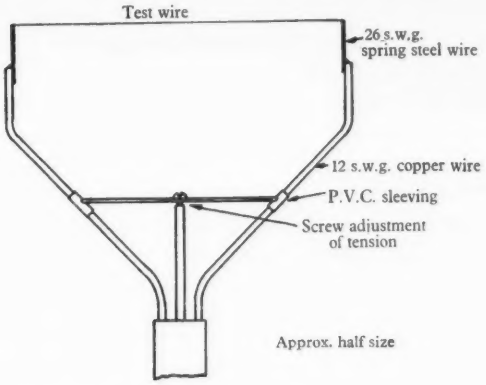

(*a*) 0·00535 and 0·00090 cm diameter wires

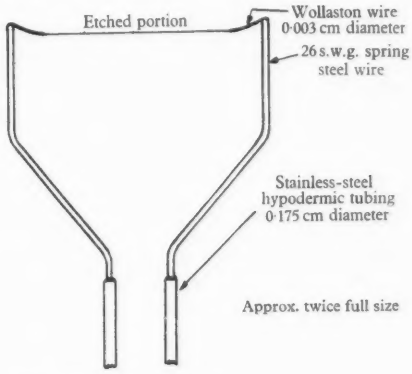

(*b*) 0·000295 cm diameter wire

FIGURE 1. Wire support geometry.

3.3. *Properties of the heated wires*

Wires of nominally pure platinum were employed for all of the measurements. The dimensions of each wire and the temperature coefficient of electrical resistance of the material are given in table 2. An optical interference method was used to determine the diameters of the finer specimens of wire whilst a similar technique combined with the use of slip gauges was used for the thickest wire. Accuracy of the two methods was about 2 and 1 %, respectively. A travelling microscope was used for the length measurements. The temperature coefficients of resistance were measured over the interval 0–100 °C, using melting ice and steam baths. The variation of this coefficient is indicative of impurities in the platinum.

The length of each specimen was made as great as practicable to minimize both the metallic conduction heat transfer and other three-dimensional effects. Free convection measurements (Collis & Williams 1954) have shown that all end effects (including metallic conduction) are small for $l/d \geqslant 20{,}000$, even at

very small values of the Nusselt number. As the Nusselt number increases the hot air film diminishes in thickness, and rough calculations based on the Langmuir concept of a concentric cylindrical film suggested that $l/d > 1000$ would be adequate for these experiments. However, the concentric film concept is not valid for forced convection, so that in the absence of a more reliable guide a large margin of safety in the aspect ratio was considered desirable. The most critical condition occurred with the finest gauge wire at the lowest velocities. The specimen with $l/d = 5370$ was therefore used for all measurements at speeds less than 6 ft./sec. At higher speeds most of the measurements were made with a shorter, and therefore stronger specimen in order to minimize errors arising from strain and permanent deformation of the wire.

Diameter d (cm)	Length l (cm)	Aspect ratio l/d	Temp. coeff. of resistance
0·000295	0·872	2950	0·00370
0·000295	1·585	5370	0·00370
0·00090	7·80	8660	0·00380
0·00535	11·10	2070	0·00342

TABLE 2

3.4. *Measurement of heat-transfer coefficients*

The wires under test were heated electrically and the power dissipated in the wire was computed from measurements of the heating current and wire resistance. The heat lost by convection is equated to the electrical power dissipation, less losses to the supporting wires. The temperature loading was determined by using the test wire as an electrical resistance thermometer. Temperatures on the International Temperature Scale were obtained by first calculating temperatures on the platinum scale using the measured temperature coefficients and then applying a correction by the Callendar method (Kaye & Laby 1948), assuming the difference coefficient $\delta = 1{\cdot}5$. Resistance of the wire at ambient temperature was determined by extrapolating to zero power dissipation. Ambient temperature was measured on a mercury thermometer prior to a run and corrected for rapid changes by reference to the platinum thermometer referred to in § 3.1.

Radiation losses were computed and found to be negligible throughout.

3.5. *Eddy shedding observations*

A hot wire anemometer was mounted in the wake of an unheated wire, of 0·00535 cm diameter, and a turbulence amplifier with a useful frequency range up to about 70 kilocycles per second was used to detect eddies shed from the upstream wire. Turbulence level and scale were varied by inserting square-mesh wire grids into the working section upstream of the wires. Determinations of the Reynolds number at which eddy shedding commenced was made for a range of turbulence conditions.

4. Results

The results discussed in §§ 4.1 to 4.4 refer to horizontal wires in a horizontal airstream normal to the wire. The effect of orientation is considered in § 4.5.

4.1. *Method of correlation*

When formulating empirical relationships it is customary to attempt to remove explicit dependence of the Nusselt number on temperature loading by evaluating the physical properties of the fluid at some suitable temperature. Choosing this temperature on the grounds of physical significance does not always lead to a unique simple relationship between the variables. Here, the system used by Hilpert has been followed (except where otherwise stated) as it leads to a compact expression of the results in the Reynolds number range concerned. Thus, the fluid properties—thermal conductivity, density and viscosity —are evaluated at a temperature which is the arithmetic mean of the free stream (or ambient) and cylinder temperatures. This system, it will be recalled, differs from that used by McAdams, who evaluated density at the free stream temperature.

Values of the thermal conductivity of air were computed from a formula given by Kannuluik & Carman (1951) which, for thermal conductivity in electrical units, is

$$k_t = 2{\cdot}41 \times 10^{-4}(1 + 0{\cdot}00317t - 0{\cdot}0000021t^2), \tag{11}$$

where k_t W cm^{-1} deg.$^{-1}$ is the thermal conductivity at temperature t °C. The ratio of viscosity to density of air, i.e. the kinematic viscosity μ/ρ, was obtained from tables in Goldstein (1938).

4.2. *Correlation of forced convection data*

The range of Knudsen number K, involved in these measurements is too small to attempt an accurate evaluation of the effect of temperature jump on heat transfer. However, in order to reduce all of the data to comparable conditions a correction was applied to reduce the measured heat-transfer coefficients to continuum values. Figure 2 has been drawn to exhibit the magnitude of the correction necessitated by temperature jump. A low-temperature loading was chosen for this illustration to avoid complications arising from temperature dependence of the fluid properties. The derivation of a correction for temperature jump based on kinetic theory is given in Appendix A. It is assumed that the measured rate of heat transfer is that which would occur in a continuum under the temperature difference which exists in the gas outside the region of discontinuity. The continuum Nusselt number N_C is then related approximately to the apparent or measured value N_M in the following way for low temperature loadings:

$$\frac{1}{N_M} - \frac{1}{N_C} = 2K. \tag{12}$$

For high-temperature loadings, allowance must be made for the temperature dependence of mean free path and thermal conductivity as shown in Appendix A.

Applying the correction enables all data pertaining solely to forced convection to be consolidated into a single curve for each temperature loading. This is demonstrated on a logarithmic scale for a low- and a high-temperature loading by means of figure 3. The series of points which diverge sharply from the upper forced convection curve at low Reynolds numbers are associated with heat transfer due to mixed free and forced convection. The conditions under which free convection becomes important are discussed in a later paragraph. The

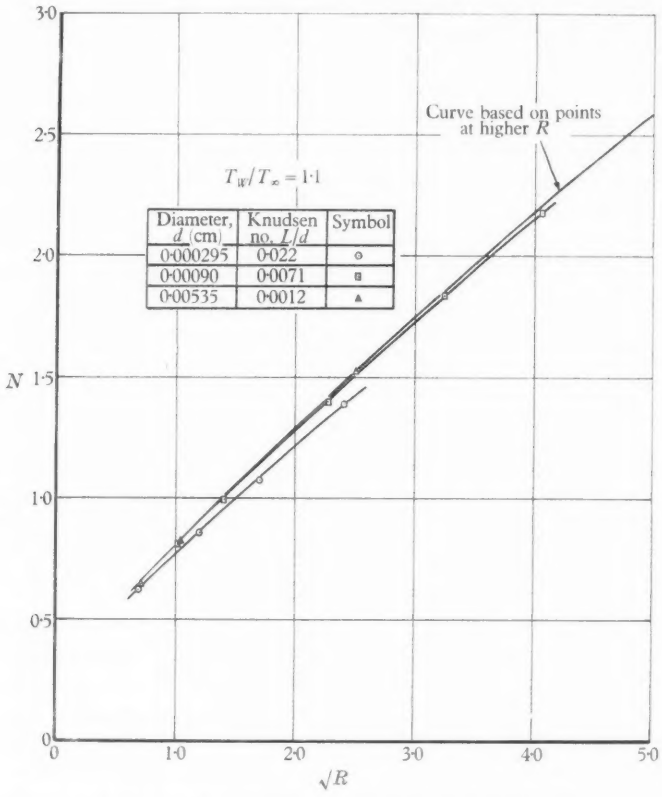

FIGURE 2. Effect of temperature jump on heat transfer.

evaluation of fluid properties at the arithmetic mean temperature T_m clearly does not entirely eliminate the temperature loading T_W/T_∞ or T_m/T_∞ as a necessary parameter. Nevertheless, the residual effect of temperature loading is small and is essentially independent of Reynolds number. The effect amounts to roughly 7 % increase in Nusselt number for an increase in temperature difference from 30 to 320 °C. Thus, for the range of variables covered in this work, the dimensionless heat-transfer coefficient, temperature loading and mass flow can be correlated by an equation of the form

$$N \cdot g\left(\frac{T_m}{T_\infty}\right) = f(R), \tag{13}$$

where g and f are functions to be determined. A satisfactory form for the temperature function is

$$g\left(\frac{T_m}{T_\infty}\right) = \left(\frac{T_m}{T_\infty}\right)^{-0\cdot17}. \tag{14}$$

It should be noted that this function is somewhat dependent on the values chosen for the thermal conductivity, and various sources differ somewhat in their values at elevated temperatures. In figure 4 the effectiveness of relations (13) and (14) in condensing the whole body of forced convection data into a single curve is demonstrated.

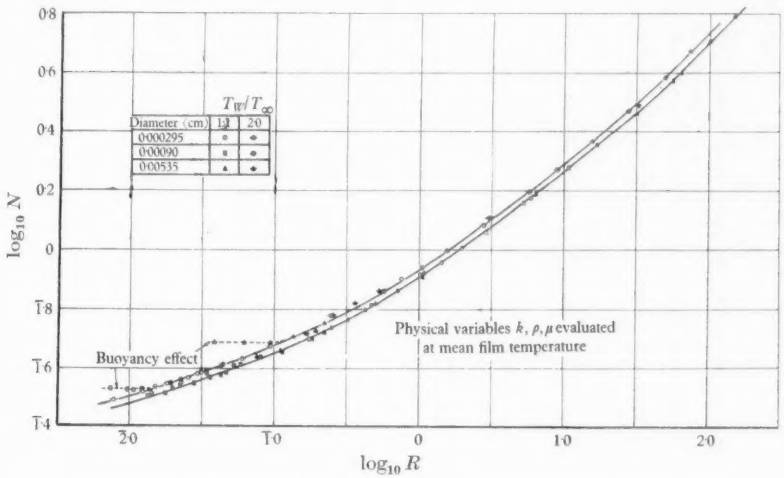

FIGURE 3. Variation of continuum Nusselt number with Reynolds number showing residual effect of temperature loading.

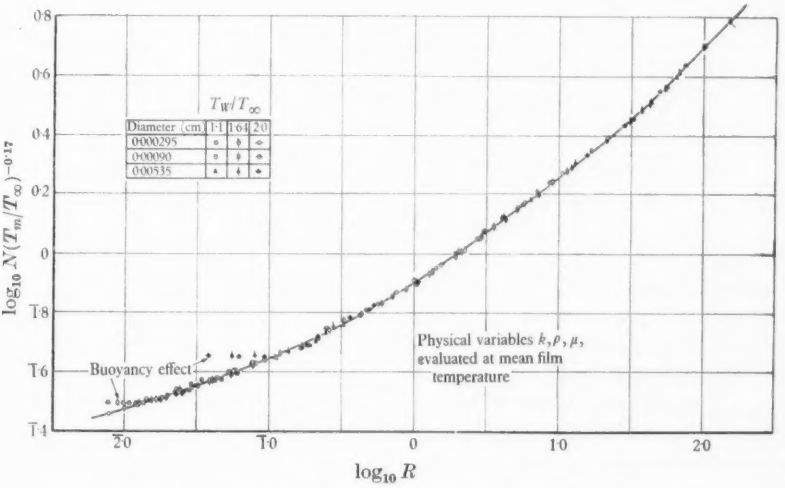

FIGURE 4. Nusselt number uniquely correlated with Reynolds number and temperature loading.

The next step is to find a convenient analytical approximation to the flow function $f(R)$. Since it is usually accepted that the data conform to King's equation (with modified constants), it will be instructive to make the comparison, remembering that the investigation was undertaken because of suspected departures from King's law. Figure 5 shows clearly that the supposed linear

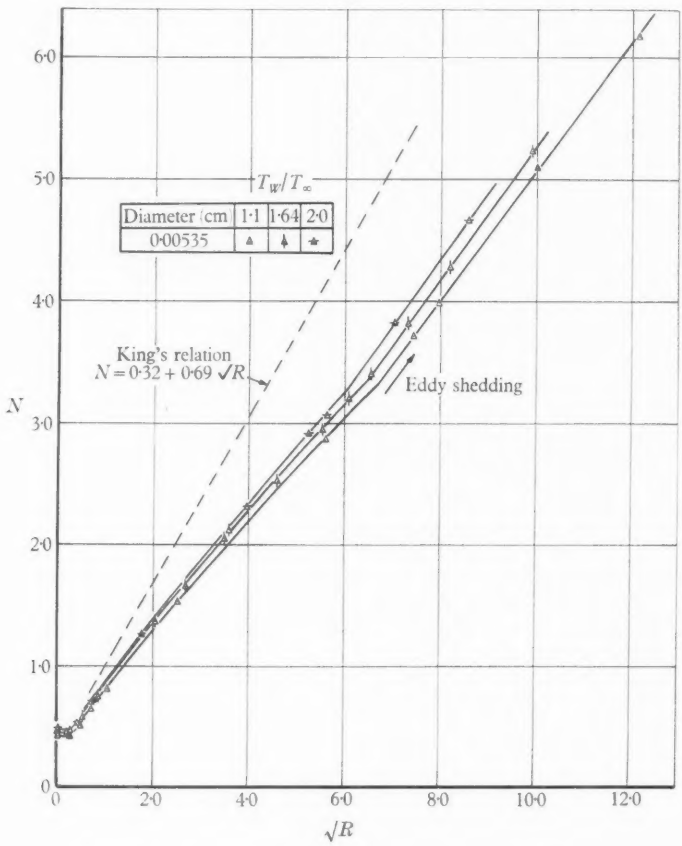

FIGURE 5. Demonstration of the inadequacy of the heat transfer relation $N = A + B\sqrt{R}$.

relation between N and $\sqrt{R}$ is no more than a rough approximation at Reynolds numbers less than about 44. Thus, the constants of King's law as determined by experiment must be somewhat arbitrary, because of the latitude available in approximating the curves of figure 5 by straight lines. In particular the slope of such lines is very variable, which explains a great deal of the inconsistency common in turbulence measurements by hot wire. At Reynolds numbers greater than 44 or thereabouts, eddies are shed from the rear of the cylinder. The change in the velocity distribution, which occurs abruptly, gives rise to the marked change of slope of the heat-loss curves which can be seen in figure 5, at about

$\sqrt{R} = 6{\cdot}6$. The function $f(R)$ thus has some sort of discontinuity at this critical Reynolds number. By trial and error it was found that the experimental data were in good agreement with the equation

$$N\left(\frac{T_m}{T_\infty}\right)^{-0{\cdot}17} = A + BR^n \tag{15}$$

if the constants A, B, n have the values given in table 3 in the Reynolds number ranges prescribed there. Most of the data shown in figure 4 are replotted in figure 6, showing how the 0·45 power law is satisfied in the range specified in table 3. The change following the onset of eddy shedding is clearly defined. At

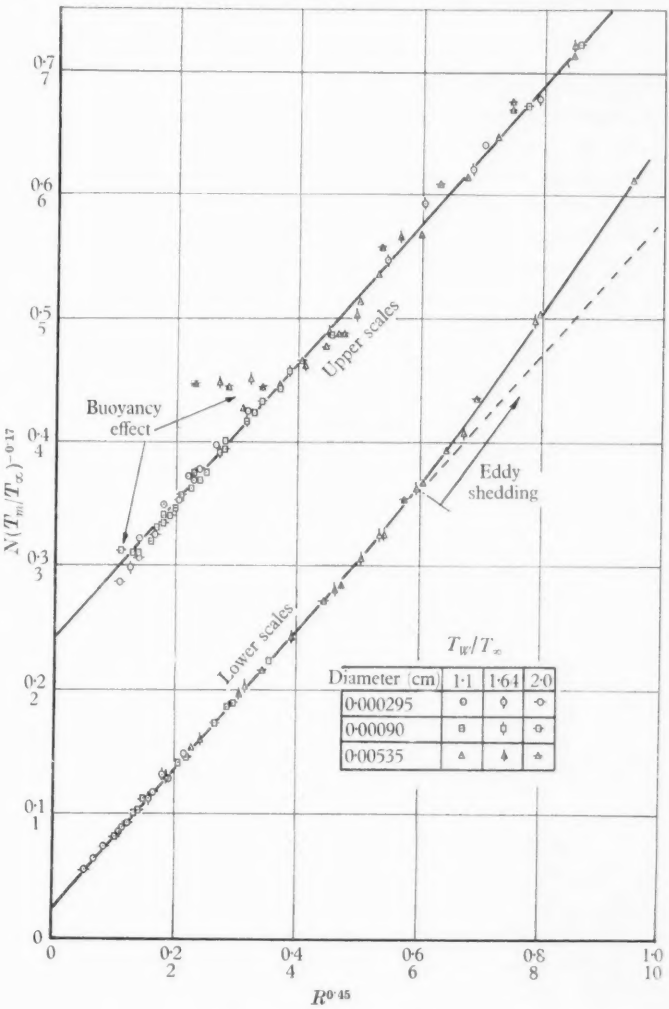

FIGURE 6. Heat transfer data correlated by 0·45 power law in the range $0{\cdot}02 < R < 44$.

$R = 0{\cdot}02$, equation (15), with appropriate constants, overestimates the Nusselt number by 2 or 3 % and the error increases rapidly if the same relation is used at smaller Reynolds numbers.

	$0{\cdot}02 < R < 44$	$44 < R < 140$
n	0·45	0·51
A	0·24	0
B	0·56	0·48

TABLE 3

4.3. *Forced convection at very low Reynolds numbers*

The theoretical solution for two-dimensional forced convection from cylinders obtained by Cole & Roshko (1954) using the Oseen method, is believed to be correct in the limit as $R \to 0$, and should not be greatly in error for $R \ll 1$. A comparison of the experimental results at low Reynolds numbers, with the Oseen solution, thus provides a check on the general soundness of the measurements and in particular of their approach to two-dimensionality. This comparison is made in figure 7 for large and small temperature loadings. The straight (broken) line represents the Oseen solution (equation (10)). Some data depart noticeably

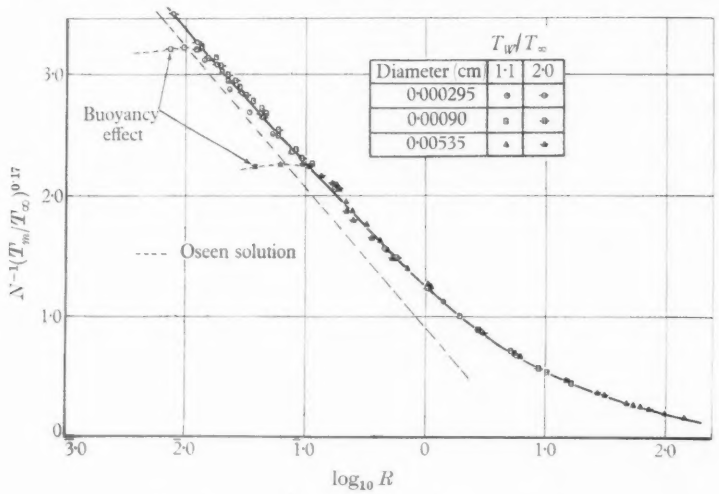

FIGURE 7. Comparison with Oseen solution.

from the forced convection curve because of buoyancy effects, but the smooth curve through the bulk of the points asymptotes to the Oseen solution as $R \to 0$. This curve deviates from the theoretical one by about 5 % at $R = 0{\cdot}01$, and diverges steadily as the Reynolds number increases, as would be expected. The discrepancy is thus too great for the Oseen solution to have much value as a working rule for forced convection at low Reynolds numbers. However, a relation

of similar form can be used to describe the experimental results for $R < 0{\cdot}5$ with an error less than the experimental scatter:

$$N\left(\frac{T_m}{T_\infty}\right)^{-0{\cdot}17} = \frac{1}{1{\cdot}18 - 1{\cdot}10\log_{10}R}. \tag{16}$$

This equation agrees with equation (15) to within 2 % in the range $0{\cdot}02 < R < 0{\cdot}5$, and is in better agreement with experiment at $R \leqslant 0{\cdot}02$ than is equation (15). Equation (16) will almost certainly be a good approximation for two-dimensional heat transfer at any lower Reynolds numbers which are attainable under continuum conditions (or nearly such) and in the absence of significant buoyancy effects.

4.4. *Mixed free and forced convection*

As we have noted, certain series of points diverge quite sharply from the forced convection curve near the lower end of the Reynolds number range. This divergence occurs because the components of velocity, induced in the heated

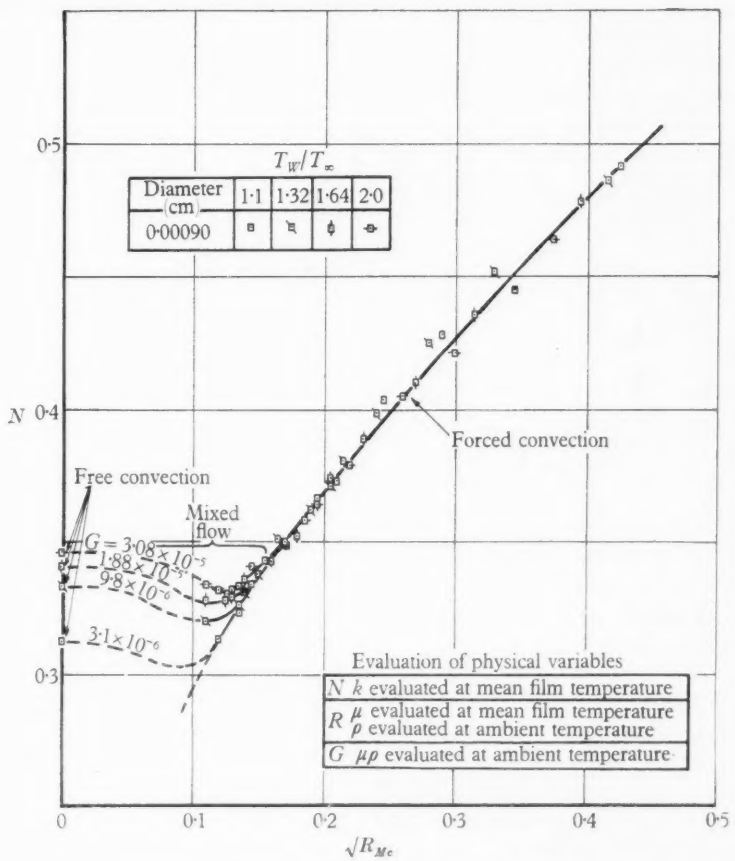

FIGURE 8. Interaction of free and forced convection.

fluid adjacent to the cylinder by buoyancy forces, become comparable in magnitude with components of the forced draught. Figures 3, 4, 6 and 7 show that the points of divergence depend markedly on cylinder diameter. By plotting the very low Reynolds number data on an enlarged scale as in figure 8, a temperature dependence is also observed. In this figure the method of correlation has been modified to the extent that the gas density embodied in the Reynolds number is evaluated at ambient temperature after the practice of McAdams (1954). This allows the temperature function of equation (15) to be discarded for the particular

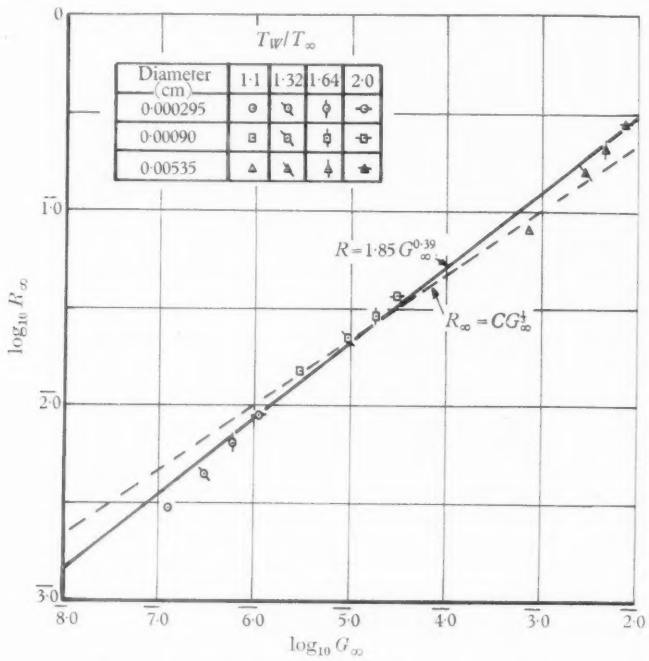

FIGURE 9. Criterion for onset of buoyancy effect.

small range of Reynolds numbers involved—a fact which will prove convenient presently (Appendix B). The data pertain to one wire diameter only, but the buoyancy effect sets in at different Reynolds numbers for each temperature. It is also clearly shown that, as the Reynolds number is further reduced, the heat-transfer rate passes through a shallow minimum before reaching the free convection value at zero Reynolds number. This curious phenomenon was apparently first observed by Ower & Johansen (1931) and later confirmed by others. However, except for special cases, the conditions governing the occurrence of mixed free and forced convection do not appear to have been quantitatively determined. Some information on this question can now be derived.

Since free convection and forced convection in a particular fluid (σ = const.) depend primarily on the Grashof and Reynolds numbers, respectively, a criterion for mixed flow involving only these two parameters should exist. This is con-

sistent qualitatively with the observed dependence on diameter and temperature. As a characteristic point of the mixed flow régime, we have chosen the condition for which the Nusselt number of mixed convection equals that for pure free convection at the same Grashof number. This point has the practical significance that it defines the lowest Reynolds number at which the hot wire in question can be used as an anemometer without ambiguity. Furthermore, the trend of the data with increasing Reynolds numbers indicates that the effect of buoyancy on the forced convection rapidly becomes negligible. In figure 9, the values of Reynolds and Grashof numbers, associated with these points of equal Nusselt number, have been plotted. Points pertaining to the finest wire could only be obtained by extrapolation. Giving less weight to these points, the conclusion was reached that buoyancy effects are small provided†

$$R_\infty > G_\infty^{\frac{1}{2}}. \tag{17}$$

The suffixes denote evaluation of the fluid properties at ambient temperature, but the conclusion, being very approximate, is not sensitive to the temperature dependence of these properties.

Another criterion based on a greater volume of data is obtained in Appendix B, and is probably more accurate for a limited range of Reynolds number. It is derived by assuming that there is no deviation from the pure forced convection relation (equation (16)) due to buoyancy effect until the Nusselt number reaches that due to free convection alone. The details of this analysis are given in Appendix B. The criterion derived for Reynolds numbers less than about 0·1 is that

$$R_\infty = 1{\cdot}85\, G_\infty^{0{\cdot}39} \left(\frac{T_m}{T_\infty}\right)^{0{\cdot}76}. \tag{18}$$

The straight line corresponding to zero temperature loading ($T_m/T_\infty = 1$) is shown in figure 9. The overall trend of the experimental points is followed, but in general the Reynolds number predicted is too high for a given Grashof number because of the assumption of no-deviation from the forced convection relation (16). The groups of points belonging to two of the three wires show additional dependence on temperature in good agreement with equation (18). Apart from the numerical factor it seems that equation (18) provides a fair criterion for the onset of buoyancy effects. In particular, it follows that

$$V_{\min} \doteqdot \text{const.} \times d^{\frac{1}{3}} (T_W - T_\infty)^{\frac{2}{3}} \left(\frac{T_m}{T_\infty}\right)^{\frac{3}{4}}, \tag{19}$$

where $V_{\min}$ is the lowest velocity which can be measured without ambiguity by a hot wire of large aspect ratio. It is interesting to note that the lower limit of usefulness of the hot wire is very little dependent on diameter. This discussion applies, of course, only to wires of large aspect ratio, where the heat flow is two-dimensional. For sufficiently small aspect-ratio wires three-dimensional heat

† It has recently been pointed out by Dr J. J. Mahony that this conclusion could be derived by the method of Appendix B if the heat transfer relations used are the Oseen solution (10) and Mahony's asymptotic formula for free convection at very low Grashof numbers (Mahony 1956).

transfer may modify the heat flux at Reynolds numbers higher than those defined by equation (18).

Since the preceding discussion is based on that segment of the experimental results for which errors were greatest, the quantitative aspects should be regarded as being essentially exploratory in nature, and the results treated with appropriate reserve.

4.5. *Effect of orientation*

The orientation with respect to the vertical, of the hot wire and of the plane of the airstream, is important in free convection and consequently has a bearing on the interaction of free and forced convection. As already stated, the preceding discussion (§§ 4.1 to 4.4) refers only to horizontal wires in a horizontal stream. It has been shown (Collis & Williams 1954) that in free convection two-dimensional heat transfer from vertical wires at very low Grashof numbers ($< 10^{-4}$) is not attained even for aspect ratios as large as 20,000. It is certain therefore that the aspect ratio would be significant in the case of mixed free and forced convection from vertical wires, for all practical values of the aspect ratio. The limited accuracy of the equipment available for very low Reynolds number observations did not justify a detailed study of this complicated phenomenon. However, it has been demonstrated previously (Ower 1949; Simmons 1949) that the region of interaction between buoyancy effects and forced convection extends over a much smaller velocity range for vertical wires than it does for horizontal wires. It may therefore be predicted that the forced convection heat-transfer coefficients for vertical and horizontal wires will not differ sensibly for all Reynolds numbers substantially greater than the value defined by equation (18). Some measurements which bear out this conclusion have been published by Simmons (1949), and further evidence is presented in figure 10 of this paper. Heat transfer measurements from a single wire of large aspect ratio ($l/d = 5400$) were made for both horizontal and vertical orientations. No significant difference was found within the Reynolds number range (about 0·25 to 4) which was covered. A systematic discrepancy between the two orientations, rising to $1\frac{1}{2}$ % at the highest Reynolds number is discernible, but is within the limit of reproducibility imposed by changes in the wire due to strain and annealing. The effect of orienting the airstream in other than a horizontal plane has not been examined at all. It is clear that with a vertical stream the mechanism of the interaction between free and forced convection will differ from that occurring in a horizontal stream, since buoyancy forces will be acting in a line parallel to the free stream instead of normal to it. The ambiguity in Nusselt number is unlikely to be present in the case of an upward directed stream, but will undoubtedly exist for a stream directed downwards.

4.6. *Effect of turbulence*

In the low-turbulence airstream of the wind-tunnel the onset of periodic vortex shedding was just detectable at $R = 46$. A small increase in Reynolds number (about 5 %) caused the intensity of the velocity fluctuation to rise sharply to a level which remained roughly constant as the Reynolds number was further

increased. The kink in the heat transfer curve was estimated to occur at $R = 44$, which agrees well with the start of eddy shedding.

Square-mesh turbulence grids of mesh size $\frac{1}{8}$, $\frac{1}{2}$ and $\frac{15}{16}$ in. were placed in turn across the stream 10 in. ahead of the 0·002 in. (0·00535 cm) wire. The turbulence level was thus increased in steps (Batchelor & Townsend 1948) whilst maintaining the scale of small eddies (the microscale λ) about the same. Observations of the vortex street became steadily more difficult but vortex shedding still

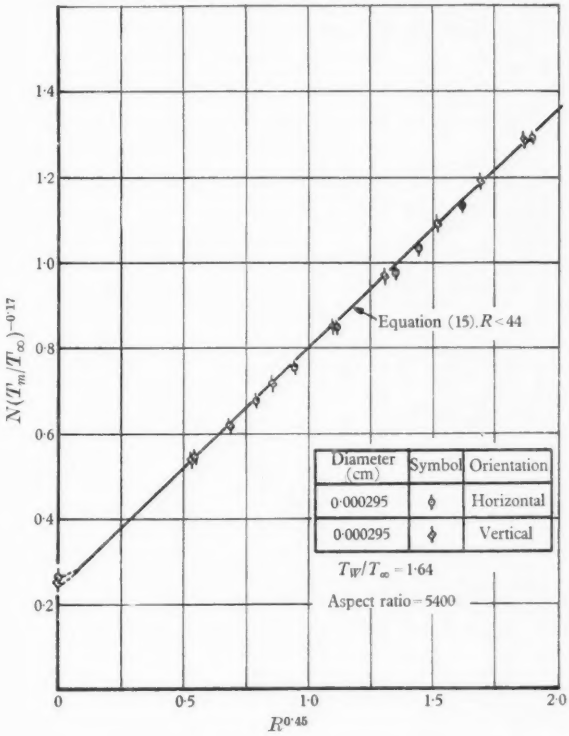

FIGURE 10. Effect of orientation on heat transfer.

commenced close to $R = 46$. The frequency of vortex shedding became increasingly uncertain, due apparently to frequency modulation arising from the fluctuating stream velocity, and to lateral displacements of the wake as a whole. However, no significant change in the Strouhal number was observed. Since the maximum effect of turbulence on the detachment of the vortex layer from the cylinder might be expected to occur with high intensity and small scale turbulence, the $\frac{1}{8}$ in. mesh was installed a distance of 20 mesh lengths upstream. Again no significant effect was observed.

It is perhaps of some interest to note that the vortex shedding frequency in these observations varied from 27 to 68 kilocycles per second.

5. Further discussion and comparison with earlier work

The experiments were designed to provide information pertaining to two-dimensional heat transfer. The results show that the effect of aspect ratio is certainly small, since agreement within the limits of error is obtained between wires of aspect ratio varying from 2070 to 8660. Again, the agreement with the Oseen solution for two-dimensional convection at very low Reynolds numbers (§ 4.3) is indicative that three-dimensional effects are small even at the lowest Reynolds numbers involved, although this situation cannot, of course, continue to indefinitely small Reynolds numbers.

A comparison with representative results taken from King (1914) and Hilpert (1933) is made in figure 11. The first impression is of haphazard scatter, but closer

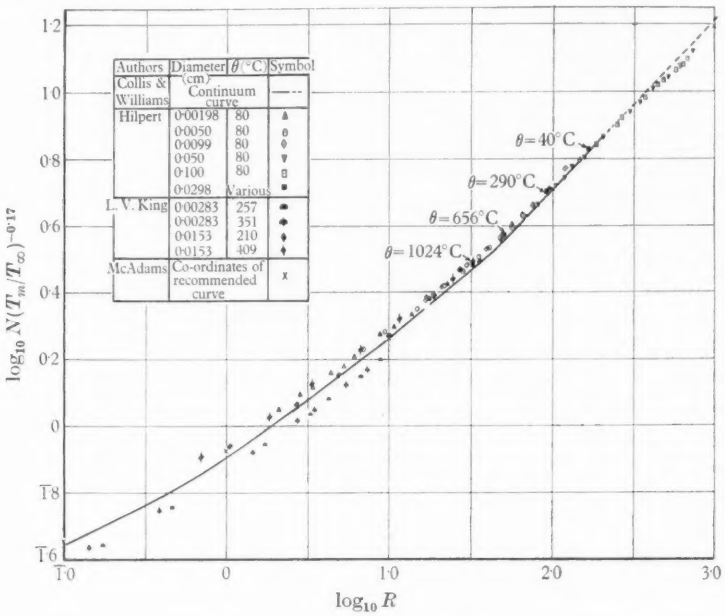

FIGURE 11. Comparison with previous forced convection investigations.

study shows that the differences between results are very largely systematic. Hilpert's work shows a high degree of self-consistency, and while exhibiting similar trends to the authors' curve the mean slope of a curve fitted to Hilpert's results would be somewhat less. Thus, while there is good agreement in values of N in the vicinity of $R = 100$, Hilpert's heat transfer is some 8 % greater at $R = 2$, and at high values of R Hilpert's curve falls below the authors' extrapolated curve. The change of slope of the $N - R$ relationship due to establishment of a vortex street is discernible at about the same point ($R \doteqdot 40$) as the bend in the authors' curve. The latter does not exhibit a gradual bend at $R = 4$ as found by Hilpert, but the occurrence of this bend was deduced from an insubstantial number of data. Where the vortex street exists, the plot of Hilpert's results

shows an irregularity involving at least one point of inflexion in the range $40 < R < 500$ which is not reflected in his constants of table 1. Unfortunately, the authors' results are too sparse in this range to clarify the matter. The correct relation for this range therefore remains in some doubt. Hilpert's data below the eddy-shedding Reynolds numbers conform well to a law involving the 0·45 power of the Reynolds number as shown in figure 12. However, the constants differ from those given in table 3, for equation (15), particularly the constant, A.

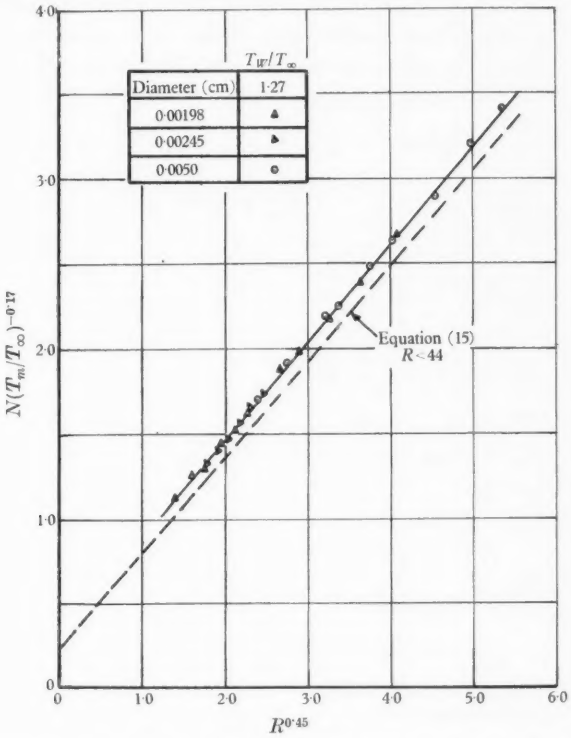

FIGURE 12. Comparison of Hilpert's data with equation (15); $R < 44$.

The data taken from King and plotted in figure 11 represent results for the lightest and heaviest wire gauges used by that author, two moderate temperature loadings being selected in each case. Near $R = 1$, heat transfer from the thicker wire is undoubtedly augmented slightly by the effect of buoyancy (see § 4.4). Apart from this it is remarkable that each series of points (of given diameter and temperature loading) is spaced a constant distance in the ordinate direction from each other and from the authors' curve. These discrepancies are evidently due to some deficiency in the measurement of the heat-transfer coefficient rather than of the Reynolds number. Regardless of the precise nature of this deficiency, it may be concluded that King's heat-transfer coefficients show the same form of dependence on the Reynolds number in the range $0·1 < R < 40$ as the work described here.

With regard to the effect of temperature loading, the authors' results constitute the only extensive body of consistent data available. The development of a method of correlating the heat-transfer coefficient with temperature loading was described in § 4.2 (equations (13), (14)). The method satisfactorily accounts for the few measurements taken by Hilpert at temperatures other than 100 °C. This can be seen from figure 11 where representative points at temperature loadings up to 1024 °C are included. The effectiveness of equations (13) and (14) in dealing with King's results cannot be determined due to the uncertainties in those results. King's own analysis showed deviations of the temperature coefficients γ and δ of equation (6) of up to 50 % from their mean value. For $R < 44$, equation (15) can be reduced to a dimensional form equivalent to King's equation (6), viz.

$$H = A'[1+\gamma(T_W - T_\infty)] + B'[1+\delta(T_W - T_\infty)]\,(Vd)^{0\cdot45}, \tag{20}$$

where A' and B' embody physical properties of the fluid and $T_\infty \doteqdot 290$ °K. No significance attaches to differences between the values of A' and B' and the constants A and B of King's equation because of the changed power of Vd in the second term, but it is of interest to compare the representative values of γ and δ. The authors' values given in table 4 together with those of King are calculated assuming the following variation of conductivity and viscosity with temperature:

$$\frac{k}{k_0} = \left(\frac{T}{T_0}\right)^{0\cdot80}; \quad \frac{\mu}{\mu_0} = \left(\frac{T}{T_0}\right)^{0\cdot76}. \tag{21}$$

The larger values found here have some significance in practical hot wire anemometry, as discussed by Collis (1956).

	γ	δ
King	0·00114	0·00008
Collis & Williams	0·00164	0·00025

TABLE 4

In the lower end of the Reynolds number range (R of order 1), comparison must be made with the work of Cole & Roshko (1954). Reference has already been made to the fact that good agreement has been found with the Oseen solution (equation (10)) obtained by these authors. Cole & Roshko did not find such agreement, but their experimental accuracy may have suffered greatly through use of nominal values of wire diameter and of temperature coefficient of resistance. Again, although very fine wires involving Knudsen numbers of up to $\frac{1}{6}$ were used, no account was taken of 'rarefaction' effects. According to equation (12) these might exceed 30 % of the measured heat transfer coefficient. In view of this, a direct comparison with the authors' results is not possible.

Some interesting indirect evidence consistent with the 0·45 power of R or V in equations (15) and (20), respectively, is found in measurements by Newman (1951) of the sensitivity of hot wire anemometers to yaw. It was originally accepted that a hot wire responded to the normal component of velocity $V \sin\psi$, where ψ is the angle of yaw, so that according to equation (6) the heat-transfer

coefficient varied linearly with $\sqrt{(V \sin \psi)}$. Newman reached the conclusion, however, that the wire responded to $V^{\frac{1}{2}}(\sin \psi)^{0.457}$. In the light of equation (20) and a close examination of Newman's data, it seems probable that the wire actually responds to the 0·45 power of the normal component of velocity, i.e. $(V \sin \psi)^{0.45}$.

Conclusions

1. Based on experiments in the Reynolds number range 0·01 to 140, a new relation for two-dimensional forced convection from cylinders normal to an airstream has been established. The law has the form

$$N\left(\frac{T_m}{T_\infty}\right)^{-0.17} = A + BR^n, \tag{15}$$

where the values of n, A, B depend on whether the Reynolds number is above or below the value for which a vortex street exists in the wake of the cylinder (see table 3). Fluid properties k, ρ and μ used in computing N and R are evaluated at mean film temperature T_m, and T_∞ is in the normal range of room temperatures.

2. The extensively used relation of King was based on measurements made at Reynolds numbers below this critical value. In that region the new relation differs from King's in that the Reynolds number enters to the 0·45 power rather than the 0·5 power, and the effect of temperature loading is found to be significantly larger. These differences, particularly the former, appear to arise mainly in the analysis of the results rather than in the measurements themselves.

3. Hilpert's measurements at low Reynolds numbers ($R < 44$) are satisfied by equation (15), except for the value of the constant A. Hilpert's temperature function differs in form from that in equation (15), but no data available are sufficiently accurate to discriminate between them. For $R > 44$, there is a discrepancy between Hilpert's results and those of the authors which cannot be resolved without further investigation.

4. The theoretical heat transfer relation based on the Oseen approximation (equation (10)) is approached asymptotically as $R \to 0$, provided free-convection or aspect-ratio effects do not intervene. A relation of similar form (equation (16)) satisfactorily describes two-dimensional forced convection for $R < 0{\cdot}5$.

5. Free convection effects die out quickly with increasing Reynolds number (at least for horizontal airstreams), so that except at very low velocities, the orientation of the wire with respect to the vertical has negligible influence on the heat transfer coefficient.

6. A rough criterion for the onset of buoyancy effects has been derived for horizontal wires (equation (18)). This gives quantitative expression to earlier observations that the minimum speed $V_{\min}$ which can be measured with a hot-wire anemometer increases with temperature loading, and also shows that $V_{\min}$ varies only as the $\frac{1}{5}$-power of the wire diameter.

7. Molecular effects reduce the heat transfer from fine wires below the continuum value (equation (15)) by an amount which can be estimated by assuming that the temperature differential is reduced by the 'temperature jump' calculated from kinetic theory.

8. The intensity and scale of the turbulence in the airstream does not affect the Reynolds number at which the vortex street develops in the wake of fine wires. Thus the change in constants of equation (15) likewise occurs at the same Reynolds number ($R = 44$) regardless of the stream turbulence.

The authors are indebted to the Chief Scientist, Australian Defence Scientific Service, Department of Supply, Melbourne, for permission to publish this paper.

Appendix A

Effect of temperature jump on the heat-transfer coefficient

It has been established (Kennard 1938) that when thermal conduction takes place between a rarefied gas and a bounding wall, there is a discontinuity in temperature at the wall. If the wall temperature is T_W, and T_s is what the temperature of the gas would be if the temperature gradient along the outward-drawn normal, $\partial T/\partial r$, continued right up to the wall, then the discontinuity, or temperature jump, is given by

$$T_W - T_s = -\xi \frac{\partial T}{\partial r}. \tag{A 1}$$

The constant ξ has dimensions of length and is known as the temperature jump distance.

Two assumptions are made in calculating the continuum value of the heat-transfer coefficient from the values measured in the presence of temperature jump: (*a*) the measured rate of heat transfer is the same as would take place from a cylinder of the same diameter, at a temperature T_s, immersed in a perfectly continuous gas; (*b*) the correction can be made directly to the measured value of the heat-transfer coefficient, which is of course an average of the local value taken over the circumference of the cylinder. Kennard derives an expression for ξ in terms of the properties of the gas and the surface:

$$\xi = \frac{2-\alpha}{\alpha} \frac{4c}{\gamma+1} \frac{k}{\mu c_v} L, \tag{A 2}$$

where α is the accommodation coefficient of the surface for the particular gas, k is the thermal conductivity of the gas, $\gamma = c_p/c_v$ is the ratio of specific heats of the gas at constant pressure and constant volume, μ is the viscosity of the gas, and L is the mean free path of gas molecules. Here L is defined by the relation $\mu = c\rho\bar{v}L$, in which $\bar{v} = \sqrt{(8RT/\pi)}$, where R is the gas constant per unit mass, ρ is the density of the gas, and c is a constant such that $0{\cdot}491 \leqslant c \leqslant 0{\cdot}499$. Rearranging and putting $4c = 2$, we get

$$\xi = \frac{2\gamma}{\gamma+1} \frac{1}{\sigma} \frac{2-\alpha}{\alpha} L, \tag{A 3}$$

where $\sigma = \mu c_p/k$ is the Prandtl number.

For air, $\gamma = 1{\cdot}4$ and $\sigma = 0{\cdot}72$, and for platinum in air $\alpha \doteqdot 0{\cdot}9$, so that, with little error,

$$\Delta\theta = T_W - T_s = -2L \frac{\partial T}{\partial r}. \tag{A 4}$$

If a wire is maintained at a temperature loading $\theta_W = T_W - T_\infty$, and q the heat loss per unit area is measured, then the heat-transfer coefficient h_W is calculated from the relation

$$q = h_W \theta_W, \tag{A 5}$$

and on the basis of assumptions (a) and (b) above it follows that the continuum heat-transfer coefficient h_s is given by

$$q = h_s \theta_s. \tag{A 6}$$

Combining (A 5) and (A 6), we obtain

$$h_s = h_W \left(1 + \frac{\Delta\theta}{\theta_s}\right), \tag{A 7}$$

where $\Delta\theta = T_W - T_s = \theta_W - \theta_s$.

From the conduction equation, we have

$$q = -\left(k \frac{\partial T}{\partial r}\right)_{T_s}, \tag{A 8}$$

and evaluating the quantities in equation (A 4) at temperature T_s, we also have

$$\Delta\theta = -2\left(L \frac{\partial T}{\partial r}\right)_{T_s}. \tag{A 9}$$

By eliminating q and $\partial T/\partial r$ from equations (A 6) to (A 9), it can be shown that

$$h_s = h_W \left[1 + \left(\frac{2L}{k}\right)_{T_s} h_s\right], \tag{A 10a}$$

which may be written alternatively as

$$\frac{1}{h_s} = \frac{1}{h_W} - 2\left(\frac{L}{k}\right)_{T_s}. \tag{A 10b}$$

In figure 13, $2L/k$ has been plotted against $T - T_0$, using values of k and L taken from Kannuluik & Carman (1951) and Kennard (1938). The correct value of $1/h_s$, must be obtained by successive approximation, starting with $T_s = T_W$.

Actually the maximum correction to the present results amounted to 11 %, giving a jump of about 30° at a wire temperature of 300 °C. In this case the error in h_s arising from evaluating $2L/k$ at T_W instead of T_s is less than $\frac{1}{2}$ %.

In order to determine the continuum Nusselt number N_C from h_s, the thermal conductivity at the mean film temperature $T_m = T_\infty + \frac{1}{2}\theta_s$ must be substituted in the expression

$$N_C = \frac{h_s d}{k_m}. \tag{A 11}$$

In the example quoted above, the adjustment to k_m arising from the diminished temperature loading amounts to -2 %, so that the continuum Nusselt number (calculated from (A 11)) is 13 % greater than the measured value.

At low temperature loadings although the jump correction $\Delta\theta/\theta_s$ may be large, the absolute temperatures T_W, T_s and T_∞ are very nearly equal. If $2L/k$ is evaluated at T_∞ then

$$N_C = \frac{h_s d}{k}. \tag{A 12}$$

The measured Nusselt number

$$N_M = \frac{h_W d}{k}, \tag{A 13}$$

and substituting in (A 10*b*) we have the simple non-dimensional formula

$$\frac{1}{N_C} = \frac{1}{N_M} - 2K, \tag{A 14}$$

where $K = L/d$ = Knudsen number.

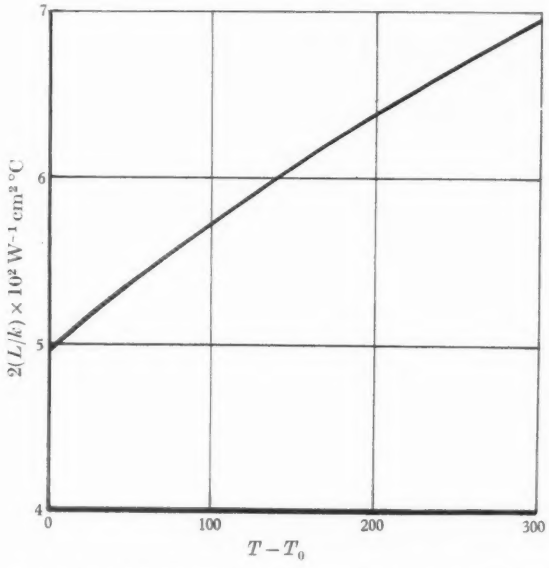

FIGURE 13. Variation of $2L/k$ with temperature for air at atmospheric pressure.

Appendix B

Criterion for the onset of buoyancy effects

This is derived for horizontal wires on the assumption that there is no deviation from the forced convection relation for low Reynolds numbers, equation (16), until the Reynolds number is reduced to the point where the forced convection Nusselt number equals that due to free convection alone. The experimental results of this paper show that this is substantially true.

In the very low Reynolds number range where buoyancy effects are likely to be significant, the forced convection relation (see § 4.3) is

$$\frac{1}{N}\left(\frac{T_m}{T_\infty}\right)^{0\cdot17} = 1\cdot18 - 1\cdot10\log_{10} R. \tag{B 1}$$

In the range $10^{-10} < G_\infty < 10^{-2}$, free convection data of Collis & Williams (1954) have been re-examined in the light of Mahony's (1956) theoretical work. It was found that a semi-logarithmic relation similar to equation (B 1) fits the experimental results very satisfactorily:

$$N^{-1} = 0\cdot88 - 0\cdot43\log_{10} G_\infty. \tag{B 2}$$

In this relation the temperature loading has been eliminated by the method of correlation employed, previously discussed at some length by the authors (1954). Equating the Nusselt number in equations (B 1) and (B 2) yields a criterion of the type required, i.e.

$$\log R = 0{\cdot}39\left(\frac{T_m}{T_\infty}\right)^{0{\cdot}17} \log G_\infty + 1{\cdot}07 - 0{\cdot}80\left(\frac{T_m}{T_\infty}\right)^{0{\cdot}17}. \tag{B 3}$$

This is not a convenient equation to deal with, but fortunately a simpler approximate result can be obtained. In the range $10^{-2} < R < 0{\cdot}2$ the temperature function of equation (B 1) may be omitted if McAdams's correlation (see § 2) is used (see note below). If R_{Mc} denotes Reynolds number evaluated in the manner of McAdams, then in lieu of equation (B 3) we obtain the condition

$$\log R_{Mc} = 0{\cdot}39 \log G_\infty + 0{\cdot}27, \tag{B 4}$$

or

$$R_{Mc} = 1{\cdot}85\, G_\infty^{0{\cdot}39}. \tag{B 5}$$

If the viscosity-temperature relation be taken as $\mu \propto T^{0{\cdot}76}$, the relation connecting R_∞ and R_{Mc} is

$$R_{Mc} = R_\infty \left(\frac{T_m}{T_\infty}\right)^{-0{\cdot}76}. \tag{B 6}$$

Equation (B 5) can therefore be written as

$$R_\infty = 1{\cdot}85\, G_\infty^{0{\cdot}39} \left(\frac{T_m}{T_\infty}\right)^{0{\cdot}76}, \tag{B 7}$$

whence

$$V_{\min} \doteqdot \text{const.} \times d^{\frac{1}{5}} (T_W - T_\infty)^{\frac{2}{5}} \left(\frac{T_m}{T_\infty}\right)^{\frac{3}{4}}, \tag{B 8}$$

where $V_{\min}$ is the lowest velocity that can be measured without ambiguity by a hot-wire anemometer and the constant depends on the flow conditions (ρ, μ, T_∞).

Note on McAdams correlation

A simple power law can be fitted locally to any part of the $\log N$ *vs* $\log R$ curve by determining the local slope p. Thus

$$N\left(\frac{T_m}{T_\infty}\right)^{-0{\cdot}17} = \text{const.} \times R^p. \tag{B 9}$$

A relation connecting R and R_{Mc} may be written as

$$R = R_{Mc}\left(\frac{T_m}{T_\infty}\right)^{-1{\cdot}0}, \tag{B 10}$$

and equation (B 9) may be written

$$N = \text{const.} \times R_{Mc}^p \left(\frac{T_m}{T_\infty}\right)^{0{\cdot}17 - p}. \tag{B 11}$$

It can be seen that, provided p lies near 0·17, the temperature function is nearly annulled.

The slope p may be determined by graphical methods or by differentiation of the empirical law which describes the particular range of interest. Upon differentiating (B 1) and obtaining p, it is found that in the range $10^{-2} < R < 10^{-1}$ McAdams system will correlate data to within 1 % at temperatures up to 300 °C.

REFERENCES

Batchelor, G. K. & Townsend, A. A. 1948 Decay of isotropic turbulence in the initial period. *Proc. Roy. Soc.* A, **193**, 539–58.

Beckers, H. L., ter Haar, L. W., Tjoan, Lie Tiam, Merk, H. J., Prins, J. A. & Schenk, J. 1956 Heat transfer at very low Grashof and Reynolds numbers. *Appl. Sci. Res.* A, **6**, 82.

Cole, J. & Roshko, A. 1954 Heat transfer from wires at Reynolds numbers in the Oseen range. *Proc. Heat Transfer and Fluid Mechanics Inst. Univ. of Calif. Berkeley, Calif.*

Collis, D. C. 1956 Forced convection of heat from cylinders at low Reynolds numbers. *J. Aero. Sci.* **23**, 697–8 (Readers' Forum).

Collis, D. C. & Williams, M. J. 1954 Free convection of heat from fine wires. *A.R.L. Aero.* note 140.

Corrsin, S. 1949 Extended applications of the hot-wire anemometer. *N.A.C.A., T.N.* 1864.

Goldstein, S. (Editor). 1938 *Modern Developments in Fluid Dynamics.* Vols. I and II, Chaps. I and XIV. Oxford.

Hilpert, R. 1933 Wärmeabgage von geheizten Drähten und Rohren im Luftstrom. *ForschArb. IngWes.* **4**, 215–24.

Kannuluik, W. G. & Carman, E. H. 1951 The temperature dependence of the thermal conductivity of air. *Aust. J. Sci. Res.* **4**, 305–14.

Kaye, G. W. C. & Laby, T. H. 1948 *Tables of Physical and Chemical Constants*, tenth edition. Longmans, Green and Co.

Kennard, E. H. 1938 *Kinetic Theory of Gases.* New York and London: McGraw-Hill Book Co. Inc.

King, L. V. 1914 On the convection of heat from small cylinders in a stream of fluid. Determination of convection constants of small platinum wires with application to hot-wire anemometry. *Phil. Trans.* A, **214**, 373–432.

Mahony, J. J. 1956 Heat transfer at small Grashof numbers. *Proc. Roy. Soc.* A, **238**, 412–23.

McAdams, W. H. 1954 *Heat Transmission*, third edition, Chap. X. McGraw-Hill Book Co. Inc.

Newman, B. G. 1951 Some contributions to the study of the turbulent boundary-layer near separation. *Australian Council for Aeronautics. Report* ACA–53.

Ower, E. & Johansen, F. C. 1931 On a determination of the pitot static tube factor at low Reynolds numbers with special reference to the measurement of low air speeds. *R & M* 1437, *British A.R.C.*, Appendix IV.

Ower, E. 1949 *The Measurement of Airflow*, third edition, Chap. X. Chapman and Hall Ltd.

Simmons, L. F. G. & Beavan, J. A. 1934 Hot wire type of instrument for recording gusts. *R & M* 1615, *British A.R.C.*

Simmons, L. F. G. 1949 A shielded hot wire anemometer for low speeds. *J. Sci. Instrum.* **26**, 407–11.

Heat transfer in slip flow at low Reynolds number

By H. C. LEVEY
Department of Mathematics, University of Western Australia

(Received 10 January 1959)

The transfer of heat by forced convection from a hot wire in a low Mach number rarefied gas stream is investigated for small Reynolds numbers. A simple expression is found for the Nusselt number, and it is suggested that this has reasonable validity over a wide range of Knudsen numbers, even into the free-molecule flow régime.

1. Introduction

The hot-wire anemometer is in extensive use as a means of measuring velocity fluctuations, and for quick response the wires used are of very small diameter. Thus, in rarefied gases it is quite easy to achieve the condition where the mean free path in the gas is comparable with the wire diameter. For example, wires of 0·0001 in. diameter are often used; and while this is 40 times the mean free path in air at room conditions, it is about equal to the mean free path in air at a pressure of 2 cm of mercury and at room temperature.

While molecular effects are significant in such conditions, the Reynolds number R based on the wire diameter can be quite small, and this is the case we consider here. We are then able to use the Oseen approximation (§3), since convection terms are only important at large distances (Cole & Roshko 1954), and this effectively enables us to treat the energy equation without a knowledge of the velocity field. The model we take for the wire is an infinite cylinder of circular cross-section, so that the flow is two-dimensional; it appears likely from available measurements that this is a good approximation in forced convection for wires of aspect ratio greater than a few thousand (Collis & Williams 1957).

The significance of molecular effects is determined by the magnitude of the Knudsen number K, the ratio of the mean free path in the gas L, to the wire diameter d. When K is negligible the gas behaves as a continuum; and when it is large, intermolecular collisions are unimportant and the oncoming gas molecules are unaffected by the presence of the wire (free-molecule flow). Slip flow occurs when K is small but not negligible, and here the mean tangential gas velocity is not zero at the wire and the gas temperature at the wire differs from the wire temperature. Finally, there is a so-called transition régime between the slip-flow and free-molecule régimes about which little is known.

We work throughout with the Navier–Stokes equations. This has often been suggested, for example, by Laitone (1956), but a consideration of the Burnett terms led Lin & Street (1954) to regard them as valid if the product of K and the

Mach number M is small. Now K may also be expressed in terms of M and R, in fact

$$K = \pi^{\frac{1}{2}}\gamma^{\frac{1}{2}}2^{-\frac{1}{2}}M/R \tag{1.1}$$

very closely, so that on these grounds the Navier–Stokes equations would be valid if M^2/R is small. We consider only the case when the density and temperature perturbations referred to their main-stream values, s and t respectively, are small; in §2.1 we show that this again demands that M^2/R should be small, and accordingly we restrict ourselves to this condition. The present writer nevertheless believes, on closer examination of the Burnett terms, that t^2/R should also be small, which is slightly more restrictive still. Note, however, that under these conditions K may still be large.

In §2.2 the boundary condition at the cylinder-gas interface is considered at some length, and arguments are given to support the use of a simple temperature-jump boundary condition when K ranges from zero to large values. Briefly, the reasons justifying this are its accordance with the boundary conditions associated with the Burnett equations and its *a posteriori* plausibility—in that order-of-magnitude agreement is achieved with the low Mach number free-molecule result when K is large.

The solution for the Nusselt number N_u, the non-dimensional heat transfer parameter, is carried through in §3 without restriction on the magnitude of K. The Oseen approximation to the energy equation together with the temperature-jump boundary condition leads to an infinite set of algebraic equations for an infinite number of unknown coefficients. Their asymptotic solution for small R is obtained and leads to a simple expression for N_u, which of course reduces to the continuum result when K is zero, and for large K predicts that N_u is proportional to σ/K, where σ is the Prandtl number. This agrees with the free-molecule low Mach number result, but in numerical magnitude is out by a factor of about 1·8, and it is suggested that our result could be used as an interpolation formula between the free-molecule and continuum régimes by adjustment of the value of the 'jump' parameter. It may be added that our result shows that the continuum result would be seriously in error when $K = O(\log[8/\sigma R])$.

2.1. The governing equations

Let p, ρ, T be the pressure, density and temperature in an ideal gas which flows steadily past a body, and denote by $p_\infty, \rho_\infty, T_\infty$ their values at a large distance where the flow is uniform in the x_1 direction with speed U. We define

$$s = (\rho - \rho_\infty)/\rho_\infty, \quad t = (T - T_\infty)/T_\infty, \quad P = (p - p_\infty)/(\rho_\infty U^2), \tag{2.1}$$

and suppose that s and t are small compared with unity. If u_i are the non-dimensional velocity components referred to U, and the x_i are non-dimensional Cartesian co-ordinates referred to a typical body dimension, then the Navier–Stokes equations become, when terms of order s, t are neglected compared with terms of order unity,

$$\partial u_i/\partial x_i = 0, \tag{2.2}$$

$$u_j \partial u_i/\partial x_j = -\partial P/\partial x_i + R^{-1}\nabla^2 u_i, \tag{2.3}$$

$$u_j \partial t/\partial x_j - R^{-1}\sigma^{-1}\nabla^2 t = (\gamma - 1)M^2 u_j \partial P/\partial x_j + R^{-1}(\gamma - 1)M^2(\partial u_i/\partial x_j + \partial u_j/\partial x_i)^2, \tag{2.4}$$

and

$$s + t = \gamma M^2 P, \tag{2.5}$$

where R is the Reynolds number referred to the typical body dimension, σ is the Prandtl number, γ is the ratio of specific heats, and M is the Mach number at infinity. It is consistent here to suppose that the thermal conductivity and the viscosity are constant. Note that (2.2) and (2.3) are the usual 'incompressible' equations which are independent of the temperature distribution, so that (2.4) is linear. The inhomogeneous terms are retained because t is not necessarily large compared with M^2.

We suppose now that R is small, so that we expect P to be of order R^{-1} roughly (for two-dimensional continuum flow past a circular cylinder it is of order $R^{-1}/\log(R^{-1})$ (Lamb 1945)); and hence if s and t are to be small then, from (2.5), M^2R^{-1} must be small. However, MR^{-1} may still be large.

2.2. The boundary conditions

We intend to use the well-known argument (Cole & Roshko 1954) that, because convection terms are small near the body and become dominant at large distances where the velocity is uniform (that is, the term $R\sigma u_j \partial\theta/\partial x_j$ is only important when $u_j \sim (1, 0)$), then no knowledge of the velocity field is needed to find a first approximation to solutions of the energy equation; and thus we shall only consider boundary conditions for t. (If this argument is applied when the perturbations t and s are not small, however, equation (2.4) is still non-linear due to the dissipation terms.)

From now on we shall be concerned with two-dimensional flow past a circular cylinder, and will take the cylinder radius as the typical length. However, by convention the Reynolds number will now be referred to the cylinder diameter, so that in the previous equations R is replaced by $\frac{1}{2}R$. Further, we will work in terms of plane polar co-ordinates (r, θ) with

$$x_1 = r\cos\theta, \quad x_2 = r\sin\theta. \tag{2.6}$$

As boundary conditions on t, we have

$$t \to 0 \quad \text{when} \quad r \to \infty, \tag{2.7}$$

and at the cylinder surface, $r = 1$, we will impose the temperature-jump condition

$$T_s - T_w = g\,\partial T_s/\partial r, \tag{2.8}$$

where T_s is the gas temperature at the wall, T_w is the wall temperature and g is a 'jump distance'. An explicit value for g often quoted, for example by Lin & Street (1954) and by Collis & Williams (1958), is

$$g = \frac{2-\alpha}{\alpha}\frac{4c\gamma}{\gamma+1}\frac{L}{\sigma}, \tag{2.9}$$

where L is the mean free path (evaluated at T_∞ to our order of approximation), α is the accommodation coefficient, usually in the neighbourhood of 0·9 for platinum-air interfaces, and c is a constant which depends on the molecular model chosen, but is anyway very close to 0·5. The derivation is referred back to Kennard (1938), although he took some pains to point out that T_s and $\partial T_s/\partial r$ do not refer to actual gas temperatures and their derivatives at the wall in his derivation. Nevertheless (2.8) and the equivalent of (2.9) appear as the significant part of the

boundary condition for the Burnett equations (Lin & Street 1954), provided that MK and tK are small even though K is not. If account is taken of (2.5) and the remarks at the end of §2.1, these conditions together with those quoted in the introduction for the validity of the Navier–Stokes equations would allow M to be as great as $R^{\frac{1}{2}}$, for example, and hence K to be of order $R^{-\frac{1}{2}}$.

We intend then to adopt the boundary condition (2.8) for both small and large values of K, with g given by (2.9), although perhaps the variation of g with $\sigma^{-1}L$ may be taken with less reserve than the remaining factor. Further grounds for the plausibility of this boundary condition are that it produces some aspects of free-molecule theory when K becomes large, in that the gas temperature tends to become independent of the wall temperature, and certainly the predicted Nusselt number in this case is of the right order of magnitude when compared with that given by free-molecule theory.

In terms of the non-dimensional temperature, the boundary condition becomes

$$t_{r=1} - t_w = h(\partial t/\partial r)_{r=1}, \tag{2.10}$$

$$h = \frac{2-\alpha}{\alpha}\frac{8c\gamma}{\gamma+1}\frac{K}{\sigma}. \tag{2.11}$$

3. The heat transfer

The energy equation now has the form

$$\nabla^2 t - \tfrac{1}{2}\sigma R u_i \partial t/\partial x_i = -\sigma M^2 \chi(x_1, x_2), \tag{3.1}$$

where χ is a known function of x_1 and x_2, and the boundary conditions are (2.7) and (2.10). Let $t^{(1)}$ be the temperature field satisfying (3.1) for which the total heat transfer from the cylinder is zero and the cylinder has the constant temperature T_e, the equilibrium temperature, and let $t^{(2)}$ be the corresponding temperature field when the cylinder is at constant temperature T_w. Then

$$t^{(3)} = t^{(2)} - t^{(1)} \tag{3.2}$$

satisfies

$$\nabla^2 t^{(3)} - 2\lambda u_i \partial t^{(3)}/\partial x_i = 0, \tag{3.3}$$

where

$$\lambda = \tfrac{1}{4}\sigma R, \tag{3.4}$$

and also satisfies the boundary conditions (2.7) and

$$t^{(3)}(1,\theta) - (t_w - t_e) = h(\partial t^{(3)}/\partial r)_{r=1}. \tag{3.5}$$

If Q is the total thermal flux from the cylinder, then this together with the contribution from the source field $\sigma M^2\chi$ must appear at infinity. Thus, if C is a very large circle surrounding the cylinder, Q together with the contribution from the source field must equal the rate of thermal transfer across C by conduction and convection, that is

$$\frac{Q}{kT_\infty} = -\oint_C \left(\frac{\partial t^{(2)}}{\partial r} - 2\lambda t^{(2)} u_n\right) ds - \iint \sigma M^2 \chi \, dS,$$

while

$$0 = -\oint_C \left(\frac{\partial t^{(1)}}{\partial r} - 2\lambda t^{(1)} u_n\right) ds - \iint \sigma M^2 \chi \, dS,$$

where k is the thermal conductivity and u_n is the outward normal velocity component on C.

Thus
$$\frac{Q}{kT_\infty} = -\oint_C \left(\frac{\partial t^{(3)}}{\partial r} - 2\lambda t^{(3)} u_n\right) ds.$$

Of course, it is obvious from these expressions that equation (3.1) commits us to take the thermal flux from the cylinder as $-k(\partial T/\partial r)_{r=1}$.

Let us finally change the dependent variable to

$$\phi = t^{(3)}/(t_w - t_e), \tag{3.6}$$

and then with the Oseen approximation we have

$$\nabla^2\phi - 2\lambda\,\partial\phi/\partial x_1 = 0, \tag{3.7}$$

$$\phi(1,\theta) - 1 = h(\partial\phi/\partial r)_{r=1}, \tag{3.8}$$

and
$$\phi \to 0 \quad \text{as} \quad r \to \infty, \tag{3.9}$$

while
$$N_u = \frac{Q}{\pi k(T_w - T_e)} = -\frac{1}{\pi}\oint_C \left(\frac{\partial\phi}{\partial r} - 2\lambda\phi\cos\theta\right) ds, \tag{3.10}$$

where N_u is the Nusselt number.

We follow Cole & Roshko (1954) and let

$$\phi = \psi \exp(\lambda r\cos\theta), \tag{3.11}$$

so that in terms of ψ
$$\nabla^2\psi - \lambda^2\psi = 0, \tag{3.12}$$

with boundary conditions

$$\psi \exp(\lambda r\cos\theta) \to 0 \quad \text{when} \quad (r \to \infty) \tag{3.13}$$

and
$$(1 - h\lambda\cos\theta)\,\psi_{r=1} - \exp(-\lambda\cos\theta) = h(\partial\psi/\partial r)_{r=1}. \tag{3.14}$$

Since ψ must be symmetrical about the x_1 axis, the appropriate solution which meets the boundary condition of infinity is of the form

$$\psi = \sum_0^\infty A_n K_n(\lambda r)\cos n\theta, \tag{3.15}$$

and from (3.10)

$$N_u = \lim_{r\to\infty} \frac{\lambda r}{\pi}\int_0^{2\pi} \exp(\lambda r\cos\theta) \sum_{n=0}^{\infty} A_n\{K_n(\lambda r)\cos n\theta\cos\theta - K_n'(\lambda r)\cos n\theta\}\,d\theta.$$

If we use the relation

$$2\pi I_n(z) = \int_0^{2\pi} \cos n\theta \exp(z\cos\theta)\,d\theta \tag{3.16}$$

and the known asymptotic forms for $I_n(z)$ and $K_n(z)$, this reduces to

$$N_u = 2\sum_0^\infty A_n. \tag{3.17}$$

It remains now to satisfy the boundary condition (3.14) at the cylinder wall, and since

$$\exp(-\lambda\cos\theta) = I_0(\lambda) + 2\sum_{n=1}^{\infty} (-1)^n I_n(\lambda)\cos n\theta,$$

we arrive at the set of equations

$$\left.\begin{aligned} [K_0(\lambda) - h\lambda K_0'(\lambda)]\,A_0 - \tfrac{1}{2}h\lambda K_1(\lambda)\,A_1 &= I_0(\lambda), \\ -h\lambda K_0(\lambda)\,A_0 + [K_1(\lambda) - h\lambda K_1'(\lambda)]\,A_1 - \tfrac{1}{2}h\lambda K_2(\lambda)\,A_2 &= -2I_1(\lambda), \\ -\tfrac{1}{2}h\lambda K_1(\lambda)\,A_1 + [K_2(\lambda) - h\lambda K_2'(\lambda)]\,A_2 - \tfrac{1}{2}h\lambda K_3(\lambda)\,A_3 &= 2I_2(\lambda), \\ \textit{etc.} \end{aligned}\right\} \tag{3.18}$$

We propose to discuss the asymptotic solution of this infinite set of equations for small λ by considering the first N, say, where N is large, and then allowing N to become infinite.

The determinant Δ of the finite set is a continuant whose diagonal terms, superdiagonal terms and subdiagonal terms are now denoted by a_n, b_n, c_n, respectively, where

$$\left.\begin{aligned} a_n &= K_{n-1}(\lambda) - h\lambda K'_{n-1}(\lambda) \quad (n \geqslant 1), \\ b_1 &= h\lambda K_1(\lambda), \\ b_n &= -\tfrac{1}{2}h\lambda K_n(\lambda), \qquad (n \geqslant 2), \\ c_1 &= -h\lambda K_0(\lambda), \\ \text{and} \quad c_n &= -\tfrac{1}{2}h\lambda K_{n-1}(\lambda), \qquad (n \geqslant 2). \end{aligned}\right\} \tag{3.19}$$

Then by Cramér's rule we have

$$A_m \Delta = D_{m+1}, \tag{3.20}$$

where D_n is the determinant obtained by replacing the nth column of Δ by the column with elements d_n defined by

$$\left.\begin{aligned} d_1 &= I_0(\lambda), \\ d_n &= (-1)^n 2I_{n-1}(\lambda) \quad (n \geqslant 2). \end{aligned}\right\} \tag{3.21}$$

Now, since Δ is a continuant, it is easy to show that if a non-diagonal element, say b_n, occurs in a term of its expansion, then c_n must also occur. If we then take account of the behaviour of $I_n(\lambda)$ and $K_n(\lambda)$ for small λ, it is possible to show that the dominant term in the expansion of Δ is given by the product of the diagonal elements, and in fact

$$\Delta = \left(\prod_{m=1}^{N} a_m\right)(1+\epsilon). \tag{3.22}$$

where

$$\left.\begin{aligned} \epsilon &= O(\lambda^2 \log \lambda) \quad \text{if} \quad h^{-1} = o(1), \\ &= O(\lambda^2) \quad \text{if} \quad h = O(1), \\ &= O(h^2\lambda^2) \quad \text{if} \quad h = o(1). \end{aligned}\right\} \tag{3.23}$$

A discussion of the determinants D_n proceeds similarly although with rather more complication, and we can show that

$$D_1 = d_1\left(\prod_{m=2}^{N} a_m\right)(1+\epsilon), \tag{3.24}$$

and

$$D_n/D_1 = O(\lambda^{2n-2}\log\lambda) \quad (n \geqslant 2), \tag{3.25}$$

for all h.

Hence

$$a_1 A_0 = d_1(1+\epsilon), \tag{3.26}$$

and

$$\sum_{n=0}^{N} A_n = A_0(1+\epsilon). \tag{3.27}$$

Thus, finally, for small λ and uniformly for all h,

$$\begin{aligned} N_u = 2\sum_{n=0}^{\infty} A_n &\sim 2d_1/a_1 \\ &\sim 2(h - \Gamma + \log(2/\lambda))^{-1}, \end{aligned} \tag{3.28}$$

where Γ ($\doteqdot 0{\cdot}5772$) is Euler's constant. In terms of the Reynolds number this result may be written

$$N_u^{-1} = \tfrac{1}{2}h - \tfrac{1}{2}\Gamma + \tfrac{1}{2}\log(8\sigma^{-1}R^{-1}) = \tfrac{1}{2}h + N_{uc}^{-1}, \tag{3.29}$$

where N_{uc} is the continuum result of Cole & Roshko.

When h is large,

$$N_u \sim 2h^{-1} = \frac{\gamma+1}{4c\gamma}\frac{\alpha}{2-\alpha}\frac{\sigma}{K}. \tag{3.30}$$

The low Mach number free-molecule result for a diatomic gas is (Stalder, Goodwin & Creager 1951)

$$N_u \sim \frac{3}{2}\frac{\gamma-1}{\gamma}\alpha\frac{\sigma}{K}, \tag{3.31}$$

so that although (3.30) predicts the correct variation with σ and K the accompanying factor is too large by a factor of about 1·8. However, in view of the assumptions made, this is quite reasonable, and it is plausible that (3.29) would provide a reasonable interpolation formula between the free-molecule régime and continuum flow if h was redefined to make (3.30) and (3.31) agree. For there are only *strong* grounds for accepting the original definition of h, i.e. equation (2.11), in a range of K where the continuum result is not greatly affected.

It is interesting to note that on other grounds Collis & Williams (1958) have attempted to fit an empirical expression of similar type to available experimental results for larger Reynolds numbers than those considered here, and have to take the rather unrealistic value of 0·695 for α in (2.11) (which reduces the above discrepancy to a factor of 1·18).

The writer wishes to thank Dr D. C. Collis, Aeronautical Research Laboratories, Melbourne, for drawing his attention to this problem and for valuable discussions.

REFERENCES

Cole, J. & Roshko, A. 1954 *Proc. Heat Transfer and Fluid Mechanics Inst., Univ. of California.*

Collis, D. C. & Williams, M. J. 1957 Australian Ministry of Supply, Aeronautical Research Laboratories, Report A 105.

Collis, D. C. & Williams, M. J. 1958 Australian Ministry of Supply, Aeronautical Research Laboratories, Report A 110.

Kennard, E. H. 1938 *Kinetic Theory of Gases.* 1st ed. New York: McGraw-Hill.

Laitone, E. V. 1956 *J. Aero. Sci.* **23**, 843.

Lamb, H. 1945 *Hydrodynamics*, 6th ed. New York: Dover.

Lin, T. C. & Street, R. E. 1954 NACA Rep. 1175.

Stalder, J. R., Goodwin, C. & Creager, M. O. 1951 NACA Rep. TN 2438.

Interactions of detonation waves

By E. LARISCH
Institute of Applied Mechanics, Bucharest

(Received 24 January 1959)

The interactions of discontinuities, in which detonation waves participate, are analysed. For this purpose detonation polars are introduced and their properties are examined. A full list of possible interactions is then given, and the use of the polars for the quantitative solution of intersection problems is illustrated.

1. Introduction

In one-dimensional flow, interaction problems involving detonation waves have been extensively treated. The literature on oblique detonation waves, however, is still very poor. The behaviour of steady-state detonation has been discussed by Rutkowski & Nicholls (1956).† The possibility of stabilizing a detonation wave on an edge has been analysed by the author (1958*a*). It has been suggested by Dunlap, Brehm & Nicholls (1958), and by the author (1958*b*), that a steady-state detonation wave be used for the combustion in a ramjet-type engine.

In the present paper, we examine the various configurations of intersections in which detonation waves participate, together with shock waves, expansion waves and shear discontinuities. The steady-state problem in which the waves 'intersect' one another is essentially equivalent to the non-steady one in which non-parallel waves 'collide'.

The data on detonation, necessary for the analysis, are first presented, and detonation polars are introduced. A complete list of possible intersections, based on the distinction introduced by Landau between incident and emerging waves, is then given; and finally a number of characteristic cases are discussed in detail.

2. Some properties of detonation waves

We start by recalling the features of detonation in gaseous combustible mixtures. An ordinary detonation wave is composed of two distinct zones; its front is a thin shock wave in which the flow is compressed and heated, and combustion then occurs in a much wider zone. This picture is altered when the thickness of the shock wave is for some reason increased, as happens for very weak or very strong shocks. The two zones may then become partially intermixed. (It is of importance that the total width of the wave is small so that its treatment as a surface of discontinuity is appropriate for all practical purposes.)

In a combustible mixture in which burning releases an amount of heat q per unit mass, detonation waves can propagate with all velocities greater than a

† The author is acquainted with this paper only from a reference in Dunlap *et al.* (1958).

characteristic minimum velocity v_J. The wave has this minimum velocity when the detonation process occurs at the Jouguet point on the detonation adiabatic. Jouguet detonation is of particular importance, since spontaneously appearing waves, or those in a flow on which sufficiently weak constraints are imposed, are always of this sort.

In a frame of reference in which a Jouguet wave in an ideal gas is at rest, the following relations hold for the normal detonation wave:

$$\left.\begin{aligned} &(a)\ v_1 = v_J = a_1 M_J = \sqrt{\left(\frac{\kappa_2-1}{2}\left[(\kappa_2+1)q + \frac{(\kappa_1+\kappa_2)p_1}{(\kappa_1-1)\rho_1}\right]\right)} \\ &\qquad\qquad + \sqrt{\left(\frac{\kappa_2+1}{2}\left[(\kappa_2-1)q + \frac{(\kappa_2-\kappa_1)p_1}{(\kappa_1-1)\rho_1}\right]\right)}, \\ &(b)\ \frac{v_2}{v_1} = \frac{\rho_1}{\rho_2} = V = \frac{1+1/(\kappa_1 M_J^2)}{1+1/\kappa_2}, \quad (c)\ \frac{p_2}{p_1} = \frac{\kappa_1 M_J^2+1}{\kappa_2+1}. \end{aligned}\right\} \tag{1}$$

More generally, the velocity v_D of the detonation wave is greater than v_J, owing to the process not taking place at the Jouguet point. The formulae are now more complicated and have the form:

$$\left.\begin{aligned} &(a)\ \frac{v_2}{v_D} = V = \frac{\kappa_2}{\kappa_2+1}\left(1+\frac{1}{\kappa_1 M_D^2}\right) - \frac{\kappa_2}{\kappa_2+1} \\ &\qquad \times \sqrt{\left(\left(1+\frac{1}{\kappa_1 M_D^2}\right)^2 - \frac{\kappa_2^2-1}{\kappa_2^2}\left\{1+\frac{M_J^2}{M_D^2}\left[\frac{\kappa_2^2}{\kappa_2^2-1}\left(1+\frac{1}{\kappa_1 M_J^2}\right)^2 - 1\right]\right\}\right)}, \\ &(b)\ M_2^2 = \frac{V}{\kappa_2(1-V+1/(\kappa_1 M_D^2))}, \quad (c)\ \frac{p_2}{p_1} = \frac{\kappa_1 M_D^2+1}{\kappa_2 M_2^2+1}. \end{aligned}\right\} \tag{2}$$

In the above relations, v is the velocity, M the Mach number, p the pressure, ρ the density, and κ the adiabatic coefficient. Indices 1 and 2 have been used to denote the gas before and after detonation.

In a flow of a combustible gas, the velocity v_J is a function of position. We now introduce the locally defined number

$$J = \frac{v}{v_J}, \tag{3}$$

which plays a role in the geometry of detonation waves analogous to that of the Mach number for shocks in inert gases. In regions of flow where $J > 1$, stationary (oblique) detonation waves, propagating with a velocity $v \geqslant v_D \geqslant v_J$ can be produced. They are inclined to the streamlines at an angle δ given by

$$\sin\delta = \frac{v_D}{v} = \frac{1}{J}\cdot\frac{v_D}{v_J}. \tag{4}$$

To obtain relations for oblique detonation waves, a tangential velocity component is superimposed on the normal wave. In the oblique detonation wave, the flow is rotated through an angle β (figure 1) given by

$$\tan\beta = \frac{(1-V)\tan\delta}{1-V\tan^2\delta}. \tag{5}$$

For the solution of problems involving oblique detonation waves it is opportune to introduce the detonation polars. In the v_{2y}–v_{2x} plane, we have

$$\left.\begin{aligned} \tan\delta &= \frac{v_1 - v_{2x}}{v_{2y}}, \\ V &= \frac{v_{2x}\sin\delta - v_{2y}\cos\delta}{v_1 \sin\delta}. \end{aligned}\right\} \tag{6}$$

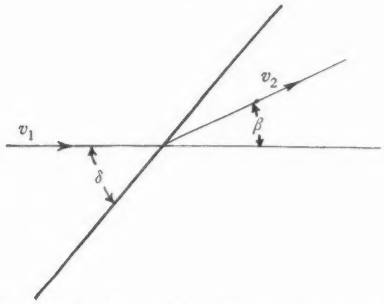

FIGURE 1. The oblique detonation wave.

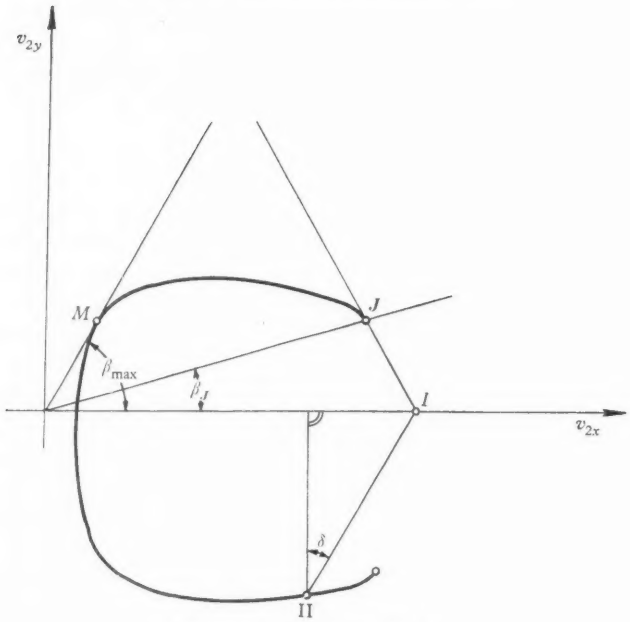

FIGURE 2. The v_{2y}–v_{2x} polar.

These equations define the polar parametrically, the parameter being the slope δ of the wave. (V depends on δ only.) The angle δ has the usual geometric representation (see figure 2). The expression $f(v_{2x}, v_{2y}) = 0$, which is an algebraic curve of the sixth degree, is long and we do not give it here. On this curve, the Jouguet detonation is represented by the point J. Only the part on the

left-hand side from (J) of the curve (6) represents detonation waves, so that the detonation polar is an open curve.

The radical in formula (6) which depends only on δ vanishes for $M_D = M_J$; hence the angle δ is a minimum at the point J. It is easily seen from this that the tangent at J to the polar passes through the point I, which represents the unburned gas. We also remark that $(d\delta/d\beta)_J = 0$. This is typical of detonation; and when $M_J - 1 \to 0$ so that the point J approaches I, $(d\delta/d\beta)_J \neq 0$. The detonation polar is always completely enclosed by the shock polar. For values of $J \gg 1$, the detonation polar approaches the shock polar for a gas moving at a Mach number M_1/J_1.

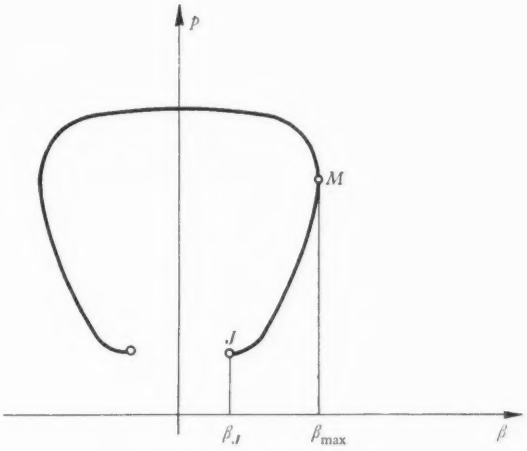

FIGURE 3. The p–β polar.

The point M, at which maximum deviation of the flow ($\beta = \beta_{max}$) is obtained, divides the polar into a region of 'weak' and one of 'strong' waves. Deviations of the flow through angles between β_J and β_{max} can be achieved by both weak and strong waves. A deviation through an angle less than β_J is not possible by a weak wave, as there is no detonation wave with Mach number less than M_J. We expect the flow pattern with detonation waves to tend, for vanishing heat release, to the usual one with shock waves. In order to achieve this correspondence, the weak wave should be chosen when possible. More details and numerical results for the flow with oblique detonation waves can be found in Larisch (1958*a*).

We shall also need the polar in the p–β plane. It is given parametrically by equations (2*c*) and (5), and its appearance is as in figure 3.

We have seen that at the Jouguet points, $d\delta/d\beta = 0$. We must have there also $dp/d\beta = 0$, so that the pressure is minimum.

Shock waves can, of course, propagate in a combustible mixture; but their intensity must be moderate, so that two conditions have to be satisfied. First, the mixture has not to be at ignition conditions behind the shock. Secondly, as can be seen from (3), the number J falls in a shock (as v decreases, v_J increases) and in a sufficiently strong shock becomes less than unity. A flow with $J < 1$ should, however, be considered as unstable with respect to the spontaneous

appearance of detonation and in the stable flow configuration the shock is replaced by a detonation wave. Shock waves which satisfy these two restrictions will be called 'permitted'.

3. Classification of intersections

We now examine the cases in which detonation waves, shock waves and shear discontinuities interact.

As usual, only a small zone surrounding a point on the line of intersection will be considered; this line can then be assumed to be straight. The motion, in a conveniently chosen frame of reference, is steady and lies in a plane normal to the intersection line. The flow pattern is obviously composed of sectors of parallel flow limited by centred expansion waves and various discontinuity surfaces.

In the treatment proposed by Landau for shock intersections, which we follow in our exposition, the distinction between 'incident' and 'emerging' waves is of chief importance. Waves in which the tangential component of the velocity is directed toward the intersection line are called incident; in the opposite case

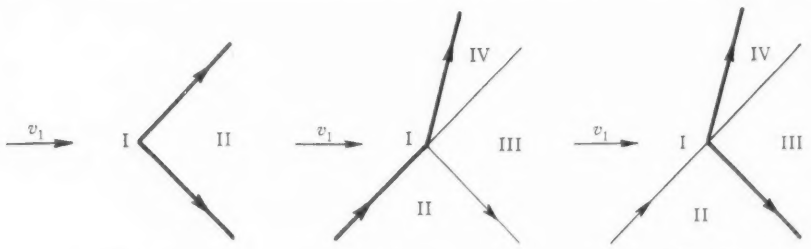

Case $A1$ Case $B1$ Case $B2$

FIGURE 4 FIGURE 5

FIGURE 4. Case A, no incident wave. Spontaneous detonation.

FIGURE 5. Case B, one incident wave. Case $B1$, splitting of a detonation wave. Case $B2$, splitting of a shock wave.

they are called emerging. Since the incident waves are produced by factors which do not depend on the intersection itself, the meeting of more than two such waves should happen only exceptionally. The same must be said of more than one incident wave intersecting a particular surface at a given point.

The known rule, asserting that a streamline cannot cross more than one emergent wave, has, in our case, an exception. Jouguet waves travel through the burned gas with sound velocity (see (1)), so that if there is such a wave among the emerging ones, it is generally continued by an expansion wave.

In zones where a combustible gas flows, we always assume that $J > 1$, and also that the burning, which occurs after the interaction, takes place in a detonation wave. Shock waves in the unburned zone are supposed to have what we have called a 'permitted intensity'.

We can now examine all possible cases of interactions. On the diagrams, fat arrows are used to denote detonation waves, thin arrows for shock waves, thin lines for shear discontinuities and dotted lines for the boundaries of expansion

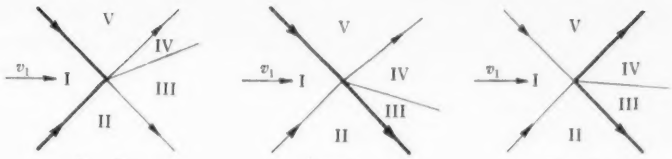

FIGURE 6. Case C, two incident waves. Intersections of waves from different families, cases $C1$, $C2$, $C3$.

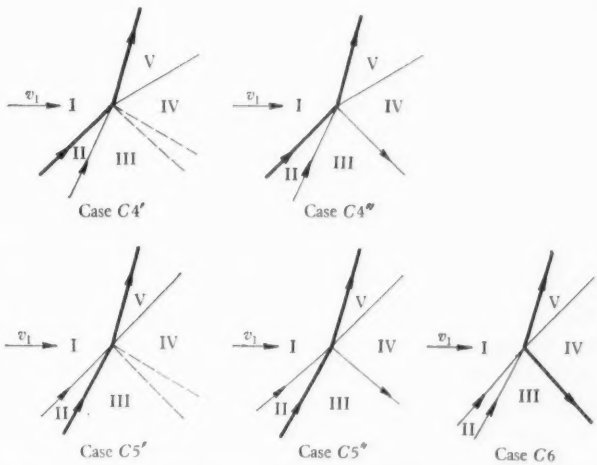

FIGURE 7. Case C, two incident waves. Intersections of waves from the same family, cases $C4'$, $C4''$, $C5'$, $C5''$, $C6$.

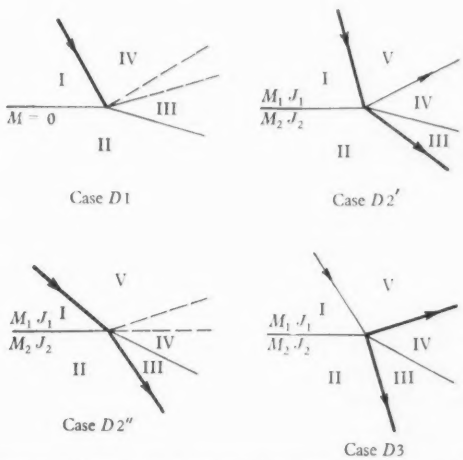

FIGURE 8. Case D, intersections with a discontinuity surface. Case $D1$, reflexion from a zone of subsonic flow. Cases $D2'$ and $D2''$, interaction of a detonation wave with a shear discontinuity. Case $D3$, interaction of a shock wave with a shear discontinuity.

fans. Expansion waves, which occur behind emergent Jouguet waves, are not specified. The intersections are classified by the number of incident waves which interact. At the end, the possible configurations for a wave intersecting a shear discontinuity surface are given.

We now briefly discuss each interaction separately. Detonation can occur in a flow spontaneously; accordingly, there is a case of intersection with no incident wave and two emerging Jouguet waves (case $A\,1$), while there are two intersections possible with one incident wave. The diagram of case $B\,1$ represents a detonation wave splitting into a more intense one and a shock wave. The inverse case, with the emerging wave weaker than the incident one and with a reflected expansion wave instead of the shock, could be observed only if the incident wave were from the strong family and is therefore not of interest. On the diagram of case $B\,2$ a shock wave is splitting and there are two emerging detonation waves.

Two types of intersections with two incident waves are possible, according as the waves deflect the flow in opposite directions or in the same one. All configurations may be met, the pair of incident waves being composed of two detonation waves, a detonation wave and a shock wave, or two shock waves. As to the intensity of the incident waves, the cases $C\,4$ and $C\,5$ might occur in two variants, with an expansion wave or a shock wave being reflected.

Three schemes might be expected to occur in the interaction with a discontinuity surface. In the case $D\,1$ the flow is subsonic on one side of the surface. The configuration of case $D\,2$ is possible in the usual two variants. In the case $D\,3$, the detonation is initiated by a shock wave. In degenerate cases the flow is inert on one side of the surface; the corresponding detonation wave is then replaced by a shock wave.

When the two incident waves are of the same intensity, the case $C\,1$ represents also the reflexion of a steady-state detonation wave from a rigid surface. It is known, however, from the case of shock waves, that this formal solution for all the cases D is to be used with care, in a steady-state motion, owing to the interaction with the boundary layer which can change the situation radically.

4. On the quantitative analysis of interactions

In order to determine the parameters of the emerging waves and those of the flow in the various zones, we make use of the fact that the pressure and the direction of the flow are the same on both sides of a shear discontinuity. The problem of finding out the intersections of the corresponding p, β polars involves here a much more intricate algebra than in the cases when shock waves only interact. There are three given parameters for the cases B, four for the cases C and five for the cases D. Obviously, solutions will exist only for a part of the domain in which these parameters are defined.

We now give indications of the way in which the most typical situations can be analysed.

It was mentioned that emerging Jouguet waves are continued by expansions. When emerging waves are looked for, the detonation polars are conveniently

drawn with the 'expansion polars' which are their continuations from the Jouguet point.

The polars for case $B2$ are drawn on figure 9. The configuration starts to be possible formally, when the p, β polar of zone II intersects the polar of zone I on its top. In this situation the intensity of the splitting shock wave is a minimum. The splitting would be actually observable only if this intensity be 'permitted'.

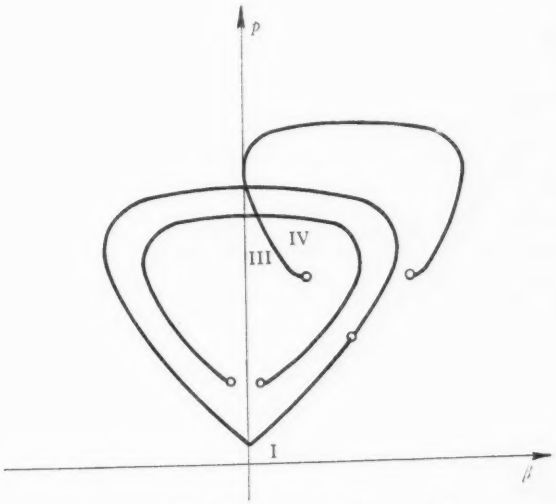

FIGURE 9. Polar diagram for case $B2$.

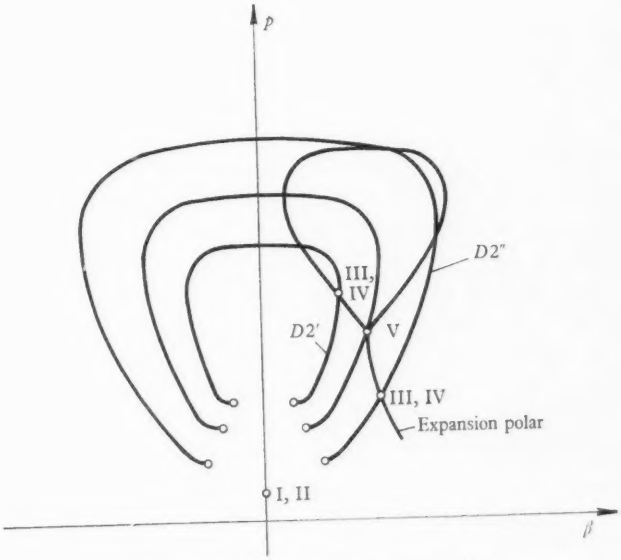

FIGURE 10. Polar diagram for cases $C4$.

It is of importance to determine when the regular reflexion of detonation waves (a particular case of $C1$) is possible. This situation has been investigated by Staniukovich (1955). When there is an incident Jouguet wave, and $\kappa = 3$, the calculations show that regular reflexion is possible as long as $\delta \gtrsim 70°$.

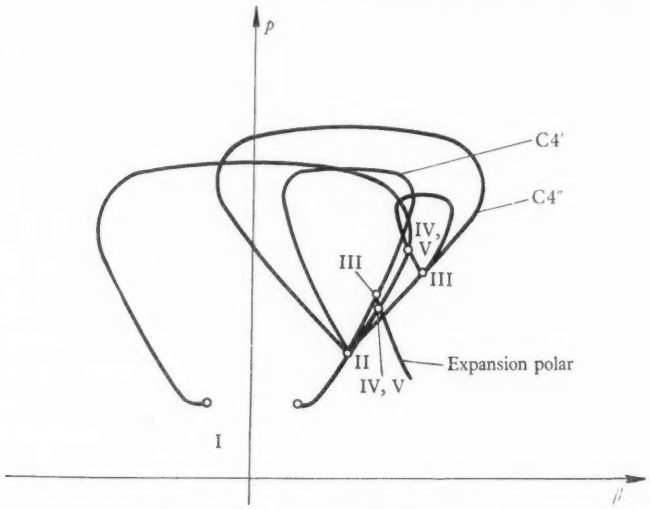

FIGURE 11. Polar diagram for cases $D2$.

In figure 10, the polar diagram for the cases $C4$ is given. The reflected wave is an expansion or a shock according as the point III lies inside or outside the detonation polar of zone I. The results are similar for the interaction case $C5$.

Finally, we show in figure 11 the polar diagram for the cases $D2$. Similar criteria as before apply as to the nature of the reflected wave. It is a shock when the detonation polar of zone II lies inside that of zone I, and an expansion in the other case.

REFERENCES

DUNLAP, R., BREHM, R. L. & NICHOLLS, J. A. 1958 *Jet Propulsion*, **28**, 7.

LARISCH, E. 1958*a* *Comunicarile Academiei R.P.R.* no. 6.

LARISCH, E. 1958*b*. *The ramjet with standing detonation wave.* Paper presented at the Meeting of the Rumanian Academy, Timisoara.

RUTKOWSKI, J. & NICHOLLS, J. A. 1956 *Proceedings of the Gas Dynamics Symposium, Northwestern University.*

STANIUKOVICH, K. P. 1955 *Neustanovivshiesia dvizenia sploshnoï sredi.* Moscow.

Horizontal diffusion in the atmosphere as determined by geostrophic trajectories

By C. S. DURST,* A. F. CROSSLEY† AND N. E. DAVIS†

* 7 Alton Road, London, S.W. 15

† Meteorological Office, Air Ministry, London, W.C. 2

(Received 24 April 1958 and in revised form 7 March 1959)

If a series of air trajectories is drawn from a fixed point at a certain height above the earth's surface, the end-points of the superimposed trajectories, after each has been followed for a time t, will have a standard vector deviation S. The purpose of this paper is to discuss the form of S. One expression is obtained by relating S empirically to the magnitude of the mean vector position $[\mathbf{x}]$ of the ends of the trajectories, so that

$$S = CL\,|[\mathbf{x}/L]|^a,$$

where L is a certain length and C and a are dimensionless constants; a is found to be about 0·870 and C is nearly proportional to $\sqrt{T}$, where T is the total period over which the series of trajectories is initiated.

A more satisfying expression for S connects it with the variability of the wind during the period of initiation of the trajectories, i.e. with the standard vector deviation of wind (σ) which is itself dependent on T. The relationship involves the Lagrangian correlation coefficient $r(t)$ of wind with time along the trajectories. It is found that the variation of S with time t agrees well with that deduced from the exponential formula $r(t) = e^{-\alpha t}$. Moreover, α, the reciprocal of the characteristic time of the 'eddies', is identified with σ^2/K where K is the coefficient of eddy viscosity for lateral mixing.

Introduction

If a trajectory of a particle of the free air is drawn from a point it will follow a meandering path; if at subsequent times a second, third and successive trajectories are initiated from the same point at equal time intervals, their paths will form a plume flowing out in the direction of the general wind stream, as shown in figures 1*a* and 1*b*. These plumes are not of exactly the same type as, for example, the plume of smoke from a chimney emitting a continuous source of pollution but are more closely paralleled by the pattern on the ground of the pollution deposited from such a chimney. The analogy is not exact in the case of geostrophic trajectories, because in a smoke plume the individual particles are free to move vertically as well as horizontally, whereas a geostrophic trajectory is the quasi-horizontal path of a point element.

To discuss these plumes of trajectories we should follow the true paths of selected elements of air, but since it is not in general possible to do so on the scale of synoptic charts, there have been substituted instead 'geostrophic

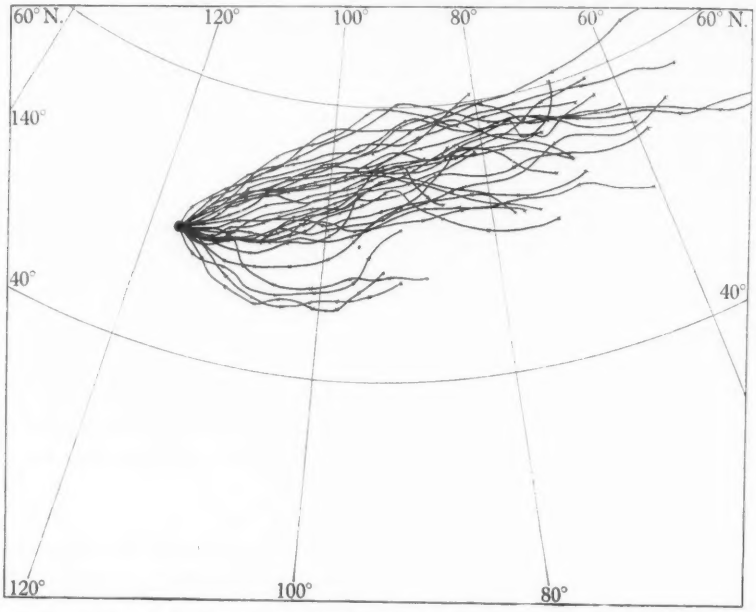

FIGURE 1*a*. Trajectories initiated twice a day and pursued for 4 days during 1–15 Aug. 1947 at 700 mb.

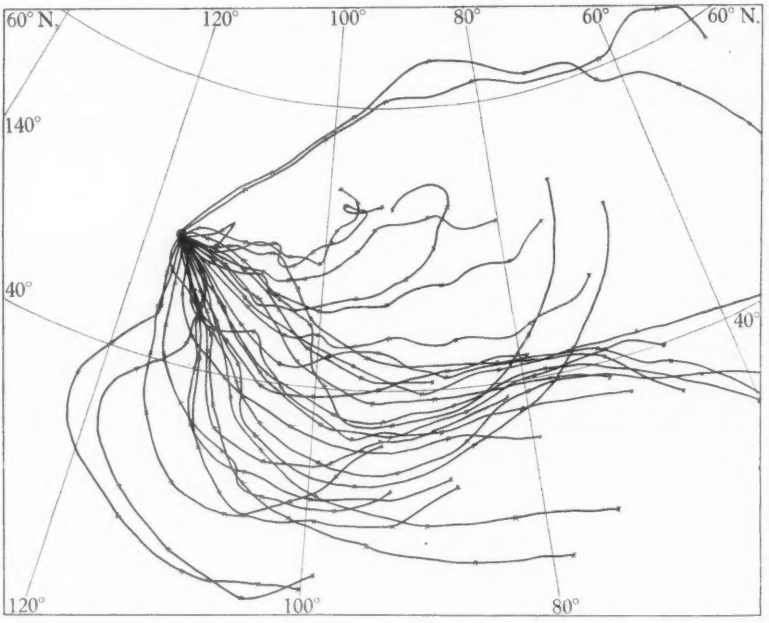

FIGURE 1*b*. Trajectories initiated twice a day and pursued for 4 days during 1–15 Nov. 1947 at 700 mb.

trajectories'. These are formed, according to common practice, by measuring the geostrophic wind near the point of origin on a synoptic or pressure contour chart, plotting the position which the air at that point will have reached after half the time interval to the next chart, measuring the geostrophic wind on the next chart, at the position at which the air will probably have arrived at the time of that (second) chart, drawing the probable track of the air up to the mid-time between the second and third charts and so on. Although individual geostrophic trajectories will no doubt vary at times considerably from the trajectories traced out by the real winds, it is believed that the standard deviation of the end-points of the geostrophic trajectories is not very different from that of the

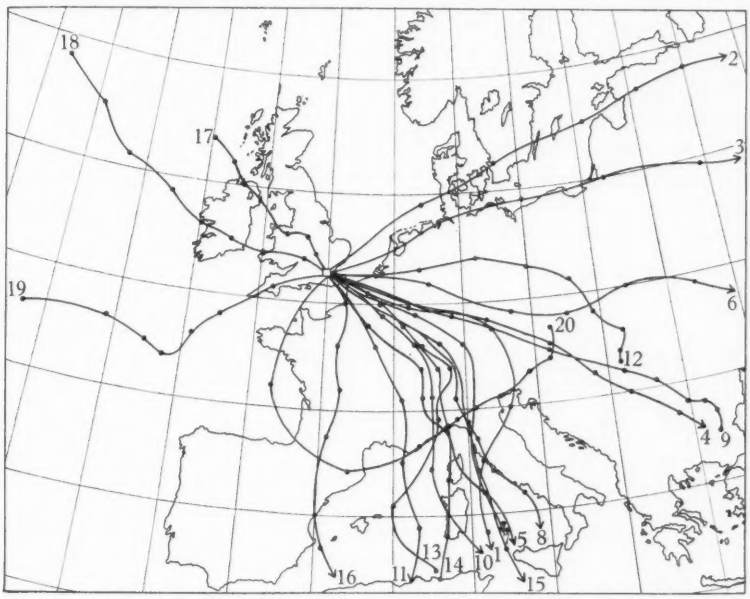

FIGURE 2. Daily trajectories, 1–20 Feb. 1948 at 700 mb.

true wind trajectories. It is hoped such studies as are given in this paper may enable the fundamental characteristics of large-scale turbulence to be more clearly understood. For that reason we have included the summarized data concerning the trajectories in an appendix so that they may be available to other workers.

The purpose of this paper is to discuss the distribution of the end-points of air trajectories initiated at regular intervals i at a point above the earth's surface and pursued for a given length of time t. It is clear that the distribution is related, not only to the time during which the trajectories are pursued, but also to the length of the period T over which they are regularly initiated. Thus there are three time scales, but if N is the number of trajectories followed $(N-1)\,i = T$ and provided N is reasonably large for a given i, the plume can be considered fairly representative of the wind régime and so the magnitude of i does not appear to be significant to the same extent as that of t and T. It is clear that the value of T is of importance in relation to the general pattern of the wind régime prevailing

during the period when the trajectories are being drawn. This is at once apparent in the comparison of figures 1*a* and 1*b* which are drawn at 700 mb over North America where data for a large area are most complete. In the former case the general circulation was strong and uniform, in the latter there was much greater meandering of the trajectories and greater variability of the individual winds. The effect is not necessarily seasonal, but it can readily be seen to be dependent on the frequency and type of eddies (depressions and anticyclones) which were passing during the period. For instance, if numerous centres of disturbances

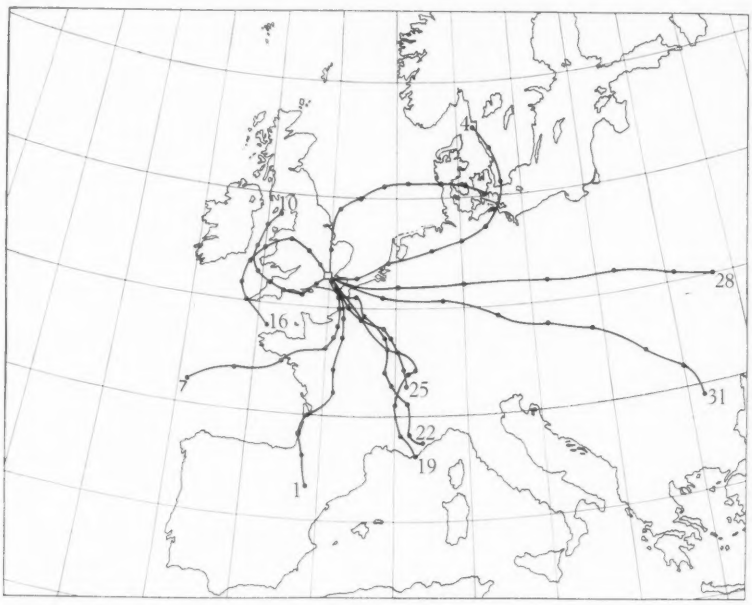

FIGURE 3. Trajectories starting every third day, July 1949 at 700 mb.

were passing over the neighbourhood of the initiation point the plume would have greater spread than if the centres of depressions were following a track to the north. Another pair of plumes is shown in figures 2 and 3 also initiated at 700 mb. In these cases the date of the individual trajectories is indicated by a figure at the end.

The expression of S as a power of the distance of the mean end-point

By a purely empirical approach, the standard vector deviation of the end-points of the trajectories can be related to the magnitude of the mean vector position $[\mathbf{x}]$ of the end-points. The formula used here is the power law

$$S = CL\,|[\mathbf{x}/L]|^a, \qquad (1)^*$$

where L is a length which is constant for any one type of trajectory and C and a are arbitrary constants. By introducing the length L, the constant C becomes

* The square brackets indicate an average over the set of N trajectories, or, equivalently, over the period of initiation T.

non-dimensional; however, it varies according to the value selected for L, being proportional to L^{a-1}.

For numerical work, L is taken to be 1 km, and this value will be assumed henceforth unless otherwise indicated. Regression equations were formed of $\log S$ on $\log |[\mathbf{x}]|$, for various time intervals up to 24 or 36 h, for the 27 cases set out in Appendix I. The correlation coefficients were very high, being 0·94 or over in all cases and 0·99 or over in 25 out of the 27 cases, but not too much weight can be attached to such values when the logarithms of numbers are being correlated. The value of a varied from 0·53 to 1·21 with an average of 0·870. It is curious that this value agrees closely with the value 0·875 deduced by Sutton (1953, p. 287) for the very different case of diffusion near the earth's surface in conditions of neutral equilibrium. The values of C varied with the period of initiation—3 months, 1 month, 2 weeks or 24 h as the case might be; more will be said of this below.

On quite a different scale there are some rather similar data available from series of smoke puffs fired from an aircraft above a camera obscura, as described by Durst (1948). These puffs were plotted in the camera obscura with trajectories lasting 1 min or $1\frac{1}{2}$ min; the period of initiation was generally $\frac{3}{4}$–1 h. From these trajectories a plume could be made up in just the same way as is shown in figure 1 and standard vector deviations of the end-points of these trajectories were found after various time intervals. Ten such families of trajectories were worked up; the mean value of a was 0·926, and that of C was 0·15.

A further collection of wind observations obtained from smoke puffs at various heights has been discussed by R. F. Jones (unpublished). Trajectories were initiated over half-hourly periods and the value of C found was 0·06 if we assume arbitrarily that the index a is 0·87.

In addition, Sutton (1932) made an estimate of the value of C from the dispersion of balloons described by Richardson & Proctor (1925). They were released over about 3 h and the value of C was 0·22 corresponding with an assumed value for a of 0·875.

Summary of values of C, a and T

The values of C derived from all the observations mentioned above have been collected together in table 1 and classified according to the period of initiation T.

The modal values of C are put in parentheses when they can be derived. The modal value of a for all the geostrophic trajectories combined is 0·878 and for the 10 smoke puffs is 0·95.

The logarithm of the period of initiation T is plotted against the logarithm of the mean value of C in figure 4. The correlation coefficient between $\log T$ and $\log C$ is 0·85, and the regression equation is

$$\log C = 0{\cdot}487 \log T - 2{\cdot}535, \tag{2}$$

whence to a close approximation $C = 0{\cdot}003T^{\frac{1}{2}}$, where T is in seconds, or $C = 0{\cdot}18T^{\frac{1}{2}}$, where T is in hours.

In these calculations, the length L as already explained has been taken as 1 km, but it is a simple matter to convert the constant C to the appropriate value for any other length; for example, if a is 0·87 and L is 10 km, the above values of C

must be multiplied by the factor 0·75; if L is 100 km, the factor is 0·56, and if L is 3000 km the factor is 0·37. It has been suggested that L might suitably be the radius of the earth, since geostrophic trajectories often extend over distances of this order within a few days. More probably perhaps L should be related to the characteristic size of the larger eddies concerned, say about 1000 km for the geostrophic trajectories considered, but only a few kilometres for the smoke puffs. However, this matter has not been pursued further.

Type of observation	Period of initiation (T)	Duration of trajectories	No. of cases	Mean value of a	Value of C ($L = 1$ km)
Geostrophic trajectories	91–92 days	36 h	2	0·865	7·67
	47 days	36 h	1	0·815	5·40
	28–31 days	36 h	8	0·844	(8·36)
	15–20 days	36 h	8	0·909	(2·23)
	24 h	24 h	8	0·848	(1·43)
Richardson's balloons	5 h	—	—	—	0·22
Smoke puffs	$\frac{3}{4}$ h	1 min	10	0·926	(0·12)
	$\frac{1}{2}$ h	—	—	—	0·06

TABLE 1. Mean values of a and C arranged according to the duration of the period of initiation T

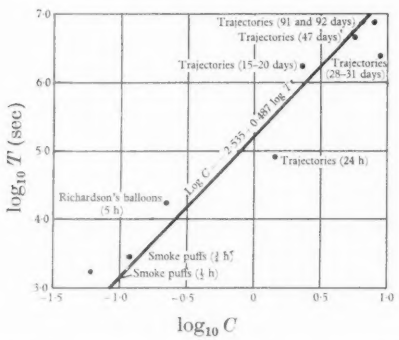

FIGURE 4. Relationship between log C and log T.

Theory

We wish to express the dispersion of the end-points of a series of trajectories, each of which has been followed for a time t from their common point of initiation, as a function of time and of the standard vector deviation of wind during the period of initiation of the trajectories. Let us suppose that a large number N of trajectories be drawn at regular intervals of time $T/(N-1)$ from a particular point in the earth's atmosphere. After an interval of t h, a typical trajectory has extended to a point with position vector $\mathbf{x}$ relative to the point of origin. Let $\mathbf{V}$ be the vector wind at any point on the trajectory. Then by vector summation

$$\mathbf{x} = \int_0^t \mathbf{V}\,dt. \tag{3}$$

Further, if we average over the N trajectories, and subtract from (3), we get

$$\mathbf{x}-[\mathbf{x}] = \int_0^t (\mathbf{V}-[\mathbf{V}])\,dt = \int_0^t \mathbf{v}\,dt, \tag{4}$$

where $\mathbf{v}$ is the vector departure from mean. That is, the vector departure from the mean of the trajectory ends can be obtained from the integral with time of the vector departure from the mean of the wind. Moreover, if S is the standard vector deviation of the end-point of the trajectories at time t after initiation,

$$S^2 = [(\mathbf{x}-[\mathbf{x}])^2] = \left[\int_0^t\int_0^t \mathbf{v}(a).\mathbf{v}(b)\,da\,db\right]. \tag{5}$$

If we assume $\mathbf{v}(t)$ to be a stationary random function of t, and write σ for the standard vector deviation of wind in the period T, i.e.

$$\sigma^2 = [\mathbf{v}(a)]^2 = [\mathbf{v}(b)]^2,$$

equation (5) becomes

$$S^2 = 2\sigma^2 \int_0^t da \int_0^a r(a-b)\,db, \tag{6}$$

where $0 \leqslant a \leqslant t$, $0 \leqslant b \leqslant t$ and $r(a-b)$ is the stretch vector correlation coefficient (Durst 1954) between $\mathbf{v}(a)$ and $\mathbf{v}(b)$. Since $r(a-b)$ is an even function, it may be shown that (6) is equivalent to

$$S^2 = 2\sigma^2 \int_0^t \int_0^{\xi'} r(\xi)\,d\xi\,d\xi', \tag{7}$$

an expression which is of the same form as that given by Taylor (1921) for diffusion parallel to a fixed axis. In order to discuss S in terms of σ we need therefore to know the behaviour of $r(t)$.

It is convenient to note here that

$$[\{\mathbf{V}(a)-\mathbf{V}(b)\}^2] = [\{\mathbf{v}(a)-\mathbf{v}(b)\}^2] = 2\sigma^2 - 2\sigma^2 r(a-b), \tag{8}$$

provided $[\mathbf{V}(a)] = [\mathbf{V}(b)]$.

The form of $r(t)$

Large-scale diffusion in the free air is controlled by the largest eddies, which in middle latitudes consist of travelling cyclones and anticyclones and the general long-wave pattern. The eddies in the free atmosphere that are concerned in any long period of diffusion may indeed be of various sizes, but their average size does not change with time in any systematic way. Taylor (1921) and others have considered the applicability of an exponential form for the Lagrangian correlation coefficient $r(t)$; in particular, Brunt (1941) argues that it holds when the eddies are all of one size. The rough constancy of the size distribution of the largest atmospheric eddies then suggests that for large-scale diffusion the form of $r(t)$ might well approximate to the exponential,

$$r(t) = e^{-\alpha t}, \tag{9}$$

in which $1/\alpha$ may be looked on as the characteristic time of those eddies which have the major effect on the motion of a particle. These eddies contain the principal part of the energy and play an important part in determining the wind

fluctuation at a fixed point (σ) and the eddy viscosity at a fixed point (K). The latter is to be regarded in the present context as the coefficient of eddy viscosity of lateral mixing. Moreover, σ^2/K has the same dimensions as α, and evidence will be produced that they are approximately equal, so that

$$r(t) \doteqdot e^{-\sigma^2 t/K}. \tag{10}$$

It is worth noting that in the sequel we find that, for geostrophic trajectories in the upper air, $1/\alpha$ is of the order of 24 h which is the time scale that would be expected from the passage of the large-scale atmospheric disturbances.

It is important to realize that for testing the form of $r(t)$ measurements must be made within ranges which are rather strictly confined. It has been pointed out by Taylor that when t is small and $r(t)$ is nearly unity, then S is initially nearly σt; also that if $r(t)$ is effectively zero for all $t \geqslant t_1$, $\int_0^t r(\xi)\,d\xi$ tends to a finite limit as t increases and consequently S varies as $t^{\frac{1}{2}}$ when t is much greater than t_1, no matter what the form of $r(t)$ is for values of t less than t_1. More precisely, we have for $t \geqslant t_1$,

$$S^2(t) \approx k(t-t_1)+S^2(t_1), \tag{11}$$

where $k = 2\sigma^2 \int_0^\infty r(\xi)\,d\xi$ is a constant. This gives a simple formula for diffusion for times exceeding t_1 and incidentally shows clearly that if we wish to examine the form of $r(t)$, it will not help if we extend the time during which the samples are followed much beyond this critical time t_1. In the case of geostrophic trajectories in the free air the critical time t_1 would appear to be about 36 h but for the surface trajectories about 18 h.

However, if we assume that $r(t)$ is exponential in form we can calculate the dispersion of the end-points of the trajectories after they have been followed for a given time t by use of (7), which on integration gives

$$\frac{S^2}{\sigma^2} = \frac{2}{\alpha^2}(\alpha t - 1 + e^{-\alpha t}) \tag{12}$$

and the values of S can then be compared with data such as those given in Appendix I.

For times greater than t_1, the exponential term in the preceding equation may be neglected; this leads to an approximation to the value of α in the form

$$\alpha = 2\sigma^2 \frac{t-t_1}{S^2-S_1^2} \quad (t > t_1). \tag{13}$$

If we now put $\alpha = \sigma^2/K$, the eddy viscosity for lateral mixing (K) is seen to be obtainable from the spread of the end-points of the trajectories; K does not depend explicitly on the standard deviation of the wind.

Magnitude of errors involved in using geostrophic trajectories

Before proceeding to the discussion of the results a word must be said as to the errors likely to arise in taking the geostrophic trajectories as representative of the true motion of the atmosphere. The principal causes of error are inaccuracy in measurement of geostrophic winds and the inherent unrepresentativeness of the geostrophic wind as a picture of the true air flow. The magnitude of these

errors over the British Isles is given by Murray (1954) and a note on their effects on trajectories by Durst & Davis (1957).

Let the true wind be $\mathbf{V}+\mathbf{v}$ and the error in its measurement be $\boldsymbol{\epsilon}$; then the calculated correlation coefficient between $\mathbf{v}(a)$ and $\mathbf{v}(b)$ becomes

$$r' = \frac{[\{\mathbf{v}(a)+\boldsymbol{\epsilon}_1\}\{\mathbf{v}(b)+\boldsymbol{\epsilon}_2\}]}{\sigma^2+[\boldsymbol{\epsilon}^2]},$$

instead of the true value $[\mathbf{v}(a)\,\mathbf{v}(b)]/\sigma^2$. Moreover, if we can assume there is little or no correlation between $\boldsymbol{\epsilon}_1$ and $\boldsymbol{\epsilon}_2$ or between $\boldsymbol{\epsilon}$ and $\mathbf{v}$ except very near time $t=0$, then

$$r' = \frac{[\mathbf{v}(a)\,\mathbf{v}(b)]}{\sigma^2+[\boldsymbol{\epsilon}^2]}.$$

If $[\boldsymbol{\epsilon}^2]$ is small in comparison with σ^2 we get

$$r-r' = [\boldsymbol{\epsilon}^2]\,r/\sigma^2.$$

If we go back to equation (7), and use the value of σ^2 deduced from the actual measurements of velocities (i.e. if we really use $\sigma^2+[\boldsymbol{\epsilon}^2]$), we see that $\sigma^2+[\boldsymbol{\epsilon}^2]$ occurs in both numerator and denominator, and in consequence there is no consistent error in S due to errors in the measurements of velocities.

It is true that a large value of $\boldsymbol{\epsilon}_1$ will lead to the apparent trajectory running away from the true trajectory with in consequence a large value of $\boldsymbol{\epsilon}_2$. This effect is discussed by Durst and Davis (1957). After 36 h the results of this effect might produce an error of 250–350 km for individual trajectories at 700 mb, and when one looks at the magnitude of the standard deviation of end-points given in Appendix I it is clear that an error of such an amount may on some occasions produce an effect which is an appreciable proportion of the true S. However, on the whole the error involved in using geostrophic trajectories in determining the values of S is probably not more than 10 %, at any rate for trajectories extending to 36 or 48 h.

Values of the correlation coefficient $r(t)$

The values of $r(t)$ have been evaluated from three types of data: (*a*) from a series of constant level balloons which were flown at 300 mb for periods of 2, 3 or 4 days (Mastenbrook & Anderson 1953); (*b*) from a considerable series of geostrophic trajectories at levels of 500 and 700 mb; and (*c*) from surface charts. The values from the constant level balloons are set out in Table 2, those of the geostrophic trajectories in Table 3.

(*a*) *Derivation from constant level balloons*

In table 2 the value of $r(t)$ has been calculated from the mean square differences between observed velocities at each time interval by means of equation (8). By proceeding in this way it was possible to obtain a considerable number of comparisons from a limited number of trajectories. The correlation coefficients nearly follow an exponential law and values of α have been calculated on the assumption that $r(t)$ is of the form $e^{-\alpha t}$.

There is, however, a difficulty in that there are errors in the positioning of the balloons which are stated to range from 20 miles in the case of good fixes to 40 miles in the case of moderately good fixes and up to 60 miles in the case of poor fixes. From internal evidence, however, it is clear that these figures are excessively high, and although any correction for position error will tend to increase all the correlation coefficients, the resulting increase in the value of K would be hardly significant.

Time interval (h) (t)		2	4	6	8	10	12	14
No. of pairs of observations		59	51	43	35	31	27	24
Standard differences (knots)	N.–S.	19	22	28	30	33	38	39
	E.–W.	17	19	22	25	28	30	32
	Vector	26	29	35	39	43	49	50
$r(t)$		0·72	0·66	0·50	0·38	0·24	0·02	−0·02
$\alpha \times 10^5\,\mathrm{sec}^{-1}$		4·5	2·9	3·2	3·4	3·9	—	—

$\sigma = 35\,\mathrm{kt}$, mean $\alpha = 3{\cdot}6 \times 10^{-5}\,\mathrm{sec}^{-1} = 0{\cdot}13\,\mathrm{h}^{-1}$, $K = \alpha/\sigma^2 = 9{\cdot}3 \times 10^{10}\,\mathrm{cm}^2\,\mathrm{sec}^{-1}$.

TABLE 2. Values of $r(t)$ derived from constant level balloons flown at 300 mb over America and the North Atlantic in latitudes north of 40° N

(*b*) *Derivation from geostrophic trajectories at* 700 *and* 500 *mb*

For a number of groups of geostrophic trajectories the winds have been tabulated after each time interval and the actual correlation coefficients between the velocity at one time and that at a subsequent time on the same trajectory have been calculated. In table 3 there are given the correlation coefficients between measured geostrophic winds at one time and at the appropriate point on the same trajectory at a subsequent time. The number of trajectories on which they are based is given. On each trajectory a number of pairs of points can be taken with the same time interval so that the correlation coefficients are based on several times as many pairs as the number of trajectories, the number of pairs being entered in parentheses in the table. Correlation coefficients are given separately for the south–north direction (S) and the west–east direction (W) and a vector correlation coefficient is also calculated and entered below the others. In October and November 1949, each month was split up into six periods of 5 days and departures from 5-day means were formed so that the average correlation coefficients were calculated for 5-day periods of initiation. Some specimens of the relationship between $\log_{10} r(t)$ and t are shown in figure 5.

The logarithms of the mean stretch-vector correlation coefficients entered in table 3 have been plotted in figure 6; these lie on a straight line and so fit a relationship such that

$$r(t) = e^{-\alpha t},$$

where $\alpha = 1{\cdot}13 \times 10^{-5}\,\mathrm{sec}^{-1}$ or $0{\cdot}041\,\mathrm{h}^{-1}$.

If, then, $\alpha = \sigma^2/K$ and $\sigma = 17{\cdot}6$ knots

$$K = 7{\cdot}2 \times 10^{10}\,\mathrm{cm}^2\,\mathrm{sec}^{-1}.$$

The exponential form of $r(t)$ has also been applied by Solot & Darling (1958)

Date	Height (mb)	No. of trajectories	Standard deviation ($k\ell$) of first 36 h		Time interval													
					6 h		12 h		18 h		24 h		30 h		36 h		42 h		48 h	
			S.	W.	S.	W.	S.	W.	S.	W.	S.	W.	S.	W.	S.	W.	S.	W.	S.	W.
1–20 Feb. 1948	700	20	19·5	21·5	0·696	0·797	0·539	0·513	0·402	0·487	0·366	0·522	0·326	0·435	0·262	0·346	—	—	—	—
			29·0		0·745 (240)		0·517 (200)		0·437 (160)		0·428 (120)		0·364 (80)		0·299 (40)					
17 Apr.–4 May 1950	700	16	10·0	11·7	0·723	0·779	0·577	0·628	0·369	0·440	0·262	0·350	0·100	0·282	0·076	0·295	0·020	0·386	—	—
			15·4		0·777 (224)		0·609 (192)		0·409 (160)		0·314 (128)		0·210 (96)		0·210 (64)		0·246 (32)			
5–20 May 1950	700	16	6·1	6·8	0·731	0·760	0·709	0·520	0·500	0·457	0·428	0·420	0·271	0·438	0·302	0·381	0·140	0·183	—	—
			9·2		0·715 (224)		0·560 (192)		0·477 (160)		0·423 (128)		0·362 (96)		0·345 (64)		0·162 (32)			
1–15 June 1950	700	15	6·2	9·3	0·666	0·828	0·463	0·750	0·326	0·607	0·304	0·505	0·232	0·500	0·262	0·337	0·276	0·139	—	—
			11·2		0·785 (210)		0·663 (180)		0·512 (150)		0·443 (120)		0·416 (90)		0·310 (60)		0·377 (30)			
17 Apr.–15 June 1950	700	47	7·8	9·5	0·721	0·785	0·575	0·652	0·368	0·496	0·329	0·411	0·190	0·376	0·191	0·326	0·129	0·295	−0·422	0·109
			12·3		0·760 (658)		0·621 (564)		0·477 (470)		0·380 (376)		0·303 (282)		0·272 (188)		0·227 (94)		−0·150	(30)
Oct. 1949	500	30	21·2	18·1	—	—	0·600	0·408	—	—	0·356	0·230	—	—	−0·013	0·148	—	—	−0·057	0·156
			27·9				0·490 (120)				0·275 (90)				0·057 (60)				0·055	(30)
Nov. 1949	500	30	13·3	18·0	—	—	0·468	0·784	—	—	0·257	0·641	—	—	0·154	0·392	—	—	−0·582	0·249
			22·4				0·671 (120)				0·499 (90)				0·293 (60)				−0·075	(15)
Apr. 1948	700	15	11·5	12·8	—	—	0·560	0·651	—	—	0·219	0·472	—	—	−0·115	0·284	—	—	−0·009	0·080
			17·3				0·613 (60)				0·369 (45)				0·095 (30)				0·037	(16)
May 1948	700	16	11·1	12·1	—	—	0·615	0·607	—	—	0·221	0·238	—	—	0·079	0·173	—	—	0·535	0·195
			16·4				0·610 (72)				0·229 (48)				0·126 (32)				0·328	(15)
June 1948	700	15	8·2	8·8	—	—	0·723	0·737	—	—	0·540	0·524	—	—	0·336	0·206	—	—	−0·110	0·390
			12·2				0·725 (60)				0·528 (45)				0·262 (30)				0·188	(46)
Apr., May, June 1948	700	46	10·7	12·8	—	—	0·620	0·719	—	—	0·299	0·518	—	—	0·029	0·420	—	—	0·214	0·324
			16·7				0·680 (192)				0·433 (138)				0·266 (92)				0·244	(30)
1–15 Nov. 1947	700	30	13·0	9·2	—	—	0·782	0·638	—	—	0·529	0·516	—	—	0·403	0·453	—	—	0·035	0·440
			15·9				0·723 (120)				0·521 (90)				0·415 (60)				0·290	(30)
1–15 Apr. 1947	700	30	6·6	4·2	—	—	0·464	0·412	—	—	0·410	0·319	—	—	0·498	0·362	—	—	—	—
			7·8				0·445 (120)				0·273 (90)				0·430 (60)					
			r.m.s.		Mean (logarithmic)		0·604		—	—	0·381		—	—	0·228		—	—	−0·380	0·132
5-day periods Oct. 1949	500	30	13·1	12·2	—	—	0·336	0·168	—	—	0·135	0·060	—	—	−0·117	−0·021	—	—	−0·162	(30)
			17·9				0·251 (120)				0·118 (90)				−0·072 (60)					
Nov. 1949	500	30	10·5	12·2	—	—	0·378	0·680	—	—	0·149	0·441	—	—	0·193	0·392	—	—	−0·006	0·315
			16·1				0·554 (120)				0·312 (90)				0·324 (60)				0·207	(30)

TABLE 3. Values of $r(t)$ derived from geostrophic trajectories

to the same problem of the spread of end-points of trajectories in the free atmosphere; the value taken for α corresponds with $0{\cdot}038\,h^{-1}$, in good agreement with the value found above.

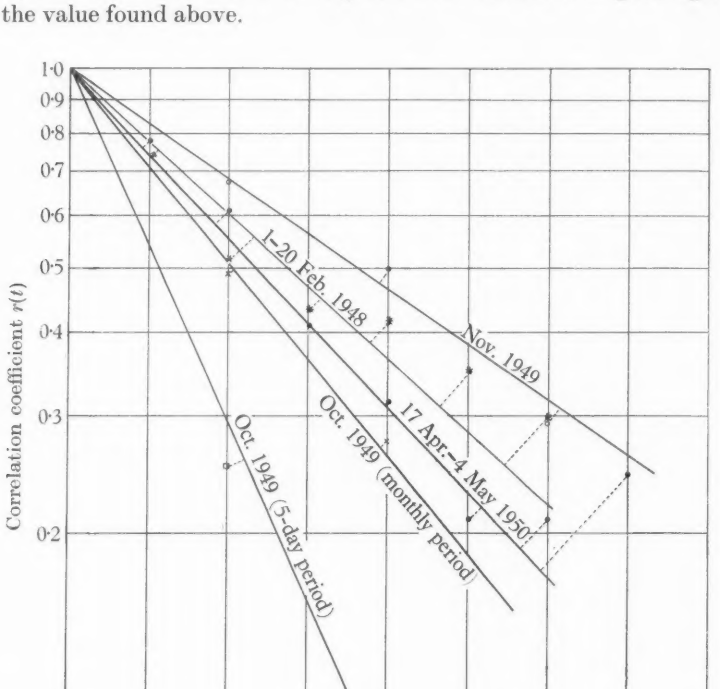

FIGURE 5. Relation between correlation coefficient, $r(t)$, and the duration of each trajectory, t.

(*c*) *Derivation from geostrophic trajectories at the surface*

From 1943 to 1946 a very close network of meteorological stations was maintained over the British Isles, and observations were plotted at 3 h intervals. Surface geostrophic trajectories were drawn from two points over the British Isles on 8 days chosen at random. These trajectories were pursued for 24 h and new ones initiated every 3 h (nine times in all) so that the period of initiation of each family of trajectories was 24 h. The winds were measured every 3 h and correlation coefficients were calculated for 6, 12, 18 and 24 h intervals from the eighteen comparisons for each family. The results are set out in table 4.

The values of α at the foot of table 4 are derived from the exponential form (9) for $r(t)$, and the value of K follows from $K = \sigma^2/\alpha$. In Appendix I there are set out the standard vector deviations of the end-points after the trajectories had been followed for various times and also the vector mean distance that the end-points had reached during those times.

In table 5 values of α and K are set out which have been derived in three independent ways. First in columns 7 they have been derived by the direct calculation of correlation coefficients from the velocities at various intervals of time. These coefficients given in tables 3 and 4 have been fitted to an exponential function from which α has been derived and hence K. Secondly, in the columns 8,

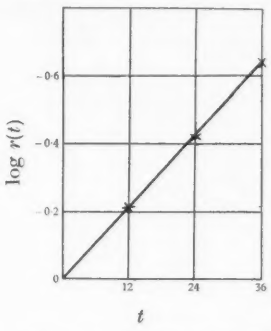

FIGURE 6. Mean value of $\log r(t)$ as function of t.

Date	No. of trajectories	Standard vector deviation (kt)	Time interval (h) 6	12	18	24
21–22 Sept. 1943	18	11·3	0·27	0·04	0·02	−0·06
25–26 Sept. 1943	18	7·7	0·43	0·59	0·10	0·21
3–4 March 1944	18	8·7	0·18	−0·08	0·01	0·13
6–7 March 1944	18	6·9	0·16	0·02	0·18	0·01
16–17 June 1944	18	12·9	0·56	0·14	0·07	−0·33
22–23 June 1944	18	6·9	0·36	−0·29	−0·59	−0·55
12–13 Dec. 1946	18	4·9	0·19	−0·04	0·17	−0·16
16–17 Dec. 1946	18	8·7	0·09	0·07	0·35	0·33
Mean	—	8·5	0·28	0·06	0·04	−0·05
$\alpha \times 10^5\,\mathrm{sec}^{-1}$	—	—	6·1	6·4	5·0	—
Mean K				$3{\cdot}3 \times 10^9\,\mathrm{cm}^2\,\mathrm{sec}^{-1}$		

TABLE 4. Vector correlation coefficients from surface geostrophic trajectories over the British Isles

the values of S/σ have been calculated from the data in Appendix I for various values of t up to 36 h for the trajectories in each group at 300, 500 and 700 mb. and up to 18 h for the surface trajectories. These have been plotted on diagrams such as figure 7 and the value of α was chosen for which the plots of S/σ gave the best fit, and again K was appropriately calculated. Figure 8 shows some specimens of the fits. Thirdly, in columns 9 the value of K has been calculated from the data in Appendix I by the use of equation (13) and the relation $\alpha = \sigma^2/K$. In these calculations t_1 was chosen to be 36 h in the upper air groups and 18 h in the surface trajectories, while t was taken as the biggest value available, which was 72 h in many cases.

Thus there were two, and in some cases three, estimates of α and K; in the case of columns 7 and 9 they were derived by quite different methods and from

(1)	(2)	(3)	(4)		(5)		(6)		(7)		(8)		(9)	
					Standard deviation vector of wind (σ)				Coefficient of eddy diffusivity for lateral mixing					
					(a) At point of initiation		(b) From all points up to 36 h		Derived from correlation coefficients		Derived from end-points of trajectories (0 to 36 h)		Derived from end-points of trajectories by $K=S^2-S_1^2/2(t-t_1)$	
Date	Height (mb)	Period of initiation (days)	Average velocity over 36 h						α	$K\ (=\sigma^2/\alpha)$	α	$K\ (=\sigma^2/\alpha)$	$\alpha\ (=\sigma^2/K)$	K
			kt	m/s	kt	m/s	kt	m/s	(h^{-1})	(cm^2/sec)	(h^{-1})	(cm^2/sec)	(h^{-1})	(cm^2/sec)
Apr.–June 1948	700	91	7	3·6	17	8·9	17	8·6	0·035	$7·6\times10^{10}$	0·05	6×10^{10}	0·033	$8·0\times10^{10}$
Oct.–Dec. 1949	500	92	20	10·3	28	14·4	—	—	—	—	0·05	15×10^{10}	0·071	$10·5\times10^{10}$
17 Apr.–15 June 1950	700	47	9	4·6	14	7·2	12	6·3	0·040	$3·6\times10^{10}$	0·05	4×10^{10}	0·029	$5·0\times10^{10}$
Apr. 1948	700	30	14	7·0	19	9·8	17	8·9	0·049	$5·8\times10^{10}$	0·07	4×10^{10}	0·041	$7·0\times10^{10}$
May 1948	700	31	6	3·1	15	7·7	16	8·4	0·053	$4·8\times10^{10}$	0·03	8×10^{10}	0·057	$4·5\times10^{10}$
June 1948	700	30	3	1·3	11	5·5	12	6·4	0·030	$4·9\times10^{10}$	0·02	7×10^{10}	0·027	$5·5\times10^{10}$
Oct. 1949	500	31	25	12·6	33	16·9	28	14·4	0·064	$11·6\times10^{10}$	0·03	2×10^{10}	0·071	$10·5\times10^{10}$
Nov. 1949	500	30	13	6·9	27	14·0	22	11·5	0·032	$14·8\times10^{10}$	0·07	7×10^{10}	0·041	$11·5\times10^{10}$
Dec. 1949	500	31	21	10·8	21	10·5	—	—	—	—	0·06	7×10^{10}	0·034	$12·0\times10^{10}$
July 1949	700	20	8	4·2	14	7·4	—	—	—	—	0·01	2×10^{10}	—	—
Aug. 1949	700	20	13	6·8	21	10·6	—	—	—	—	0·04	10×10^{10}	—	—
Feb. 1948	700	20	23	12·0	24	12·1	29	14·9	0·042	$19·0\times10^{10}$	0·06	13×10^{10}	—	—
17 Apr.–4 May 1950	700	16	10	4·9	16	8·1	15	7·9	0·046	$4·7\times10^{10}$	0·04	6×10^{10}	0·035	$6·5\times10^{10}$
5–20 May 1950	700	16	9	4·8	10	5·1	9	4·7	0·041	$1·9\times10^{10}$	0·06	1×10^{10}	0·027	$3·0\times10^{10}$
1–15 June 1950	700	15	8	3·9	11	5·4	11	5·8	0·034	$3·5\times10^{10}$	0·05	2×10^{10}	0·022	$5·5\times10^{10}$
1–15 Aug. 1947	700	15	13	6·8	9	4·8	8	4·0	0·039	$1·5\times10^{10}$	0·01	6×10^{10}	0·015	$3·9\times10^{10}$
1–15 Nov. 1947	700	15	17	8·5	15	7·9	16	8·2	0·027	$9·0\times10^{10}$	0·02	12×10^{10}	0·040	$6·0\times10^{10}$
July 1947	300	30	21	11·0	38	19·6	—	—	—	—	0·10	14×10^{10}	0·141	$9·8\times10^{10}$
Feb. 1948	300	28	25	13·0	45	22·9	—	—	—	—	0·15	13×10^{10}	0·151	$12·5\times10^{10}$
Oct. 1949	500	5	—	—	—	—	18	9·2	0·070	$4·4\times10^{10}$	—	—	—	—
Nov. 1949	500	5	—	—	—	—	16	8·3	0·043	$5·8\times10^{10}$	—	—	—	—
		(h)	Over 24 h				Up to 24 h				(0–18 h)		(18–24 h)	
21–22 Sept. 1943	Surface	24	15	7·8	10	5·0	11	5·8	—	—	0·15	8×10^9	0·12	10×10^9
25–26 Sept. 1943	Surface	24	14	7·1	8	4·1	8	3·9	—	—	0·10	5×10^9	0·55	1×10^9
3–4 Mar. 1944	Surface	24	18	9·2	6	2·9	9	4·4	—	—	0·20	3×10^9	0·10	7×10^9
6–7 Mar. 1944	Surface	24	11	5·7	4	1·9	7	3·5	—	—	0·35	1×10^9	0·22	2×10^9
16–17 June 1944	Surface	24	13	6·4	14	7·0	13	6·6	—	—	0·10	16×10^9	0·11	14×10^9
22–23 June 1944	Surface	24	8	4·0	5	2·6	7	3·5	—	—	0·50	$0·7\times10^9$	0·44	1×10^9
12–13 Dec. 1946	Surface	24	13	6·8	3	1·6	5	2·5	—	—	0·75	$0·3\times10^9$	0·22	1×10^9
16–17 Dec. 1946	Surface	24	13	6·8	5	2·4	9	4·4	—	—	0·30	2×10^9	0·10	7×10^9

Note. The values of K in columns 7 and 8 have been derived from $K=\sigma^2/\alpha$, where σ is the standard deviation taken from column 6 when available, and otherwise from column 5. The value of α in column 9 has been derived from $\alpha=\sigma^2/K$.

TABLE 5. Values of α and K deduced from the geostrophic trajectories by various methods

different portions of the trajectories, and in the case of columns 8 and 9 they were derived by somewhat the same method (i.e. by the assumption before integration that $r(t)$ followed an exponential law) but the measurements were made at different parts of the trajectories.

The agreement between the values of K is closer than that between the values of α, the correlation coefficient between the values of columns 7 and 9 being 0·92

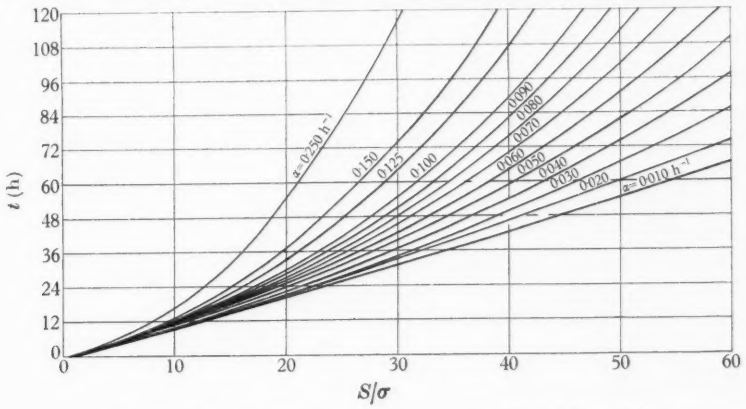

FIGURE 7. Values of ratio S/σ for various values of α and t.

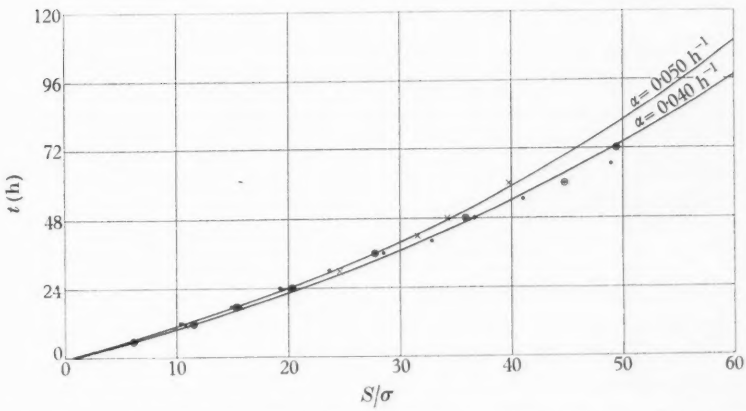

FIGURE 8. Illustration of method of deducing α from the relationship of S/σ to t.
●, 17 Apr.–15 June 1950; ⊙, Apr.–June 1948; ×, Oct.–Dec. 1949.

in the case of K and 0·64 in the case of α. In figure 9 is shown a dot diagram illustrating the relationship of the values of α and K given in column 9 with those given in column 7.

The agreement is sufficiently good to give confidence that the variations in the values of α and K are not due to casual errors. The means of the 12 available pairs of values of K are 6·1 and $6{\cdot}4 \times 10^{10}$ cm^2 sec^{-1} for columns 7 and 9 respectively; the corresponding mean values of α are 0·041 and 0·037 h^{-1}.

In table 6 there are set out the best values of σ, α and K that can be deduced

from table 5. σ is taken from column 6 of that table when possible, otherwise from column 5, and α and K are derived from the average of columns 7 and 9 (or from 8 if neither 7 nor 9 was available).

At the higher levels where the standard deviation of wind is in general greater there is clearly a tendency for both α and K to be greater. In figure 10 there is shown the relationship between K and σ; the observations at different pressure levels are indicated by various symbols.

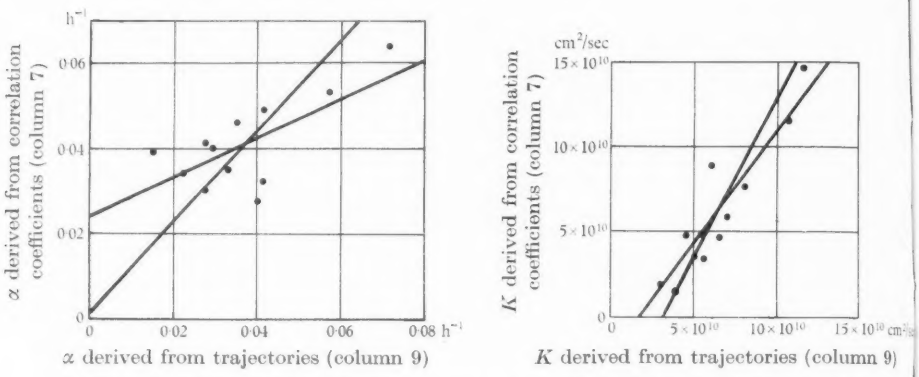

FIGURE 9. Comparison of values of α and K derived by two independent methods (see table 5).

On the diagram have also been put crosses at points representing the mean value of K against σ for tables 2 and 3. That for table 3 fits the regression line; that for table 2 (constant level balloons) is in agreement with the two 300 mb groups of geostrophic trajectories.

The relationship between K and σ for the 19 cases with observations at 500 and 700 mb is shown in figure 10, the regression of K on σ being given by

$$K = (1{\cdot}12\sigma - 2{\cdot}8)\,10^{10}\,\mathrm{cm^2\,sec^{-1}}.$$

K, however, is not in general a function of σ alone. If α were constant, K would be proportional to σ^2. On the other hand, K may be regarded as the product of eddy velocity (σ) and characteristic eddy size (σ/α), so that if the size is constant then K is proportional to σ. No doubt the truth usually lies somewhere between these two extremes.

It seems from this examination that there is fairly strong evidence that the correlation coefficients between the winds at the end-points of the trajectories follow closely an exponential law, particularly in view of the linearity in the points on figure 6 and of the agreement between the values of α shown in columns 7 and 9 of table 5. Moreover, it seems that K is probably the coefficient of eddy viscosity for lateral mixing. It is of the same order of magnitude as the values deduced by Haurwitz (1941), who quotes 4×10^7 g/cm sec for the exchange coefficient derived from the transport of heat across parallels of latitude. To obtain the corresponding figure for the eddy viscosity we have to divide this quantity by the density, i.e. by 9×10^{-4} g/cm^3 at 700 mb and 7×10^{-4} g/cm^3 at

500 mb, so obtaining 4×10^{10} cm^2/sec for 700 mb and 6×10^{10} cm^2/sec for 500 mb. Other values of the exchange coefficient have been derived by Lettau (1936) which vary with latitude from $4{\cdot}4 \times 10^7$ g/cm sec in latitude 35° to a maximum of $8{\cdot}2 \times 10^7$ g/cm sec in latitude 50°–55°; these correspond with $K = 5 \times 10^{10}$ and 9×10^{10} cm^2/sec respectively.

Date	Apr.–June 1948	17 Apr.–15 June 1950	Apr. 1948	May 1948	June 1948	July 1949	Aug. 1949
Pressure (mb)	700	700	700	700	700	700	700
σ (m sec.$^{-1}$)	8·6	6·3	8·9	8·4	6·4	7·4	10·6
α (h$^{-1} \times 10^2$)	3·4	3·5	4·5	5·5	2·9	1·0	4·0
K (cm^2 sec$^{-1} \times 10^{10}$)	7·8	4·3	6·4	4·7	5·2	2·0	10·0
Period of initiation (days)	91	47	30	31	30	20	20
Date	Feb. 1948	17 Apr.–4 May 1950	5–20 May 1950	1–15 June 1950	1–15 Aug. 1947	1–15 Nov. 1947	Oct.–Dec. 1949
Pressure (mb)	700	700	700	700	700	700	500
σ (m sec^{-1})	14·9	7·9	4·7	5·8	4·0	8·2	14·4
α (h$^{-1} \times 10^2$)	4·2	4·1	3·4	2·8	2·7	3·3	7·1
K (cm^2 sec.$^{-1} \times 10^{10}$)	19·0	5·6	2·5	4·5	2·7	7·5	10·5
Period of initiation (days)	20	16	16	15	15	15	92
Date	Oct. 1949	Nov. 1949	Dec. 1949	Oct. 1949	Nov. 1949	July 1947	Feb. 1948
Pressure (mb)	500	500	500	500	500	300	300
σ (m sec^{-1})	14·4	11·5	10·5	9·2	8·3	19·6	22·9
α (h$^{-1} \times 10^2$)	6·7	3·7	3·4	7·0	4·3	14·1	15·1
K (cm^2 sec$^{-1} \times 10^{10}$)	11·1	13·1	12·0	4·4	5·8	9·8	12·5
Period of initiation (days)	30	30	31	5	5	30	28

TABLE 6. Best values of σ, α and K derived from Table 5

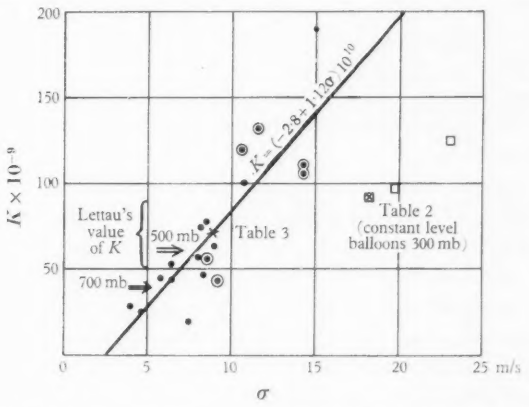

FIGURE 10. Relationship between standard deviation of wind (σ) and K. □, observations at 300 mb; ⊙, observations at 500 mb; •, observations at 700 mb; ×, results from tables 2 and 3; ⇒, Haurwitz's value of K.

The diffusion laws in relation to time scale

From this work it would seem that there is a remarkable agreement between the values of K (interpreted as the coefficient of large-scale horizontal diffusion) which we have found and those derived by other workers by quite different methods. The inference is that the Lagrangian correlation coefficients follow an exponential law. However, the empirical relation between C and T set out above would seem to support the hypothesis that the power law also applies to this type of diffusion.

We believe that both are indeed applicable for short times and that the scheme below sets out in a practical and convenient form the modes of 'diffusion' of the end-points of successive trajectories of duration t.

	$t=0$	small	moderate	large	$t\to\infty$
$r(t)$	Near unity	power law *or* exponential law			effectively zero
s.d. of end-points	σt	$CL\left\|\frac{[\mathbf{V}]t}{L}\right\|^{a}$ *or* $\frac{\sqrt{2}\sigma}{\alpha}(\alpha t-1+e^{-\alpha t})^{\frac{1}{2}}$			$P\sigma t^{\frac{1}{2}}$ *or* $(2Kt)^{\frac{1}{2}}$

Here P is a constant. It may be noted that not only is C a function of T, but σ is also a function of T, as can be seen in Appendix II; therefore C must itself be a function of σ.

Application of results to large-scale diffusion

Instantaneous emission. In this case a 'cloud' is produced instantaneously at the source. The centre of gravity of the cloud travels along a wind trajectory, meanwhile the cloud itself grows by small-scale diffusion. The examination of (geostrophic) trajectories through the source shows the area within which the centre of gravity of the cloud will have arrived after time t from the moment of generation. The most probable position will be that point arrived at by the mean trajectory (the trajectory followed by the mean wind) through the source (e.g. the appropriate monthly mean wind). If the distribution of the trajectory end-points is assumed to be Gaussian and their standard deviation is known, the probability of the centre of gravity of the cloud arriving at any particular point at time t can be set down.

Continuous emission. In this case only a point source need be considered. The particles are emitted as a continuous plume which broadens by small-scale diffusion as it gets further and further (in time) from the source. First, however, we ignore the broadening of the plumes and consider the distribution which results from the variation of the trajectories with time. If the end-points obtained by following each of a succession of trajectories for a time t have a Gaussian distribution, then the mean concentration χ of diffusing substance along a horizontal axis normal to the mean trajectory is given approximately by

$$\chi=\frac{Q}{\pi^{\frac{1}{2}}S\,|[\mathbf{V}]|}\,e^{-y^2/S^2}, \tag{14}$$

where Q is the rate of emission of diffusing substance at the source, S is the standard deviation of the distance of the end-points of the trajectories from their centre of mass, and y is distance from the mean trajectory.

If the broadening of the instantaneous plume by small-scale diffusion is taken into account, it may be remarked that (14) remains valid as a first approximation since the 'coefficient of diffusion' appropriate to the trajectories is several magnitudes greater than the coefficient of small-scale diffusion.

Moreover, S is dependent on the period of initiation in the way that has been discussed for the geostrophic trajectories; hence we can see how the mean plume gradually broadens with time as S increases.

Vertical diffusion. Hitherto only the horizontal spread has been considered. If the coefficient of eddy diffusion in the vertical K_z were known, it would be possible to estimate the vertical spread. Thus for sufficiently large t the standard deviation of the vertical spread is $\sqrt{(2K_z t)}$. Information about the value of K_z in the free atmosphere is scanty; a value of 10^3 or 10^4 cm/sec is appropriate to the friction layer, but in the free atmosphere the value is probably greater, perhaps of the order 10^5 or 10^6, or even more, according to circumstances. After 48 h the standard deviation of the vertical spread would be 0·6, 2 or 6 km according as the value of K_z is 10^4, 10^5 or 10^6 cm/sec and after 8 days would be 1, 4 or 12 km respectively.

It is seen from these figures that if the coefficient of eddy diffusion is no greater in the free atmosphere than it is in the friction layer the diffusing material would have spread out in a flat disk after a week or so, but if the diffusion coefficient is as great as 10^6 it would have spread vertically throughout the troposphere after 1 or 2 days. There is evidently need for further examination of the magnitude of the coefficient of eddy diffusion in the vertical.

When the vertical spread is pronounced, the horizontal distribution of the material may be distorted from the supposed Gaussian form by the effects of wind shear in the vertical.

We acknowledge with thanks the permission to publish this paper given by the Director-General of the Meteorological Office. We also wish to thank Sir Graham Sutton, F.R.S., and Dr F. Pasquill for the interest they have shown in our researches and for the valuable suggestions they have given us.

REFERENCES

Brunt, D. 1941 *Physical and Dynamical Meteorology*, 2nd ed. Cambridge University Press.
Durst, C. S. 1948 *Quart. J. Roy. Met. Soc.* **74**, 349.
Durst, C. S. 1954 *Geophys. Mem., Lond.*, no. 93.
Durst, C. S. & Davis, N. E. 1957 *Met. Mag.* **86**, 138.
Haurwitz, B. 1941 *Dynamic Meteorology*. New York: McGraw-Hill.
Lettau, H. 1936 *Beitr. Phys. frei. Atmos.* **23**, 45.
Mastenbrook, H. J. & Anderson, A. D. 1953 *Naval Res. Lab. Memo. Rep.* no. 240.
Murray, R. 1954 *Prof. Notes, Met. Off., Lond.*, no. 110.
Richardson, L. F. & Proctor, D. 1925 *Mem. Roy. Met. Soc.* **1**, no. 1.
Solot, S. B. & Darling, E. M. 1958 *Geophys. Res. Papers*, no. 58, Air Force Cambridge Research Center, Bedford, Mass.

SUTTON, O. G. 1932 *Proc. Roy. Soc.* A, **135**, 158.
SUTTON, O. G. 1953 *Micrometeorology*. New York: McGraw-Hill.
TAYLOR, G. I. 1921 *Proc. Lond. Math. Soc.* **20**, 196.

Appendix I

Standard vector deviation S of end-points of trajectories after various times

(N = number of trajectories, T = period of initiation)

A. Cases at 300 mb

Time (h)	July 1947 $N=30$, $T=30$ days [x] (km)	July 1947 $N=30$, $T=30$ days S (km)	February 1948 $N=28$, $T=28$ days [x] (km)	February 1948 $N=28$, $T=28$ days S (km)
6	483	423	258	494
12	805	780	610	800
18	970	1060	940	990
24	1160	1210	1190	1180
30	1340	1420	1490	1410
36	1420	1570	1680	1580
42	1570	1760	1900	1750
48	1730	1820	2100	1890

B. Cases at 500 mb

Time (h)	Oct. 1949 $N=31$, $T=31$ days [x] (km)	Oct. 1949 $N=31$, $T=31$ days S (km)	Nov. 1949 $N=30$, $T=30$ days [x] (km)	Nov. 1949 $N=30$, $T=30$ days S (km)	Dec. 1949 $N=31$, $T=31$ days [x] (km)	Dec. 1949 $N=31$, $T=31$ days S (km)	Oct.–Dec. 1949 $N=92$, $T=92$ days [x] (km)	Oct.–Dec. 1949 $N=92$, $T=92$ days S (km)
6	197	364	87	302	183	226	150	310
12	442	688	218	509	372	424	330	566
18	690	1042	380	658	541	583	523	800
24	980	1337	510	890	770	744	755	1050
30	1291	1600	682	1100	1066	882	1030	1270
36	1630	1675	897	1378	1375	1028	1330	1430
42	1924	1870	1033	1562	1710	1160	1620	1630
48	2255	1973	1253	1760	2100	1285	1950	1770
54	2485	2087	1500	1915	2358	1427	2225	1910
60	2655	2155	1710	2042	2750	1598	2530	2060
66	2820	2155	1937	2157	2840	1827	2700	2110
72	—	—	2250	2205	3530	2035	2800	2170

C. Cases at 700 mb

Time (h)	1–15 Aug. 1947 $N=30$, $T=15$ days [x] (km)	1–15 Aug. 1947 $N=30$, $T=15$ days S (km)	1–15 Nov. 1947 $N=30$, $T=15$ days [x] (km)	1–15 Nov. 1947 $N=30$, $T=15$ days S (km)
6	124	83	211	171
12	237	209	417	362
18	409	266	597	510
24	513	344	765	687
30	666	390	905	805
36	887	430	1100	950
42	1026	460	1288	1098
48	1253	521	1500	1198
54	—	—	1742	1293
60	—	—	1975	1391

D. Cases at 700 mb

Time (h)	Apr. 1948 $N=15$, $T=30$ days [x] (km)	Apr. 1948 $N=15$, $T=30$ days S (km)	May 1948 $N=16$, $T=31$ days [x] (km)	May 1948 $N=16$, $T=31$ days S (km)	June 1948 $N=15$, $T=30$ days [x] (km)	June 1948 $N=15$, $T=30$ days S (km)	Apr.–June 1948 $N=46$, $T=91$ days [x] (km)	Apr.–June 1948 $N=46$, $T=91$ days S (km)
6	198	225	81	166	25	123	98	192
12	392	462	161	317	51	245	193	363
18	500	603	197	464	103	352	252	482
24	575	727	260	617	129	458	297	650
36	915	922	405	838	167	644	462	888
48	1255	1162	489	985	240	933	621	1142
60	1685	1435	563	1208	312	1168	801	1436
72	2045	1630	710	1357	423	1343	1014	1686

E. Cases at 700 mb

Time (h)	17 Apr.–4 May 1950 $N=32$, $T=16$ days [x] (km)	17 Apr.–4 May 1950 $N=32$, $T=16$ days S (km)	5–20 May 1950 $N=32$, $T=16$ days [x] (km)	5–20 May 1950 $N=32$, $T=16$ days S (km)	1–15 June 1950 $N=30$, $T=15$ days [x] (km)	1–15 June 1950 $N=30$, $T=15$ days S (km)	17 Apr.–15 June 1950 $N=94$, $T=47$ days [x] (km)	17 Apr.–15 June 1950 $N=94$, $T=47$ days S (km)
6	99	181	96	138	81	135	89	155
12	203	339	197	240	176	226	186	274
18	317	470	328	349	262	340	302	393
24	408	604	441	440	358	432	397	501
30	523	754	565	523	447	534	510	618
36	600	947	670	576	533	628	600	743
42	717	1067	805	682	621	747	716	853
48	837	1174	885	756	722	856	815	950
54	972	1325	975	832	810	968	912	1064
60	1127	1415	1110	914	867	1049	1046	1157
66	1244	1520	1225	995	1130	1220	1195	1270
72	1389	1613	1387	965	1410	1358	1388	1348

F. Cases at 700 mb

Time (h)	1–20 Feb. 1948 $N=40$, $T=20$ days [x] (km)	1–20 Feb. 1948 $N=40$, $T=20$ days S (km)	July 1949 $N=20$, $T=20$ days [x] (km)	July 1949 $N=20$, $T=20$ days S (km)	Aug. 1949 $N=20$, $T=20$ days [x] (km)	Aug. 1949 $N=20$, $T=20$ days S (km)
6	375	261	134	160	171	230
12	675	490	223	317	287	450
18	918	629	329	469	453	631
24	1113	807	405	615	594	827
30	1327	987	480	759	749	973
36	1549	1160	547	887	887	1137

G. Surface cases ($N = 18$, $T = 24$ h)

Time (h)	21–22 Sept. 1943 [x] (km)	21–22 Sept. 1943 S (km)	25–26 Sept. 1943 [x] (km)	25–26 Sept. 1943 S (km)	3–4 Mar. 1944 [x] (km)	3–4 Mar. 1944 S (km)	6–7 Mar. 1944 [x] (km)	6–7 Mar. 1944 S (km)
3	87	54	49	44	105	31	77	21
6	183	103	90	79	202	63	145	43
9	275	144	174	103	295	94	201	59
12	375	186	261	144	407	113	254	71
15	472	223	351	158	502	148	311	88
18	554	257	453	180	613	167	345	113
21	618	293	528	191	709	210	419	134
24	671	331	611	197	792	247	496	150

Time (h)	16–17 June 1944 [x] (km)	16–17 June 1944 S (km)	22–23 June 1944 [x] (km)	22–23 June 1944 S (km)	12–13 Dec. 1944 [x] (km)	12–13 Dec. 1944 S (km)	16–17 Dec. 1944 [x] (km)	16–17 Dec. 1944 S (km)
3	81	75	45	28	77	17	82	26
6	168	138	88	59	151	37	165	59
9	253	194	130	79	225	48	236	81
12	321	242	167	91	300	55	300	104
15	381	283	201	89	378	61	378	143
18	447	321	244	79	452	68	453	169
21	504	365	290	81	520	80	527	195
24	553	365	343	95	587	93	585	225

Appendix II

The values of σ over Southern England

The standard deviation of wind $\sigma(T)$ taken over periods of duration T bears a ratio to the standard deviation σ' over a long period depending on the value of T.

Some ratios have been set out in tables A and B. Table A was derived from the comparison of winds at 500 mb observed during 15 years at Larkhill (or Crawley) in the months of January and July. Table B was derived from data given by Durst (1954) which enabled the ratio of $\sigma(T)$ to σ' to be calculated.

T	1 day	2 days	4 days	8 days	1 mth.	3 mth.	5 mth.	15 mth.
January $\sigma(T)$	17·7	24·4	29·4	32·6	38·8	40·6	41·6	41·8
$\sigma(T)/\sigma$ (15 mth.)	0·40	0·58	0·70	0·78	0·93	0·97	0·99	1·00
July $\sigma(T)$	11·6	16·2	19·4	22·6	28·4	29·3	29·5	29·6
$\sigma(T)/\sigma$ (15 mth.)	0·39	0·55	0·65	0·76	0·96	0·99	1·00	1·00

TABLE A. Value of $\sigma(T)$ in knots for various values of T

T	5 min.	15 min.	30 min.	1 h	6 h	12 h	24 h
$\sigma(T)/\sigma'$	0·037	0·062	0·088	0·111	0·22	0·30	0·41

TABLE B. Values of $\sigma(T)/\sigma'$ for various values of T

σ' is the long period value of the standard vector deviation of wind, which is a constant for the appropriate region, season and level.

Turbulent entrainment in stratified flows

By T. H. ELLISON AND J. S. TURNER
Department of the Mechanics of Fluids, University of Manchester

(Received 19 February 1959)

When a fluid which is lighter than its surroundings is emitted by a source under a sloping roof (or a heavier fluid from a source on a sloping floor), it may flow as a relatively thin turbulent layer. The motion of this layer is governed by the rate at which it entrains the ambient fluid. A theory is presented in which it is assumed that the entrainment is proportional to the velocity of the layer multiplied by an empirical function, $E(\mathrm{Ri})$, of the overall Richardson number for the layer defined by $\mathrm{Ri} = g(\rho_a - \rho)\, h/\rho_a V^2$. This theory predicts that in most practical cases the layer will rapidly attain an equilibrium state in which Ri does not vary with distance downstream, and the gravitational force on the layer is just balanced by the drag due to entrainment together with friction on the floor or roof.

Two series of laboratory experiments are described from which $E(\mathrm{Ri})$ can be determined. In the first, the spread of a surface jet of fluid lighter than that over which it is flowing is measured; in the second, a study is made of the flow of a heavy liquid down the sloping floor of a channel. These experiments show that E falls off rapidly as Ri increases and is probably negligible when Ri is more than about 0·8.

The theoretical and experimental results allow predictions to be made of flow velocities once the rate of supply of density difference is known. An estimate is also given of the uniform velocity which the ambient fluid must possess in order to cause the motion of the layer to be reversed.

1. Introduction

There are many situations in nature in which a thin layer of fluid lighter than its surroundings flows up under a sloping roof, or a layer of fluid heavier than its surroundings flows down a sloping floor. In some cases such flows are of considerable economic importance. For example, katabatic winds in the atmosphere, in which air cooled by contact with cold ground flows downhill, are of importance to agriculture because of their influence on frost damage; also they may carry smoke or fog and so affect visibility at airfields and ports. The accumulation of smog in valleys is a slightly different but related problem (Scorer 1954). In some regions, such as the coasts of Greenland and Antarctica, katabatic winds may attain great strength (Ball 1956). Some bottom currents in the ocean are similar; Dietrich (1956) has described the flow of cold water from the Arctic over a submarine ridge between Iceland and the Faroes. In estuaries, where lighter river water meets the sea, a variety of complicated

phenomena may occur (Stommel 1953); but in certain fjord-like estuaries, such as the Alberni Inlet (Tully 1949), the fresh water flows out on the sea surface in a manner which closely resembles the experiments to be described in §5.

Heavy layers may also be formed on account of the extra weight of suspended solids. This is the case in turbidity currents in the oceans (Kuenen 1952) and probably to some extent in dust-storms in the atmosphere such as the Sudan haboob (Freeman 1952). In these cases, and also in connexion with some phenomena of sea-breezes, interest centres more on the rate of advance of the leading edge of the heavy fluid than on the steady state (Berson 1958) though the latter is still important. Density currents in reservoirs (Bell 1942) are of interest to engineers because of their effect on silting. The most important example of a flow in which the moving layer is lighter than its surroundings is to be found in coal mines. Methane can accumulate near the roof and the way in which it flows and the extent to which it mixes with air have an important bearing on safety. It was this aspect of the problem which led to the work reported here being undertaken.

When planning an investigation of the flows listed above, it is useful to realize that the range of conditions which may be encountered in one context, such as the flow of methane in mines, may be greater than the difference between that situation and an apparently disconnected one, such as the flow in an estuary. It is therefore desirable to classify the flows according to fundamental hydrodynamical properties and not geophysical context. One obvious group of such properties is the relative depth, velocity and level of turbulence in the thin layers and the ambient fluid. In order to illustrate this, let us consider a source of methane in the roof of a sloping gallery in a mine. If the ambient air is at rest, the methane will form a thin layer and move up along the roof; the thickness and velocity of the layer will depend on the slope and the rate of emission of methane. If the velocity is small enough the layer may remain laminar for a considerable distance; otherwise it will become turbulent. If we now add the possibility that the ambient air may itself be moving and may either be effectively laminar (in most practical cases a very low level of turbulence would be implied rather than true laminar flow) or highly turbulent, it will be seen that a large number of cases must be considered. Each of these is likely to show its own phenomena and require its own theory.

This paper is concerned only with the case when the thin layer is turbulent and the ambient fluid either at rest or moving with a very low level of turbulence. The situation has similarities both with the motion of a buoyant plume and with the ordinary flow of water in an open channel. A theory is presented, describing the overall properties of the layer, which is based on the same physical principles as the theory of plumes but takes account of the stabilizing effect of the density difference across the edge of the layer. In place of a single entrainment constant, an entrainment function, $E(\mathrm{Ri})$, depending on the overall Richardson number of the layer, is used. This function has to be determined empirically. The theory leads to a generalization of the equations for slowly varied flow in hydraulics.

Two sets of experiments are reported which enable the function $E(\mathrm{Ri})$ to be deduced and the profiles of velocity and density in the layers to be studied. From these it is seen that stability will normally have a drastic effect on entrainment in many natural situations. While the experiments give general support for the theory, they reveal a number of minor complications.

In the final part of this paper, the application of the work is discussed and the effect of movement of the ambient fluid is calculated.

2. Entrainment

The concept of entrainment

Plumes and jets are examples of free turbulent flows; the region of turbulence is of finite extent and adjoins non-turbulent fluid of almost uniform mean velocity. The turbulent region grows with distance downstream as the non-turbulent fluid becomes *entrained* in it. This entrainment implies a flow of ambient fluid into the turbulent layer, and so, in the case where the ambient fluid is initially at rest, a small mean velocity perpendicular to the main flow.

Although the distribution of stress is not exactly the same in plumes as in jets, it is known that the velocity profiles are roughly Gaussian in both cases, and it is likely that the large-scale features of the turbulence are also much the same. It is also probable that the turbulence is not far from a state of local equilibrium uninfluenced by upstream history; and if so it must be determined by local scales of velocity and length.

Provided the Reynolds number is high enough, we should not expect molecular viscosity to influence the flow greatly (Townsend 1956). There is just a chance that the Prandtl (or Schmidt) number, ν/D, may influence the turbulent diffusion of the agent causing the density variation (temperature, salt concentration, etc.) even at very high Reynolds numbers. This was suggested by Batchelor & Townsend (1956); but since they were unable to predict the magnitude of the effect, their ideas have not been widely accepted. The point is an important one, since it bears on the relevance of experiments in a water channel to large-scale situations where the fluid is a gas, but in the absence of further information we can only ignore it for the present with a note of caution. If this is done, the velocity of inflow into the turbulent region must be proportional to the velocity scale of the layer; the constant of proportionality is called the *entrainment constant*, E.

The idea of an entrainment constant was first used explicitly by Morton, Taylor & Turner (1956) who made it the basis for their theory of plumes. More recently Morton (1959) has extended the theory to *forced plumes*, which are emitted with high momentum and so behave initially as jets. In all these cases the boundaries of the turbulent region have been not far from vertical, so it has been unnecessary to consider the action of a stable density gradient in inhibiting mixing; we refer to them as neutral cases. In the cases with which this paper is particularly concerned, such stability has a drastic influence on the value of the entrainment constant.

The numerical value of E clearly depends on the definition of the length scale that is used, and the use of scales associated with particular shapes of profile

has led to some confusion in the past. Our presentation is in terms of integrals over the profiles and avoids any assumption about their shape. For brevity, we consider only the two-dimensional case.

Definition of the entrainment constant

Take the x-axis along the plume or jet, and the y-axis perpendicular to it, measuring y from the plane of symmetry when both sides of the flow are free and from the boundary when the plume is along a floor or roof. Let $v(x, y)$ denote the mean velocity relative to that in the ambient fluid, and let $V(x)$, $h(x)$ and $\Delta(x)/g$ be the velocity, length and density scales in the cross-section, and A the flux of density difference (which is independent of x). Then the quantities V, h, A and Δ are defined by the relations:

$$Vh = \int v\,dy, \tag{1}$$

$$V^2h = \int v^2\,dy, \tag{2}$$

$$A = \int \left(\frac{\rho_a - \rho}{\rho_a}\right) g(v + V_a)\,dy$$

$$= (V + V_a)h\Delta, \tag{3}$$

where the suffix a refers to the ambient fluid.

The entrainment constant, E, can now be defined in accordance with the qualitative definition given earlier by

$$\frac{dh(V + V_a)}{dx} = E\,|V|. \tag{4}$$

Entirely analogous definitions can be given in the case of a circularly symmetrical plume or jet.

Evaluation of $E(0)$ for plumes and jets

Values of E for the neutral case can be determined from published measurements of plumes and jets.

For the two-dimensional jet (Townsend 1956, p. 193), $V \propto x^{\frac{1}{2}}$, $h = 0{\cdot}15x$, so $E = 0{\cdot}075$. For the circular jet (Townsend 1956, p. 186) we find $E = 0{\cdot}070$.

Measurements of plumes are notoriously unreliable, since the velocities involved are small and only a very little movement in the ambient fluid is needed to cause a waving of the plume and so a spurious spreading. Rouse, Yih & Humphreys (1952) have given measurements of the spread of circular and two-dimensional plumes. In the circular case their measurements lead to $E = 0{\cdot}12$ and in the two-dimensional case to $E = 0{\cdot}22$.

Although these are probably the best available measurements of plumes, they cannot be regarded as definitive. In the two-dimensional case, the source was surrounded by a wall which may have affected the flow. Measurements to be presented later in this paper do in fact confirm that the value found for two-dimensional plumes is far too high.

Another method of estimating the entrainment constant for plumes was used by Morton *et al.* (1956). They observed the height to which a plume would rise in a stably stratified environment. Allowing for the different definition used in their paper, they also found E to be 0·12 for circular plumes. Here again the measurements cannot be considered to be very precise; in particular, the greatest widths of their plumes were not small compared with the width of the tank and there must have been some downflow in the ambient fluid.

To sum up, we may say that there is some suggestion that E is greater in plumes than in jets, but that measurements on plumes have not been sufficiently precise to settle the point.

Effect of a boundary

Bakke (1957) has published measurements of a wall-jet, in which the velocity profile resembles that of one half of an ordinary two-dimensional jet, modified by the presence of a thin boundary layer along the wall. His measurements lead to a value for E of 0·072. The slight extent of the modification caused by the presence of the wall suggests that it can be taken into account by including a frictional force in the momentum equation. The outer parts of the flow are little affected by the wall, and E is in excellent agreement with the values given earlier for jets.

We shall see below, however, that in the case of inclined plumes the situation is more complex. At the rather low Reynolds numbers attainable in the laboratory, there is a tendency for the region between the wall and the velocity maximum not to become fully turbulent, and this can influence the whole flow.

3. The effect of stable stratification

It is well known that a stable density gradient strongly inhibits turbulent mixing. Richardson (1920) showed that this was to be expected from consideration of the turbulent energy balance, and in recent work (Ellison 1957; Townsend 1958) further suggestions have been put forward about the mechanism whereby the buoyancy forces destroy the turbulence. Thus when the presence of a roof or floor causes a plume to be inclined so that the mixing zone is no longer nearly vertical as in the ordinary plume, the density difference between it and the ambient fluid will give rise to a change in the value of E.

If we assume a state of local equilibrium to obtain and ignore molecular effects, we see that the only relevant dimensionless groups upon which E can depend are the absolute density difference $(\rho-\rho_a)/\rho_a$, and some parameter in the form of a Richardson number specifying the stability of the layer. This we define by:

$$\mathrm{Ri} = \frac{\Delta h \cos\alpha}{V^2} = \frac{A\cos\alpha}{V^2(V+V_a)}, \tag{5}$$

where α is the slope of the floor. Note that the Richardson number used in this discussion is a parameter specifying the *overall* state of a cross-section of the layer; and it must not be confused with the local parameter based on gradients of density and velocity. Ri is equal to the inverse square of the internal Froude

number for the layer, and the analysis could equally have been written in terms of Fr, which necessarily represents the same physical quantity as Ri.

Now it is generally agreed (Batchelor 1953) that provided the density difference is small enough, it can be neglected except where multiplied by g as in the Richardson number. This is equivalent to ignoring $(\rho-\rho_a)/\rho_a$ in the inertia terms in the equations of motion; in other words, the fluid is treated as having uniform mass but variable weight. We should note, however, that there are cases of practical importance, such as unmixed methane layers, where the density differences are large and it may not be justifiable to neglect this parameter.

Thus we may assert that provided the Reynolds number is sufficiently large and the density differences are small, E is a function only of the Richardson number, Ri. This assertion forms the basis of the theory presented in the next section. One should remember, however, that there are many situations in the laboratory and in nature when the Reynolds number is not sufficiently high to be unimportant; we shall discuss these further later.

4. The theory of inclined plumes

We consider the steady state of a layer moving up a roof over a stationary ambient fluid. The velocity and density profiles are left arbitrary, their shape being taken into account by the inclusion of two dimensionless coefficients S_1 and S_2 in the theory.

It is assumed that the ambient fluid is in hydrostatic equilibrium and that the velocities in the plume at right angles to the boundary are sufficiently small for the pressure to be found everywhere by integrating the hydrostatic equation in that direction.

The equations for continuity of mass deficiency and for entrainment can now be written as follows:

$$Vh\Delta = A = \text{constant}, \tag{6}$$

$$\frac{1}{V}\frac{d(Vh)}{dx} = E, \tag{7}$$

where E is a function of Ri, which in this case may be written $A\cos\alpha/V^3$. The momentum equation is

$$\frac{d(V^2h)}{dx} = -CV^2 - \frac{1}{2}\frac{d(S_1\Delta h^2\cos\alpha)}{dx} + S_2\Delta h\sin\alpha, \tag{8}$$

where

$$S_1\Delta h^2 = \int_0^\infty 2g\left(\frac{\rho_a-\rho}{\rho_a}\right)y\,dy \tag{9}$$

and

$$S_2\Delta h = \int_0^\infty g\left(\frac{\rho_a-\rho}{\rho_a}\right)dy. \tag{10}$$

In the momentum equation (8), we have made use of the fact that $(\rho_a-\rho)/\rho_a$ can be neglected except where it is combined with g. Equation (8) represents the momentum balance of the fluid contained in the elementary volume of unit width bounded by x, $x+dx$, $y=0$, $y=\infty$. On the left-hand side is the rate of change of momentum of the fluid. The first term on the right is the frictional

drag of the roof; the second expresses the pressure force on the layer due to its changing depth and density, that is, the difference of the integrated hydrostatic pressure on the planes x and $x+dx$; and the last term represents the force of gravity accelerating the layer. Note that while we have written the friction term as a force proportional to the square of velocity, the drag coefficient C will not be a constant even for a given wall; it will vary with the shape of the profiles and the local stability in the region near the wall. A similar effect is observed in the lower atmosphere where the drag coefficient referred to the wind at a fixed height decreases with increasing stability.

If any variation of S_1, S_2 and α with x is ignored, and use is made of (5), (8) can be written:

$$S_2 \mathrm{Ri} \tan\alpha - C = (1+\tfrac{1}{2}S_1\mathrm{Ri})\frac{dh}{dx} - \frac{(2-\tfrac{1}{2}S_1\mathrm{Ri})\,h}{3\mathrm{Ri}}\frac{d\mathrm{Ri}}{dx}. \tag{11}$$

It will be useful to have in mind the magnitudes of S_1 and S_2 during our theoretical discussion. In the experiments on inclined plumes to be described in §5 we found values ranging from 0·2 to 0·3 for S_1 and from 0·6 to 0·9 for S_2. The terms in (11) involving S_1 are likely to be relatively unimportant.

The development of the layer

The entrainment equation (7) now enables us to derive from (11) separate equations for dh/dx and $d\mathrm{Ri}/dx$. These are:

$$\frac{dh}{dx} = \frac{(2-\tfrac{1}{2}S_1\mathrm{Ri})\,E - S_2\mathrm{Ri}\tan\alpha + C}{1-S_1\mathrm{Ri}}, \tag{12}$$

and

$$\frac{h}{3\mathrm{Ri}}\frac{d\mathrm{Ri}}{dx} = \frac{(1+\tfrac{1}{2}S_1\mathrm{Ri})\,E - S_2\mathrm{Ri}\tan\alpha + C}{1-S_1\mathrm{Ri}}. \tag{13}$$

These equations play a role in the theory of inclined plumes analogous to that played by Bresse's (1860) equation in the mathematical theory of gradually varying flow of a homogeneous liquid in an open channel; if one sets $E = 0$, they reduce to Bresse's equation.

In ordinary hydraulics h and Ri are directly connected through the equation of continuity (which is simply Vh = constant in that case) so there is a certain depth at which $\mathrm{Ri} = 1$ and another depth for which $dh/dx = 0$ and $d\mathrm{Ri}/dx = 0$. In the case of the inclined plume, the behaviour of Ri is little different from that in ordinary hydraulics, but h is no longer connected uniquely with it. There is a particular value of Ri, called the *normal* value, Ri_n, determined by the slope and friction, for which the right-hand side of (13) vanishes and $d\mathrm{Ri}/dx = 0$; to determine Ri_n one must know S_1 and S_2 and use measured values for E as a function of Ri. It is found that in many practical flows Ri attains the value Ri_n in a short distance, afterwards remaining constant, but h continues to increase steadily; in fact when $\mathrm{Ri} = \mathrm{Ri}_n$,

$$\frac{dh}{dx} = E(\mathrm{Ri}_n). \tag{14}$$

The analogy with hydraulic theory may be pursued further. Equations (12) and (13) have six different forms of solution depending on the relative sizes of

$S_1\mathrm{Ri}$ at the origin, $S_1\mathrm{Ri}_n$ and 1. The distinction can still be made between tranquil (subcritical) flow in which $S_1\mathrm{Ri}$ is greater than unity and the velocity of long internal waves on the layer is greater than the flow velocity, and shooting (supercritical) flow in which $S_1\mathrm{Ri}$ is less than unity and disturbances are unable to propagate upstream. It will appear that the entrainment becomes very small when Ri is still somewhat less than unity, so that all tranquil flows are similar to the corresponding flows in ordinary hydraulics. We shall avoid the use of the words 'subcritical' and 'supercritical' to describe the state of the flow, since there is risk of confusion with the idea of a critical Richardson number at which the entrainment effectively vanishes.

The type of solution of most concern to us is that for flow down steep slopes (discussed, for example, by Bakhmeteff (1932, pp. 75–81)) in which $S_1\mathrm{Ri}_n$ and $S_1\mathrm{Ri}_0$ are both less than unity. The flow is shooting throughout. If it starts too slowly, gravity accelerates the flow until Ri approaches Ri_n; if it starts too fast, increased mixing occurs until Ri_n is again approached and there is a balance between gravity and bottom friction and entrainment.

A numerical solution of equations (12) and (13), using the knowledge of $E(\mathrm{Ri})$ obtained in a later section of this paper, shows that if, for example, the layer was initiated with $\mathrm{Ri} = 1$ and depth h_0 on a slope of 0·1, then at $x = 10h_0$, Ri would have attained a value within 0·01 of Ri_n. In fact, the rate of change of Ri near the origin is so rapid that the theory cannot be expected to be at all accurate; nevertheless the conclusion that the normal state is reached rapidly should be correct. This conclusion probably applies to a wide range of cases, and it is used in interpreting our experiments. It implies that, at a given slope, the velocity of an inclined plume depends on the rate of output of density deficiency, A, alone. The rate of spread of the edge of the plume and the entrainment E will not depend on the depth of the layer nor on the distance downstream.

5. The experimental determination of entrainment: the surface jet

The foregoing theoretical discussion leads us to expect the entrainment to depend principally on the Richardson number, but it is not yet possible to predict its magnitude or the form of the function $E(\mathrm{Ri})$ on purely theoretical grounds; these must be found experimentally. In this and the following sections two sets of experiments are described. The first were begun before the ideas of this paper had been developed, and there are therefore several features of them which may be criticized in the light of our present knowledge; however, they gave the first indication of the shape of the E *vs* Ri relation and seem worth presenting for comparison with the later independent measurements, which relate more directly to the theory.

The surface jet

The early experiments were carried out while the second author was in Cambridge and were influenced by the equipment available in the Cavendish Laboratory. It was convenient to use a tank about 15 cm wide, 20 cm deep and 5 m long, with plate-glass sides and wooden bottom and ends. At first this was fitted with

a sloping floor and attempts were made to study gravity flows directly. The essential difficulties will be discussed in connexion with the next set of experiments, but this attempt was abandoned in favour of a simpler experiment which permitted the mixing to be studied without the complications due to slope and friction. The tank was divided into two short end sections and a long centre compartment as shown in figure 1, by watertight partitions which were fastened to the sides and bottom but were slightly lower than the top of the tank. The experiment consisted of filling the centre section (*b*) with salt solution of a known density, and allowing a steady supply of tap water to fill (*a*) and flow over into (*b*) and thence to the tank (*c*), which was simply to catch this overflow.

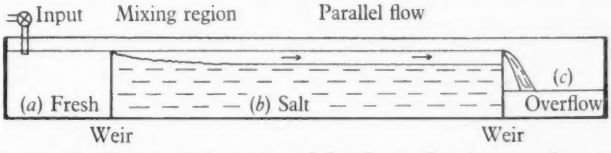

FIGURE 1. Sketch of channel used for the surface jet experiments.

With no density difference between (*a*) and (*b*) the flow formed a simple two-dimensional half-jet which at sufficiently high rates of flow became fully turbulent after a few centimetres. This then increased its depth nearly linearly with distance until the flow in (*b*) became too disturbed for it to be possible to follow the jet further. When the fluid in (*b*) was heavier than that in (*a*), there was a very different picture. Mixing began as before, but the rate of increase of depth soon became smaller and at a certain distance downstream, depending on the density difference and the rate of flow, the 'jet ' region changed smoothly to one whose depth changed very little with distance. The turbulence in the mixed layer was damped out, and there was no further mixing with the salt solution below; the layer then remained of constant depth until it reached the second weir.

These conditions could be maintained only for a relatively short time. The loss of salt from the centre reservoir meant that the flow was not really steady, but, in any case, the flow was finally disturbed by a wave on the interface travelling back from the second barrier. However, it was found possible to make all the desired measurements during the few seconds between the establishment of a nearly steady state and the breakdown due to the passage of this wave.

In order to measure velocity, small plastic particles were introduced into the flow and photographed with a cinecamera. The particles, of density slightly less than that of fresh water so that they would rise slowly through it, were released when required from a device laid along the centre of the bottom of the tank; they were spaced at about 2 cm intervals over a distance of 60 cm. The films showed the particles rising through the salt solution, moving slightly backwards because of the back flow necessary to replace the salt removed by mixing, and then moving very quickly forward as they reached the lighter layer on top. The position of no horizontal flow was slightly below that where the sudden density change occurred. To extract numerical values for the velocities, the film was

projected on to graph paper and the positions of the particles plotted frame by frame; the process is tedious, and only a few runs have been filmed and analysed completely in this way. However, the input velocity can readily be found from the flow rate and the depth at the weir; and it will be shown that useful information can be found using only this and the depth of the layer far downstream.

In the rather peculiar flow conditions of the tank, there is some doubt whether or not the velocity of the backflow should be considered a true flow in the ambient fluid; there is some suggestion that a circulation had been set up in the tank, in which case it should be ignored. In view of this doubt and the poor quality of the velocity profiles obtainable from the film, it was decided to compromise and analyse the experiments by taking the sum of one half the back flow

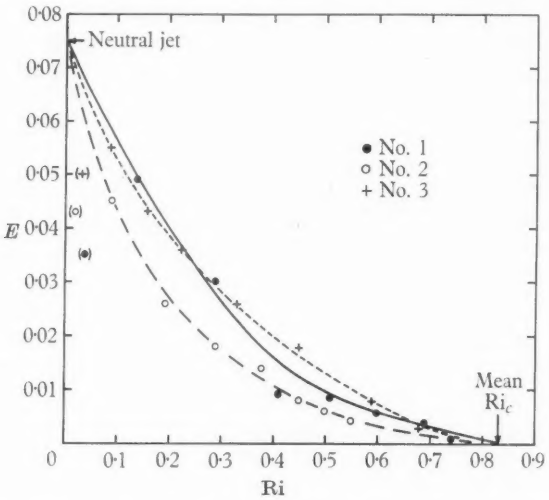

FIGURE 2. Entrainment, E, as a function of Richardson number, Ri, for three experiments on surface jets. The value of $E(0)$ has been taken from published results on neutral jets, and Ri_c obtained from a more extensive series of measurements of the depth of the final layer.

with the velocity near the top of the layer as V, and to assume that V_a was zero. For h an average of the depth of greatest density gradient and the depth of greatest velocity gradient was used. The individual points showed considerable scatter, but by averaging over a number of particles, smooth curves of $V(x)$ and $h(x)$ could be drawn. These functions were then inserted in the momentum equation (11) and it was usually found that they were not quite consistent; in that case, further small adjustments were made until (11) was satisfied. It was then possible to find E from (7) and Ri from (5). The results of three runs which have been fully analysed are shown in figure 2. The most important feature of the results is the rapid fall of E with increasing Ri.

It is of particular interest to know whether there is a 'critical' Richardson number, Ri_c, above which mixing is negligible; for example, in Expt. 1 it appears from figure 2 that Ri_c is about 0·74. A method of finding Ri_c is available which

can be applied simply to a longer series of experiments. The momentum equation (11), with $S_1 = 1$, can be integrated and written in the form

$$\frac{h(1+\frac{1}{2}\mathrm{Ri})}{\mathrm{Ri}^{\frac{3}{2}}} = \text{constant}. \tag{15}$$

This shows that we need know only the input conditions and the ultimate depth of the layer in order to find Ri_c. This depth was determined from photographs of flows in which the fresh water was dyed. The mean of the values of $\mathrm{Ri}_c^{\frac{3}{2}}/(1+\frac{1}{2}\mathrm{Ri}_c)$ was evaluated from eleven experiments (since this quantity was much more nearly normally distributed than Ri_c itself), and from this we obtain a 'best' value of $\mathrm{Ri}_c = 0{\cdot}83 \pm 0{\cdot}10$. This value is marked on figure 2.

To sum up, we have found from this series of preliminary experiments that E falls off rapidly as Ri increases, and that for values of Ri greater than about 0·8 mixing is very small. A few words of caution are necessary before we attempt to compare these results with those of the later experiments. The numerical values of E and Ri depend on the definition of the velocities and depths; we used the velocity near the surface, which in this type of flow is likely to be close to but not identical with the mean velocity assumed in the development of the theory. In applying the theory we have also tacitly assumed that there is local equilibrium at any cross-section; this is clearly not so for points near the weir (as is shown by the low values of E obtained before the jet has become fully turbulent), and any later 'memory' effects will tend to overestimate E. Also it should be noticed that the smooth E *vs* Ri curves are a result of the method of analysis, and the difference between separate experiments, not the scatter on any one curve, should be used as an indication of the magnitude of random experimental errors.

6. The experimental determination of entrainment: inclined plumes

(*a*) *Earlier measurements*

The only previous measurements on inclined plumes known to us are those of Georgeson (1942). She liberated methane or hydrogen from a shallow box on the roof of a concrete gallery 5 ft. wide, 6ft. high and 100 ft. long, having a slope of 1 in 10, and measured the depth of the layer 25 ft. and 75 ft. from the source, and the velocity of the leading edge of the layer. Her interpretation was based on an arbitrary assumption about the rate of spread of the layer, but the results may be re-evaluated using the theory of §4. She found that the velocity was proportional to the cube root of the rate of inflow and varied little with x; this agrees with our equation (5) and our conclusions about a normal Richardson number provided we assume, as Georgeson did, that the velocity she measured was equal (or at least proportional) to the velocity of the layer. If we use this velocity to calculate Ri, and obtain E by (14) from the measured rate of growth of the layers (the depth grew from 8 in. at 25 ft. to 14 in. at 75 ft.), we find $E = 0{\cdot}01$ at $\mathrm{Ri} = 0{\cdot}37$. In view of the uncertainty of interpretation of these measurements, they are in good agreement with our results. A point representing these values is shown in figure 10.

More extensive experiments of the same type are currently being conducted by Leach (1959), and we are grateful to him for permission to quote his results before publication. He releases methane into a gallery having a slope of 1:25. This has a curved roof, so that the flow is not properly two-dimensional, but due allowance has been made for the effective width and depth of the layer in calculating entrainment. Leach measures methane concentration as a function of distance from the source and from the roof, and uses the continuity of density flux to define a mean velocity—a process which is equivalent to the use of equations (6) and (10) with $S_2 = 1$. An average of four experiments, with measurements at three cross-sections, leads to values of $E = 0{\cdot}0039$ and $\mathrm{Ri} = 0{\cdot}46$; these also are shown in figure 10. Note that Ri is increased and the point brought very nearly into agreement with our curve if S_2 is taken as 0·9, which we shall see is a plausible value at high Reynolds numbers.

(*b*) *Laboratory experiments*

(i) *The experimental channel*

In planning the laboratory experiments on inclined plumes emphasis was placed on the production and maintenance of a steady state. We required a nearly two-dimensional flow whose properties remained constant in time and which could be controlled over a wide range of flow rates, density differences and slopes. As in the surface jet experiments, salt solution and water were chosen as the working fluids in preference to gases since this enabled reasonable Reynolds numbers to be obtained with apparatus of practical size. (For a given Richardson number, Reynolds number and ratio of densities, the size of the apparatus is proportional to the two-thirds power of the kinematic viscosity, so if we had used air instead of water, the apparatus would have had to be six times as large.)

The channel which was used for most of the measurements was made as large as possible consistent with the available water supply. It consisted of a Perspex box $200 \times 60 \times 10$ cm, mounted with the largest faces vertical; it could be tilted to any angle between horizontal and vertical.

The channel was filled with fresh water, and salt solution supplied from a tank in the roof of the laboratory to an opening at the upper end of the bottom of the channel. The rate of flow was controlled by a series of nozzles which could be inserted into the supply pipe. The flow provided by each of these was measured, and so, knowing the density of the salt supply (determined by weighing), one could calculate the flux of density excess, A. The solution flowed in a 10 cm wide stream down the full length and was removed, together with the fresh water that it had entrained, from the bottom corner. There was a considerable body of water above the flowing layer, so the effect of the top of the channel was negligible; but, in order to maintain a steady state, fresh water had to be added to make up for that lost by entrainment. We knew from the theory that the velocity of flow and the entrainment at a fixed slope should be independent of distance, and hence that the inflow velocity should also be constant. Therefore extra water was supplied gently at a constant rate all along the top of the tank

by forcing it through a long 'sock' about 10 cm in diameter made of cotton sheeting and connected at both ends through control valves to a constant head tank of fresh water. The arrangement is shown in figure 3.

Provision was made at 10 cm intervals along the centre of the bottom of the channel for the insertion of measuring instruments which could be traversed across the flow to give density and velocity profiles; since the flow was steady, there was sufficient time for such traverses to be made.

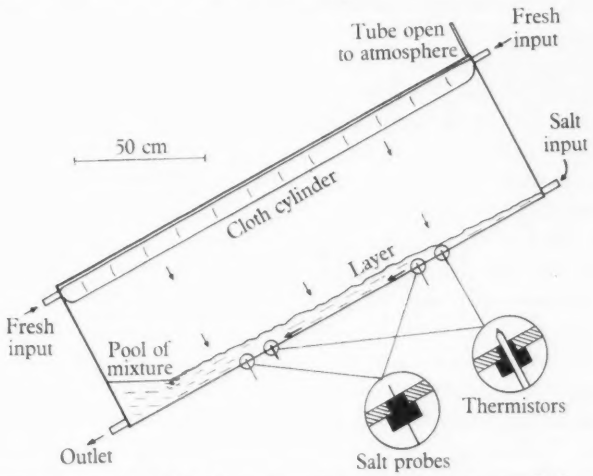

FIGURE 3. Sketch of the channel used to investigate inclined plumes.

The density was found by withdrawing samples from the desired position in the flow with a fine stainless steel tube and measuring salinity continuously in a simple conductivity cell. This consisted of two lengths of stainless steel tube (1 mm diameter for most of the experiments, but 3 mm diameter for experiments with the channel vertical when very weak samples had to be measured) mounted rigidly and joined by a short length of insulating polythene tubing leaving a 3 mm gap. A potential of 2·3 V, 50 c/s, was established across the cell and the current read on a meter; calibration was carried out directly against density using samples of known dilution.

The velocity profiles were obtained by using thermistors encased in the tips of glass tubes (Standard Telephones and Cables Ltd., Type F 23) set transversely to the flow. Each of the thermistors, which were heated with a current of about 40 mA, 50 c/s, was placed in one arm of a Wheatstone bridge adjusted to balance when there was no flow. Movement of the water cooled the thermistor and threw the bridge off balance; the out-of-balance was indicated by a meter and used as a measure of the velocity at the tip of the thermistor. Calibration was carried out directly by placing the thermistors in a pipe where dyed patches of water could be timed between fixed marks. As with all instruments working on the 'hot-wire' principle, the output is highly non-linear (the instrument being most sensitive at low speeds) and depends on the temperature of the fluid, which was therefore recorded in each experiment and calibration run.

The averaging of the considerable fluctuations in the meter readings caused by the turbulence in the flow was done by eye, making a somewhat subjective allowance for the non-linearity of the instrument.

(ii) *Description of the flow*

The salt solution can be dyed so that it can be followed easily by eye. When this is done, a wide variety of phenomena can be directly observed, and it will be instructive to describe these briefly in qualitative terms before proceeding to the detailed results of the measurements.

When the flow is started, a rounded nose moves through the static water, usually overhanging its base slightly. At low slopes and large density differences this advances at about the mean flow rate of the layer behind it; it stays about the same depth as the layer apart from a small bump at the tip followed by a depression and grows only very slowly. At large slopes and smaller density differences the nose becomes very turbulent and builds up continually to many times the thickness of the layer. Its velocity is then much smaller than that of the layer behind. This fact must be kept in mind in interpreting measurements, such as those of Georgeson already discussed or the results for turbidity currents, in which only the nose velocity was determined (although in each of these cases it is in fact likely that the nose travelled at much the same speed as the layer). The properties of noses and the factors which determine their behaviour make an interesting study in themselves, but one which cannot be pursued here.

At low flow rates and small slopes, the steady layer behind the nose remains laminar with a sharp top and no mixing with the fluid above. If the flow rate is increased, waves appear on the interface, and increase in size until their amplitude is comparable with the depth of the layer. They eventually break and transfer material upwards into the overlying water. This is a mechanism of mixing which can operate in very stable conditions, even when the density gradients are so steep that no turbulence can persist.

At high flow rates and greater slopes, the whole of the salt layer becomes turbulent, and the layer spreads out as it entrains fresh water. The outer edge is an irregular succession of large eddies, but there is an inner region, a few millimetres thick, near the floor, which is less disturbed, and which appears as strongly coloured fluid with an irregular surface. This inner layer becomes less noticeable as the flow rate increases, but at intermediate Reynolds numbers it is very important. It appears from the measured profiles that the velocity maximum occurs near the position of steep density gradient; this means that the shear is zero near the top of the inner layer and so there is locally no source of turbulent energy at this level. It is not therefore surprising that there is little transfer across the interface. There is clearly strong interdependence of Reynolds number and Richardson number effects in the range of Reynolds numbers at which we can study inclined wall plumes in the laboratory; at high slopes (and hence low Ri) very low rates of flow give turbulent plumes with no appreciable inner layer, while at low slopes (and hence high Ri) much larger rates of flow are required for the plume to become fully turbulent. A quantitative discussion

of the criterion for turbulence is beyond the scope of this paper, which must be confined to the turbulent case.

The nature of the entrainment process and the effectiveness of our method of adding fresh water to the channel may be demonstrated as follows. Dye is added briefly to the fresh water supply; this seeps out through the sock and travels straight across the channel perpendicular to the plume at all slopes. At the edge of the plume it is trapped by the large eddies and, as it becomes part of the plume fluid, travels at right angles to its previous direction and much faster. None of the fluid in the plume escapes: transfer is always into the turbulent fluid.

If too little fresh water is supplied, a pool of dilute salt solution builds up at the bottom of the tank. Usually, the supply of fresh water is adjusted until this pool just disappears, but for some purposes it is desirable to retain it; its position may be used as a measure of the entrainment as described later.

In the following sections three approaches to the problem of measuring entrainment as a function of Richardson number are described. We started with measurements involving the recording and integration of velocity profiles, but as our understanding of the process increased, proceeded to use simpler and more effective methods of characterizing the flow.

(iii) *Measurements of profiles*

In figure 4 are shown typical mean profiles of velocity and density difference for an inclined plume with a slope of 14°. Note that the velocity profiles have a steep increase to the maximum and then a gentle, nearly linear decrease to zero at the edge; the salt profiles show a very concentrated layer near the wall, but the concentration falls off sharply at about the height of the velocity maximum. The edge of the measurable salt is close to the edge of the layer

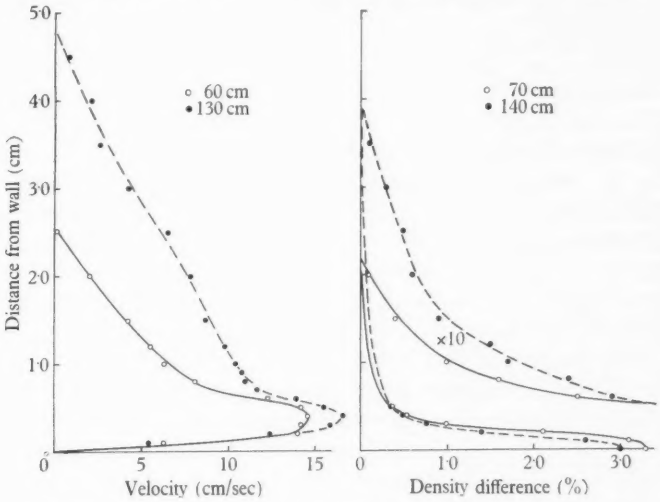

FIGURE 4. Typical profiles of (*a*) velocity, and (*b*) density in an inclined plume. 14°; $A = 144$.

indicated by the velocity profiles. The dilution of the plume and the increase of its depth with distance downstream are clearly shown.

We have integrated profiles such as these to obtain V and h defined by (1) and (2) and have then calculated E and Ri using (4) and (5). The process is tedious, but the results for a series of experiments covering a wide range of conditions are presented in figure 5. It is clear that we do not obtain by this means a single value of Ri for each slope or even a single curve of E *vs* Ri. Part of the difficulty is the limited accuracy of the velocity measurements (probably not better than $\pm 10\,\%$) and the fact that the measured velocities have to be cubed to obtain Ri. There is, however, a trend in the results suggesting that E is lower at higher Reynolds numbers (the numbers marked on the points are

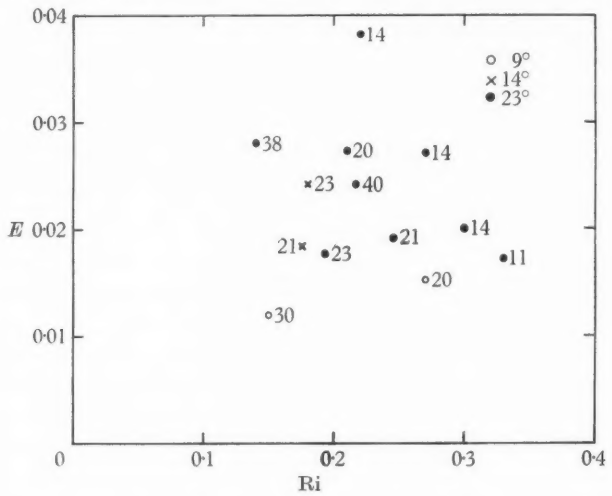

FIGURE 5. Entrainment into plumes as a function of Richardson number, obtained by integration from measured profiles. The numbers marked on the points represent the mean value of Vh during the runs.

values of Vh in the middle of the length over which E was measured). This odd effect may be attributed to the inner concentrated layer of salt. At low Reynolds numbers this carries most of the salt flux; little salt can pass the velocity maximum, but there is a turbulent region above it which is therefore hardly stabilized at all by the salinity gradient. At higher Reynolds numbers the salt is spread right across the moving layer and has a stronger inhibiting action on entrainment. This view is supported by a calculation of the factor S_2 defined by (10), which gives a measure of the spread of the salt relative to the velocity profile. We find that lower entrainment is associated with higher values of S_2, the range of S_2 for the observations shown in figure 5 being from 0·6 in a flow at low Reynolds number at 23° to 0·9 at the highest Reynolds number obtainable at 9°.

The same integration of salinity profiles enables us to estimate the friction coefficient C from (13). This is found to take values greater than would be found if the region below the velocity maximum were laminar but less than

that associated with pipe flow in a uniform fluid. The measurements are not sufficiently accurate for it to be possible to describe how the friction coefficient depends on stability and Reynolds number. Also, when the layer has thickened, its depth is no longer negligible compared with its width, and friction on the side wall is an additional complication.

(iv) *Analysis of the outer parts of the layer*

The full analysis of the profiles gave very little useful information after a great deal of labour. We shall now concentrate on the region beyond the velocity maximum, and present a quicker method of analysis. Instead of measuring V and h by integrating the profiles, we choose a characteristic velocity and

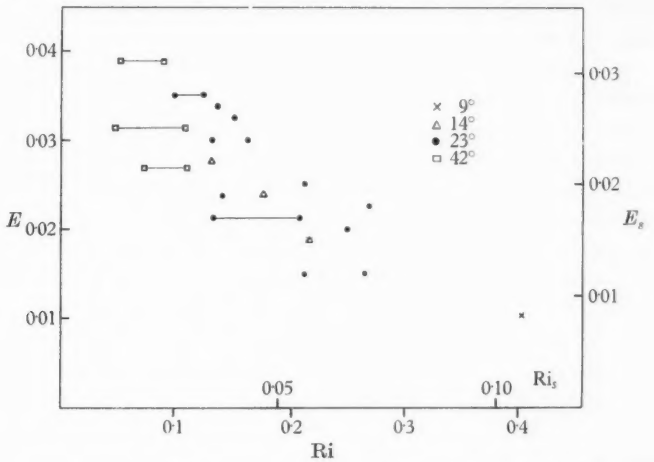

FIGURE 6. Entrainment as a function of Richardson number based on measurements of the outer parts of the plume. Scales are shown for the directly measured E_s and Ri_s, and also for the equivalent E and Ri which relate to mean properties.

length which may be found by inspection in each case. We note that the outer parts of the velocity profiles are nearly linear and so we use the intercepts of this straight portion on the height axis and on a parallel to the velocity axis through the velocity maximum, to define h_s and V_s; the density at a standard distance above the velocity maximum, $0{\cdot}2h_s$, is used to define a flux $A_s = \Delta_{\frac{1}{2}} h_s V_s$. A single integral over each velocity profile is used to determine $d(Vh)/dx$ and hence E.

The relations between V_s and V, and Ri_s and Ri, were found from a study of those cases for which both types of analysis were available to be $V = 0{\cdot}80V_s$ and $\mathrm{Ri} = 3{\cdot}8\mathrm{Ri}_s$. It should be noted, however, that these conversion factors are based almost entirely on experiments at 23° and there is some uncertainty in applying them to higher slopes; and in fact at the lower Richardson numbers the results of this method do not agree well with those of our other methods (figure 10).

The results of the simplified analysis are plotted in figure 6, where scales for both Ri and Ri_s and for E and E_s are shown. Although there is still a considerable scatter, it is less than in figure 5 and a detailed examination shows no

trend with Reynolds number. Note that sometimes two values of Ri are shown for the same E; these represent occasions on which the flow was accelerating slightly between the two measuring positions. There is clearly a decrease of entrainment with increasing Richardson number and an increase of normal Ri with decreasing slope.

(v) *Direct measurement of velocity and entrainment as a function of slope*

The success of the simple method of analysis used for the outer parts of the plume in the last section encouraged us to simplify even further and to seek a definition of a characteristic velocity which could be measured without the need to obtain profiles at all.

We have noted that the velocity maximum occurs close to the region of large density changes, which with coloured salt solution is visible as a sharp interface a few millimetres from the wall. Irregularities or turbulent eddies at this level may be followed by eye and their passage between fixed marks on the channel timed to give a reproducible measure of velocity. Comparison of velocities obtained in this way with measured profiles shows that, when a sharp layer is present, one tends to follow waves on the interface and find a velocity slightly larger than the maximum mean particle velocity. The relation between V and the layer velocity, V_L, is $V = 0{\cdot}60V_L$ at 23°; at higher slopes, when there is no sharp inner layer, there is evidence that V_L is close to the maximum velocity and that $V = 0{\cdot}7V_L$. (Note that if V_L was exactly the maximum velocity, the factor would be 0·70 for Gaussian profiles and 0·67 for triangular profiles.) The results have been interpreted on the assumption that the factor is a linear function of slope varying from 0·60 at 23° to 0·70 at 90°. Any uncertainty introduced by this somewhat arbitrary procedure is not large. Richardson numbers have been calculated using A found from the known input rates and densities of the salt supply.

The entrainment was measured by making use of the pool of dyed salt solution at the bottom corner of the channel. When the flow rates are adjusted so that a steady small pool forms, we know that the length of the entraining layer extends from the input to the top surface of this pool; mixing within the pool does not remove any further fresh water from the channel. The total rate of output was measured with a bucket and a stop-watch, and so, after subtracting the salt input, $d(Vh)/dx$ could be found. Thus with the aid of the velocities obtained from the timing of the layer we can evaluate E. The method is much less laborious than the earlier ones, and a more extensive series of measurements has been possible.

The results, which cover a wide range of output rates, density differences and slopes, are shown in figure 7. We have also plotted E and A/V^3 as functions of slope in figures 8 and 9, since these relations are often required in practice. It is of particular interest to note that the value of E found for a vertical wall plume is 0·087, compared with the value of 0·075 for a neutral jet. We would not attach much significance to the difference between these values; but we can say confidently that E is not as high as 0·22 which, as mentioned earlier, is the value corresponding to the measurements of Rouse *et al.* (1952).

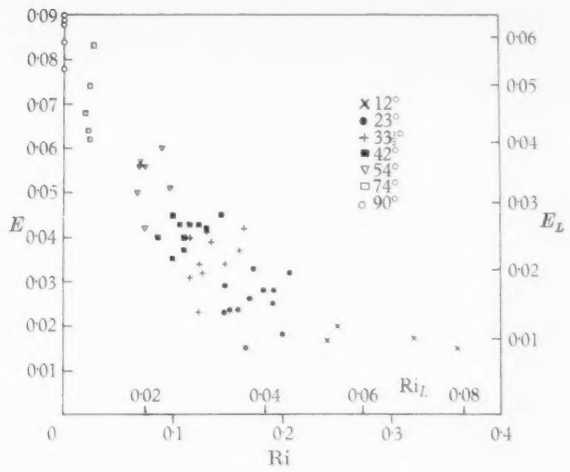

FIGURE 7. Entrainment as a function of Richardson number for inclined plumes, using the direct visual measurements of velocity and entrainment. The scales E_L and Ri_L relate to the 'layer velocity' and E and Ri to the mean velocity.

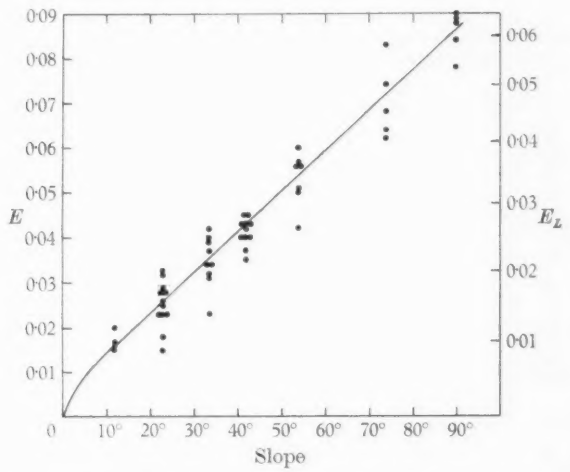

FIGURE 8. Measurements of entrainment into an inclined plume as a function of slope. Scales show both E_L based on the 'layer velocity' and E based on the equivalent mean velocity.

(vi) *Comparison of the several methods*

In figure 10 we have collected together the mean curves of E *vs* Ri found by the three methods: the surface jet, the profile measurements analysed using the outer parts of the plume and the timing of the layers. Agreement is good, particularly when it is remembered how sensitive the values of Ri are to the velocity measurements. The surface jet tends to give the highest values of E for a given Ri; if this is regarded as significant, it might be explained as a 'memory'

effect arising because the jet is not exactly in local equilibrium. It is likely that the Richardson numbers taken from the profile measurements are systematically too low at small values of Ri, as mentioned in (iv) above.

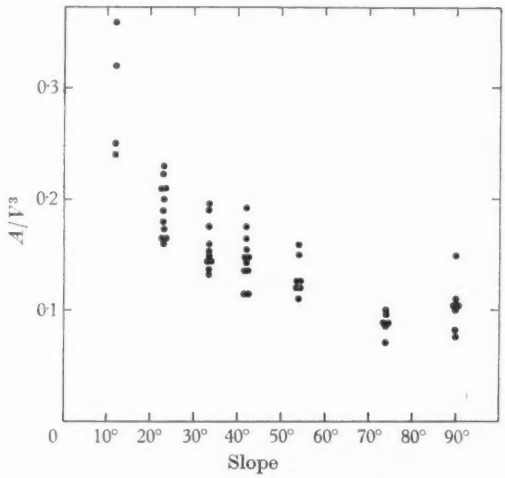

FIGURE 9. Measurements of A/V^3 as a function of slope. The points have been obtained by the 'layer velocity' method but are plotted using the equivalent mean velocities.

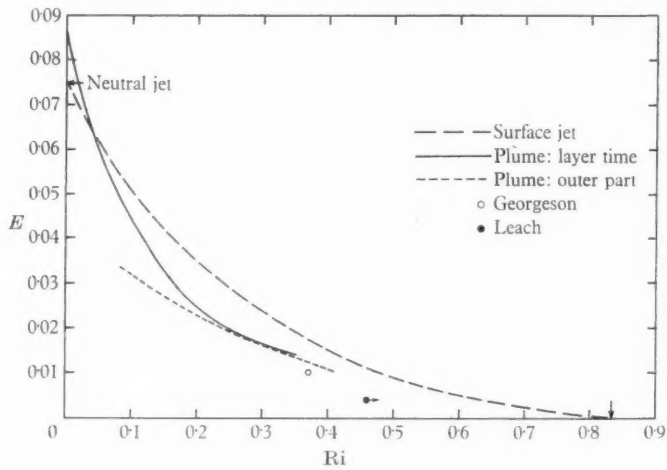

FIGURE 10. Comparison of the three series of measurements of entrainment as a function of Richardson number, all based on equivalent mean velocities. Also shown are points calculated from the measurements of Georgeson and Leach.

The curves are less firmly based at high values of Ri than elsewhere. This is a pity since important flows occur at low slopes, but in order to obtain satisfactory measurements in this region, a much larger scale experiment than is practical in the laboratory seems to be required. However, as we shall see in the

next section, when the ambient fluid is in motion the relevant Richardson numbers are smaller and the region which we have examined in detail is important even at low slopes.

7. The application of the results

(*a*) *Prediction of mean velocity and concentration*

The laboratory results may be used confidently to make predictions of the velocity of flow of a larger scale turbulent density current on a steep slope. All that is required is an estimate of the rate of output of light or heavy fluid; small changes in Ri due to Reynolds number effects or changes in the friction coefficient will be unimportant since V is proportional to $\mathrm{Ri}^{\frac{1}{3}}$. This point is brought out clearly in figure 11, in which we show measurements of V based on profiles recorded at a slope of 23°, plotted against A on logarithmic scales; V is proportional to $A^{\frac{1}{3}}$ over a wide range of A and the relation should continue to hold at higher values. The constant of proportionality could have been obtained from figure 9.

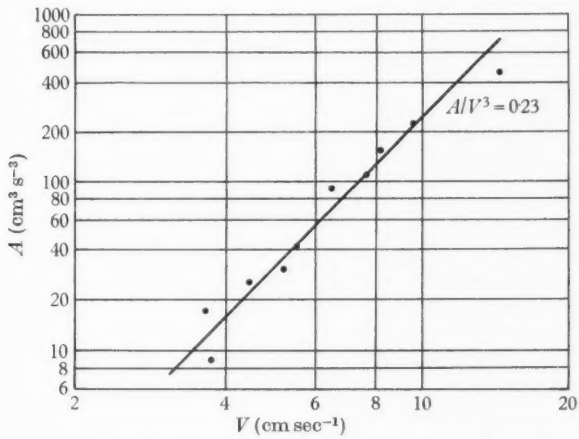

FIGURE 11. Measurements of the flux of density difference, A, as a function of the velocity V at 23°, plotted on logarithmic scales.

At low slopes, our results suggest that E becomes very small, so that even at large Reynolds numbers there should be negligible mixing of a current with its surroundings and so little friction at the interface. The weight of the layer must then be balanced solely by friction on the floor and

$$S_2 \frac{A}{V^3} \sin\alpha = C. \tag{16}$$

This result is important in the theory of turbidity currents (Charnock 1959).

At a given slope and rate of emission and hence a fixed V, the concentration in a plume at high Reynolds number is inversely proportional to h. Since $dh/dx = E$, the dilution can readily be calculated using the results for E as a function of slope (figure 8).

(b) The effect of motion of the ambient fluid

There is considerable interest in the question of how a steady velocity in the ambient fluid affects the flow of a wall plume. The meteorologist wishes to know how large an upper wind is necessary to destroy a katabatic flow at the surface; and the mining engineer is interested in how fast a downhill ventilating flow is needed to prevent a methane layer flowing uphill along the roof of a sloping mine roadway.

Using the measurements of E *vs* Ri, we can now supply rough answers to these questions. The results are not very sensitive to small changes in this relation, and are probably adequate even if there is a tendency for an opposing flow of ambient fluid to increase the apparent value of E (as might perhaps be inferred from a remark of Townsend (1956)).

Let us again consider the case where there is a line source of density difference of strength A, though this is a considerable simplification of the meteorological situation where cooling may extend over tens of kilometres. The equations required are

$$\Delta(V+V_a)\,h = A = \text{constant}, \tag{3}$$

$$\frac{dh(V+V_a)}{dx} = E\,|V|, \tag{4}$$

where E is a function of the Richardson number which is given by

$$\mathrm{Ri} = \frac{h\Delta\cos\alpha}{V^2} = \frac{A\cos\alpha}{V^2(V+V_a)}; \tag{5}$$

and the momentum equation, which in this case may be written

$$\frac{d(V+V_a)\,Vh}{dx} = -(V+V_a)^2 C\,\mathrm{sgn}\,(V+V_a) + S_2\Delta h\sin\alpha - \tfrac{1}{2}\cos\alpha\frac{d\Delta h^2 S_1}{dx}. \tag{17}$$

These equations will be valid only when V is positive, that is, when the motion of the ambient fluid is either opposed to the natural motion of the layer or, if in the same direction, is less than the speed at which the layer is travelling. In the case where the ambient fluid is dragging the layer forward in the same direction as gravity with friction as the only retarding force, the profiles will be very different from those assumed for plumes and our values of E are unlikely to apply. The velocity of the layer itself, $V+V_a$, can take either sign.

In the normal state in which $dV/dx = 0$, the equations lead to

$$\left(1+\tfrac{1}{2}S_1\,\mathrm{Ri}\,\frac{V}{V+V_a}\right)E = S_2\,\mathrm{Ri}\tan\alpha - C\,\frac{(V+V_a)^2}{V^2}\,\mathrm{sgn}\,(V+V_a). \tag{18}$$

For given values of α and C, and using our results for $E(\mathrm{Ri})$, the equation (18) can be solved numerically to give $(V+V_a)/A^{\frac{1}{3}}$ as a function of $V_a/A^{\frac{1}{3}}$, that is, the non-dimensional layer velocity as a function of that in the ambient fluid. The calculation has been carried out using $S_1 = 0{\cdot}25$ and $S_2 = 0{\cdot}75$, for $\alpha = 0{\cdot}02$ and $\alpha = 0{\cdot}1$, with $C = 0$ and $C = 0{\cdot}02$. The latter friction coefficient is a high value

which is unlikely to be reached except in small-scale laboratory experiments. The results are shown in figure 12. It will be seen that when V_a opposes the natural flow and is greater than a value ranging between $2{\cdot}4A^{\frac{1}{3}}$ when $C = 0$, $\alpha = 0{\cdot}02$, and $3{\cdot}2A^{\frac{1}{3}}$ when $C = 0{\cdot}02$, $\alpha = 0{\cdot}1$, it is possible for the layer to flow in either direction. Three values of $(V+V_a)$ satisfy (18), but it is fairly clear that the middle one is unstable and that the layer can either flow very slowly with gravity, concentrating the available density difference so as to achieve the

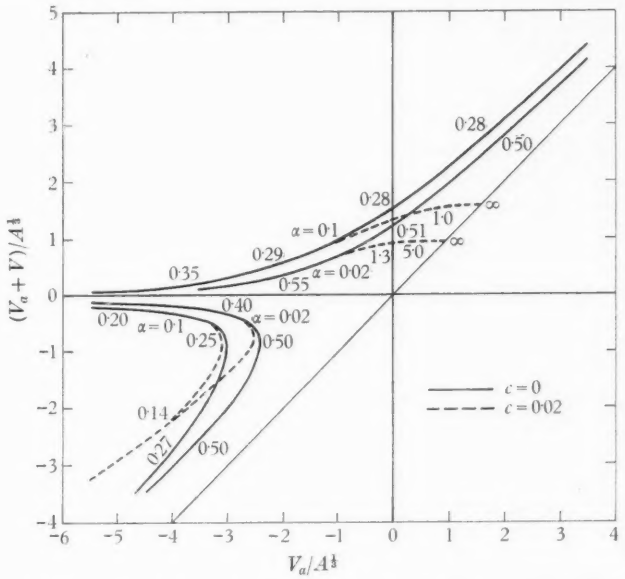

FIGURE 12. Calculations of the velocity of an inclined plume with a moving ambient stream, based on the experimental E(Ri) relation shown in figure 10. $V+V_a$ is the velocity of the layer, V_a that of the ambient stream. Curves are shown for two values of the slope and two friction coefficients; the velocity necessary to reverse the direction of flow is seen to be relatively insensitive to changes in these parameters.

necessary Richardson number, or at a moderate speed in the reverse direction. Physical intuition urges that since only a small fluctuation in speed from the slow forward moving state is needed to take the layer to the unstable solution, it is likely that in practice the reverse flow will be realized whenever it can exist.

The curves of figure 12 for different slopes and friction coefficients lie close together, showing that the velocity of ambient fluid required to produce reversal, like the free forward velocity, varies only slowly with these parameters and all that is needed to predict it is a good estimate of A. However, the Richardson number, values of which are marked on figure 12, does depend on the slope, and the corresponding values of E, which is a strong function of Ri, vary more markedly. We note, as mentioned previously, that small values of Ri are relevant when the ambient fluid is acting against gravity; and for a given ambient velocity there is much more mixing when the slope is steep. The

entrainment becomes very small in the case of moderate ambient flows assisting gravity.

Although these conclusions and the numerical values are strictly applicable only to the case of a turbulent layer and laminar ambient stream, it is unlikely that they will be affected greatly by a low level of turbulence in the ambient flow. It is not possible for us to test the theory in our large channel because of the amount of water which would be required to produce the ambient stream, but we have begun some experiments in a small tiltable channel 10 cm wide by

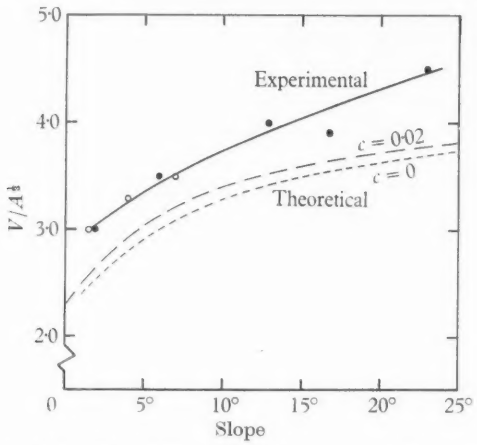

FIGURE 13. Experimental values of the reversal velocity as a function of slope, compared with calculations carried out for two values of friction coefficient. Dots: $A = 21$. Circles: $A = 63$.

5 cm deep and 250 cm long, which are of interest in this connexion. Salt solution is released from a slit across the bottom of the channel near the centre of its length, and may travel either with or against the main stream (which in this channel is necessarily turbulent at moderate velocities), depending on the rate of output, the main stream velocity and the slope. In figure 13 are shown the measured mean velocities of the main flow necessary to produce reversal of the layer for a range of slopes. These are compared with the theoretical values, calculated on the basis of diagrams like figure 12, for two values of friction coefficient. The agreement is satisfactory and the measurements demonstrate the small dependence on slope. Note particularly that flow against the main stream is possible at very small slopes.

(*c*) *Typical values of A*

Finally we may give some estimates of typical values of A in practical cases, from which velocities may be calculated.

For a katabatic wind, suppose there is a line source equivalent to an area 50 km long in the direction of greatest slope which is cooled at 0·1 cal cm^{-2} min^{-1}: then $A = 10^8$ cm^3 sec^{-3}. The velocity of free flow would be about

$$600 \text{ cm sec}^{-1} = 12 \text{ knots},$$

and the velocity of upper wind necessary to reverse it is

$$2{\cdot}6A^{\frac{1}{3}} = 1200 \text{ cm sec}^{-1} = 24 \text{ knots}.$$

These values are not unreasonable. It is hoped in a later investigation to compare the theory with meteorological observations, and for this purpose it may be necessary to extend the theory slightly to take account of the Coriolis force due to the earth's rotation.

As an example of the release of methane in a mine gallery, let us suppose that 10 ft.^{3} min^{-1} is released in a roadway 5 ft. wide. A is then 10^4 cm^3 sec^{-3} and the ventilating flow needed to reverse the layer would be 57 cm sec^{-1} = 120 ft. min^{-1}.

In the case of turbidity currents, our results may be used in reverse. There are well-documented cases in which turbidity currents have broken a succession of telegraph cables on the ocean floor and so their front velocity is well known. In this case E is very small so it is only necessary to guess C. For example, in the Grand Banks turbidity current of 1929, velocities of 55 knots were reported, so with $C = 0{\cdot}003$, we find $A = 6 \times 10^{10}$ cm^3 sec^{-3}.

8. Conclusion

The assumption that the rate of entrainment into a turbulent inclined plume is a function of the overall Richardson number has led to a consistent picture of such flows. Our experiments have determined the empirical function $E(\mathrm{Ri})$ with an accuracy sufficient for most applications except in the range of high Richardson numbers where E is very small. Here much larger scale experiments are desirable.

It is not claimed that this approach is in any sense fundamental, but it forms a natural extension of an idea which has been used successfully in uniform fluids. The experiments could, perhaps, be refined further to investigate systematically the effects of Reynolds number (for example, to explain the details of figure 5). This seems to be taking the 'overall' approach too far, however; it is likely to be more profitable to look at the local rates of transfer of salt and momentum and to try to relate them to local stability parameters at different parts of the flow. Work is now being continued along these lines, both for simple wall plumes and (in the smaller channel mentioned in the last section) for a flow with an opposing turbulent ambient fluid.

9. Acknowledgements

The first part of the experimental work was carried out in the Cavendish Laboratory while the second author held an Overseas Scholarship from the Royal Commission for the Exhibition of 1851. The second author also wishes to acknowledge the financial support of the Ministry of Power during the period of the later work in Manchester.

REFERENCES

BAKHMETEFF, B. A. 1932 *Hydraulics of Open Channels.* New York and London: McGraw-Hill Book Co.

BAKKE, P. 1957 *J. Fluid Mech.* **2**, 467–72.

BALL, F. K. 1956 *Aust. J. Phys.* **9**, 373–86.

BATCHELOR, G. K. 1953 *Quart. J. R. Met. Soc.* **79**, 224–35.

BATCHELOR, G. K. & TOWNSEND, A. A. 1956 Turbulent diffusion. *Surveys in Mechanics*, pp. 352–99. Cambridge University Press.

BELL, H. S. 1942 *Misc. Publ. U.S. Dep. Agriculture*, no. 491.

BERSON, F. A. 1958. *Quart. J. R. Met. Soc.* **84**, 1–16.

BRESSE, J.-A.-Ch. 1860. *Cours de mécanique appliquée, Hydraulique.* Paris.

CHARNOCK, H. 1959 *Nature, Lond.*, **183**, 657–9.

DIETRICH, G. 1956 *Dtsch. Hydrograph. Z.* **9**, 78–89.

ELLISON, T. H. 1957 *J. Fluid Mech.* **2**, 456–66.

FREEMAN, M. H. 1952 *Met. Rep., Met. Off., Lond.* no. 11.

GEORGESON, E. H. M. 1942 *Proc. Roy. Soc.* A, **180**, 484–93.

KUENEN, P. H. 1952 *Amer. J. Sci.* **250**, 874–84.

LEACH, S. J. 1959 *Safety in Mines Research Establishment Report* (in the Press).

MORTON, B. R. 1959 *J. Fluid Mech.* **5**, 151–63.

MORTON, B. R., TAYLOR, G. I. & TURNER, J. S. 1956 *Proc. Roy. Soc.* A, **234**, 1–23.

RICHARDSON, L. F. 1920 *Proc. Roy. Soc.* A, **97**, 354–73.

ROUSE, H., YIH, C. S. & HUMPHREYS, H. W. 1952 *Tellus*, **4**, 201–10.

SCORER, R. S. 1954 *Sci. Progr.* **42**, 396–405.

STOMMEL, H. 1953 *Proc. Minnesota Intern. Hydraulics Convention*, pp. 305–12.

TOWNSEND, A. A. 1956 *The Structure of Turbulent Shear Flow.* Cambridge University Press.

TOWNSEND, A. A. 1958 *J. Fluid Mech.* **3**, 361–72.

TULLY, J. P. 1949 *Bull. Fish. Res. Bd Can.*, no. 83.

Electron density and ionization rate in thermally ionized gases produced by medium strength shock waves

By Y. MANHEIMER-TIMNAT
Scientific Department, Israel Ministry of Defence

AND W. LOW
Department of Physics, The Hebrew University, Jerusalem

(Received 11 February 1959)

A method, based on the measurement of attenuation of microwaves, which allows the electron density and the ionization rate of shock-heated gases to be obtained, is described. Results obtained for air in the shock Mach range 8·2–10·4, and for nitrogen containing 0·25 % oxygen in the range 7·4–8·8, show that the electron density is in agreement with theoretical calculations based on thermodynamic equilibrium. Ionization time measurements in air are presented in this range and these results extend the measurements of Niblett & Blackman (1958) to a lower Mach range.

Introduction

The electrical properties of thermally ionized gases, produced by shock waves, have been studied by a number of authors. Lin (1952) and Lin, Resler & Kantrowitz (1955) measured the electrical conductivity of argon in the shock Mach range 4–16 by hydromagnetic methods. Lamb & Lin (1957) obtained data on the electrical conductivity of air in the shock Mach range 11–17 with the same type of equipment. Petschek & Byron (1957) studied the ionization mechanism of argon behind shock waves in the shock Mach range 10–18 and gathered data on the ionization times involved. Recently, Niblett & Blackman (1958) measured the ionization rate in air for shock Mach numbers 11–17 by a photographic method.

This paper presents new data on the ionization rate and electron density in air between shock Mach numbers 8·2 and 10·4 and in nitrogen, containing 0·25 % oxygen, in the shock Mach range 7·4–8·8.

The method described here (see also Low & Manheimer, 1959) is based on the interaction of microwaves with the ionized gaseous medium. The attenuation coefficient of the microwaves is related to the electrical conductivity and the dielectric coefficient of the gas. Margenau (1946) showed that these quantities may be calculated if the electron density of the gas and the collision frequency of electrons with other particles are known. Assuming thermal equilibrium it is possible (Bethe 1942; Glass, Martin & Patterson 1953; Gilmore 1955) to calculate the chemical composition of the shocked gas, and its temperature and density as functions of shock Mach number for given initial conditions.

These data enable one to calculate the electron density as well as the collision frequency of electrons with those species whose collision cross-section is known. It is, therefore, possible to obtain a theoretical curve for the attenuation coefficient of microwaves of given frequency as a function of shock Mach number for specified initial conditions.

In this work the attenuation coefficient of microwaves of 3 cm wavelength and the shock velocity are measured experimentally and compared with the results of the theoretical calculations.

By observing the attenuation as a function of time as the shock-heated gas passes through the waveguide, one can estimate the rate of ionization and obtain information about the rate of approach to thermodynamic equilibrium and the mechanisms involved.

Theory

The attenuation coefficient, α, of microwaves of circular frequency ω ($\omega = 2\pi f$, where f is the frequency in cyc/sec) which pass through a gaseous medium, assumed to be in thermal equilibrium, is given by the following relation, due to Margenau (1946):

$$\alpha^2 = \frac{\omega^2 \epsilon}{2c^2}\left\{-1 \pm \left[1 + \left(\frac{4\pi\sigma_r}{\epsilon\omega}\right)^2\right]^{\frac{1}{2}}\right\}. \tag{1}$$

For $(4\pi\sigma_r/\epsilon\omega)^2 \ll 1$ this may be approximated by

$$\alpha = \frac{2\pi\sigma_r}{c}. \tag{1a}$$

Here ϵ is the dielectric constant of the gas ($\epsilon = \epsilon_0 - 4\pi\sigma_i/\omega$), σ_r and σ_i are the real and imaginary part of the complex conductivity, and c the velocity of light in vacuum. The positive sign should be taken for $\epsilon > 0$, and the negative one for $\epsilon < 0$, since α is always real. σ_r and σ_i are given by

$$\sigma_r = \frac{4}{3\sqrt{\pi}} \frac{e^2 N_e}{m\gamma} K_2\left(\frac{\omega^2}{\gamma^2}\right) \to \frac{8}{3\sqrt{\pi}} \frac{e^2 N_e \gamma}{m\omega^2} \quad \text{as} \quad \frac{\omega^2}{\gamma^2} \to \infty, \tag{2}$$

and

$$\sigma_i = \frac{4}{3\sqrt{\pi}} \frac{e^2 N_e \omega}{m\gamma^2} K_{\frac{3}{2}}\left(\frac{\omega^2}{\gamma^2}\right) \to \frac{e^2 N_e}{m\omega} \quad \text{as} \quad \frac{\omega^2}{\gamma^2} \to \infty, \tag{3}$$

where e denotes the electron charge, m its mass, N_e the density of free electrons, and γ their mean collision frequency in the ionized mixture. $K_2(x)$ and $K_{\frac{3}{2}}(x)$ are special functions defined by Margenau (1946).

The mean collision frequency γ can be defined by the gas kinetic formula

$$\gamma = v \sum_j n_j \bar{Q}_j. \tag{4}$$

n_j is the number of particles of species j per cm^3, $\bar{Q}_j$ is the average electron cross-section of particles of species j, and v is the mean velocity of the free electrons, which is related to their temperature T by (k being Boltzmann's constant):

$$\frac{mv^2}{2} = kT. \tag{5}$$

Since the temperatures reached in the experiments do not exceed 4000 °K it is justifiable to assume that the electron temperature is equal to the gas temperature. For the electron velocities obtained in this work (well below 1 eV) one should use the electron diffusion cross-section (this point is discussed at some length by Lamb & Lin 1957). The species which may contribute appreciably to the total electron collison probability $\sum_j n_j \bar{Q} j$ are, in our case: N_2, O_2, NO, N, O and A (this can be seen from figure 6 of Lamb & Lin (1957) for air and from calculations described in the Appendix for nitrogen). Data on the average electron diffusion cross-sections for all these species have been compiled by Lamb & Lin (1957). For the molecular species N_2, O_2, NO and A, their values are based on experimental data, reported by Massey & Burhop (1952). For atomic oxygen and nitrogen they used the theoretical calculations of Hammerling, Shine & Kivel (1957), which showed good agreement with their experimental results.

Since our experimental results indicate that thermodynamic equilibrium has essentially been reached in these experiments, the composition of the ionized gas (the various n_j, including the electron density N_e), its temperature and density at a given shock velocity and initial temperature and density, can be calculated from the Rankine–Hugoniot equations across the shock front, according to a method first developed by Bethe & Teller (1940) and Bethe (1942), and described in detail by Glass, Martin & Patterson (1953) and Gilmore (1955).

Techniques

The shock waves were produced in a small brass shock-tube of circular cross-section, built for this investigation (see figure 1). The internal diameter of the high-pressure section is 1 in. and that of the low-pressure section 0·5 in. This gives a higher shock strength for the same pressure ratio than a constant section shock tube (Glass *et al.* 1953).

Interchangeable sections were used so that the overall length of the tube could be varied between 80 and 130 cm. The shock velocity was measured by the ionization plug method (Birk, Erez, Manheimer & Nahmani 1954; Campbell, Malin, Boyd & Hull 1956). The metal tube incorporates a Teflon section, where the attenuation of the microwaves is measured. Teflon was chosen because of its favourable mechanical and electrical properties (good sealing properties and low losses at microwave frequencies).

Hydrogen was used as driver gas, which, owing to its low molecular weight, gives strong shock waves with reasonable pressure ratio (Glass *et al.* 1953). The gas was obtained from commercial cylinders, at a maximum pressure of 140 atm. The diaphragm, dividing the chamber from the channel, was made of several cellulose acetate sheets of 0·4 mm thickness (2–4 pieces according to desired shock strength). The channel was evacuated by a conventional vacuum system including a rotary oil pump, a 3-stage mercury diffusion pump, a cold trap filled with dry ice, and a shortened McLeod manometer. The vacuum obtained in the shock tube was better than 10μ Hg. After evacuating the system, the low-pressure section was filled with the gas under study and its flow regulated in order to obtain the

desired pressure. At a pressure of 10 mm Hg, which was used in the experiments with nitrogen, the impurity level due to leaks was 0·2 %. Experiments with air as test gas were conducted at lower pressure, between 1 and 3 mm Hg, since there were no purity limitations here while safety reasons favoured low air pressure when using hydrogen as driver gas.

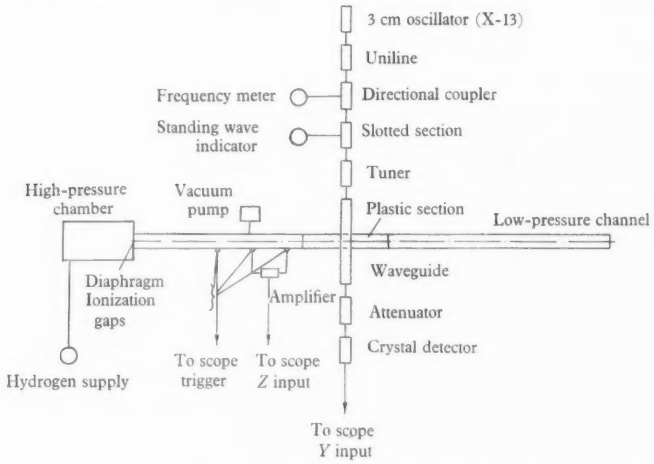

FIGURE 1. Block diagram of shock tube and microwave equipment.

The Mach numbers obtained experimentally were 20–25 % lower than those expected for an ideal shock tube. This is caused by imperfect rupture of the diaphragm, heat losses to the walls, and boundary layer effects. These perturbations are pronounced owing to the small bore of the tube (Lin 1952), for example, observed a difference of 12 % between ideal and actual Mach number even with a shock tube of internal diameter 1·5 in.). The velocity of the shock during its downward travel was measured between three stations immediately before the test section. No attenuation was detected within the accuracy of our shock velocity measurements (± 1 %).

The microwave equipment used was in the 3 cm range (exploratory experiments in the 1 and 10 cm ranges showed that the method may be used successfully with these wavelengths too). A Varian X-13 oscillator was our power source; the line included conventional components for the measurement of standing wave ratio, as indicated in figure 1. The standing wave ratio was minimized (about 1·05) before each experiment. The microwave output was displayed on the Y input of a Du Mont 329 oscilloscope and photographed by a Du Mont Oscillorecord camera. The scope was triggered by a signal coming from an ionization plug through a video amplifier. Two further ionization plugs were connected, through a second channel of the same amplifier, to the Z input of the scope and darkened the trace at the passage of the shock front.

A typical oscillogram is shown in figure 2. M is here 9·8 (the speed of sound in air is 340 m/sec). We can distinguish (from left to right) the arrival of the shock front at the first plug (onset of the trace, point A), its passage over the second and

third plug (darkening of the trace, points B and C). As the shock front arrives at the waveguide we see a decrease in microwave power, the maximum attenuation (0·03 V), point D, being reached after about 9 μsec. The undisturbed output is 0·3 V. From the voltage ratio V_0/V_1 the attenuation coefficient, α, is calculated by the relation

$$\alpha\,(\text{db/cm}) = \frac{8{\cdot}7}{2l_{\text{eff}}} \ln \frac{V_0}{V_1}. \tag{6}$$

Here l_{eff} is the effective path of the microwaves through the attenuating medium. This quantity, which depends on the microwave field and the geometrical configuration, was determined experimentally to be 0·73 cm.

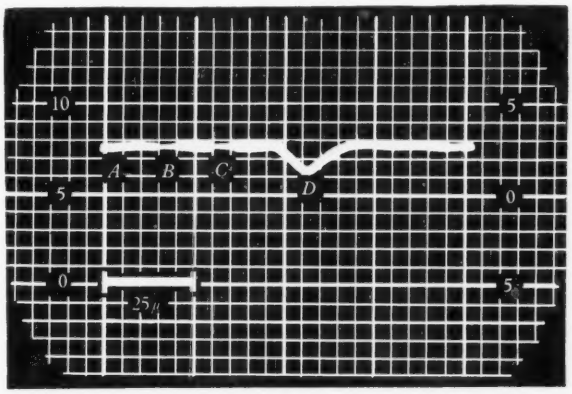

FIGURE 2. Oscillogram of microwave attenuation as a function of time. Shock wave in air, at pressure 1 mm Hg, $M = 9{\cdot}8$. Time base 5 microseconds per scale division. Amplification 20 mV per scale division. The first spark plug triggers the trace. The passage of the shock wave over the second and third spark plugs are indicated by a darkened trace at B and C. The maximum attenuation at point D is about 0·03 V and is reached after 9 μsec.

Calibration experiment

The attenuation caused by a gas discharge in our microwave system was compared with results of Udelson, Creedon & French (1957). Instead of the shock tube, a discharge tube of the same diameter was passed through the waveguide and a d.c. discharge in hydrogen was produced using a power supply of variable voltage (0–5000 V), which enabled us to raise the discharge current to a maximum of 7·5 mA. The ratio of the microwave power without discharge and during discharge was measured by the current in the crystal detector and a sensitive galvanometer. The crystal was operated in the square law region and the attenuation constant, α', is therefore given by a relation analogous to (1):

$$\alpha\,(\text{db/cm}) = \frac{8{\cdot}7}{2l_{\text{nom}}} \ln \frac{i_0}{i_1}, \tag{7}$$

taking a nominal path l of 1 cm (i_0 is the current without discharge, i_1 the current during discharge). This was compared with the attentuation constant, α, calcu-

lated from Udelson's data and Margenau's theory; the ratio α/α' was found to be approximately constant ($1{\cdot}37 \pm 0{\cdot}09$) for different discharge currents and hydrogen pressures; the mean value of the effective path l_{eff} was therefore 0·73 cm.

Results

(*a*) *Experiments in air*

The experiments in air were performed with two different lengths of the channel in the shock tube (65 and 80 cm); the initial pressure of air in the channel being varied between 1 and 3 mm Hg in order to obtain different Mach numbers. Hydrogen from a commercial container at pressures between 80 and 120 atm. was the driver gas. The shock Mach numbers obtained ranged from 8·2 to 10·4. The frequency of the microwaves employed was 10,000 Mc/sec.

Mach number	Collision frequency (sec^{-1})	Electron density (cm^{-3})	Real part of electrical conductivity (c.g.s.)	Imaginary part of electrical conductivity (c.g.s.)	Dielectric coeff. (c.g.s.)	Attenuation coeff. (db/cm)
8	$5{\cdot}5 \times 10^9$	$1{\cdot}3 \times 10^{10}$	$6{\cdot}75 \times 10^6$	$5{\cdot}1 \times 10^7$	0·99	0·012
8·4	6·3	2·25	$1{\cdot}30 \times 10^7$	8·75	0·98	0·024
8·9	7·35	4·7	3·20	$1{\cdot}8 \times 10^8$	0·96	0·059
9·5	8·8	$1{\cdot}1 \times 10^{11}$	8·70	4·2	0·92	0·17
9·8	9·75	1·7	$1{\cdot}50 \times 10^8$	6·4	0·87	0·29
10·15	$1{\cdot}1 \times 10^{10}$	2·8	2·65	$1{\cdot}05 \times 10^9$	0·79	0·55
10·4	1·15	4·0	4·00	1·45	0·70	0·87
11	1·25	9·5	$1{\cdot}00 \times 10^9$	3·8	0·24	3·50

TABLE 1. Data on high-frequency (10,000 Mc/sec) electric properties of shock-heated air. Initial pressure: 1 mm Hg. Initial temperature: 293 °K.

The theoretical attenuation coefficient, α, for an initial pressure of 1 mm Hg and an initial temperature of 293 °K, was calculated for a shock Mach range 8–11 from equations (1), (2) and (3). The data required for the computations (electron density, composition, density and temperature of the shock-heated air and electron diffusion cross-sections) were all taken from Lamb & Lin (1957). The results are tabulated in Table 1, which includes the attenuation coefficient, α, in db/cm, the real and imaginary parts of the complex conductivity, σ_r and σ_i, and the dielectric coefficient, ϵ (all in c.g.s. units).

Table 2, in which the experimental results are presented, includes the measured Mach number, M; the ratio of the microwave output before passage of the shock wave, V_0, to the output at maximum attenuation, V_1; the attenuation coefficient, α, which is obtained from V_0/V_1 by means of equation (6); the initial air pressure, p_1, and the time, τ, between ionization onset and the moment when its maximum value is reached.

In addition, a normalized coefficient of attenuation, for an initial pressure of 1 mm Hg, has been calculated in order to make comparison possible with the data of Table 1. Normalization was achieved by dividing the experimental attenuation coefficient by the square of the initial pressure. For the low conductivity values

obtained in these experiments one may use equation (1*a*) and the asymptotic form of equation (2), getting for α the relation:

$$\alpha = \frac{16\sqrt{\pi}\, e^2 N_e \gamma}{3 m\omega^2}. \tag{8}$$

Use of this approximation, instead of the exact equations (1), (2) and (3), introduces for $M = 10{\cdot}4$, the maximum experimental value, an error less than 0·5 %. Equation (8) shows that α is proportional to the product $N_e\gamma$ and both these quantities increase linearly with the initial pressure p_1.

Mach number	Output ratio	Initial pressure (mm Hg)	Attenuation coefficient (db/cm)	Ionization time (μsec)	Normalized atten. coeff. (db/cm)
8·2	1·025	2·9	0·15	10	0·018
8·45	1·03	2·5	0·175	11	0·028
8·5	1·065	3	0·38	9	0·042
8·9	1·045	2	0·26	9	0·065
9·1	1·035	1·5	0·205	8	0·091
9·2	1·075	1·8	0·45	9	0·14
9·3	1·04	1·4	0·25	12	0·13
9·5	1·065	1·4	0·38	9	0·19
9·5	1·05	1·2	0·29	10	0·20
9·5	1·05	1·2	0·29	10	0·20
9·5	1·11	1·6	0·62	8	0·24
9·8	1·085	1·2	0·48	8	0·34
9·8	1·06	1·0	0·35	8	0·35
9·8	1·075	1·1	0·45	7	0·35
9·8	1·095	1·2	0·54	8	0·37
9·8	1·10	1·2	0·565	9	0·39
9·8	1·12	1·3	0·67	8	0·40
9·8	1·11	1·2	0·62	10	0·43
10·0	1·11	1·1	0·62	10	0·51
10·4	1·175	1·0	0·96	10	0·96

TABLE 2. Results of experiments in air.

A comparison between the calculated attenuation coefficient and the experimental results is given in figure 3. The agreement is seen to be good; the slight tendency to higher values shown by the experiments may be explained by assuming that the effective path l_{eff} is somewhat longer than the one used. No difference was observed between results obtained with different lengths of the channel in the shock tube. This is to be expected, since the duration of the uniform flow is longer than the ionization time in all experiments (the shortest duration of uniform flow was 14 μsec, while the largest ionization time measured reached only 12 μsec). This fact shows that thermodynamic equilibrium has indeed been reached in the heated air. (Experiments performed in argon, where the ionization time is known to be longer than the duration of uniform flow in our tube (Petschek & Byron 1957), showed indeed larger attenuation for a longer shock tube.)

The time elapsed between ionization onset and the attainment of its maximum value (where thermodynamic equilibrium is reached) varies between 7 and 12 μsec.* The product of this ionization time, τ, by the initial pressure, p_1, is plotted as function of Mach number, M, in figure 4, where the results of Niblett &

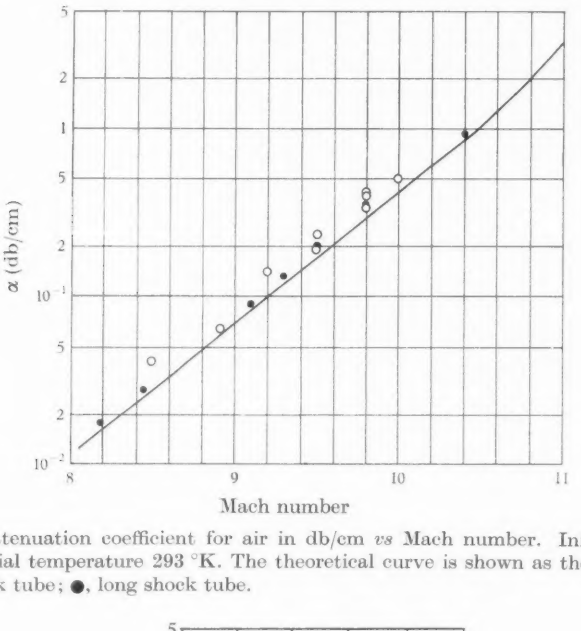

FIGURE 3. Attenuation coefficient for air in db/cm *vs* Mach number. Initial pressure 1 mm Hg, initial temperature 293 °K. The theoretical curve is shown as the heavy line. ○, Short shock tube; ●, long shock tube.

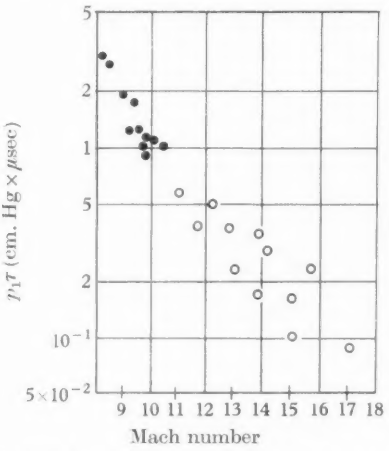

FIGURE 4. Experimental values of ionization time in air *vs* Mach number. ○, Niblett & Blackman; ● present work.

* It might be objected that the ionization time cannot be measured with any accuracy with a microwave waveguide whose cross-section is of the order of 1 in. × ½ in. We therefore performed several experiments with a specially constructed waveguide with cross-section 1 in. × 0·1 in. The results were approximately the same.

Blackman (1958) for higher Mach range are also reproduced. Our experimental points give an extension of their results and their scatter is of the same order of magnitude.

The good agreement obtained for the electron density between experiment and theory confirms the fact that the principal contribution to ionization in air in the shock Mach range 8–10·5, corresponding to equilibrium temperatures of 2800–3500 °K, is due to nitric oxide, NO, whose ionization potential is the lowest of all abundant species. The same conclusion was reached by Lamb & Lin (1957) for the shock Mach range 11–17.

The short ionization times measured agree with the hypothesis put forward by Glick, Klein & Squire (1957) that nitric oxide is formed by reaction of atomic oxygen with molecular nitrogen, since the relaxation times involved are all very short.

(*b*) *Experiments in nitrogen*

The nitrogen used in our experiments was obtained from commercial containers of low purity (containing 2 % of oxygen); the gas was purified by passing through a column of heated colloidal copper and its oxygen content reduced to about 0·2 %. At the pressure of 10 mm Hg used, the impurity level (air) due to leaks was 0·2 %. The total oxygen content of the gas was, therefore, of the order of 0·25 %. The driver gas was again hydrogen at pressures between 80 and 140 atm. The shock Mach numbers obtained ranged from 7·45 to 8·8.

The theoretical attenuation coefficient, α, for an initial pressure of 10 mm Hg and an initial temperature of 300 °K has been calculated for a shock Mach range of 7·4–9, according to equations (1), (2) and (3).

The temperature and density of the shocked gas as a function of Mach number were taken from Waldron (1958). Although his data were computed for pure nitrogen, a numerical check showed that the inclusion of 0·25 % O_2 changed the results by less than 0·5 % and this could be neglected at the accuracy level used in the computations. The composition of the gas was calculated from the chemical equilibrium, conservation of matter, and conservation of charge equations. Details of the computational method are given in the Appendix. Data on the electron diffusion cross-sections were taken again from Lamb & Lin (1957). Results of the calculations are tabulated in table 3.

Theoretical computations of the equilibrium composition for pure N_2 in the same temperature range were also performed. They show that the addition of a small amount of O_2 causes a very marked increased in the electron density, N_e. For pure nitrogen N_e is $4{\cdot}75 \times 10^6$ cm^{-3} at $M = 7{\cdot}4$, while the value for the mixture containing 0·25 % O_2 is $1{\cdot}45 \times 10^{10}$; the figures for $M = 9$ are $1{\cdot}65 \times 10^{10}$ and $1{\cdot}05 \times 10^{12}$, respectively. It appears, therefore, that the dominating factor in the ionization process in the mixture is nitric oxide, NO, whose ionization potential, 9·25 eV, is the lowest of all species present.

The experimental results are gathered in table 4, which includes the measured Mach number, the ratio of microwave outputs and the coefficient of attenuation.

Figure 5 shows comparison between the experimental data and the calculated values. The agreement is fair. The fact that some of the experimental values are

somewhat higher than the theoretical curve may be caused by some slight increase in the oxygen content of the gas, possibly due to poor purification by the copper column.

Mach number	Collision frequency (sec^{-1})	Electron density (cm^{-3})	Real part of electrical conductivity (e.g.s.)	Imaginary part of electrical conductivity (e.g.s.)	Dielectric coeff. (e.g.s.)	Attenuation coeff. (db/cm)
7·4	$4{\cdot}35 \times 10^{10}$	$1{\cdot}45 \times 10^{10}$	$2{\cdot}80 \times 10^{7}$	$2{\cdot}95 \times 10^{7}$	0·994	0·05
7·9	4·9	7·20	$1{\cdot}35 \times 10^{8}$	$1{\cdot}25 \times 10^{8}$	0·975	0·25
8·2	5·25	$1{\cdot}65 \times 10^{11}$	3·05	2·60	0·948	0·57
8·35	5·45	2·45	4·55	3·95	0·921	0·86
8·8	5·9	6·85	$1{\cdot}25 \times 10^{9}$	$1{\cdot}0 \times 10^{9}$	0·798	2·57
9	6·2	$1{\cdot}05 \times 10^{12}$	1·95	1·30	0·742	4·14

TABLE 3. Data on high-frequency (20,000 Mc/sec) electrical properties of shock-heated nitrogen, containing 0·25 % O_2. Initial pressure: 10 mm Hg. Initial temp.: 300 °K.

Mach number	Output ratio	Attenuation coefficient (db/cm)
7·45	1·01	0·06
7·95	1·07	0·40
8·1	1·075	0·43
8·15	1·08	0·46
8·25	1·15	0·83
8·35	1·16	0·89
8·35	1·17	0·94
8·4	1·19	1·03
8·4	1·20	1·09
8·4	1·22	1·19
8·45	1·22	1·19
8·45	1·23	1·23
8·45	1·27	1·42
8·55	1·32	1·65
8·55	1·32	1·65
8·6	1·34	1·75
8·65	1·39	1·96
8·65	1·43	2·13
8·65	1·43	2·13
8·8	1·54	2·57
8·8	1·58	2·67

TABLE 4. Results of experiments in nitrogen.

The maximum electron density, calculated from the experimental data, was reached in about 15 μsec, a somewhat longer time than in air, probably due to the lower oxygen content.

A rough estimate of the dissociative recombination coefficient of nitric oxide can be obtained from the experimental ionization rate and the general principle of detailed balancing. This calculation is in order of magnitude agreement with recombination coefficients of typical diatomic molecular ions (Loeb 1955).

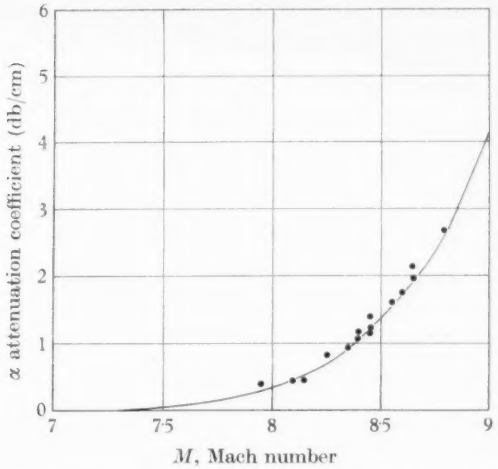

FIGURE 5. Attenuation coefficient for nitrogen with 0·25 % oxygen. Initial temperature: 300 °K. Initial pressure: 10 mm Hg.

Discussion

The attenuation range in which this method can be used most efficiently, giving results comparable in their precision to other techniques, is between 0·1 and 10 db. For attenuation smaller than 0·1 db special precautions for stabilizing the klystron's output are required, since otherwise the high amplification required will result in unfavourable signal-to-noise ratio.

This attentuation range covers a variety of conditions of the gas under test, in which a number of parameters can be varied:

(*a*) The microwave path in the ionizing medium, which determines the value of the attenuation coefficient, may be varied between wide limits by appropriate planning of the apparatus and therefore $p_1\tau$ may be measured for large and small values.

(*b*) The microwave frequency may be varied from millimetre to 10 cm waves, and therefore N_e can be measured for values between 10^{10} and 10^{14} electrons per cm^3 (this includes high Mach numbers for small gas pressures). It would at any rate be best to perform such measurements at a number of frequencies. In this case one could obtain the collision frequency, as well as the electron density from the experimental data.

(*c*) Shock strength and initial pressure.

A wide range of temperatures and pressures in different gases may therefore be covered; in particular, relatively low Mach numbers, where other known methods give unsatisfactory results, may be studied.

Appendix

Composition calculations for nitrogen, containing 0·25 % *oxygen*

Our problem is to calculate the equilibrium composition of a gas mixture, containing initially 99·75 % N_2 and 0·25 % O_2 at a pressure of 10 mm Hg and a

temperature of 300 °K, for shock Mach numbers 7·4–9. Assuming only single ionization occurs, the reactions involved are:

$N_2 \rightleftarrows 2N + 9{\cdot}7592$ eV/molecule	Dissociation of N_2
$O_2 \rightleftarrows 2O + 5{\cdot}1155$ eV/molecule	Dissociation of O_2
$\frac{1}{2}N_2 + \frac{1}{2}O_2 \rightleftarrows NO + 0{\cdot}9313$ eV/molecule	Formation of NO
$N_2 \rightleftarrows N_2^+ + e^- + 15{\cdot}58$ eV/molecule	Ionization of N_2
$N \rightleftarrows N^+ + e^- + 14{\cdot}5482$ eV/molecule	Ionization of N
$O_2 \rightleftarrows O_2^+ + e^- + 12{\cdot}05$ eV/molecule	Ionization of O_2
$O \rightleftarrows O^+ + e^- + 13{\cdot}6173$ eV/molecule	Ionization of O
$NO \rightleftarrows NO^+ + e^- + 9{\cdot}25$ eV/molecule	Ionization of NO

From these we derive the following system of eleven simultaneous algebraic equations (concentrations of the various species, in terms of number of particles per original gas mixture molecule, are indicated by square brackets):

(*a*) $[N_2] + \frac{1}{2}[NO] + \frac{1}{2}[N] = 0{\cdot}9975$

(*b*) $[O_2] + \frac{1}{2}[NO] + \frac{1}{2}[O] = 0{\cdot}0025$

(*c*) $K_1 = [N]^2/[N_2]$

(*d*) $K_2 = [O]^2/[O_2]$

(*e*) $K_3 = [NO]/([N_2].[O_2])^{\frac{1}{2}}$

(*f*) $K_4 = [N_2^+].[e^-]/[N_2]$

(*g*) $K_5 = [N^+].[e^-]/[N]$

(*h*) $K_6 = [O_2^+].[e^-]/[O_2]$

(*i*) $K_7 = [O^+].[e^-]/[O]$

(*j*) $K_8 = [NO^+].[e^-]/[NO]$

(*k*) $[N_2^+] + [N^+] + [O_2^+] + [O^+] + [NO^+] = [e^-]$

(*a*) and (*b*) are conservation of matter equations, (*c*) to (*j*) chemical equilibrium equations, and (*k*) is the conservation of charge. The K_n are equilibrium constants, given in terms of concentrations and may be calculated according to the following relation (Gilmore 1955):

$$K_n = \left(\frac{\rho_0 T_0}{\rho T}\right)^{\Delta n} \exp\left[\frac{\Delta E_0^0}{RT} - \Delta\left(\frac{F^0 - E_0^0}{RT}\right)\right],$$

where Δn is an integer, indicating the change in the number of particles in the reaction, ΔE_0^0 the energy of reaction at 0 °K, $\Delta(F^0 - E_0^0)$ the change in the standard free energy caused by the reaction, R the universal gas constant, ρ_0 and T_0 standard reference density and temperature (1 atm. and 0 °C).

Since we showed that it is permissible to employ Waldron's (1958) data for the temperature and density of the shocked gas, ρ and T, it is possible to calculate all equilibrium constants using free energy and reaction energy data tabulated by Gilmore (1955).* These computations were performed for six values of M in the range of interest.

One can now solve the equation system (*a*)–(*k*), but its non-linearity makes this a rather laborious task. Preliminary calculations indicate that the degree of ionization is small (less than 10^{-6}) and it is therefore permissible to perform the calculations in two steps. In the first step ionization is neglected and a system consisting of equations (*a*)–(*e*) is solved by an iterative method. In the second

* For N and N_2 more detailed tables by Woolley (1956) were used.

step we are interested in finding the electron density N_e; for this purpose we need only to know the electron concentration $[e^-]$. From equations (f)–(k) we obtain:

$$[e^-] = \sqrt{(K_4[N_2] + K_5[N] + K_6[O_2] + K_7[O] + K_8[NO])}. \qquad (A\,1)$$

An order of magnitude check of the equilibrium constants and concentrations involved shows that in the range of interest all terms of the sum under the square root in equation (A 1) can be neglected in comparision with $K_8[NO]$. This is a consequence of the fact that the ionization potential of nitric oxide is much lower than that of the other components.

Results of the computations, including concentrations of all non-ionized particles and electron concentration and number density are tabulated in table 5.

Mach number	$[N_2]$	$[N]$	$[NO]$	$[O_2]$	$[O]$	$[e^-]$	N_e (cm^{-3})
7·4	0·9964	$1{\cdot}4 \times 10^{-5}$	$2{\cdot}3 \times 10^{-3}$	$3{\cdot}2 \times 10^{-4}$	$2{\cdot}1 \times 10^{-3}$	$6{\cdot}9 \times 10^{-9}$	$1{\cdot}45 \times 10^{10}$
7·9	0·9966	7·7	1·75	1·2	3·05	$3{\cdot}3 \times 10^{-8}$	7·20
8·2	0·9967	$3{\cdot}95 \times 10^{-4}$	1·35	$5{\cdot}8 \times 10^{-5}$	3·5	7·3	$1{\cdot}65 \times 10^{11}$
8·35	0·9967	3·15	1·2	4·1	3·65	$1{\cdot}1 \times 10^{-7}$	2·45
8·8	0·9966	$1{\cdot}05 \times 10^{-3}$	$8{\cdot}3 \times 10^{-4}$	1·6	4·15	2·95	6·85
9	0·9964	1·75	6·8	1·0	4·3	4·5	$1{\cdot}05 \times 10^{12}$

TABLE 5. Gas composition and electron density for nitrogen with 0·25 % oxygen in shock Mach range 7·4–9. Initial pressure: 10 mm Hg. Initial temperature: 300 °K.

REFERENCES

BETHE, H. A. 1942 *Rep. Dep. Commerce*, PB-27307.

BETHE, H. A. & TELLER, E. 1940 *Rep. Ballistic Res. Lab., Aberdeen Proving Ground*, X-117.

BIRK, M., EREZ, A., MANHEIMER, Y. & NAHMANI, G. 1954 *C.R. Acad. Sci., Paris*, **238**, 654.

CAMPBELL, A. W., MALIN, M. E., BOYD, T. J. JR. & HULL, J. A. 1956 *Rev. Sci. Instrum.* **27**, 567.

GILMORE, F. R. 1955 *Rand. Corp. Res. Memorandum*, RM-1543.

GLASS, I. I., MARTIN, W. A. & PATTERSON, G. N. 1953 *Rep. Inst. Aerophysics, Univ. Toronto, UTIA*, no. 2.

GLICK, H. S., KLEIN, J. J. & SQUIRE, W. 1957 *J. Chem. Phys.* **27**, 850.

HAMMERLING, P., SHINE, W. W. & KIVEL, B. 1957 *J. Appl. Phys.* **28**, 760.

LAMB, L. & LIN, S. C. 1957 *J. Appl. Phys.* **28**, 754.

LIN, S. C. 1952 Thesis, Cornell University.

LIN, S. C., RESLER, E. L. & KANTROWITZ, A. R. 1955 *J. Appl. Phys.* **26**, 95.

LOEB, L. B. 1955 *Basic Processes of Gaseous Electronics*. Berkeley: University of California Press.

LOW, W. & MANHEIMER, Y. 1959 *Proc. IX Int. Astronautical Congress*. Vienna: Springer (in the Press).

MARGENAU, H. 1946 *Phys. Rev.* **69**, 508.

MASSEY, H. S. W. & BURHOP, E. H. S. 1952 *Electronic and Ionic Impact Phenomena*. Cambridge University Press.

NIBLETT, B. & BLACKMAN, V. H. 1958 *J. Fluid Mech.* **4**, 191.

PETSCHEK, H. E. & BYRON, S. 1957 *Ann. Phys.* **1**, 270.

UDELSON, B. J., CREEDON, J. E. & FRENCH, J. C. 1957 *J. Appl. Phys.* **28**, 717.

WALDRON, H. F. 1958 *Rep. Inst. Aerophysics, Univ. Toronto, UTIA*, no. 50.

WOOLLEY, H. W. 1956 *NACA TN* 3271.

The stability of viscous flow between rotating concentric cylinders with a pressure gradient acting round the cylinders

By R. C. DIPRIMA
Department of Mathematics, Rensselaer Polytechnic Institute, Troy, New York

(Received 6 February 1959)

The stability of a viscous fluid between concentric cylinders is analysed, for the case in which the basic velocity distribution is the sum of a velocity distribution due to the rotation of the cylinders (Taylor 1923), and a 'pumping' velocity distribution due to a pressure gradient acting round the cylinders (Dean 1928). The critical Taylor number is computed for a wide range of values of the ratio of average velocity of pumping to average velocity of rotation for the case in which the outer cylinder is stationary. It is assumed that the spacing between the cylinders is small.

1. Introduction

The stability of a viscous flow between two concentric rotating cylinders was first considered experimentally and theoretically by Taylor (1923). Using the assumption that the spacing between the cylinders is small compared to the mean radius, he obtained a criterion for the onset of a secondary motion with a cellular form which was verified by his experiments. The eigenvalue problem which arises in this analysis is of considerable interest, and has been discussed by several authors, including Pellew & Southwell (1940), Chandrasekhar (1954*a*) and DiPrima (1955).

A similar type of instability occurs when a viscous fluid flows in a curved channel under a pressure gradient acting round the channel. This problem was first considered by Dean (1928), for the case in which the annulus is thin compared to the mean radius. The resulting eigenvalue problem has also been studied by Reid (1958) and Hämmerlin (1958). Their results verify those of Dean (1928).

In a number of engineering applications, stability problems of the type just described are of considerable interest. One such problem, which has been considered recently by Brewster & Nissan (1958) and Brewster, Grosberg & Nissan (1959), is that of the stability of a viscous fluid between concentric cylinders when the inner cylinder is rotating (the Taylor problem) and at the same time the fluid is being pumped round the annulus (the Dean problem). The pumping may be in the direction of the rotation or opposed to it. The theoretical conclusions of Brewster *et al.* (1959) are based on the use of the necessary condition for instability that the square of the circulation should decrease outwards from the inner cylinder. The eigenvalue problem is explicitly solved only in the case when the average velocity of rotation is equal to, but opposite in direction to, the

average velocity of pumping. In general their conclusions are supported by their experimental results.

In this paper the stability problem for the above type of velocity distribution is formulated. In the case when the spacing between the cylinders is small compared to the mean radius, the eigenvalue problem is solved by the methods first suggested by Chandrasekhar (1954*a*). Numerical results for the critical value of the parameter governing stability are given for a wide range of ratios of average velocity of pumping to average velocity of rotation. The results are in good agreement with the experimental data of Brewster *et al.* (1959).

2. The disturbance equations

Let (r, θ, z) be cylindrical co-ordinates, with the z axis coinciding with the axis of the cylinders, and let R_1, R_2, Ω_1 and Ω_2 denote the radii and angular velocities of the inner and outer cylinders, respectively. If u_r, u_θ, and u_z denote the components of velocity in the increasing r, θ and z direction and p denotes the pressure, the Navier–Stokes equations admit a steady solution of the form

$$u_r = u_z = 0, \quad u_\theta = V(r), \quad \frac{\partial p}{\partial r} = f(r). \tag{1}$$

Now superimpose on this steady motion a small disturbance of a form such that the θ-component of velocity is

$$u_\theta(r, \theta, z, t) = V(r) + v(r) \cos \lambda z \, e^{\sigma t}. \tag{2}$$

The motion will be stable if the real part of σ is less than zero, and unstable if it is greater than zero. It can be anticipated, from similar problems and the experimental results, that for the problem studied here the secondary motion will be of a stationary cellular nature. Hence, we shall only consider the marginal state $\sigma = 0$. In this case the linearized equations for the disturbance velocities are

$$\left.\begin{aligned} (L - \lambda^2)^2 u &= \frac{2\lambda^2}{\nu} \frac{1}{r} V(r) v, \\ (L - \lambda^2) v &= \frac{1}{\nu} \left(\frac{dV}{dr} + \frac{V}{r} \right) u, \end{aligned}\right\} \tag{3}$$

where u is the disturbance velocity in the r direction, ν is the kinematic viscosity, and

$$L = \frac{d^2}{dr^2} + \frac{1}{r} \frac{d}{dr} - \frac{1}{r^2}.$$

In the case that $d = R_2 - R_1$ is small compared with $\frac{1}{2}(R_1 + R_2)$, the operator L can be replaced by d^2/dr^2, and V/r and $dV/dr + V/r$ can be approximated by

$$V(r)/r = \Omega_1 \{1 - (1-k)x\} + \frac{d^2}{2\mu R_1^2} \frac{\partial p}{\partial \theta} (x^2 - x), \tag{4}$$

$$\frac{dV}{dr} + \frac{V}{r} = 2A + \frac{d}{2\mu R_1} \frac{\partial p}{\partial \theta} (2x - 1), \tag{5}$$

where $k = \Omega_2/\Omega_1$, $r = R_1 + dx$, $A = \Omega_1 \{1 - (kR_2^2/R_1^2)\}/\{1 - (R_2^2/R_1^2)\}$, and μ is the viscosity. These approximations are correct up to terms $O(d/R_1)$. The first term on the right of equation (4) represents the velocity profile due to the rotation of

the cylinders, and the second term represents the velocity profile due to pumping. Using equations (4) and (5), the system of differential equations (3) becomes

$$(D^2-a^2)^2 u = \{1-(1-k)x-Q(x^2-x)\}v, \tag{6}$$

$$(D^2-a^2)v = -a^2 T\left\{1+\frac{Q}{1-(kR_2^2/R_1^2)}(2x-1)\right\}u, \tag{7}$$

where u has been redefined as $(\nu/2a^2\Omega_1 d^2)u$ and

$$\left.\begin{aligned} D=\frac{d}{dx}, \quad a=\lambda d, \quad T=-\frac{4A\Omega_1 d^4}{\nu^2}, \quad Q=3(1+k)\frac{V_P}{V_R}, \\ V_R=R_1\Omega_1\frac{1+k}{2}, \quad V_P=-\frac{d^2}{12\mu R_1}\frac{\partial p}{\partial\theta}. \end{aligned}\right\} \tag{8}$$

The quantities V_R and V_P are the average velocities due to rotation and pumping, respectively. The parameter, T, is commonly referred to as the Taylor number.

The requirement of no slip at the boundaries gives the boundary conditions

$$u = v = Du = 0 \tag{9}$$

at $x = 0$ and $x = 1$.

The system of equations (6) and (7), together with the boundary conditions, determine an eigenvalue problem for T as a function of k, R_2/R_1, Q and a. For fixed values of k, R_2/R_1, and Q, the minimum value of T with respect to a determines the critical value, T_c, at which instability will first set in. Notice that when the pumping is zero, i.e. $Q = 0$, equations (6) and (7) reduce to the Taylor problem as treated by Chandrasekhar (1954*b*). In order to obtain the problem of a viscous flow in a curved channel under a pressure gradient acting round the channel, i.e. $Q \to \infty$, it is necessary to redefine u as u/Q, and then let $Q \to \infty$, noting that the combination TQ^2 is $72(V_P d/\nu)^2/(d/R_1)$.

The determination of T_c for the general case is a four parameter problem, and would require a considerable number of computations. We shall now restrict ourselves to the physically interesting case (see Brewster & Nissan (1958) or Brewster *et al.* (1959)) when the outer cylinder is at rest.

3. The outer cylinder at rest

In this case $k = 0$ and equations (6) and (7) reduce to

$$(D^2-a^2)^2 u = \{1-x-Q(x^2-x)\}v, \tag{10}$$

$$(D^2-a^2)v = -Ta^2\{1+Q(2x-1)\}u. \tag{11}$$

Thus T is now defined as a function of a and $Q = 3V_P/V_R$; and for fixed values of Q the minimum value of T with respect to a gives the critical Taylor number, T_c, at which instability will occur.

The method that was used in obtaining approximate values of T_c and a_c is completely analogous to that used by Chandrasekhar (1954*a*) in treating similar problems. The function $v(x)$ is expanded in a set of complete functions satisfying $v(0) = v(1) = 0$. In this case

$$v(x) = \sum_{m=1}^{\infty} A_m \sin m\pi x, \tag{12}$$

and with this expansion for $v(x)$, equation (10) is solved for $u(x)$.

The four constants of integration that appear in the solution are determined by the conditions $u = Du = 0$ at $x = 0$ and 1. The functions u and v are then substituted in equation (11), the result is multiplied by $\sin n\pi x$, $n = 1, 2, \ldots$ and integrated from 0 to 1. This leads to infinitely many equations for the A_m. If all of the A_m are not to vanish identically the determinant of the coefficients must be zero, and this gives a relation between T, a and Q. The details of the analysis, while straightforward, are quite lengthy and are given in the Appendix.

Q	$a = \lambda d$	T/π^6	N	T_{N-1}/T_N
30	3·76	0·085	3	0·982
21	3·70	0·155	—	0·984
15	3·60	0·266	—	0·987
10	3·45	0·474	—	0·992
6	3·30	0·866	—	0·996
3	3·14	1·54	—	1·006
1·0	3·13	2·53	—	1·006
0·50	3·13	2·96	—	1·005
0	3·12	3·53	—	1·004
− 0·50	3·17	4·35	—	1·002
− 1·0	3·24	5·64	—	0·9997
− 1·5	3·40	7·97	—	0·9992
− 2·0	3·80	13·1	—	1·02
− 2·5	5·0	24·7	4	1·002
− 2·75	5·73	33·1	—	1·016
− 3·00	6·35	42·6	—	1·045
− 3·25	7·05	53·7	—	1·094
− 3·50	7·4	66·4	—	1·109
− 3·75	5·8	64·5	—	0·949
− 4·00	5·5	47·8	—	0·969
− 4·50	5·37	29·1	—	0·981
− 5·00	5·20	19·0	—	0·987
− 6·00	5·00	10·0	—	0·995
− 8·00	4·70	4·00	3	1·02
− 10·00	4·55	2·10	—	1·01
− 15·00	4·35	0·720	—	0·984

TABLE 1. Critical Taylor Numbers and corresponding values of a for assigned values of Q. (N = number of terms used in approximation)

The numerical results for T_c and a_c for a range of values of Q from -15 to 30, i.e. V_P/V_R ranges from -5 to 10, are tabulated in table 1, and shown graphically in figures 1 and 2. It is clear from table 1 that for most values of Q a three-term approximation gives satisfactory results; however, for the range $-8 < Q < -2$ it was necessary to use another term in the approximation.

For $Q = 0$ the values of T_c and a_c are in agreement with those of Chandrasekhar (1954*b*). When the average velocities of pumping and rotation are equal but in opposite directions, i.e. $Q = -3$, the values of $T_c/\pi^6 = 42{\cdot}6$, and $a_c = 6{\cdot}35$ may be compared with the values 40·7 and 5·7* found by Brewster *et al.* (1959) using a six-term approximation and following the methods of Dean (1928). It is impossible to compare the present results with the results for zero rotation;

* In part, the poor agreement for a_c probably follows from the fact that, in the neighbourhood of the minimum value, T is very insensitive to changes in a and hence an accurate determination of a_c is quite difficult.

however, as $Q \to \pm\infty$ it appears from figure 2 that a_c is approaching a value of about 4, and Reid (1958) gives $a_c = 3{\cdot}96$ for this case.

The experimental results* given by Brewster *et al.* (1959) have been used to compute values of T_c/π^6 which are shown in figure 1. As can be seen the experimental points are in good agreement with the theoretical curve obtained here.

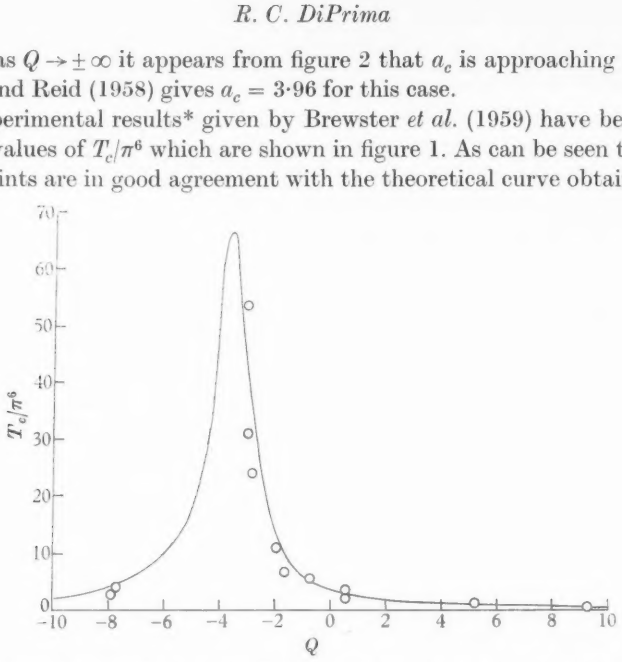

FIGURE 1. The variation of the critical Taylor number, T_c, as a function of $Q = 3V_P/V_R$. Values of T_c computed from the experimental data of Brewster *et al.* (1959) are also shown. ○, experimental points, Brewster *et al.* (1959).

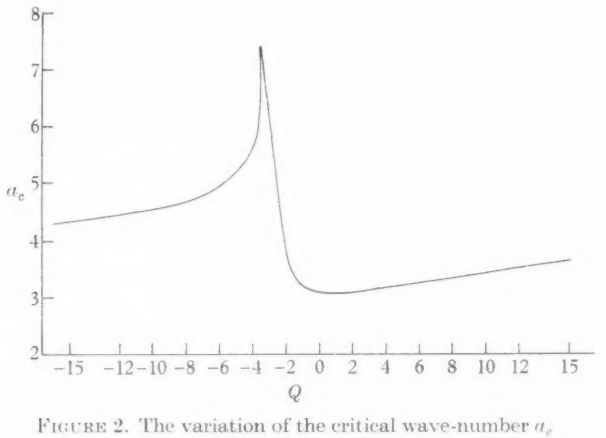

FIGURE 2. The variation of the critical wave-number a_c as a function of $Q = 3V_P/V_R$.

* The experiments were run with a glycerine solution as the fluid. The value of R_1 was 15·6 cm and the value of d was 0·858 cm, which was determined by making the experimental results agree with the theoretical results of Taylor for $Q = 0$. Some experiments were also run with a water-dye solution for the range of value of $-5 < Q < -3$, but there was difficulty in making accurate observations in this case and the scatter of the results was quite large. However, in a private communication, Dr Grosberg of the University of Leeds has informed the author that the average values of the latter results do show good agreement with the theoretical curve given in figure 1.

Finally, for an assigned ratio of V_P/V_R, the curve shown in figure 1 may be used to compute the critical value of V_R at which instability will occur. Also, for given values of V_P or V_R the corresponding ranges of V_R and V_P for which the flow is stable may be computed. It should be noted that in the neighbourhood of $V_P/V_R = -1$ the value of T_c is quite large. This means that as long as the average velocities of pumping and rotation are nearly equal and opposite in sign, and hence tend to annul each other on the average, they may be quite large in magnitude before instability will occur.

The results presented in this paper were obtained in the course of research sponsored by the Mechanics Branch of the Office of Naval Research, Washington. The author would like to express his appreciation to Prof. A. H. Nissan for suggesting this problem and for his continued interest throughout the course of the analysis. Thanks are also due to Mr Burt Liebowitz who carried out the rather lengthy numerical computations.

Appendix

The solution of equation (10), corresponding to the expansion of $v(x)$ given in equation (12), that satisfies the boundary conditions $u = Du = 0$ at $x = 0$ and 1 is

$$u(x) = \sum_{m=1}^{\infty} \frac{A_m}{(m^2\pi^2+a^2)^2}\{A_1^{(m)}\cosh ax + B_1^{(m)}\sinh ax + A_2^{(m)}x\cosh ax + B_2^{(m)}x\sinh ax$$
$$+ [1+f_m-(1-Q)x-Qx^2]\sin m\pi x - e_m[(1-Q)+2Qx]\cos m\pi x\},$$

where
$$f_m = \frac{4(a^2-5m^2\pi^2)}{(m^2\pi^2+a^2)^2}, \quad e_m = \frac{4m\pi}{m^2\pi^2+a^2},$$

$$A_1^{(m)} = (1-Q)\,e_m,$$

$$B_1^{(m)} = \frac{m\pi}{\Delta}\{a\alpha_m + (\sinh a + a\cosh a)\,\beta_m - (\sinh a)\,\gamma_m\},$$

$$A_2^{(m)} = -\frac{m\pi}{\Delta}\{(\sinh a)^2\,\alpha_m + (a\sinh a + a\cosh a)\,\beta_m - (a\sinh a)\,\gamma_m\},$$

$$B_2^{(m)} = \frac{m\pi}{\Delta}\{(\sinh a\,\cosh a - a)\,\alpha_m + (a^2\sinh a)\,\beta_m - (a\cosh a - \sinh a)\,\gamma_m\};$$

and
$$\alpha_m = 1+QF_m, \quad \beta_m = -G_m(-1)^{m+1}\{(1+Q)+(1-Q)\cosh a\},$$
$$\gamma_m = (-1)^{m+1}QF_m - (1-Q)\,(a\sinh a)\,G_m, \quad \Delta = \sinh^2 a - a^2,$$

where
$$F_m = \frac{12(m^2\pi^2-a^2)}{(m^2\pi^2+a^2)^2}, \quad G_m = \frac{4}{m^2\pi^2+a^2}.$$

Substituting for u and v in equation (11) multiplying the result by $\sin n\pi x$, $n = 1, 2, \ldots$, and integrating from 0 to 1 gives the following system of equations:

$$\sum_{m=1}^{\infty}\left\{K_{nm}(a,Q) - \delta_{nm}\frac{(n^2\pi^2+a^2)^3}{2a^2T}\right\}\bar{A}_m = 0 \quad (n = 1, 2, \ldots),$$

where $\bar{A}_m = A_m/(m^2\pi^2+a^2)^2$, $\delta_{nm} = 0$ if $n \neq m$ and $= 1$ if $n = m$, and the lengthy expression $K_{nm}(a, Q)$ is given by

$$K_{nm} = \frac{n\pi}{n^2\pi^2+a^2}\{g_n A_1^{(m)} + h_n B_1^{(m)} + k_n A_2^{(m)} + l_n B_2^{(m)}\}$$
$$+\frac{\delta_{nm}}{2} - X_{nm} + QY_{nm} + Q^2 Z_{nm}.$$

In this expression

$$g_n = (1-Q)\epsilon_n + 2Q\zeta_n, \qquad k_n = (1-Q)\zeta_n + 2Q\theta_n,$$
$$h_n = (1-Q)\lambda_n + 2Q\mu_n, \qquad l_n = (1-Q)\mu_n + 2Q\nu_n,$$

with

$$\epsilon_n = 1+(-1)^{n+1}\cosh a, \qquad \theta_n = \epsilon_n H_n - 2E_n\lambda_n - 1,$$
$$\lambda_n = (-1)^{n+1}\sinh a, \qquad \nu_n = \lambda_n H_n - 2E_n(\epsilon_n - 1),$$
$$\zeta_n = \epsilon_n - 1 - E_n\lambda_n, \qquad E_n = \frac{2a}{n^2\pi^2+a^2},$$
$$\mu_n = \lambda_n - E_n\epsilon_n, \qquad H_n = 1-\frac{1}{a}E_n + 2E_n^2,$$

and

$$X_{nm} = \begin{cases} 0, & n+m \text{ even},\ n \neq m, \\ \frac{1}{4}, & n = m, \\ -4A_{nm} + 2B_{nm}e_m, & n+m \text{ odd}; \end{cases}$$

$$Y_{nm} = \begin{cases} -12A_{nm} + 4B_{nm}e_m, & n+m \text{ even},\ n \neq m, \\ \dfrac{3}{4n^2\pi^2} + \dfrac{1}{\pi n}e_n - \frac{1}{2}f_n, & n = m, \\ -4A_{nm}, & n+m \text{ odd}; \end{cases}$$

$$Z_{nm} = \begin{cases} 0, & n+m \text{ even},\ n \pm m, \\ 0, & n = m, \\ 4A_{nm} - \dfrac{12}{\pi^4}\left[\dfrac{1}{(n-m)^4} - \dfrac{1}{(n+m)^4}\right] + e_m\left\{-2B_{nm} + \dfrac{8}{\pi^3}\left[\dfrac{1}{(n-m)^3} + \dfrac{1}{(n-m)^3}\right]\right\} & \\ \quad +8A_{nm}f_m, & n+m \text{ odd}; \end{cases}$$

where

$$A_{nm} = \frac{nm}{\pi^2(n^2-m^2)^2}, \qquad B_{nm} = \frac{n}{\pi(n^2-m^2)}.$$

REFERENCES

Brewster, D. B., Grosberg, P. & Nissan, A. H. 1959 *Proc. Roy. Soc.* A, **251**, 76–91.

Brewster, D. B. & Nissan, A. H. 1958 *Chem. Engng Sci.* **7**, 215–221.

Chandrasekhar, S. 1954*a* *Amer. Math. Mon.* 7, **61**, 32–45.

Chandrasekhar, S. 1954*b* *Mathematika*, **1**, 5–13.

Dean, W. R. 1928 *Proc. Roy. Soc.* A, **121**, 402–420.

DiPrima, R. 1955 *Quart. Appl. Math.* 1, **13**, 55–62.

Hämmerlin, G. 1958 *Arch. Rat. Mech. Anal.* 3, **1**, 212–224.

Pellew, A. & Southwell, R. V. 1940 *Proc. Roy. Soc.* A, **176**, 312–344.

Reid, W. 1958 *Proc. Roy. Soc.* A, **244**, 186–198.

Taylor, G. I. 1923 *Phil. Trans.* A, **223**, 289–343.

An experimental investigation of the stability of plane shock waves

By K. C. LAPWORTH
Department of the Mechanics of Fluids, University of Manchester

(Received 12 February 1959)

The stability of plane shock waves was measured in a shock tube by perturbing the primary shock wave, formed on rupturing the diaphragm, by means of thin wedges. A time-record of the shape of the shock wave after it passed the wedges and travelled along a channel of constant cross-section was obtained by Schlieren photography. Analysis of the photographs enabled the rate at which the shock wave recovered its plane shape to be determined and this, together with the detailed shape of the wave at various instants, was compared with the first-order theory of Freeman (although all the conditions assumed in the theory could not be faithfully reproduced in the experiments).

For shock-wave Mach numbers of 1·165, 1·41 and 1·60, the time-rate of decay of the perturbations was found to agree quite well with the theoretical value, but the amplitudes of the perturbations were much larger than those given by the theory.

The experiments failed to give reliable information about the decay of the perturbations after a large time, owing, it is believed, to flow separation from the sharp corners of the wedges which constituted an additional source of disturbance to the shock waves.

1. Introduction

When a propagating shock wave enters a diverging, converging or parallel channel, it is observed, under certain conditions, that the shock always meets the channel walls perpendicularly and tends to a state of uniform curvature. Thus, on entering a converging or diverging channel the shock tends to cylindrical form, and on entering a parallel channel it tends to plane form.

Perry & Kantrowitz (1951) have noticed that as a shock wave goes from a parallel channel to a converging channel it becomes adjusted to the new conditions very rapidly and passes from plane to cylindrical form in a very short distance. It is also commonly observed that the shock wave produced by bursting the diaphragm in a shock tube attains a plane form after travelling only a few shock-tube diameters, yet it is far from plane when first formed after rupture of the diaphragm. The phenomenon of equalization of curvature along a propagating shock wave has been termed 'shock-wave stability'. The experiments described in this paper were designed to measure the stability of an initially plane shock wave and to compare it with the theoretical predictions of Freeman (1957).

A qualitative explanation of shock-wave stability may be given by considering what occurs when a plane shock propagating along a parallel channel encounters a disturbance on one wall of the channel. For simplicity suppose that the disturbance is a symmetrical wedge (figure 1*a*). As the shock meets the face AB, a cylindrical compression pulse is formed, and the part of the shock between the junction of the pulse and the face AB of the wedge is diffracted. This part of the shock is curved and meets AB perpendicularly. For this pattern to be formed the wedge angle δ must not exceed a certain value which depends on the strength of the incident shock wave. It will be assumed that δ is always small enough to give rise to the pattern shown in figure 1*a*. This pattern grows uniformly in time. The

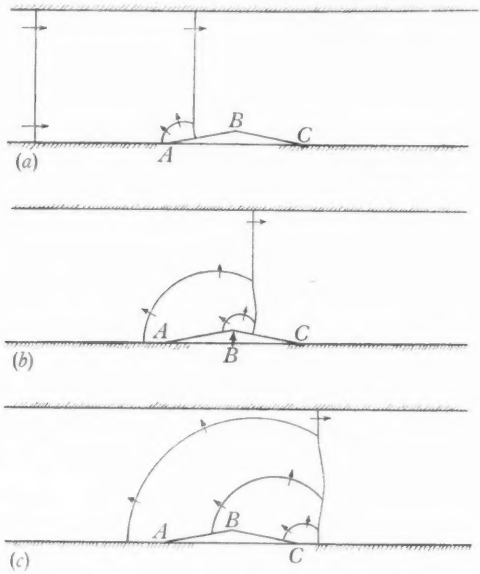

FIGURE 1. Illustration of shock-wave stability.

diffracted portion of the shock eventually reaches the apex B of the wedge. The shock is there further diffracted, and an expansion pulse is formed as shown in figure 1*b*. Finally the shock reaches the corner C of the wedge, and another compression pulse is formed, the shock again being diffracted. Each superimposed shock diffraction pattern grows uniformly with time; therefore the curvature at each point of the diffracted part of the shock must decrease with time. The effect of reflexion of the pulses at the channel walls is taken into account by introducing images of the wedge in the walls. Thus, the shape of the shock propagating along the uniform part of the channel is a combination of superimposed diffraction patterns. However, each separate pattern becomes flatter as the shock propagates and the shock becomes plane. Although only a simple disturbance has been considered, the argument is readily extended to the case of a more complex disturbance.

The phenomenon of shock-wave stability has been treated theoretically by Freeman (1957). He considered a plane shock wave propagating along a parallel

channel and meeting symmetrical wedges, one on either wall of the channel (figure 2).

The problem is linearized on the assumption of small δ; and, using the results of Lighthill's theory of shock-wave diffraction (1949), the following relation

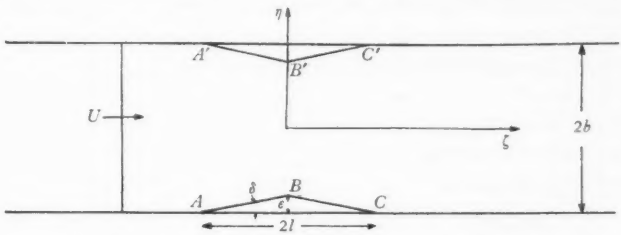

FIGURE 2. The problem treated by Freeman (1957).

between ξ, the perturbation of the shock wave from plane at any point, and the co-ordinates (ζ, η) as in figure 2 is obtained for $\zeta/b \gg 1$:

$$\frac{\xi}{b} = \frac{\epsilon}{l}\frac{\Omega}{(\zeta/b)^{\frac{3}{2}}}\left[F\left\{\frac{\pi}{b}\left(\frac{a_1 k_1}{U}\zeta+\eta\right)\right\}+F\left\{\frac{\pi}{b}\left(\frac{a_1 k_1}{U}\zeta-\eta\right)\right\}\right], \tag{1}$$

where

$$F(\alpha) = 2E(\alpha)-E\left(\alpha+\frac{\pi l}{b}\frac{a_1 k_1}{U}\right)-E\left(\alpha-\frac{\pi l}{b}\frac{a_1 k_1}{U}\right), \tag{2}$$

$$E(\beta) = \sum_{n=1}^{\infty}\frac{(-1)^n \sin n\beta}{n^{\frac{7}{2}}}-\sum_{n=1}^{\infty}\frac{(-1)^n \cos n\beta}{n^{\frac{7}{2}}}, \tag{3}$$

$$k_1 = \left[\frac{6(M_s^2-1)}{7M_s^2-1}\right]^{\frac{1}{2}}.$$

Here Ω is a function of M_s (the Mach number of the undisturbed shock wave with respect to the velocity of sound ahead of it) and has been given previously by Freeman. Also, a_1 is the velocity of sound behind the shock wave.

The functions F in (1) represent two waves travelling in opposite directions along the shock wave. These waves are due to the disturbances arising from the upper and lower wedges and their respective images.

In connexion with this problem, another effect must be considered. Suppose that the shock travels from the position AA' to BB' (figure 2) in the same time that it takes the junction between the cylindrical compression pulse and the shock wave to travel along the shock a distance equal to the channel width. Then, neglecting the depth of the wedges, when the shock reaches the position BB' the compressions arising at A and A' will just reach B' and B respectively and will coincide with the expansion pulses arising at the apices of the wedges. Similarly, when the shock reaches the position CC' the compression and expansion pulses already formed will coincide with the further compression pulses arising at C and C'. According to the linearized theory, the strength of each compression pulse is proportional to δ and the strength of each expansion pulse is proportional to 2δ. Thus, for $\zeta/b \gg 1$ where the compression and expansion pulses tend to coincide over their whole fronts, the compressions will be annulled by the expansions, and therefore $\xi = 0$.

It can readily be shown that, for this condition of cancellation to hold, $(a_1 k_1/U)(l/b) = 2n$, where n is an integer. In fact, the expression for ξ given by (1) is the leading term of an asymptotic expansion, provided that the above condition of cancellation does not hold. When the above condition does hold, the next highest term in the expansion becomes of greatest importance, in which case the decay of the perturbations would be more rapid than indicated by (1).

On the other hand, if the shock travels from AA' to CC' in the same time as the junction between the first cylindrical compression pulse and the shock wave takes to travel the width of the channel, then the compression pulses arising at A and A' tend to reinforce those arising at C' and C respectively. In this case, the distortions of the shock wave due to the two wedges are superimposed to give a larger distortion. The condition for this reinforcement to occur is $(a_1 k_1/U)(l/b) = 2n+1$.

2. Apparatus and experimental procedure

The phenomenon of shock-wave stability was investigated by allowing plane shock waves produced in a shock tube to travel along a parallel channel with symmetrical wedges on each wall as in figure 2. By taking schlieren photographs of different shock waves, all of the same—or very nearly the same—strength, at various values of ζ, the time-history of the passage of a particular shock through the channel could be deduced.

(i) *The shock tube and instrumentation*

The shock tube used is shown diagrammatically in figure 3. The internal dimensions of the cross-section were 5·875 in. by 1·500 in. Air was used in the tube. The high-pressure section of the tube was left open to the atmosphere and the low-

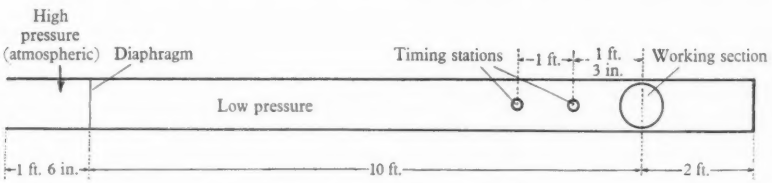

FIGURE 3. Dimensions of shock tube.

pressure section was brought to the desired pressure by a rotary pump. The high- and low-pressure sections were separated by a cellophane diaphragm 0·0015 in. thick. On bursting the diaphragm, a shock wave propagates into the low-pressure section of the tube.

The velocity of the shock wave was found by measuring the time taken by the shock to travel between two stations 1 ft. apart. Each timing station consisted of a small schlieren system with a beam of light across the tube restricted by a narrow vertical slit. The beam, after being focused on a knife-edge, was incident on a photomultiplier. Each small schlieren system was so adjusted that the passage of the shock wave caused light to be deflected off the knife-edge on to the photomultiplier. The resulting signal from the first timing station started an electronic

binary counter registering microseconds, and the signal from the second station stopped the counter. The velocity of the shock wave was then readily deduced.

The signal from the second timing station also actuated an electronic delay circuit that could be preset to trigger a spark light source at the working section of the tube at any desired time after the shock had passed the second timing station. The spark gap was the light source for a schlieren system at the working section of the tube; thus, schlieren photographs of shock waves at various positions in the working section could be obtained.

(ii) *The schlieren system at the working section*

The schlieren system is shown diagrammatically in figure 4. The source of light was provided by the discharge across a spark gap of an $0{\cdot}25\,\mu$F condenser charged to 10,000 V. The light was focused on the first knife-edge by the lens L_1 and then

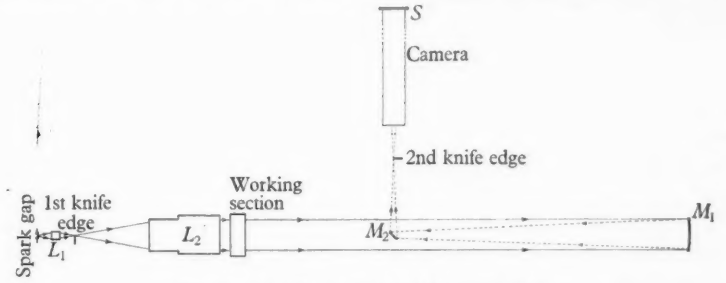

FIGURE 4. Diagram of schlieren system.

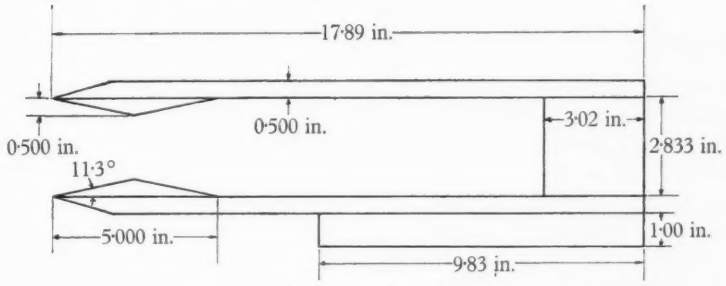

FIGURE 5. Diagram of first wedge system.

collimated by the lens L_2. The collimated beam passed through the working section of the shock tube and was then reflected by the concave mirror M_1 which brought the light to a focus at the second knife-edge. The light then passed into a camera which was focused on the working section of the shock tube.

(iii) *The wedge systems*

One wedge system is shown diagrammatically in figure 5. This was made from ground steel and the whole unit could slide into the shock tube where it could be clamped at any desired position relative to the working section.

After a series of pictures had been obtained with the wedges in one position the

whole assembly could be moved to another position and a further series of pictures obtained, thus extending the range of ζ beyond the diameter of the working-section windows, over which information about the behaviour of the shock could be recorded. It was also necessary to have a second and longer wedge system in order to obtain pictures of the flow at distances from the wedges greater than the length of the first wedge system.

The wedges were designed to satisfy as far as possible the conditions assumed in Freeman's linearized theory. In this respect a compromise had to be made: wedges of very small angle, satisfying the conditions of linearized theory, are difficult to make; furthermore, it would be difficult to measure accurately the small distortions in the shock wave caused by wedges of very small angle. The wedges used had an angle of 11·3°, and the dimensions and spacing of the wedges was such that the condition for reinforcement of the disturbances from each wedge held approximately over the range of shock-wave Mach numbers investigated.

(iv) *Measurement of shock-wave shapes*

The co-ordinates of the shock waves were measured directly from the film records by means of a measuring microscope equipped with a travelling stage movable in two perpendicular directions. The positions of the compressions travelling along the shock waves were also noted, except in the cases of shocks a long distance past the wedges when the compressions become too weak to be observable.

It was found by experience that any measurement could be repeated with an accuracy of better than 0·001 in. An estimate of the setting error of the measuring microscope is $\pm$ 0·0005 in., which corresponds to $\pm$ 0·0003 channel widths.

3. Results

Shock waves of Mach numbers 1·165, 1·41 and 1·60 were investigated. A sequence of photographs showing a shock wave of Mach number 1·41 passing over the wedges and along the parallel channel is shown in the composite picture of figure 6, plate 1. The numbers below the picture give the distance in channel widths along the channel measured from the trailing edges of the wedges.

The results obtained by plotting the measured shock-wave co-ordinates are shown in figure 7*a*. In this picture the scale in the direction along the channel has been made 10 times greater than the scale perpendicular to the channel, thus serving to emphasize the shock-wave perturbations. It can be seen from figure 6, plate 1, that the compression waves arising from the leading edge of one wedge and the trailing edge of the opposite wedge are very close together on the shock wave, indicating that the condition for reinforcement holds very nearly. The actual shape of the shock wave at any instant depends on the positions of the compression waves.

Some idea of the rapidity with which the shock tends to plane form may be gained from figure 7*a*. Over the length of the channel shown (approximately 3 channel widths) the compressions travel across the channel 1½ times, and the maximum perturbation of the shock at the end of this short distance is only about one-tenth the perturbation when the shock is just past the wedges.

4. Comparison between theory and experiment

The rather complicated function denoted by F in equation (1) and given explicitly in equations (2) and (3) may be represented adequately by a sine curve provided that $(a_1 k_1/U)(l/b)$ is not too far removed from unity, i.e. if the condition for reinforcement is realized. For the three shock-wave Mach numbers investigated, $(a_1 k_1/U)(l/b)$ was close enough to unity to render the above approximation

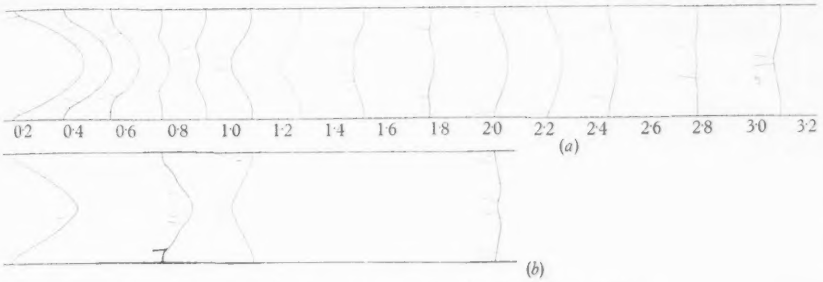

FIGURE 7*a*. Measured shock wave co-ordinates for $M_s = 1{\cdot}41$.
FIGURE 7*b*. Shock wave co-ordinates calculated using Lighthill's theory.
The scale in the direction along the channel is 10 times the perpendicular scale.

M_s	$\frac{a_1 k_1}{U}\frac{l}{b}$	Approximate form for $F(\alpha)$
1·165	0·799	$5{\cdot}11 \sin(\alpha - 3{\cdot}91)$
1·41	0·952	$5{\cdot}64 \sin(\alpha - 3{\cdot}91)$
1·60	0·965	$5{\cdot}64 \sin(\alpha - 3{\cdot}91)$

TABLE 1

for $F(\alpha)$ valid. The values of $(a_1 k_1/U)(l/b)$ and the corresponding values of $F(\alpha)$ for the three shock-wave Mach numbers investigated are shown in table 1. It is seen that, for the shock-wave Mach numbers under consideration, $F(\alpha)$ has the approximate form $A \sin(\alpha - 3{\cdot}91)$. On substituting this approximate value for $F(\alpha)$ in equation (1), the following expression for the perturbation is obtained:

$$\frac{\xi}{b} = \frac{\epsilon}{l}\frac{\Omega}{(\zeta/b)^{\frac{3}{2}}} 2A \sin\left(\frac{\pi a_1 k_1}{U}\frac{\zeta}{b} - 3{\cdot}91\right)\cos\left(\frac{\pi\eta}{b}\right). \tag{4}$$

According to this expression, the perturbation is a standing wave in the form of a cosine curve.

Direct comparison between the theoretical expression (4) and the experimental results cannot be made because the position of the plane unperturbed shock from which the perturbations must be measured is not known accurately enough. In order to overcome this difficulty, a quantity called the 'total perturbation' has been introduced. This is defined as the difference between the extreme positions of a perturbed shock wave measured in the direction of propagation (figure 8).

The theoretical expression for the magnitude of the total perturbation ψ is

$$\psi = A\frac{0{\cdot}1414\Omega}{(x+0{\cdot}883)^{\frac{3}{2}}}\left|\sin\left[\frac{\pi a_1 k_1}{U}(x+0{\cdot}883) - 3{\cdot}91\right]\right|,$$

where all lengths have been made non-dimensional by dividing by the channel width $2b$. In this system, x is the distance along the channel measured from the trailing edges of the wedges. Experimentally, the total perturbation is readily determined from the plotted shock shapes.

4.1. *Analysis of the experimental results*

For comparison with theory, a function was chosen of a form similar to the theoretical expression, and the parameters in this function were evaluated to give the best fit to the experimental results by the method of least squares.

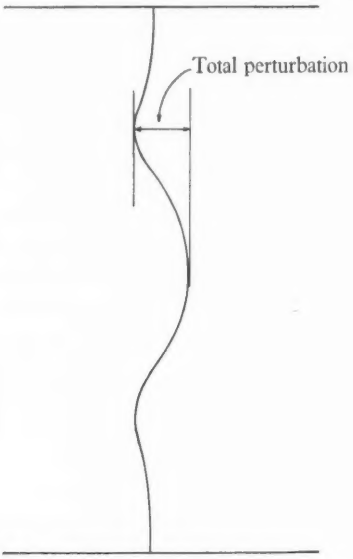

FIGURE 8. Sketch defining total perturbation of shock wave.

The function chosen to fit the experimental results was

$$\psi = \frac{G}{(x+0{\cdot}883)^n}\,|\sin\,[m(x+0{\cdot}883)+p]|,$$

where n, G, m and p are the parameters to be evaluated. m and p are easily determined; on the other hand, to evaluate G and n it was found convenient to minimize $\Sigma(\log\psi - \log\psi')^2$, where ψ' is the measured total perturbation. Evidently, the values of G and n obtained in this way would not be exactly the same as those found by minimizing $\Sigma(\psi-\psi')^2$, but they led to curves which fitted the experimental points quite well.

This analysis was carried out for shock waves of Mach numbers 1·41 and 1·60, but proved unsuccessful for shock waves of Mach number 1·165 (see figures 9–11). From the experimental results for $M_s = 1{\cdot}165$ (figure 11), it can be seen that the period of oscillation of total perturbation did not remain constant; therefore it was impossible to find constant values for m and p, and the analysis failed.

The results for $M_s = 1{\cdot}41$ and $1{\cdot}60$ in figures 9 and 10 show that for values of x greater than about 4 the measured perturbations behaved in an erratic manner and ceased to decrease with increasing x. Possible reasons for this behaviour will

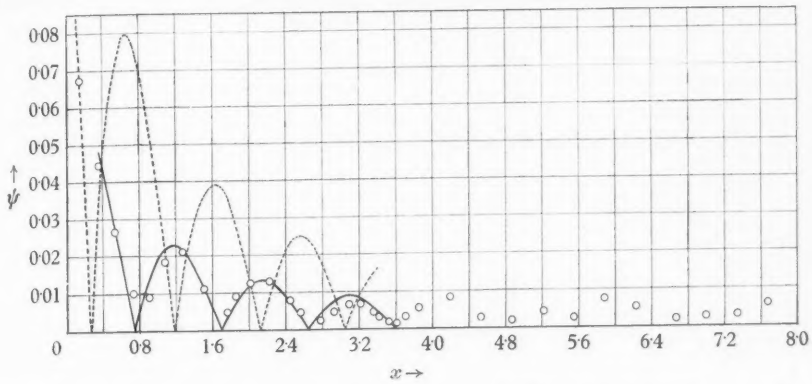

FIGURE 9. Graph of total perturbation *vs* distance. ○, Experimental results; —, fitted curve; – – –, theoretical curve.

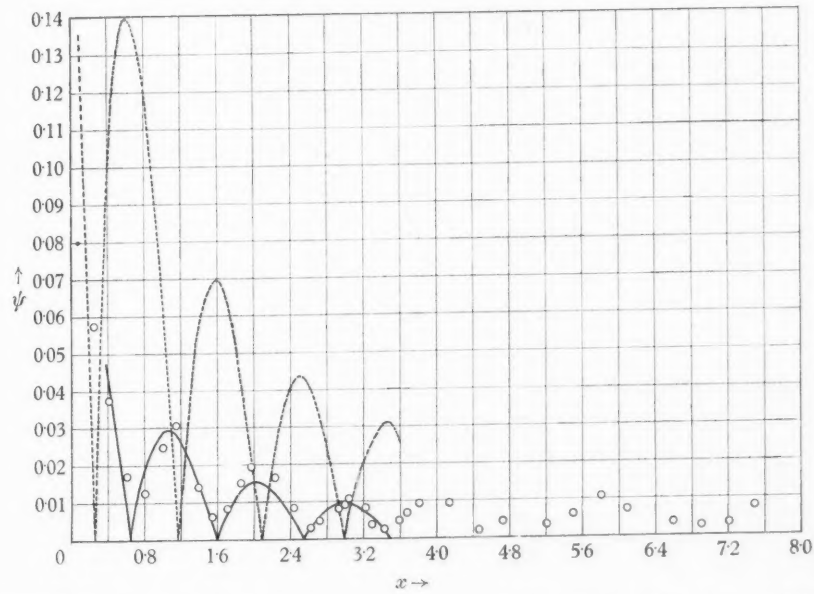

FIGURE 10. Graph of total perturbation *vs* distance. ○, Experimental results; —, fitted curve; – – –, theoretical curve.

be discussed later. These anomalous results were not used in the analyses, and the fitted curves are shown extending over the results that were used. The perturbations of the shock waves before the compressions from the trailing edges of the wedges had travelled across the channel once were not included in the analyses

either for, at such an early stage in the stabilization of the shock wave, the regions of the shock near the junctions of the compressions and the shock had not expanded far enough to affect much of the shock wave.

The results found for n and G at $M_s = 1{\cdot}41$ and $1{\cdot}60$ are tabulated in table 2 together with the theoretical values of these quantities given by Freeman's theory.

In assessing how well the 'best' curves fit the experimental results, the errors in the determination of the total perturbations must be considered. There are two sources of error: (*a*) Each point on the graph is determined from measurements

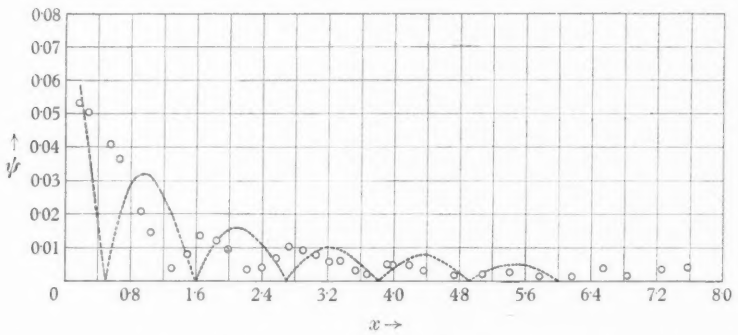

FIGURE 11. Graph of total perturbation *vs* distance. ○, Experimental results; —, fitted curve; – – –, theoretical curve.

	n		G	
M_s	Experiment	Theory	Experiment	Theory
1·41	1·45	1·5	0·066	0·157
1·60	1·65	1·5	0·090	0·273

TABLE 2

of different shock waves; the Mach numbers of these shock waves all agree to better than 1 %. The effect of the small scatter in shock-wave Mach numbers was estimated by obtaining pictures of shock waves of the same nominal Mach number at the same position in the channel. This was done for $M_s = 1{\cdot}60$, and the effect on the perturbation of the scatter in Mach number was found to be very small indeed, much less in fact than the deviation of some of the experimentally determined points from the fitted curve. (*b*) The error in the actual measurement of the perturbation has already been discussed. This is less than the deviation of some of the points from the fitted curve.

It seems likely that the form of the function chosen to fit the experimental results is too simple to give an adequate description of the phenomenon. It should be borne in mind that the form of the function chosen to fit the experimental results is the same as the form of the theoretically derived function which is valid only at a large number of channel widths beyond the wedges. Although the

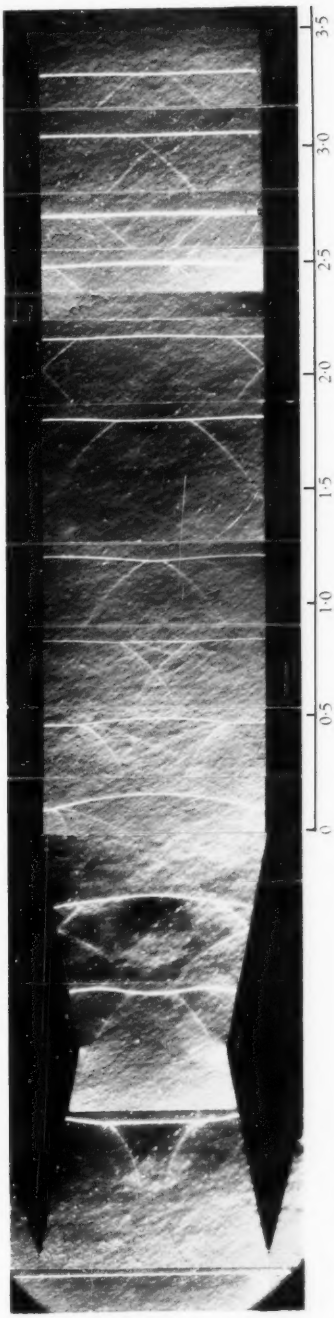

FIGURE 6 (plate 1). Photographs of shock wave at $M_s = 1{\cdot}41$.

(*Facing p.* 480)

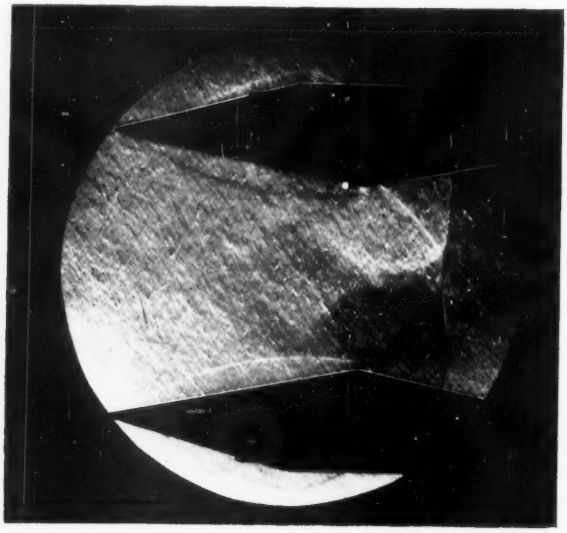

FIGURE 12 (plate 2). Photograph showing diffusion of expansion wave.

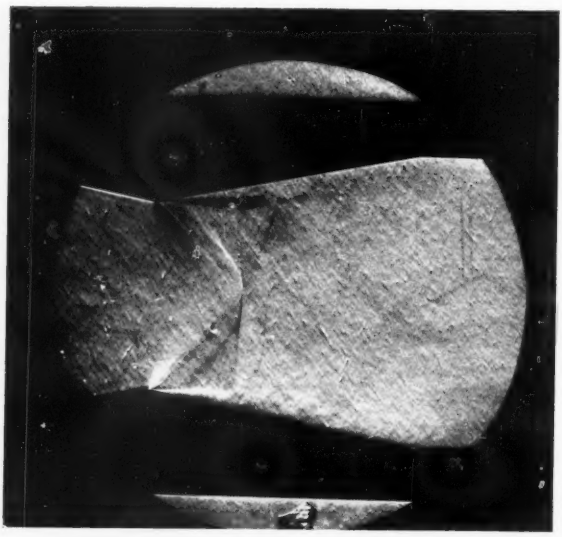

FIGURE 13 (plate 2). Photograph showing wake behind shock wave.

theory is valid only at large distances beyond the wedges, there is agreement with experiment in certain respects. The points on which theory and experiment agree are summarized below:

(*a*) The period of oscillation of the theoretical and experimental values of ψ compare well.

(*b*) The experimentally determined law for the decay of the perturbation with distance compares well with the law given by theory, viz. $\xi \propto \zeta^{-\frac{1}{2}}$.

The points of difference between experiment and theory are as follows:

(*c*) The theoretical expression for the perturbation given by equation (4) shows that the shock shape should be a cosine curve for the shock-wave Mach numbers under consideration. This was not observed experimentally. The theory also indicates that the shock perturbations should become small, i.e. $O(\zeta/b)^{-\frac{1}{2}}$, at regular intervals along the channel; observation showed that, although the shock did not become plane, the perturbations did become very small at regular intervals.

(*d*) There is a phase difference between the theoretical and experimental results.

(*e*) The maximum total perturbations predicted by theory are considerably greater than those observed experimentally.

Comparison between the observed shock shapes and those given by direct application of Lighthill's theory of diffraction of blast

Freeman's theory is based on Lighthill's theory but holds good only for $x/b \gg 1$. Direct application of Lighthill's theory may be expected to give better agreement with experiment near the origin. Shock shapes were calculated for $M_s = 1{\cdot}41$ using Lighthill's theory: these calculated shock shapes are shown in figure 7*b*, where they can readily be compared with the experimental shapes of figure 7*a*. (The dotted lines are expansion pulses which arise from the apex of each wedge.)

From figure 7*b* it is seen that the curvatures of the theoretically determined shock shapes tend to be concentrated in smaller regions of the shock waves than observed in the experiments. This is due to the fact that the theory, which is linear, treats the expansion waves as localized pulses travelling along the shock wave whereas, as can be seen from figure 12, plate 2, the expansion wave tends to become diffuse and meets the shock over a region of its length rather than at one point. This spreading out of the expansion waves (which is explained, at least qualitatively, by the non-linear theory of Whitham 1957) tends to make the curves in the shock shape smoother than those given by the linearized theory.

4.2. *Discussion on the irregular character of the perturbations at the largest values of x investigated*

From figures 9–11 it can be seen that the perturbations cease to decay in a regular manner beyond a certain distance along the channel. It is here suggested that this erratic behaviour may be attributed to the formation of a wake at the apex of each wedge after the passage of the shock wave. These wakes will lead to attenuation of the shock wave since they represent sinks of energy. It has been shown theoretically by Hollyer (1956), and by Trimpi & Cohen (1955), that the

growth of a boundary layer on the shock tube walls can account for observed shock-wave attenuation. The theoretical work treats the problem one-dimensionally and serves to give an overall attenuation of the shock wave, whereas in the present discussion interest centres on the two-dimensional effects of the wakes on the shock wave. A picture of the separated flow over the wedges is shown in figure 13, plate 2. This picture shows the situation 685 μsec after a shock wave of Mach number 1·41 had passed the apexes of the wedges. The well-developed wake can be observed and it is to be expected that this will affect the shock wave propagating along the channel. A certain time must elapse after the passage of the shock wave before a wake is formed. Whilst the wake is forming and also when it has formed, the main shock wave will be attenuated by propagation of expansion waves from the wake. This process will take a certain length of time after the shock wave has passed the wedges; therefore it may be expected that any effect the wake would have on the shock would only become apparent after the shock wave had travelled some distance along the channel. It is in fact observed that the results become erratic at a certain distance past the wedges.

The author is indebted to Prof. P. R. Owen and Prof. M. J. Lighthill for suggesting the experiment. Dr N. C. Freeman gave valuable help in discussions on the theoretical aspects of the problem. During the period of research the author was assisted by a grant from the Department of Scientific and Industrial Research.

REFERENCES

Freeman, N. C. 1957 On the stability of plane shock waves. *J. Fluid Mech.* **2**, 397–411.

Hollyer, R. N. Jr. 1956 Attenuation in the shock tube. I. Laminar flow. *J. Appl. Phys.* **27**, 254–61.

Lighthill, M. J. 1949 The diffraction of blast. I. *Proc. Roy. Soc.* A, **198**, 454–70.

Perry, R. W. & Kantrowitz, A. 1951 The production and stability of converging shock waves. *J. Appl. Phys.* **22**, 878–86.

Trimpi, R. L. & Cohen, N. B. 1955 A theory for predicting the flow of real gases in shock tubes with experimental verification. *Tech. Note Nat. Adv. Comm. Aero., Wash.*, no. 3375.

Whitham, G. B. 1957 A new approach to problems of shock dynamics. Part I. Two-dimensional problems. *J. Fluid Mech.* **2**, 145–71.

TENTH INTERNATIONAL CONGRESS OF APPLIED MECHANICS

The *Tenth International Congress of Applied Mechanics* will be held in the Congress Building at Stresa (Italy) from *Wednesday*, 31 *August through Wednesday*, 7 *September* 1960.

Apart from a number of invited general lectures the technical sessions of the Congress will be held in two sections, viz.:

SECTION 1: Fluid dynamics (hydrodynamics and aerodynamics).

SECTION 2: Mechanics of solids (rigid body dynamics, vibrations, elasticity, plasticity and theory of structures).

It should be noted that thermodynamics and computational methods as such are not included, although specific applications of computational methods to pertinent problems of one of the two sections mentioned above are acceptable subjects for papers to be read at the Tenth Congress.

Previous Congresses have demonstrated the desirability of an adequate period of time for the presentation and discussion of individual papers. In order to allow a period of 45 minutes for each paper (30 min. for presentation and 15 min. for discussion) a Programme Committee will make a selection from papers submitted for presentation. Abstracts of papers should be submitted *in four copies to the Secretary of the International Committee* (*W. T. Koiter*) *before* 1 *January* 1960. Preferably they should not exceed two type-written pages (doubly-spaced) and in no case should they exceed four pages. In order to facilitate the work of the Programme Committee it is recommended that abstracts be in *two* of the official Congress languages (English, French, German and Italian). Authors are urged to make their abstracts as clear as possible, since selection of papers has to be based upon them. *Decisions of the Programme Committee are final*, and it will be understood that it is impossible to enter into correspondence about them with authors of papers. They will be informed promptly of the decision on each paper.

Day-to-day organization of the Congress is in the hands of the Italian Organizing Committee (President: Prof. G. Colonnetti; Secretary: Dr F. Rolla, Consiglio Nazionale delle Ricerche, Ufficio relazioni internazionali, Piazza delle Scienza 7, Roma). All correspondence (apart from submission of papers) should be addressed to the Italian Organizing Committee. Information on accommodation, also registration forms, will be obtainable from Dr Rolla after 1 September 1959.

The Executive Committee of the International Committee for the Congresses of Applied Mechanics

C. B. BIEZENO, *President*; RICHARD V. SOUTHWELL; W. T. KOITER, *Secretary*; (Prof. Mekelweg 2, Delft, Netherlands).

JOURNAL OF FLUID MECHANICS

Volume 6, Part 3 October 1959

CONTENTS

A theory of dispersion in a porous medium
by P. G. SAFFMAN *page* 321

The motion of bubbles in a vertical temperature gradient
by N. O. YOUNG, J. S. GOLDSTEIN and M. J. BLOCK 350

Two-dimensional convection from heated wires at low Reynolds numbers
by D. C. COLLIS and M. J. WILLIAMS 357

Heat transfer in slip flow at low Reynolds number
by H. C. LEVEY 385

Interactions of detonation waves
by E. LARISCH 392

Horizontal diffusion in the atmosphere as determined by geostrophic trajectories
by C. S. DURST, A. F. CROSSLEY and N. E. DAVIS 401

Turbulent entrainment in stratified flows
by T. H. ELLISON and J. S. TURNER 423

Electron density and ionization rate in thermally ionized gases produced by medium strength shock waves
by Y. MANHEIMER-TIMNAT and W. LOW 449

The stability of viscous flow between rotating concentric cylinders with a pressure gradient acting round the cylinders
by R. C. DIPRIMA 462

An experimental investigation of the stability of plane shock waves
by K. C. LAPWORTH 469

Printed in Great Britain at the University Press, Cambridge
(Brooke Crutchley, University Printer)